

Influence of modified bio-oils on the fracture mechanics behavior of  
elastomers

## Dissertation

zur Erlangung des Doktorgrades der Ingenieurwissenschaften  
(Dr.-Ing.)

der

Naturwissenschaftlichen Fakultät II  
Chemie, Physik und Mathematik

der Martin-Luther-Universität  
Halle-Wittenberg

vorgelegt von

Herr M.Sc. Md Mahbubur Rahman  
geb. am 10.08.1986 in Kushtia, Bangladesch

Gutachter:

1. Prof. Dr. Kay Saalwächter
2. Prof. Dr. Beate Langer
3. Prof. Dr. Markus Stommel

Öffentliche Verteidigung: 24 Mai, 2023

# Table of Contents

List of abbreviations.....	i
List of symbols.....	iii
1 Introduction and motivation.....	1
2 Fundamentals of technical use of plasticized elastomers.....	6
2.1 Fundamentals of elastomers.....	6
2.1.1 Properties of polar and non-polar elastomers.....	6
2.1.2 Function of filler and additives.....	9
2.1.3 Crosslinking.....	11
2.1.4 Filler-rubber interactions.....	12
2.2 Fundamentals of plasticizers.....	14
2.2.1 Plasticizers.....	14
2.2.2 Working principle of plasticizer on elastomers.....	15
2.2.3 Properties of plasticizers according to their sources.....	19
2.3 Characterization of elastomers and plasticization effect.....	23
2.3.1 Structural properties.....	23
2.3.2 Fracture resistance behavior and plasticization effect.....	29
2.3.3 Mechanical behavior and plasticization effect.....	31
3 Experimental.....	34
3.1 Investigated oils and materials.....	34
3.1.1 Oils.....	34
3.1.2 Elastomers and Composition.....	34
3.1.3 Preparation of rubber mixtures.....	35
3.2 Experiments.....	36
3.2.1 Oil characterization.....	36
3.2.2 Physicochemical characterization of elastomers.....	42
3.2.3 Basic thermo-mechanical and mechanical testing.....	45
3.2.4 Resistance against crack behavior measurement methods.....	51
3.2.5 Aging behavior of plasticized elastomers.....	55
4 Results and discussion.....	57
4.1 Structure and properties of the investigated oils.....	57
4.1.1 Structure analysis by FTIR and NMR spectroscopy.....	57
4.1.2 Description of polarity, thermal behavior and molecular mass.....	60
4.2 Development of polymer-filler interaction under the influence of oil.....	65
4.3 Influence of oils on the vulcanization behavior and crosslink density.....	68
4.4 Thermo-mechanical and mechanical properties of rubber vulcanizates and their dependence on plasticizing oils.....	70
4.4.1 Influence of oil type on temperature-dependent linear viscoelastic behavior.....	70
4.4.2 Influence of oil type and content on the mechanical properties.....	76
4.5 Fracture mechanics parameters of oil-containing rubber vulcanizates.....	82
4.6 Dependence of aging characteristics on oil type.....	88
5 Structure-property correlations.....	95
6 Summary.....	99
References.....	103

"Dedicated to my beloved  
**parents**, my beautiful  
**wife**, and my little angel,  
**Maarit**"

## List of abbreviations

ATR	Attenuated total reflectance
BR	Polybutadiene rubber
CS	Compression set
CBS	N-cyclohexylbenzothiazole-2-sulfenamide
DAE	Distillate aromatic extracts
DOP	Dioctyl phthalate
DMSO	Dimethyl sulfoxide
DENT	Double-edge notched tension (specimen)
DMA	Dynamic mechanical analysis
DQ	Double-quantum
EECO	Canola oil epoxidized ester of glycerol formal
EESO	Soybean oil epoxidized ester of glycerol formal
EPFM	Elastic-plastic fracture mechanics
ERO	Epoxidized rapeseed oil
EES	Epoxidized ester of soybean and sunflower oils
E-SBR	Emulsion-styrene-butadiene rubber
EPDM	Ethylene-propylene-diene rubber
EPO	Epoxidized palm oil
ECODP	Epoxidized castor oil-based diglycidyl phthalate
EPM	Ethylene-propylene rubber
FTIR	Fourier transform infrared spectroscopy
FID	Free induction decay
FEM	Finite element method
IIR	Isobutyl-isoprene rubber
ITIT	Instrumented tensile impact test
LO	Linseed oil
LEFM	Linear-elastic fracture mechanics
MQ	Multi-quantum
NBR	Acrylonitrile-butadiene rubber
NBR-18	Vulcanized 18 % acrylonitrile content NBR with filler and additives
NBR-34	Vulcanized 34 % acrylonitrile content NBR with filler and additives
NBR-39	Vulcanized 39 % acrylonitrile content NBR with filler and additives
NO	Naphthenic oil
NR	Natural rubber
OMMT	Organically modified montmorillonite
phr	Parts per hundred parts of rubber
PCA	Polycyclic aromatic hydrocarbon
PVC	Poly-vinyl chloride
SO	Stored oil
SEM	Scanning electron microscopy
ROME	Rapeseed oil epoxidized methyl ester
ROPE	Rapeseed oil epoxidized iso-propyl ester

---

SBR	Styrene-butadiene rubber
SBR-21	Vulcanized 21 % styrene content SBR with filler and additives
S-25T	37.5 phr TDAE loaded 25 % styrene content SBR with filler and additives
SENT	Single-edge notched tension (specimen)
SSM	Single-specimen method
TPE	Thermoplastic elastomer
TDAE	Treated distillate aromatic extracted
WLF	Williams-Landel-Ferry
W/O	Without oil
ZnO	Zinc oxide

## List of symbols

$a$	(mm)	Initial crack length; physical crack length that is set before the start of the test
$a/W$	(N·mm)	Relationship of initial crack length to specimen width impact energy
$A_{el}$	(N·mm)	The elastic part of the deformation energy $A_{tot}$ of the test specimen
$A_{max}$	(N·mm)	Deformation energy results from the area under the force-deformation ( $F-I$ ) curve to $F_{max}$
$A_p$	(N·mm)	Crack propagation energy results from $A_{tot} - A_{max}$ deformation energy
$A_{pl}$	(N·mm)	The plastic part of the deformation energy $A_{tot}$ of the test specimen
$A_{tot}$	(N·mm)	Deformation energy results from the total area under the force-deformation curve
$b$	(mm)	Force-deformation curve reference length from the multifractal scaling law specimen thickness
$B$	(mm)	Specimen thickness
$\beta_f$	(K <sup>-1</sup> )	Thermal expansion coefficient above and below $T_g$
$B_p$	(K <sup>-1</sup> )	Cubic thermal expansion coefficient of plasticizer
$B_G$	(K <sup>-1</sup> )	Cubic thermal expansion coefficient of glass-like polymer
$c_R$	-	Mass concentration of carbon black
$D_{res}/2\pi$	(KHz)	Residual dipolar coupling
$E$	(MPa)	Modulus of elasticity
$E'$	(MPa)	Storage modulus
$E''$	(MPa)	Loss modulus
$f_{max}$	(mm)	The deflection occurring at the force $F_{max}$ in the instrumented impact test
$f$	(cm <sup>3</sup> g <sup>-1</sup> )	Fractional free-volume of plasticizer
$f_{exp}$	(cm <sup>3</sup> g <sup>-1</sup> )	Fractional free-volume of cubic expansion coefficient
$F_g$	(cm <sup>3</sup> g <sup>-1</sup> )	Fractional free-volume at $T_g$
$F$	(N)	Force
$F_{max}$	(N)	Maximum force, the force at which a significant drop in the force occurs without increasing deformation
$h_s$	(mm)	Height of spacer
$h_R$	(mm)	Rebound height
$h_0$	(mm)	Height of fall
$J$	(N/mm)	$J$ -integral; mathematical description of the local stress-strain field in front of the crack tip; the fracture mechanical material value is calculated using approximate solutions
$J_d$	(N/mm)	Critical $J$ value when unstable crack propagation sets in impact stress
$J_i$	(N/mm)	Physical crack initiation value, critical $J$ value when stable propagation begins
$J_{max}$	(N/mm)	Maximum $J$ value measured in the quasi-static fracture mechanics test
$l$	(mm)	Extension
$L_0$	(mm)	Output measuring length, clamping length
$l_{max}$	(mm)	Extension at the maximum force, measured in the instrumented impact test
$L$	(mm)	Specimen length
$m_1$	(g)	Initial mass
$m_2$	(g)	Final mass
$M_W$	(g/mol)	Molecular weight or Molar mass
$M_c$	(g/mol)	Molar mass of network chains
$M_e$	(g/mol)	Molar mass of entanglements
$M_x$	(g/mol)	Molar mass of crosslinks

$N_A$	(mol <sup>-1</sup> )	Avogadro number
$\rho$	(g/cm <sup>3</sup> )	Density
$R_0$	(nm)	Radius of oil molecules
$s$	-	Standard deviation
$t$	(s)	Time
$t_0$	(mm)	Thickness of sample before compression
$t_i$	(mm)	Thickness of sample after recovery
$t_{90}$	(min)	time required to 90% curing
$T$	(°C)	Temperature
$T_2$	( $\mu$ s)	Relaxation time
$T_0$	(N/mm)	Threshold tearing energy, determinable in fracture mechanical fatigue experiments
$\tan \delta$	-	Mechanical loss factor
$T_c$	(N/mm)	Critical tearing energy, ascertainable in fracture mechanical fatigue experiments
$T_g$	(°C)	Glass transition temperature
$T_i$	(N/mm)	Critical value of the tearing energy when crack propagation begins (crack initiation value)
$T_J^*$	(N/mm <sup>2</sup> )	$R$ -curve increase at the maximum achievable crack extension $\Delta a_{max}$ , crack propagation value
$T_s$	(N/mm)	Tear strength
$U$	(N·mm)	Deformation energy
$\nu$	(mm <sup>2</sup> /s)	Kinematic viscosity
$\nu_f$	(cm <sup>3</sup> g <sup>-1</sup> )	Free-volume
$\nu_t$	(cm <sup>3</sup> g <sup>-1</sup> )	Volume at a given temperature
$\nu_0$	(cm <sup>3</sup> g <sup>-1</sup> )	Volume at absolute zero temperature /occupied volume
$\nu_H$	(m s <sup>-1</sup> )	Hammer speed
$\nu_T$	(mm/min)	Crosshead speed
$V$	(%)	Coefficient of variation
$W$	(mm)	Specimen width
$Wt\%$	(%)	Weight percentage
$\delta$	(ppm)	Chemical shift (NMR spectroscopy)
$\delta_c$	(mm)	Deformation field in front of crack tip
$\Delta a$	(mm)	Changes in crack length
$\Delta K$	(MPa·mm <sup>1/2</sup> )	Stable crack extension and crack front after defined load
$\varepsilon_B$	(%)	Strain at break
$\eta$	-	Geometry function
$\varphi$	-	Filler volume fraction
$\lambda$	-	Extension ratio
$\rho$	(g/cm <sup>3</sup> )	Network density
$\sigma$	(MPa)	Stress
$\sigma_m$	(MPa)	Maximum stress; tensile strength
$\sigma_B$	(MPa)	Stress at break
$\sigma_{200}$	(MPa)	Stress at 200 % strain
$\tau$	(N·mm)	Torque

# 1 Introduction and motivation

Elastomers are mostly amorphous and weakly networked ubiquitous polymers used for different engineering instruments and commodity goods. Elastomers also named as rubbers, and it is named for specific type of elastomer. Researchers are focused on developing the quality of elastomers day by day. The goal is to improve the mechanical and thermal behavior, aging resistance, and resistance to fracture behavior. The failure of elastomers is one of the biggest problems in their daily application. There are some specific reasons for elastomers' failure, e.g., material inhomogeneities, stretching, continuous deformations during the application, long-time application, unpleasant surroundings, and weathering or overall deficient crack initiation/propagation resistance. Figure 1 shows some examples of the usual result for the failure of elastomeric components. Damage may occur on the elastomer due to bad processing, overload or overpressure, and this crack may happen due to low resistance against crack initiation and/or propagation. An elastomer can be damaged due to outside conditions like high or low temperatures or/and rain, air pollution, and so on, or a long-term application. There are some correlations of the reason for all damage to the elastomer, which are low resistance against crack initiation and propagation due to inhomogeneity of filler distribution/dispersion in a polymer matrix, incompatible plasticizers, poor several material properties, unfit in an unpleasant environment, or decreasing its resistance against crack initiation and propagation due to aging.

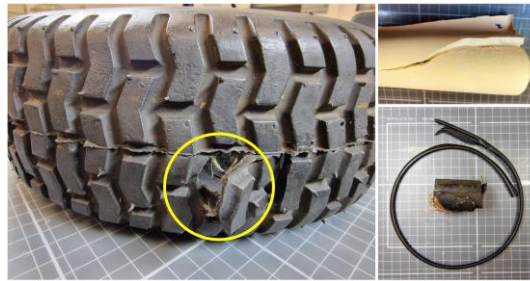


Figure 1. Examples failures of elastomeric components

The propagation of cracks in the elastomer is fundamental for many critical applications, e.g., rubber and pressure-sensitive adhesives. The failure of elastomers by crack propagation often results in a catastrophic process involving a considerable loss of life and money. When a passenger tire explodes, shown in Figure 2 (a), or when an O-ring seal fails in Figure 2 (b).

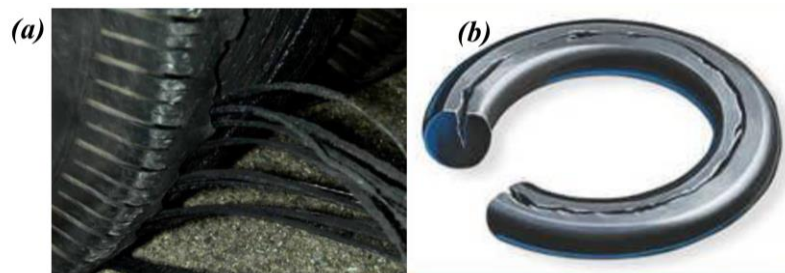


Figure 2: Catastrophic crack propagation in elastomer compounds like resulting in an exploded tire (a), and a crack in an over-compressed elastomer O-ring (b), photo reproduced with permission from ref [1]



In other ways, the failure by crack propagation is perhaps less devastating but still a nuisance, e.g., the aging of wiper blades or failure of elastomer adhesives by interfacial crack propagation, shown in Figure 3.

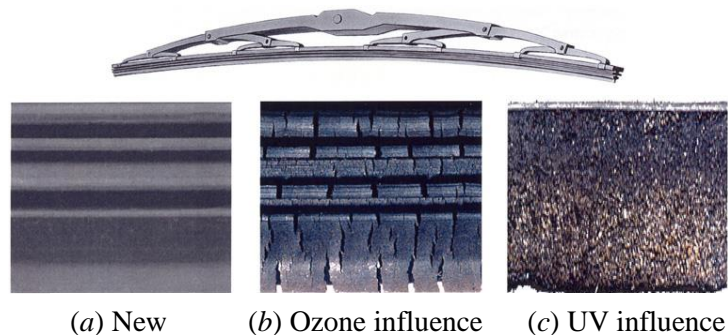


Figure 3: Aging of a wiper blade (a) by ozone (b) and ultraviolet radiation (c), photo reproduced with permission from ref [1]

An unfilled elastomer contained the internal plasticizers, although it shows poor mechanical behavior under stressful conditions [2]. Contrary, plasticizing effect reduces when a number filler reinforced to improve mechanical properties. External plasticizers are the basic solutions that enhance plasticization effect, and chain mobility of filled elastomers. Parallely, it influences on crack resistance and mechanical behavior. A compatible external plasticizer is a condition that fulfills the desired demand otherwise damage may be happened. Compatibility is a vast term that includes a positive relation between elastomer and plasticizer, such as similar polarity. So, a complete investigation is required on modified bio-oil be a plasticizer, especially its physical, chemical, and thermal characteristics are in a great concern.

In this thesis different bio-oils were characterized at the preliminary stage, making hypotheses for desired elastomers in fracture behavior. However, previous works [3] on the bio-oils estimated the efficiency of mechanical behavior, so it was tough to predict good resistance to crack behavior. The selection of optimum bio-oil quantity also was a big challenge for this thesis because they were not commercially plasticizers and do not have any data. The chemical nature of modified bio-oils was investigated using NMR and FTIR spectra. The surface tension of bio-oils on the untreated polytetrafluoroethylene (PTFE), polar and non-polar elastomers investigation help to find the polar behavior of bio-oils. Parallely density, viscosity, molecular mass, and aging information helped to see bio-oils physical, chemical, and aging behavior. These bio-oils were laboratory modifications of market fatty oils, so there were no official characteristics datasheets. Therefore, this characterization helped to predict appropriate elastomers. However, more experimental work was needed to complete this thesis on the hypotheses.

This thesis was carried out in different steps, including oil characterization, mixing, sample preparation, and materials investigations under unaged and aged conditions, and ended with the evaluation of results with comments on the study and further prospects. Figure 4 shows a diagram of the complete list of the investigation applied in this thesis. At the beginning of step 1, the oils are characterized in a physical, chemical, thermal, and aging manner. Then the samples were prepared with different concentrations of bio-oils. Nevertheless, the concentration of filler, crosslinking agent, and antioxidants were fixed for the whole thesis. In step 2, on uncured elastomers (raw mixture), filler wettability was investigated to see how bio-oils were interrupted/helped the length of rubber-filler bounding (so-called rubber-layer  $L$ ). This is a hypothesis that the information on rubber-layer  $L$  can predict the resistance against fracture

behavior because the oil penetration can change the filler surfaces and inner cavities. It was a primary prediction, and to make this prediction strong, the curing behaviors are investigated because they can influence mechanical behavior [4]. In step 3, general investigations were done, including the mechanical, fracture mechanics, thermo-mechanical, and optical (filler-macro dispersion). The crack resistance behaviors were investigated under two different loading systems. The quasi-static and impact load was used to investigate the crack through the elastomer matrix and was done to find the resistance against crack behaviors. The principal idea was to see the influence of bio-oils in the elastomer matrix against the crack under two different loads. The correlation between the resistance efficiency of the crack of plasticized elastomers and the rubber-layer  $L$  was established in this thesis. Plasticized elastomers have aged in step 4 under different conditions to see if there is any influence on the elastomer's mechanical and crack resistance behaviors. The structural properties of oil might influence its polarity and viscosity after aging; so, that also investigated. Furthermore, these properties could be influencing the rubber-layer  $L$ , crosslink density, mechanical, thermo-mechanical, crack resistance, and aging behavior of the materials. Additionally, the structure-property correlation was established in this thesis.

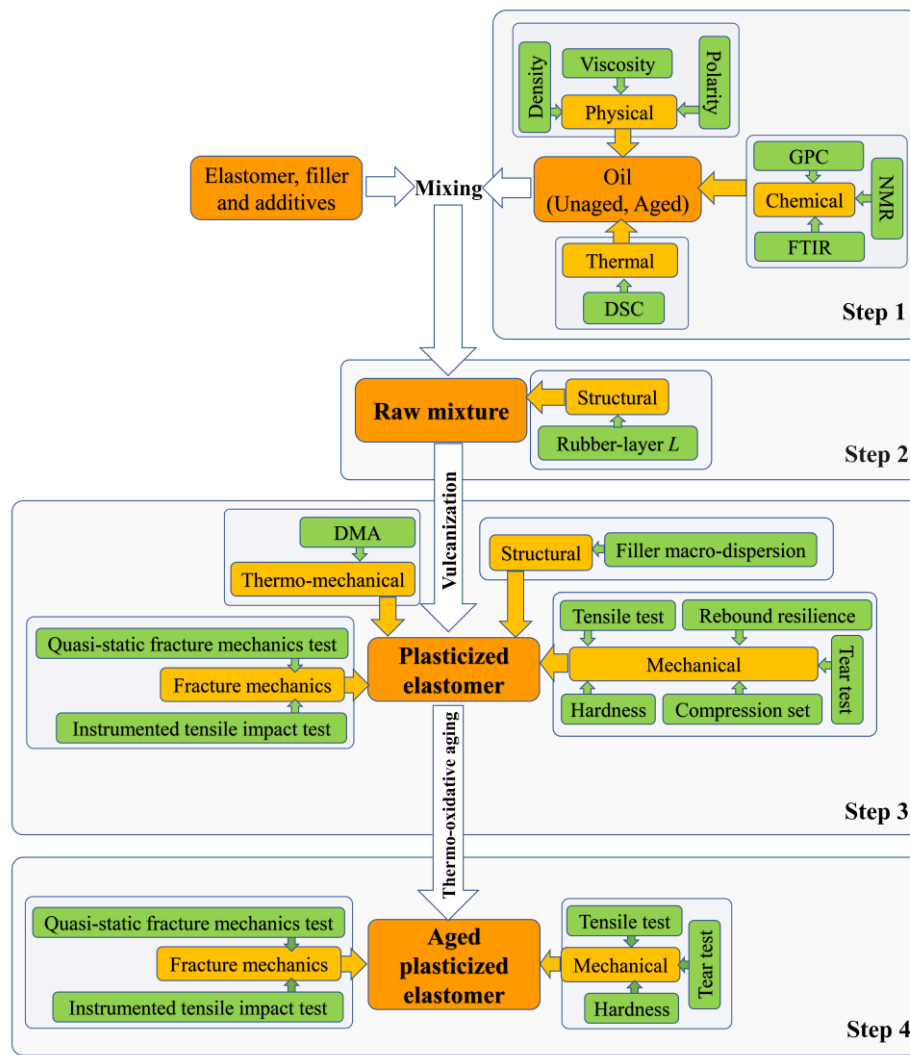


Figure 4: A complete diagram of the investigation with different steps was applied in this thesis

The related work on modified bio-oils and mechanical behaviors of polymers was published in the journal "Materials" titled "Influence of Bio-Based Plasticizers on the Properties of NBR Materials" in 2020 [3]. Some important behavior regarding mechanical, thermal, and physical of plasticized NBR were investigated in this publication. Two different modified bio-oils; epoxidized ester of canola oil (EECO) and epoxidized ester of soybean oil (EESO) were used. For the comparison a synthetic oil Mesamoll<sup>®</sup> and treated distillate aromatic extracts (TDAE). The curing behavior was investigated to notice how the bio-oils can be influence the cure kinetics and crosslinking behavior. This investigation claims that the mechanical behavior of NBR materials can be highly influenced by the type and concentration of bio-oils. Tensile, tear, hardness and compression set behavior were in concern about the mechanical behavior. Thermo-mechanical behavior was searched using DMA. Thermal behavior and structural behavior were investigated by TGA and polarized microscopy respectively. Finally, the thermo-oxidative aging was checked to see the influence of mechanical behavior of plasticized NBR materials. It was claimed that bio-oils can advantageously use as plasticizers instead of conventional oils. Positive aspects of the use of bio-oils were observed or at least a comparable level of properties as for the use of mineral oil-based plasticizers regarding characterization of the kinetics of crosslinking reactions. Based on the results shown in this article, mechanical behaviors were improved or comparable of NBR materials when it was mixed with bio-oils instead of mineral or synthetic oils.

Another part of the work on the investigation of crack resistance behavior was published as a chapter in the book named "Fatigue Crack Growth in Rubber Materials" by G. Heinrich et al [5]. The chapter title was "Influence of Plasticizers Basing on Renewable Sources on the Deformation and Fracture Behaviour of Elastomers" in 2021. The plasticized SBR and NBR were investigated where they were mixed and vulcanized with six different bio-oils in different proportion. All samples were filled with carbon black filler and vulcanized with a common recipe that was used in these investigations. Bio-oils were mainly the modified rapeseed oils, and canola oils. The mineral oil as TDAE was used to compare the results. Different mechanical investigations were done and parallelly characterized the fracture resistance behavior of plasticized rubber materials. The unplasticized rubber vulcanizates also was in the list of comparison. The aim of this investigation was to find alternatives for mineral oil-based plasticizers which are used many technical applications. A certain potential of renewable bio-oils as alternatives for traditional mineral oil-based was seen in this article. This investigation has proven that compared to the reference oil some specific bio-oils have shown their mixes increases the materials resistance against crack initiation and propagation. This article claims that the polarity between polymer and plasticizer dominates the efficiency of a bio-oil in the vulcanizates, the degree of migration during vulcanization, the molecular structure of the bio-oils, and probably the internal oil migration in the area of the fracture process zone during crack propagation leading to changed conditions at the molecular scale.

The title "Synthetical modification of plant oil-based plasticizer with CO<sub>2</sub> leads to reduced migration from NBR rubber" was published in the "Applied polymer science" journal in 2021 and contributed to my work as a second author [6]. The motive of this article was to reduce the oil migration of plasticized NBR vulcanizates and parallelly enhance the mechanical behavior. The epoxidized monoester of glycerol formal from soybean oil was used as bio-oil-1 and it was modified in the lab of Hochschule Merseburg by Mr. Irfan Shehzad. The modified oil was changed the epoxidized functional group into carbonated group as bio-oil-2. This article claims that the carbonated group contained bio-oil reduced the oil migration but the mechanical behavior of plasticized NBR was almost unchanged or a minor difference was observed.

The next chapter is “Fundamentals of technical use of plasticized elastomers.” Basic information about elastomers, especially polar and non-polar elastomers, will be discussed in this chapter, and this can help with detailed information about their property when mixed with oils, fillers, and additives. The theoretical background for different aspects of this chapter will be applied to the investigation of this thesis. The importance of vulcanization parameters is also discussed in this chapter because they can make a big difference in vulcanized elastomer behavior. The discussion on oils briefly this chapter to know their general structure and the parameters which can possibly influence the behavior of elastomers when oil is introduced during elastomer mixing. The type and content of fillers highly influence mechanical and fracture resistance behavior, and a fundamental discussion will be done here to know how they can influence their presence in elastomers. Different investigations on plasticized elastomers were a big step to getting motivation and continuing the study based on some theoretical background. However, the fracture resistance behavior study was insufficient to get complete information. It has some shortcomings in comparing the evaluation for this thesis and highly depends on different testing theories, parameters, and individual characteristics of elastomers, oils, fillers, and additives.

Filler-rubber interaction was a critical issue in influencing the elastomer behavior, and oil penetration can change their property, and it is a big issue to characterize the interactions while different types and content of oil were mixed. The application of different load and stress modes can influence the fracture resistance behavior of elastomers. They were introduced in this chapter, so it will be easy to understand the crack resistance behavior of elastomers and the theory behind them. Different types of aging can generally change the behavior of elastomers, which was applied in this thesis. The theory behind the property changes with some old studies was introduced in this chapter, which can help to know what kind of possible property change was responsible for aging time and temperature. This chapter discussed the theoretical background of plasticizer functions and their activities when mixed with elastomers based on the different theories and rules which were well established.

## 2 Fundamentals of technical use of plasticized elastomers

### 2.1 Fundamentals of elastomers

#### 2.1.1 Properties of polar and non-polar elastomers

An elastomer is considered polar if its charge can be measured as positive or negative. Acrylonitrile-butadiene rubber (NBR) is a complex family of unsaturated statistical polar copolymers of acrylonitrile and butadiene, which are synthesized by an emulsion polymerization system. Butadiene and acrylonitrile are the monomers with the water, emulsifier/soap, radical generating activator, and other ingredients that are introduced into the polymerization vessels. The polymerization reaction is carried out in solution, emulsion, suspension, and bulk [7]. The growing acrylonitrile polymer chain is head-to-tail, and the other carbon atoms are compact and highly polar nitrile units. It is widely used in the fiber industry. It is hard, stiff, thermally stable, and resistant to most organic solvents because of strong interactions between nitrile groups [8]. It is utterly inert against powerful solvents like chloroform. Commercially, polyacrylonitrile is a significant polymeric material [9]. The NBR is yellow as raw materials, although it can be orange or tinted red according to the monomer ratio. The acrylonitrile content positively influences the physical property. Nevertheless, polarity, the cure rate with sulfur, air/gas impermeability, tensile strength, abrasion resistance, and heat aging tear resistance of NBR are influenced by the presence of acrylonitrile in the polymer chain. Although, the cure rate with a peroxide system, compression set, resilience, hysteresis, and low-temperature flexibility decreases [10].

Table 1 shows the classification of well-known NBR with different acrylonitrile content, their Mooney viscosity, and specific gravities [11]. The essential factor in NBR properties is the acrylonitrile groups' ratio to butadiene groups in the polymer backbone, and it influences the resistance against oil and polarity of NBR materials.

Table 1: Classification of NBR [11]

Classification	Acrylonitrile content %	Mooney viscosity $M_{1+4}$ (100 °C)	Specific gravity
Low nitrile	15-20	43-63	0.94
Medium nitrile	26-29	56-75	0.96
Medium-high nitrile	32-36	32-85	0.97-0.98
High nitrile	37-43	45-85	0.98-1.00
Ultra-high nitrile	$\geq 48$	45	1.01

In this thesis, the NBR with medium-high nitrile and high nitrile was chosen to see the variation in the impact of polarity with oils. The property of NBR changes with changing acrylonitrile content. The lower the acrylonitrile content, the lower the  $T_g$ , and the higher the acrylonitrile content, the better the polymer's resistance to non-polar solvents, fats, oils, and motor fuel. Most applications requiring both solvent resistance and low-temperature flexibility require an acrylonitrile content of 33 % and commercially most often produced rubbers with 18 to 51 % [12]. The extensive use of NBR in various application areas requires oil, fuel, and chemical resistance. The vast application of NBR in the automotive space is used in fuel and oil handling hose, seals, and water handling applications in the temperature range of approximately -40 °C to 125 °C [13]. Polyacrylonitrile is

synthesized by the monomer acrylonitrile (see Figure 5). Polyacrylonitrile is synthesized by a reaction of an acrylonitrile monomer with a free radical or anionic initiator.

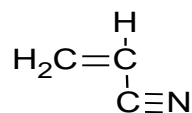


Figure 5: Chemical structure of acrylonitrile

Inside the NBR polymer backbone chain, the butadiene monomer (see Figure 6) could be possible in three different structures.

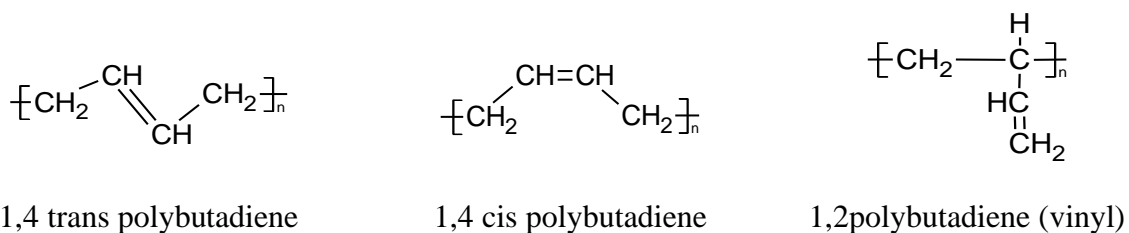


Figure 6: Chemical structure of different isomers of butadiene in NBR

The physical property of NBR largely depends on the percentage of acrylonitrile content in the NBR chain. The chemical structure of NBR is shown in Figure 7.

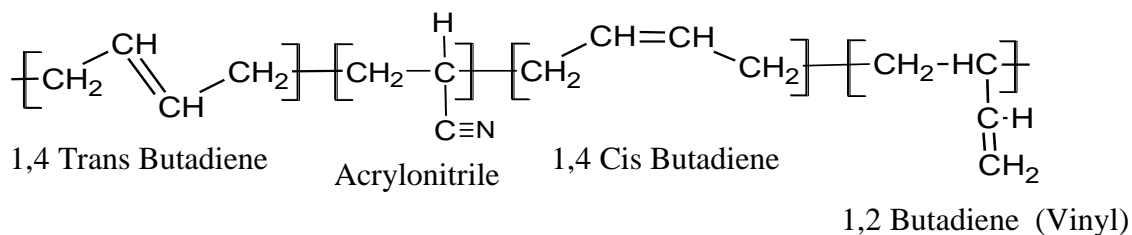


Figure 7: Chemical structure of NBR [12]

The amount of acrylonitrile positively contributes to individual properties and the solvent or oil resistance and acts as a gas barrier [14]. The carbon atom contains double bonds that are easily attacked because of electron shifts and form radicals, which initiate the thermal oxidation and crosslinking reactions, defined as thermo-oxidative aging [15]. Due to crosslinking the unsaturated double bonds in the butadiene units, the NBR gradually becomes hard and brittle; finally, cracks often occur during the thermal oxidation process because of predominant oxidation crosslinking reactions [14].

The nitrile groups ( $-\text{C}\equiv\text{N}$ ) of polyacrylonitrile might be a suitable binder because nitrile groups are strong polar due to the electronegative nitrogen (see Figure 8). Here, nitrile groups can also form strong interactions with their environments through hydrogen bonding and dipole-dipole interactions [8]. The number of acrylonitrile monomer units and the curing agents (Sulfur), fillers, and other additives affect the thermal stability of NBR compounds [16].

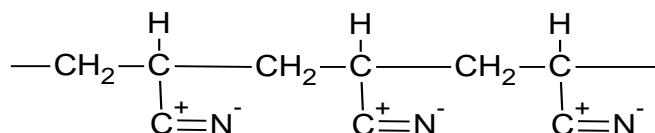


Figure 8: Ionic structure of acrylonitrile [17]

The polar nitrile group significantly influences the electrical, mechanical, thermal, and barrier properties of polyacrylonitrile. Carbon black-filled NBR makes it harder and reduces its flexibility because of the reinforcement of carbon black filler. So, a plasticizer is needed to regain flexibility. The chemical structure correlated with its polarity, so researchers looked for suitable bio-oil as NBR's plasticizer. In a general sense, the oil should be polar to get good compatibility between NBR and oil. However, there are many criteria that were dependent for oil to act as a plasticizer in the NBR matrix to enhance the resistance against crack and other mechanical behavior, which was focused on in this thesis.

Compound to NBR, there are many examples of non-polar polymers such as polypropylene, PTFE, polyethylene, butadiene, and polystyrene. Styrene-butadiene rubber (SBR) is an essential type of synthetic rubber that has a non-polar chemical nature. The manufacturing method of SBR copolymer was developed industrially for the first time by German chemists in the 1930s [18]. SBR is a highly random copolymer of non-polar butadiene and non-polar styrene, as shown in Figure 9. The content of styrene may vary from 10 to 25 %, and the properties of SBR are influenced by the presence of styrene monomer in the SBR chain. Figure 10 shows the chemical structure of SBR, where three different isomers of butadiene can be possible in the polymer chain with styrene [19,20]. SBR has become the most crucial synthetic rubber, representing about one-half of the total world production [21]. There is a vast application of SBR in the vehicle, industrial, and household applications. There is a leading application of SBR in manufacturing car tires, shoe soles, heels, drive couplings, automotive parts, and mechanical rubber goods.

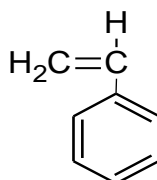


Figure 9: Chemical structure of styrene monomer [19]

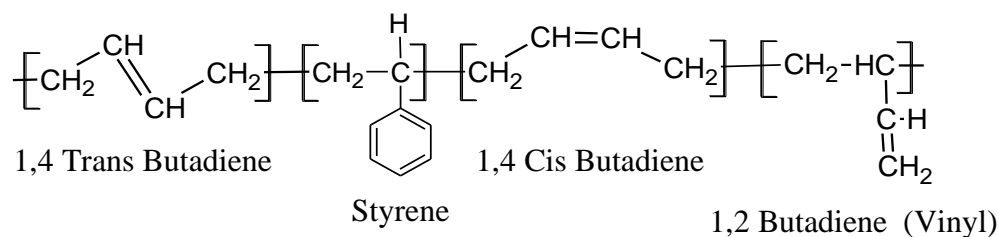


Figure 10: Chemical structure of styrene-butadiene rubber (SBR) [20]

SBR is soft and unstable without carbon black, but it is durable and abrasion-resistant when reinforced by carbon black. The styrene/butadiene ratio influences the properties of SBR. With high styrene content, the rubbers are more rigid and less rubbery [18]. The plasticizer could be the solution to rigid SBR, although commercially, TDAE is added to the SBR matrix to make it rubbery and flexible. However, researchers are trying to find an alternative to TDAE, and bio-oil was the alternative proposal. Several steps needed characterization to select the appropriate oil for the SBR matrix. So, the bio-oil was modified and characterized to make it appropriate for SBR. In principle, the non-polar SBR needed non-polar bio-oils, so polarity investigation is one of the essential tasks for finding more compatible oil as a plasticizer for SBR materials. There are typical applications of flexible plasticized SBR, including shoe soles, hoses, sponge and foam products, waterproof materials, drive couplings, haul-off pads, conveyor belts, toys, heels, adhesives, roll

coverings, and various other molded rubber goods. The typical working temperature range is -25 °C to +100 °C for static sealing [18].

### 2.1.2 Function of filler and additives

Fillers are used in various systems such as organic, biological, biomimetic, and natural polymeric materials [22]. The fillers are intentionally added to the polymer systems and rubber for manufactured products. Fillers are spherical particles of geometrically indeterminate shape, they are unoriented and isotropic that incorporated into elastomer during compounding or formulation. There are two types of filler that are defined according to their activity. The reinforcing fillers are usually called functional fillers, carbon black, precipitated silica, carbon nanotube, and partly OMMT is the typical example of functional/reinforcing fillers. Functional/reinforcing filler help to a good interaction between polymer and filler, influencing viscoelastic behavior and increasing mechanical properties.

For commercial formulation, reinforcing fillers' demand is higher due to extra economical, mechanical advantages than the nonreinforcing fillers. Carbon black and silica are the well-known used active and reinforcing fillers in the rubber industry, and these fillers have a good interaction with plasticizers [23] when compounded with elastomers. Carbon black influenced the strength and toughness of elastomers, improving the rubber's resistance to tearing, abrasion, flex fatigue, and increased traction and durability [24]. The silica fillers have weaker rubber-filler interaction and are extensively used where a high degree of reinforcement is not essential [25]. However, using a coupling group, e.g., silane with silica, enhances the activity of silica.

Carbon black is a necessary ingredient of most rubber compounding and considerably influences the final product's performance. There are no chemical reactions that happen with carbon black and plasticizers, and physical attractions are only identified. It is a universal reinforcing filler and light stabilizer [26]. The filler reinforced elastomers are presently utilized in vast application areas, such as wires, seals, cables, and automobiles.

The elastomer lacks sufficient physical strength, making it unsuitable for various applications in different environments. Vulcanizates' required properties have to be filled up with reinforcement fillers. It is the reason behind the use of fillers, such as carbon and silica. The addition filler with virgin elastomer forms the elastomer composites, improving mechanical behaviors [27,28]. The elastomer is (very low  $T_g$ ) sticky and very soft in moderately high temperatures. Elastomers without filler, the plasticizers are not stable and have the possibility of high leaching. So, the filler is a critical compound that is not made only to enhance the mechanical properties of elastomers, for homogenized dispersion plasticizers helped it. High-performance composite materials are widely used as reinforcing carbon black agents, despite carbon black being the most commonly used and the oldest active filler in rubber compounds and a massive amount of research on carbon black [29,30].

The outstanding role of carbon black was discovered at the beginning of the twentieth century [31]. Carbon black is 95% amorphous carbon, its particle size varies from 5 to 500 nm, and the main component of carbon black particles is divided into three categories, primary particles, aggregates, and agglomerates [27]. The aggregates again form loose agglomerates linked by Van der Waals interactions [32]. The carbon black surface contains the reactive groups, including acid, phenolic, quinonic, carboxyl, ketone, pyrone, and lactone groups, as shown in Figure 11 [24,33]. These reacting groups may have hydrogen bonds on Van der Waals interactions with plasticizers and elastomers.



Carbon black is a well-known filler used in this thesis, and it was previously proved that it enhances elastomer's mechanical performances. It is very important to carbon black dispersion uniformly is a basic prerequisite to achieving optimum properties after vulcanization. Many works [4,34,35] have been done to investigate the filler dispersion and different mechanical properties of filled elastomer vulcanizates. The investigation of thermogravimetric analysis of rubber-filler gel [36] is one of the well-known methods to know the activity of carbon black.

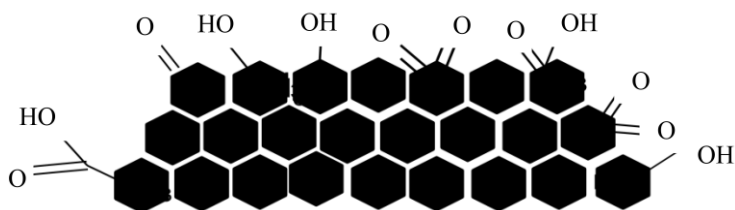


Figure 11: Surface chemistry of carbon black filler, reproduced with permission from ref [33]

The raw mixture of the elastomer compounds was investigated regarding the wetting behavior of carbon black by rubber molecules [36]. When rubber is mixed with carbon black, a part of the rubber chains bonded to the active group already on the carbon black surfaces, as shown in Figure 11, these bound-rubber cannot be detached from the filler when the raw mixture is extracted in a suitable solvent like toluene. The better rubber-filler interaction correlates to the larger amount of rubber that remains on the carbon black after extraction [37]. The interactions can explain in two ways. Rubber bounding may be caused by adsorption effects where van der Waals forces and chemisorption play the key role, and the rubber bounding formation has been formed by a chemical process. This process is predicted by the reaction of rubber with functional groups present on the filler surface [38]. During mixing, rubber radicals formed by the mechanical-chemical degradation and possibly react with the active sites which newly formed on filler due to changes its structure by friction. Extracting of raw mixtures with toluene solvent, the bound part of the rubber formed a layer on the carbon black surface remains in the rubber-filler gel. Due to agglomerate structure of carbon black, the rubber chains were not only bounded on the carbon black surfaces but infiltrate into the void and pores of the agglomerates and it is kinetic process so mixing time is factor here. A study [4] on the rubber-filler interactions claimed that a larger amount of rubber can be remains after 10 min of mixing time. The investigation of rubber-filler interactions can be done on different concepts especially bound-rubber and wetting concept [4]. The bound-rubber concept is used to determine the investigation of rubber-filler interactions in filled rubber systems, and it is defined as the structure formed by the attachment of rubber chains to the carbon black. Previous studies [39–41] on bound-rubber systems investigated the factors which were affected the bound-rubber formation. A high extraction temperature decreases the bound-rubber [42], whereas mixing time and high filler content rubber bounding increases [43]. In contrast, the wetting concept is briefly used to detect the filler localization and rubber-filler interactions. The wetting concept is an acceptable method according to the bounded rubber principle. The calculation of the wetting concept is different from the bound-rubber concept. As a part of the wetting concept, rubber-layer  $L$  is calculated, and it provides the physical and chemical interaction information about the bounded rubber layer on the filler surfaces. Rubber-layer formation continues until rubber infiltrates the filler entirely [44].

The organic chemical accelerators were not used until 1906, when the effect of aniline on sulfur vulcanization was discovered by Oenslager [45]. Typically benzothiazole or sulfonamide accelerators are used, where ZnO is an activator, and fatty acid is the co-activator [24]. The thiazole sulfonamide accelerator was used in 1937 as the fastest curing vulcanization system [46]. The accelerator is used to make a complex form with the activator and increase the activator's

efficiency. The entire crosslinking reaction process is complete by some complicated steps. Generally, the most commonly used activator is a metal oxide, such as magnesium oxide (MgO), lead oxide (PbO), and zinc oxide (ZnO). Practically ZnO was used in this thesis, and according to previous study [47] there is no change in the  $T_g$  after the ZnO incorporation. This indicates that ZnO will not affect the  $T_g$  of elastomer. ZnO is one of the rubber compounds' significant ingredients. It was chosen as activator for selected elastomers like SBR, NR, BR, NBR, which influenced the elastomer's physical, chemical, and mechanical properties.

The processing aids are the physical plasticizer used to modify compounded rubber's physical properties or the finished vulcanizate [48] and it must be compatible with elastomer. The saturated higher fatty acid is usually used as a processing aid. Stearic acid is the most common processing aid due to its 100 % saturation, with no possibility of reacting with oxygen or ozone. According to renewable sources, rice bran oil can be used as a processing aid with a polymer like NBR, SBR, and polychloroprene [48,49].

### 2.1.3 Crosslinking

One of the most important compounds of a rubber mixture is the crosslinking system. Non-crosslinked rubbers are generally not very strong, do not maintain their shape after a large deformation, and can be very sticky [24]. Even plasticizers in uncured elastomers cannot make them stable. Crosslinking is defined as converting a thermoplastic material or elastomer into a thermoset or vulcanizate [50]. It is the formation of chemical links between molecular chains to form a three-dimensional network of connected molecules [51]. The link can be an ionic bond or a covalent bond. The crosslinked molecular chains can be natural or synthetic macromolecules. The crosslinking process may occur via different reaction mechanisms, depending on the chemicals/fillers [24]. The well-known crosslinking agents for the elastomer are sulfur and peroxides. Peroxide is a crosslinking agent specially for saturated and unsaturated polymer chains.

The sulfur is usually used to crosslink unsaturated polymers like NR, SBR, NBR, and BR. Naturally, the sulfurs can be found as allotropes sulfur. The allotropes sulfur (see Figure 12) is ordinarily inert, but the cyclic sulfur homolytic or heterolytic cleavage at high temperatures (160 °C-180 °C). Cleavage's bond-breaking energy is around 429 kJ / mol [52].

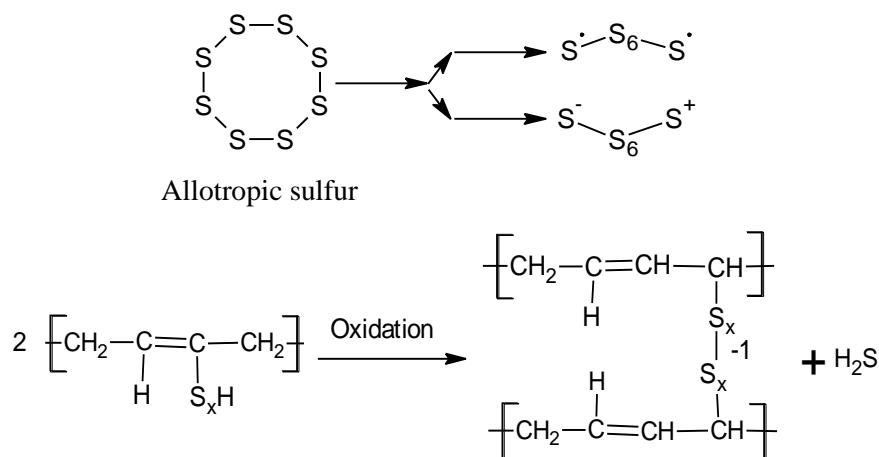


Figure 12: Scheme of sulfur crosslinking [53]

Here  $S_x$  mentioned the number of sulfurs. “x” is denoted as the number of elemental sulfurs. The name of elemental sulfur was numbered as 1, 2, 3, x accordingly mono, di, tri, and poly sulfidic, respectively.

The sulfur can be attached to carbons and links between carbon and sulfur [54]. There are some general criteria for the vulcanization of sulfur with polymer chains. It is not easy for sulfur to react with the rubber because sulfur's activation is tricky to break the C-H bond, and the required energy is around 337.2 KJ/mol [52]. If sulfur is active itself, it takes a long time to cure. The process takes approximately 6 hours at 140 °C for completion, which is uneconomical by any production standards; this is the reason behind using an activator and accelerator.

### 2.1.4 Filler-rubber interactions

For a filled elastomer, the reinforcement properties are the meaning of filler and elastomer interaction. The chemical and physical properties of the filler and rubber are responsible for interaction with them both. The rubber-rubber interactions are not the significance of the interaction between filler-rubber and filler-filler interaction. Filler-rubber interactions describe the filler's compatibility with the rubber, and filler-filler interactions are represented by the attraction of filler and the ability to form a network. The occlusion of rubbers is an essential effect of filler-rubber interactions. When the rubbers are trapped between or inside aggregates, it is a so-called occluded rubber.

The filler-filler interactions are recognized as the primary interactions in reinforcement, especially for the high filler content. The chemical interaction between the filler particle surface influences the interactions. It could be physical interactions, e.g., van der Waals forces or hydrogen bonding, fillers' morphology, and volume fractions. One of the significant factors is the surface energy of fillers, which profoundly influences fillers' compatibility with rubber. The filler's surface area means it has more sites available to interact with the rubber or the other filler particles.

Wang [55–58] broadly discusses filler-rubber interactions. Figure 13 shows the schematic figure of relation between filler and rubber after mixing. Where Figure 13 (a) is describes about how it looks like when rubber shell covered a carbon black particle. Rubber shell surrounded to carbon black aggregates were represented in Figure 13 (b). The filler aggregates trap elastomers are called occluded rubber as shown in Figure 13 (c) and (d) shows how rubber get trapped in bunch of filler agglomerates.

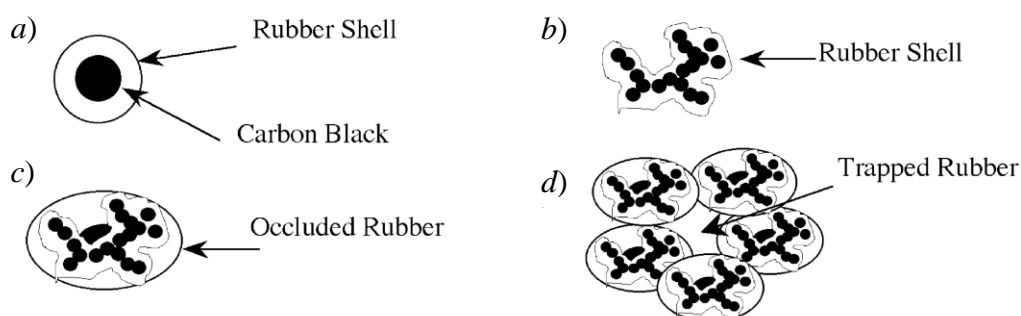


Figure 13: Models of rubber excluded from the rubber matrix, photo reproduced with permission from ref [33]

The incorporation of filler into rubber matrix can be explained by several models [33]. Figure 14 shows the model where interactions between rubber-filler describes in an easy way to understand. The rubber chains are attracted either physically or chemically to form a rubber shell on the carbon

black particle's surface. The carbon black particles are much stiffer than the rubber molecules further away if attached to the closest. The rubber shell, which is shown for the individual particle, is seen throughout the filler aggregate. As in this case, the rubber chains closest to the aggregate are the stiffest. In this shell model, bridging of bound-rubber in the aggregate leads to a higher rubber-layer  $L$ , which is defined as the mass fraction of rubber retained in the extracted compound. Rubber collects around the aggregate and the rubber shell to form an outer layer of occluded rubber. This layer is not as tightly bound to the filler aggregate but decreases mobility near the aggregate surface. Rubber is trapped between aggregates, which have formed an agglomerate. This rubber experiences slight stiffness, increases, and becomes free once the aggregate structure breaks apart during deformation [59].

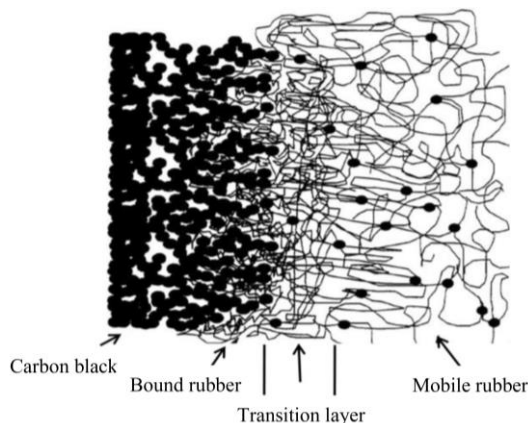


Figure 14: Sketch of the entangled bound rubber-mobile rubber model, photo reproduced with permission from ref [60]

The interaction between carbon black and rubber can be mechanical, physical, chemical, or a combination of these forms of interaction [31]. When the rubber seals are prepared, there are two possibilities to spoil when in contact with oil; firstly, the oil can extract the oil-soluble additives from the seals and expose the seal rubber to subsequent thermal oxidation with little or no protection. Secondly, the chemical that contains the additives or oils can cause elastomer degradation [14,61].

The reinforcement of elastomer by fillers is restricted to the rubbery state of the elastomer. Little or no reinforcement is observed in the glassy state below  $T_g$  [31]. NBR vulcanizates, filled with reinforcement fillers (carbon black), have higher abrasion resistance than equivalent materials from NR and SBR [62]. Filler dispersion occurs when carbon black pellets are broken up under shear forces into individual aggregates/agglomerates and distributed throughout the rubber matrix [63]. The filler in the mixing process acts as the reinforcing between the rubber matrix and the filler. The precondition for a reinforcing effect is dominated by the particle size of the filler, and particle size should be smaller than 100 nm [64]. Increasing the filler content makes the network chains shorter, and the number of entanglements between two crosslinks decreases [60]. Carbon black not only improves the strength of the rubber but also influences the curing characteristics. It also decreases the vulcanization induction time because it acts as a catalyst for the initiation of vulcanization and decreases the cure rate as several surface acid groups on the carbon black increase [24].

The reinforcing potential is attributed to two effects [65], forming a physically bonded flexible filler network and strong rubber-filler coupling. Both effects refer to very high surface activity and specific surface of the filler particles. The level of reinforcement depends on the following criteria [62]; content of particles, the filler's contact surface, activity on the filler surface, and the filler

structure. Plasticizers have solubilized the rubber and assisted in the Brownian motion of the polymer chains, thus reducing the compound's viscosity [66].

The filler, rubber, and other additives are mixed physically where Van der Waals interactions, dipole-dipole interactions, and hydrogen bonds are present in the materials. When elastomers trap the fillers, it is called the bound elastomer [33]. The elastomer and carbon black come together during smashing by rotation, try to overlap each other, make the transition layer, and finally, the bound-rubber.

## 2.2 Fundamentals of plasticizers

### 2.2.1 Plasticizers

A plasticizer is a liquid or semi-liquid compound that can be mixed into a polymer mixture to increase the elasticity and the flexibility of the vulcanizate and get better filler dispersion. The plasticizer can highly influence some essential parameters and helps in controlling the hardness, glass transition temperature and viscosity level [49,67]. It is one of the most crucial mixture components after fillers to produce rubber compounds. Plasticizer improves, in particular low-temperature performance flexibility and elasticity of the vulcanizate. They are mainly mineral oils, synthetic liquids, or esterified with alcohols having branched chains. Ester-based tri ethylene glycol and tetraethylene glycol or glycol ethers of adipic and sebacic acid and thioethers are used as low-temperature plasticizers in polymers. The characteristics of a plasticizer during the compounding of rubbers are given some different properties. It improves processability by using high filler content. A plasticizer is necessary to set processability due to the high viscosity and improvement of filler distribution. A plasticizer must meet the conditions, e.g., it should be non-toxic, should have specific compatibility to the polymer, aging and oxidation resistance, no discoloration of the mixture, no interaction with the crosslinking system, and nonvolatile during vulcanization. The frequent use of plasticizers includes mineral oils, synthetic esters, and a few natural products such as wood resin, animal glue, and vegetable oils (bio-oils) are used [49,68]. Figure 15 shows the schematic model of plasticization of a polymer which represents the low molecular weight plasticizer molecules in physical presence in the polymer chains. Plasticizer molecules increase the distance between the chains. Although a high intermolecular force between polymer-polymer, e.g., Crosslinking, strong hydrogen bonds, or crystallinity help to limit the distance between chains. In the case of polymer-plasticizer interactions are stronger than the intermolecular forces, the relaxation of the polymer chains or the dissolution of the polymer can take place [69].

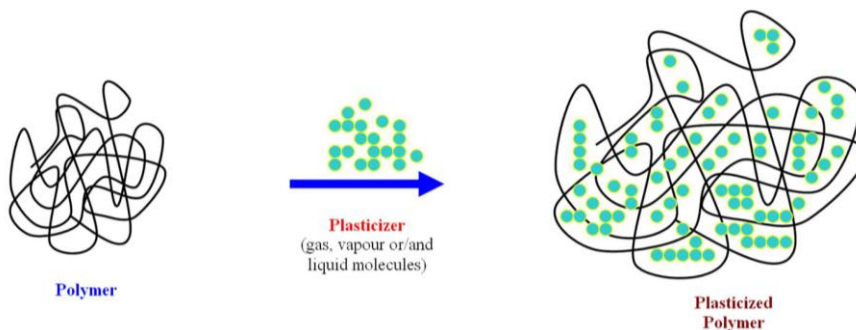


Figure 15: A schematic model of plasticization, photo reproduced with permission from ref [70]

A previous study [71] on bio-oil-based plasticizers proves that oil mixes in the elastomer matrix can be influences the elastomer bonding. Although another article [72] stated that increasing plasticizer loading gradually reduces the bounding rubber contents of the compounds, but the types

of plasticizers insignificantly influence the bound-rubber content. However, there is no previous research on the bio-oil-enriched rubbers, so this thesis could be unique in finding the bound-rubber fraction of elastomers.

## 2.2.2 Working principle of plasticizer on elastomers

The research on the working principle of plasticization started in the twentieth century and led to several theories. The most reliable theories are classical theories and free-volume theories. In classical approaches, the lubricity theory, the gel theory, and the viscosity theory were developed during the 1940s. In the 1950s, some other models were proposed.

Schematic representation of the theories was shown in Figure 16, where green balls represented the plasticizers, blue balls, and lines were polymers, and blue dots were weak secondary bonding forces.

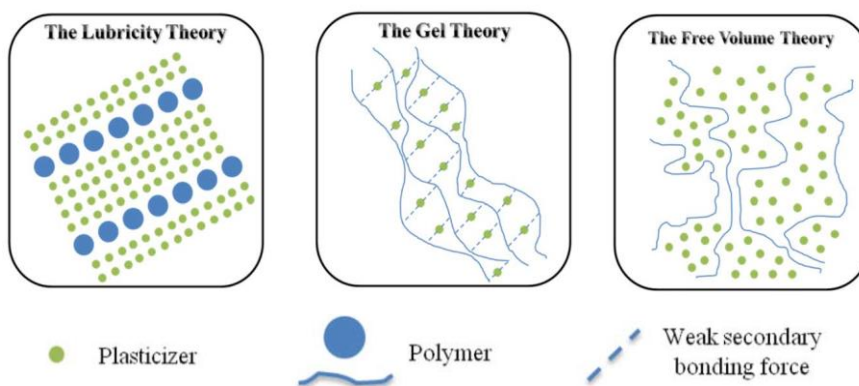


Figure 16: Plasticization theories, reproduced with permission from ref [73]

The lubricity theory is attributed to Kirkpatrick [74], Clark [75], and Houwink [76]. According to that theory, the function of a plasticizer is to reduce intermolecular friction between the polymer molecules. When the polymer molecules are mixed and compressed randomly, then they have to slip over each other. The plasticizer acts as a lubricant, allows for the movement of the molecules, and reduces their internal resistance to sliding. In general, two possibilities of gliding were postulated that could explain the softening mechanism of plasticizers, as shown in Figure 17 [76]. Figure 17 (a) shows the gliding planes are in the bulk of the plasticizers. The plasticizer molecules will preferentially stick to the macromolecules, making it probable that, on deformation, the plasticizer molecules will glide over each other, and the planes of the slip are inside the solvent. In Figure 17 (b), they are at the surface of the polymer.

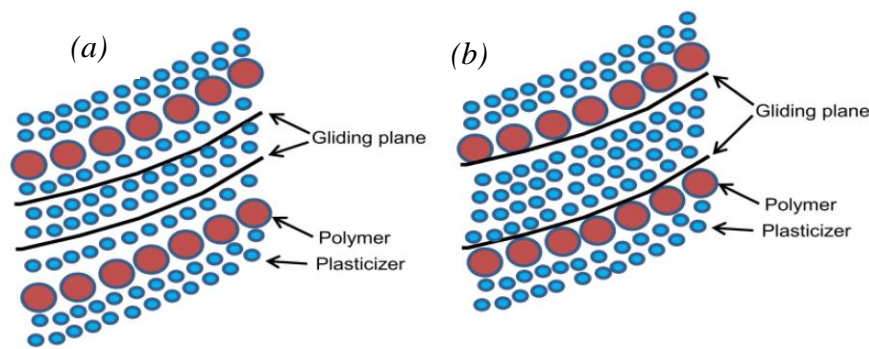


Figure 17: Model of gliding possibilities in a polymer-plasticizer system, reproduced with permission from ref [76]

Houwink [76] realized that either dissolving or swelling occurs first during the plasticization. However, Gidvani [77] was criticized the lubricity theory, and he said that the swelling of polymer is not always involved by the plasticization because the polymer could be plasticized by the lubrication effect of the plasticizers. There are some important evaluations that support the lubricity theories. The vapor pressure of plasticizers in polymers was measured by Verhoek [78] and found that the solvent retention was reduced by plasticizers, and this supports the lubricity theory. Krikpatrick [74] measured the retentivity and permeability of cellulose acetate plasticized with various sulfonamides, phthalates, and phosphates, and he realized that these properties are dependent on the attractive forces between plasticizer and polymer. Swelling of acrylonitrile-butadiene copolymers with different percentages of acrylonitrile content was measured by Houwink [77], and he proved the importance of polarity of the plasticizer and polymer.

The idea of gel theory was proposed by Aiken [79]. He worked on plasticized PVC materials for tensile creep investigation and tried to find some correlations between plasticizer effectiveness, softening compatibility, and molecular structure. It was found that the polar groups in the plasticizer and polymer could be organized in a manner to form solvating dipoles on the PVC chains. In contrast, the nonpolar tails remain incompatible with PVC. They formed in tiny cluster, leaving many unshielded polar polymer chains, forming influential polymer-polymer contacts. This forms a gel structure responsible for viscous flow and the micro-Brownian motion responsible for the plasticizer around the polymer chains. A study [79] on gel theory proved that the plasticizer containing long aliphatic chains are more potent than plasticizers containing bulky cyclic groups, especially at low temperatures and short time investigations. Although, at high temperatures and long times, they were more potent in softening than the linear type of plasticizer. The micro-Brownian motion of plasticized polymers chain segments enhanced the elasticity, and generally, the segmental motion was not enough to explain the flexibility of plasticized polymers. Aiken proposed two possibilities for the presence of a three-dimensional gel network structure of great endurance. Static mechanism describes that the polymer-plasticizer combinations have an average lifetime compared to segmental motions time scale. Another possibility was a dynamic equilibrium in the solvation and desolvation processes. This means the plasticizer diffuses through the polymer matrix, which opens the polymer-polymer attachments for the time being, then travels and allows the structure to close behind it in various positions. The idea of gel theory on the explanation of plasticization effect was matched to solvation-desolvation process. The experimental results in support of gel theory were shown by Doolittle [80] and later confirmed by Stickney [81] and Alfrey [82]. It is also considered that from gel theory, the polymers as formed by a three-dimensional honeycomb structure maintained by loose attachments between the polymer molecules along their chains. Gel theory states that the rigidity of polymers is dominated by the resistance of three-dimensional structures rather than internal frictions. There is solvation-desolvation and aggregation-disaggregation equilibrium between the polymer and plasticizer molecules [76]. According to gel theory, the plasticizer's function is to reduce the number of these polymer points, letting the polymer be deformed without breaking. Despite lubricating the glide planes, the plasticizers reduce the rigidity of polymers, thereby reducing the aggregation of the polymer molecules [76]. The behavior of plasticized polymers was proclaimed by gel theory, where Doolittle [80] found that the distensibility of plasticized polymers increased with temperature. The distensibility is defined as the capability of being distended or stretched of a rubber under pressure. However, the behavior is the opposite in some cases, especially with nitrocellulose plasticized with succinate, where the distensibility enhances at lower temperatures. When distensibility increases with increasing temperature could be explained by gel theory as polymer molecules are drawn to each other more tightly when the temperature decreases, and the same things happen when plasticizers are used. In this case, less solvation and more aggregation happen. As a result, the

polymer should behave more rigid and less distensible. Contrary, some solvents contained high molecular weight show enhancement in solvent ability on cooling and this can explain opposite behavior noticed. The plasticization of non-solvents can be explained by this theory. The molecules of non-solvents deed by holding apart the polymer molecules and so breaking some unions between active centers on the polymer. The explanation of tear resistance [83] or creep behavior [79] can be possible from the gel theory.

The lubricity and gel theory compiled by Moorshaed [84] which is based on some polar polymers. He analyzed some basic requirements of polymer to be plasticized. Polymer chains should be long enough, so they have strength, while plasticizers insist them apart. The primary bonds of crosslinked polymer chains should have held together, and forces are strong to allow the plasticizer to penetrate into the polymer. Moorshaed also stated that the polar component in plasticizer improves the tensile strength, although the flexibility of polymer enhances while there are points of high cohesion at many points along the chain. Non-polar components in plasticizers served as high flexibility in plasticized compounds. This means the presence of polar and non-polar components is required in a plasticizer if perfect compatibility and flexibility have to be earned.

The free-volume theory was postulated by Fox and Flory [85], but different authors contributed to it, and it is still being used to explain the viscoelastic properties of plasticized polymers, and it was undoubtedly the one giving a precise explanation of plasticization. The theory was attempted to explain the diminution of the glass transition temperature  $T_g$  of a plasticized polymer. The  $T_g$  is detected by a change from a hard, glass-like material to a rubbery solid. Some authors [86,87] previously proved that the specific volume decreases with the temperature until  $T_g$ ; below the  $T_g$ , specific volume decreases at a low rate. For all volume-temperature curves above the  $T_g$ , if they are extrapolated, then intersect each other practically at the same point. The free-volume is a specific volume above the transition temperature minus the solid specific volume extrapolated to the same temperature above the transition temperature. Kanig [86] defined the free-volume  $v_f$  as the difference between the volume measured for the genuine crystal  $v_t$  and the volume observed at absolute zero temperature, glass, or liquid at a given use temperature  $v_0$  (see Equation 1).

$$v_f = v_t - v_0 \quad (1)$$

The free-volume theory was corrected by Kanig [47] and summarized by Sears and Darby [87]. It comes from three primary sources: the chain ends' motion, side chains, and the main chain. The free-volume of a polymer system may be increased by increasing the number of end groups, which means lower molecular weight. Increasing the number or size of side chains means plasticization and this enhances the chance for main chain movement has been controlled by including segments of low steric hindrance and low intermolecular attraction. It represents internal plasticization.

Some models which correlate free-volume fraction to the  $T_g$  for polymers which backs the free-volume theory. Fractional free-volume,  $f$  of plasticizer is defined according to Equation 2, here  $v_p$  is free-volume and  $v_0$  is occupied volume.

$$f = \frac{v_p}{v_0} \quad (2)$$

According to Boyer-Sumha rule [88], free-volume fraction  $f_{exp}$ , of cubic expansion coefficient  $\beta_p$  of plasticizer glass-like polymer  $\beta_G$  will be given in Equation 3.

$$f_{exp} \approx (\beta_p - \beta_G) T_g \quad (3)$$



Williams-Landel-Ferry (WLF) [89] approach predicted a linear dependence of  $f$  on temperature. Here  $\beta_f$  thermal expansion coefficient above and below  $T_g$ ,  $f_g$  is a fractional free volume at  $T_g$  (see Equation 4).

$$f = f_g + \beta_f (T - T_g) \quad (4)$$

According to this free-volume theory, cyclic macromolecules that do not have any end groups provide no free-volume effect and shows high  $T_g$ . The introduction of plasticizer molecules into the polymer mass implies the addition of molecules with  $T_g$  lower than the polymer itself and the small portion of plasticizer molecules that increase the free-volume of the system. According to the free-volume theory, the plasticizer with low  $T_g$  is more efficient for reducing the  $T_g$  of the plasticized polymer. The branched plasticizer influences the free-volume. A more branched plasticizer has a higher free-volume than a linear one. According to the molecular weight of the plasticizer, increasing its molecular size increases the free-volume introduced into the polymer, but on a weight basis, the total free-volume increment could be more significant for small molecular weight plasticizers [76].

Sears and Darby [87] explained plasticization and antiplasticization of plasticized polymer in an easy-to-understand way. The elastomers are amorphous, and it contains low crosslinking, and the chains were not ordered. These amorphous areas have associated with more free-volume since conformational changes are permitted and are more flexible. Plasticizer molecules situate themselves around the polymer chains, preferentially in the amorphous areas. Thus, the plasticizers were very welcoming to amorphous elastomers. The free-volume theory predicts that introducing plasticizer molecules into the polymer involves more free-volume, flexibility, and effortless movement of macromolecules [76].

Antiplasticization terms comes for describing the opposite effect of plasticization and that is mostly happen when a small amount of plasticizers was inserted in the polymers. At a low concentration, the miscibility of the plasticizers confides on interactions with polymer chains along with constituent groups, and it envisaged as being bound to the polymer chains and restricting the rotation of short segments called  $\beta$ -relaxation and it is the reason for the antiplasticization. In contrast, at the high concentrations not all plasticizer content can be compromised as bound molecules towards the polymer chains, so the residual plasticizer starts to put apart into small clusters in a dynamic state of alignment/segregation with the polymer chains and this is the primary period of the cross-over to a plasticization behavior. The dispersed clusters were grown in number with plasticizer concentration until they got interconnected and be the full plasticization and it means there must overcome the optimum level of plasticizer concentration otherwise, it creates the antiplasticization effect. When the concentration of plasticizers increased more than the optimum level then at certain point the high concentration plasticizers leach out from polymer matrix and coagulated on the surfaces. The coagulated formation of plasticizer for elastomer is very common if plasticizer concentration is too much high or immiscible in concern of polarity. The coagulating effect can be observed when the concentration of plasticizer is high in elastomer matrix and this can swell the polymer chains with a high free-volume and resulting a high movement of polymer chains caused the chain breakage, sticky wet elastomer surface, cluster formation on the surface, high migration, and decreases the tear resistance properties. The choice of a plasticizer dependences the elastomer; thus, non-polar plasticizers are generally used for non-polar elastomers, whereas polar elastomers fit to polar plasticizers [66]. The polar property of elastomers influences the selection of plasticizers, and it is controlled by the monomer's properties in the polymer backbone chain.

### 2.2.3 Properties of plasticizers according to their sources

There are three primary sources of plasticizers: non-renewable, renewable, and synthetic plasticizers. Non-renewable plasticizers are based on mineral oils extracted from mine and purified by fractional distillation process. Renewable plasticizers are plant and animal-based oils extracted from plant seeds and animal fat, and milk. While synthetic plasticizers are more complicated chemical synthesis in laboratory. Some common types of plasticizers include phthalates, adipates, sebacates, and citrates.

The common non-renewable source of plasticizers is mineral oils, also called liquid petroleum. It is a colorless, oily, almost tasteless, water-insoluble liquid and light mixtures of higher alkanes from mineral sources and a distillate of petroleum. The solvent separation techniques are used to prepare paraffinic oil from the paraffinic crude oil. Paraffinic oil has excellent thermal and oxidative stability and good high temperature viscosity [90]. It contains much wax and yields a very high viscosity and densities around 0.86 to 0.91 g/cm<sup>3</sup>. Paraffinic oil is white in color, yellowish, or colorless transparent liquid. The paraffinic oils are saturated long-chain hydrocarbons, mainly used as the lubricant inside the polymeric compounds. It is a non-polar organic substance with major components of C<sub>16</sub> to C<sub>20</sub> n-alkanes.

The naphthenic crudes are available and inexpensive [90]. Generally, naphthenic oils are derived from naphthenic crudes. They contain a little wax, and the viscosity is medium compared to paraffinic oil and they are chemically cycloalkanes.

Aromatic oils are generally aromatic hydrocarbons, and the structure contains the aromatic structure. The aromatic extracts are procured from the selected refineries and suitably blended to meet stringent specifications that are harmful to the atmosphere and human health [91]. The aniline point can characterize the content of aromatic compounds in the oil, and this indicates the aromatic ring in oils. The higher the aromatic ring in oils, the higher the aromatic groups, and the lower the aniline point [92]. Nowadays, aromatic process oils are used as a plasticizer in the form of distillate aromatic extracts (DAE) [93]. They are used in the manufacture of oil-extended natural or synthetic rubber. The aromatic oils contain a high level of polycyclic aromatic (PCA) components, which are recognized as the cause of tumors. So the DAE is classified as carcinogenic to humans, according to the European legislation (EU Substance Directive 67/548/EEC), and must label with the risk phrase “R45” [66,91,93–95].

The latest used aromatic extracts are the treated distillate aromatic extracts (TDAE). It is called green rubber oil or nature friendly oil with higher aromatic content, environmental protection, non-toxic, non-carcinogenic characteristics, and is a highly used substitute for existing aromatic oil. These are manufactured from DAE by further severe processing such as either hydrotreating or solvent extraction to meet the PCA threshold of less than 3 wt % DMSO-extract according to IP 346 method to omit the label. According to a test of an International standard IP 346, the PCA content of DAE is 20 wt %, whereas, in TDAE, it is only 1.3 wt % [93].

Currently, researchers are focused on renewable sources for plasticizers. They are called “natural oils” or “bio-oils,” “vegetable oils,” or “modified vegetable oils.” The plant oils are called green plasticizers that are safe and renewable to meet the general requirements of environmental protection and sustainable development [96,97]. Already it was reported that modified vegetable oils could be a suitable replacement for conventional plasticizers like mineral oils or synthetic plasticizers [98]. The renewable source plasticizers are vegetable oils (bio-oils). The common word “oil” is frequently used as the plasticizer for elastomeric compounds. Oil can be defined as a less viscous organic substance. The oil can be distinguished between fatty oil, essential oils, mineral oils, and silicone oils. Fatty oils are the source of bio-oils; they are also called sweet oils [94]. The

petroleum-based oils are used extensively in elastomeric compounds as plasticizers [48]. They are generally called natural oil; chemically, they can be characterized as triglyceride esters of higher fatty acids [99]. Triglycerides are consisting of three fatty acids attached by glycerol. The plant oils are recognized as green plasticizers that are safe and renewable to meet the general requirements of environmental protection and sustainable development [96,97]. Due to renewability, cost-effectiveness, and non-toxicity, plant oils are using in the plastic and rubber industries [100].

Linseed oil is used as multipurpose additive (plasticizer, processing aids) in NBR, which improves the mechanical properties and processability and decreases the vulcanization (cure) time [101]. Soybean oil can be used as the plasticizer in natural rubber (NR) [66,98]. The vegetable oils contain phenolic components like tocopherols, potent antioxidants, and protect the elastomers from oxidation. So, vegetable oils can be potentially multipurpose ingredients in elastomeric compounds [48] and possess excellent frictional properties, such as good lubricity, low volatility, high viscosity index, solvency for lubricant additives, and easy miscibility with other fluids [102]. The physical condition is related to the chemical structure. The saturation structure is one of the relevant terms here. The color of fatty oil varies from tint red to light yellow, and some can be found as transparent, tint yellow, or white.

The oil from plants is triglyceride ester of higher fatty acid, and the instauration influences the state of matter. The liquid oils are unsaturated fatty acid substances, whereas the fats are the saturated fatty acid component. Fatty oils are a combination of fatty acids. The composition of different fatty acids in the plant oil has listed in Table 2, and it shows that mainly the oleic acid and linoleic acid dominate the properties of bio-oils. However, canola and rapeseed oil have a higher proportion of oleic acid, whereas sunflower oil has higher linoleic acid. It means that during modification, these fatty acids dominate the behavior. Soybean oil is natural fatty oil extracted from the soybean seeds, scientific name *Glycine max*. It is a drying oil class, which means it can be crosslinked due to autoxidation. The extensive consumption of this oil is edible oil.

Distribution of fatty acids may vary from different soybeans and processing methods [103]. In the 1970s, canola was produced through traditional plant crossbreeding of the rapeseed plant, which contains glucosinolates and erucic acid. However, erucic acid was removed because it was believed to be inedible or toxic in high doses. The newly developed plant was renamed “canola” - a combination of “Canadian” and “Oil” (or ola) to make this difference apparent. If a seed is labeled “canola,” it has to have less than 30  $\mu$  mol of glucosinolates and not more than 2% of erucic acid. Well-known as cooking oil, canola oil is also known as rapeseed oil. It is expelled from the seed of several varieties of the Brassicaceae family of plants. The species are *Brassica rapa* and *Brassica juncea*.

Bio-oils are composed of long chains of fatty acids that are bound to glycerol molecules through ester bonds. Plant oil (bio-oil) as a plasticizer has needed some modifications to make it more compatible. The main problem with the direct use the natural oil in rubber compounding is unsaturation. The fatty acid-containing natural oil has several double bonds. The double bond can easily be oxidized at high temperatures and air. Bio-oil contains many C=C on the fatty acid chains and can be polymerized through various methods. Previous studies [8,75] had claimed that during the vulcanization of rubbers, the bio-oils could be co-vulcanized to the rubber matrix, and sulfur may be consumed by the oils, and the modification has been done to reduce the unsaturation. The modified bio-oils have been produced for around 30 years and are available under various trade names [104], and it can be prepared by the epoxidation of bio-oils using peroxyacetic acid (peracetic acid) generated in situ in the presence of sulfuric acid as the catalyst [105]. The double bonds contained unsaturated fatty acids are converted into the more active oxirane moiety by

reaction with peroxides [106]. The epoxide group is more involved than the carbon-carbon double bond on the fatty acid chain. The melting point increases after the epoxidation extent [105]. Epoxides are generally stable compounds, and their ring structure confers some degree of protection against oxidation and other form of degradation. So, they do not typically undergo aging in the same way unsaturated compounds. The epoxides can be subject to degradation under some specific conditions such as strong acids or bases can cause of epoxide ring open and leading to the formation of new compounds [104,107].

Table 2: Fatty acid composition of different bio-oils

Fatty acid	Soybean oil ( <i>Glycine max</i> ) [108]	Sunflower oil ( <i>Helianthus annuus</i> ) [109]	Canola oil ( <i>Brassica juncea</i> ) [110]	Rapeseed oil ( <i>Brassica napus</i> ) [111]	Linseed oil ( <i>Linum usitatissimum</i> ) [108]
Palmitic (16:0)	11	0.09	4.9	4.6	5.87
Palmitoleic (16:1)	0.14	6.33	0.18	0.3	0.06
Stearic (18:0)	4.74	3.45	1.82	1.7	4.49
Oleic (18:1)	21.60	21.64	57.5	63.3	22.30
Linoleic (18:2)	52	67.28	25.4	19.6	16.67
$\alpha$ -linolenic (18:3)	7.65	0.09	8.41	1.2	49.85
Arachidic (20:0)	0.25	0.23	0.50	0.6	0.12
Eicosenoic (20:1)	0.19	0.13	1.04	9.1	0.16
Behenic (22:0)	0.36	0.72	0.25	0.4	0.10
Erucic (22:1)	0.11	0.04	0.11	0.3	0.06

Figure 18 (a) shows the chemical reaction during the conversion into epoxidized bio-oils. In the beginning, the triglycerides ester of higher fatty acid (bio-oil) leads to reaction in two ways. It can be reacted with peracetic acid under certain conditions and converted into triglyceride epoxidized ester of higher fatty acid, it is also known as epoxidized bio-oils. In other ways the bio-oil can be modified and converted into monoglyceride epoxidized ester. The bio-oil is first treated with alcohol, such as methanol in the presence of catalysts such as sodium hydroxide or potassium hydroxide. This process is known as transesterification, converts the triglycerides into fatty acid methyl ester (monoglyceride ester) and glycerol. Finally react with peracetic acid and form the monoglyceride epoxidized ester where the (-R) methyl group in the chemical structure can be replaced with isopropyl or butyl groups to change their behavior such as polarity.

A general conversion of double bonds to epoxy groups is nearly 90 % [112] although it can be controlled according to polarity of elastomers and additives. Bio-oils contain unsaturated fatty acids which are nonpolar and oxidant. Therefore the double bonds in the bio-oils have to be converted to stable compounds such as epoxide, methyl, iso-propyl, acrylate, and even some bromoacrylated triglycerides, and monoglycerides that can be develop miscibility with different polymers [104,113,114]. The stability of epoxide can depend on several factors. Epoxides are cyclic ethers with a three-membered ring containing an oxygen atom and two carbon atoms as shown in Figure 18 (b). The high ring strain associated with the small ring size makes the molecule reactive towards nucleophiles, such as acids and bases, which can lead to ring-opening reactions. However, the stability of epoxides can be increased by various factors. For example, the presence

of electron-withdrawing groups on the carbon atoms adjacent to the oxygen atom can stabilize the epoxide ring by reducing the ring strain. Additionally, some epoxides may have steric hindrance around the ring, which can also contribute to their stability. The iodine value of bio-oils plays a helpful role in changing their lubricity. The iodine values were lower when the bio-oils were epoxidized [115]. The decreases in the iodine value of epoxidized bio-oils indicate that almost 98.5% of unsaturation was converted into an oxirane ring, enhancing thermo-oxidative stability.

At room temperature, the viscosity of saturated fatty acid is higher than unsaturated fatty acid viscosity. At room temperature, canola oil's viscosity is  $78.8 \text{ mm}^2/\text{s}$ , whereas soybean oil is  $54.3 \text{ mm}^2/\text{s}$  [116]. The saturated fatty acid contained in soybean oil is 15 %, and in canola oil is 6.3 % (see Table 2). Ordinary bio-oils are slightly polar [92] from the chemical structure in finding active groups or polar part double bonds. As bio-oil is slightly polar, it is a beneficial compatible oil for polar and non-polar elastomers as a plasticizer. Bio-oils have low glass transition temperature  $T_g$ , because of it has a high free-volume and probable branched structures. The bio-oils used in this thesis are partially crystallized but if they have often double bonds, so characterization of  $T_g$  is relevant.

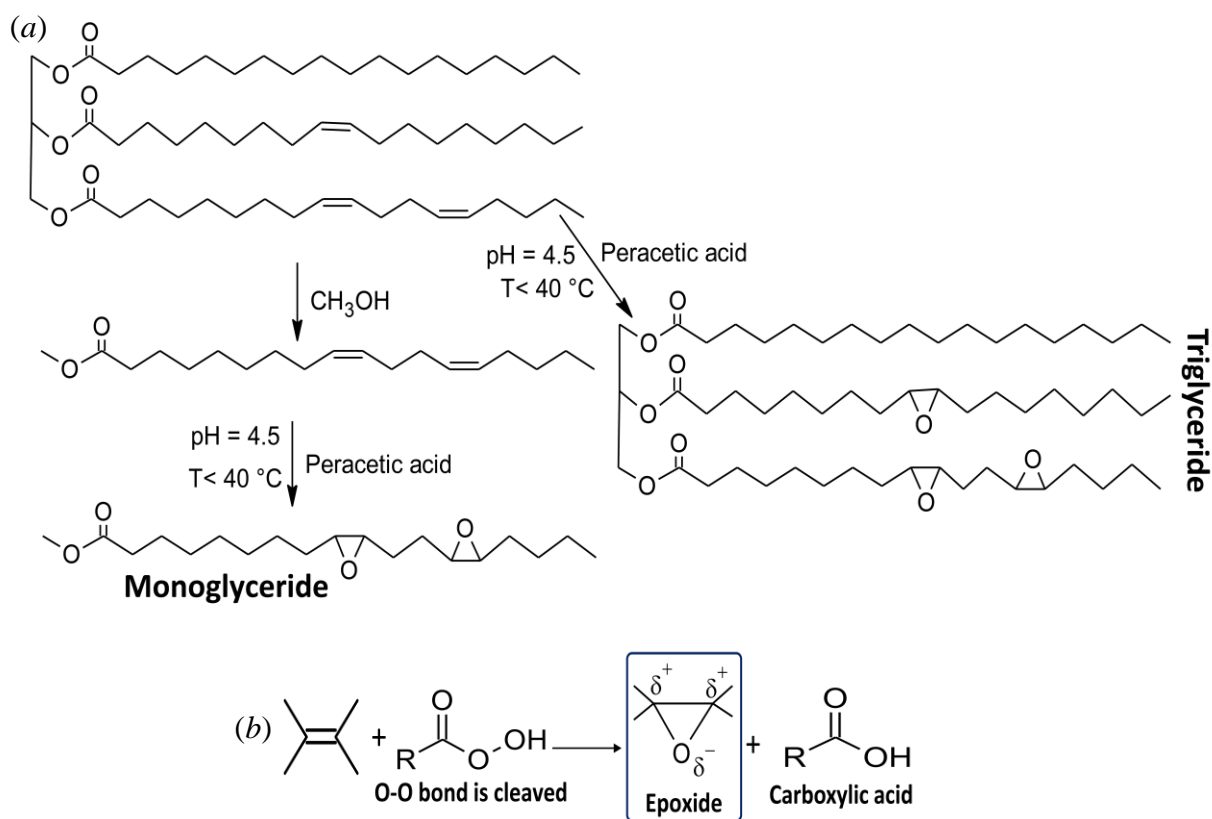


Figure 18: Different steps of conversion of epoxidized vegetable oil (a); Bond cleaved of peracetic acid and formation of epoxide (b)

Now is the point of selecting the renewable source plasticizer for elastomers. A minor modification of bio-oil is well-compatible with the elastomer. The different bio-oils have different polar behavior where the aromatic component and saturated fatty acids contribution influences the polarity of bio-oils as shown in Table 3.

Table 3: Polarity and aromatic behavior of different oils [92]

Name of oils	Clay gel analysis		
	Polar (%)	Saturates (%)	Aromatic content (%)
Aromatic oil	16	17	36
Paraffinic oil	10	69	9
Naphthenic oil	2	61	12
TDAE	12	16	30
Soybean oil	40	0	1
Canola oil	39	1	1
Rubber seed oil	41	0	1
Castor oil	16	17	1
Sesame oil	42	0	1

The epoxidized bio-oil contains fewer double bonds compared to conventional bio-oil and has the active oxirane group. The plasticizer contains OH groups that are most compatible with polar polymers, like NBR [76]. Although the hydrogen and Van der Waals bonds influence compatibility. The active groups combine a dipole-dipole interaction with elastomer. The saturation and aromatic contents were investigated using clay silica gel analysis and which is a method for determining the weight percent of asphaltenes, saturated hydrocarbons, aromatics, and polar compounds in a petroleum product, and it is done according to ASTM D 2007 [117]. Bio-oils are highly polar compared to mineral oils and have low aromatic components. These criteria vary on the species of plants, which means the modification of oil is not only essential, but the specification of the plant is also important.

## 2.3 Characterization of elastomers and plasticization effect

### 2.3.1 Structural properties

#### Structural properties on deformation behavior of elastomers

Stress and strain are two important parameters used to describe the deformation behavior of elastomer materials. Stress refers to the measure of the force that is applied to a material divided by the material's cross-sectional area. The physical unit of stress is  $\text{N/mm}^2$  or MPa and symbolized as  $\sigma$ . Strain is defined as the ratio of the change in length of an elastomer to its original length. It is typically expressed as a percentage and symbolized as  $\epsilon$ . The stress-strain behavior of unfilled elastomers (pure elastomers) can be described by the neo-Hookean model. The neo-Hookean model [123] is an isotropic model and it is used to implementation of materials which has an isotropic modulus and has negligible compressibility. When a pure elastomer undergoes deformation, its behavior is dependent on the extent of the deformation. Specifically, when the elastomer is subjected to small strains, it exhibits a linear response. The linear behavior is characterized by a direct proportionality between the applied stress and the resulting strain and can

be described mathematically by Hooke's law. The modulus of elasticity refers to the stiffness of elastomers and describes their resistance to linear-elastic deformation. pure elastomers exhibit a linear behavior within the range of small deformations due to the entropic nature of their molecular structure. The polymer chains in elastomers can be elastically stretched and recoil upon release, resulting in reversible deformation and leading to the linear relationship between stress and strain.

Neo-Hookean model assumes that the stress-strain relationship is purely elastic, and that there is no plastic deformation. Mathematically neo-Hookean model can be expressed as the Equation 5. Here  $\sigma$  is engineering stress, which is defined as the ratio of force and area before deformation. Actual modulus  $E$  is a material property that describes its resistance to extension by tensile stress, and  $\lambda$  is extension ratio is defined as the ratio of the final length of a material to its initial length.

$$\sigma = \frac{E}{3} \left( \lambda - \frac{1}{\lambda^2} \right) \quad (5)$$

Note that according to the neo-Hookean model, the stress  $\sigma$  measured at  $\varepsilon = 200\%$  strain (deformation  $\lambda = \varepsilon + 1 = 3$ ) is close to  $E$ , since  $\sigma_{200} = (E/3)(3 - 1/3^2) = 0.96 E$ . Thus,  $\sigma_{200}$  is commonly used as a reference quantity and will be used as such in this thesis. Classical rubber elasticity theory provides neo-Hookean model, and it is a physical phenomenon that describes the behavior of elastic materials when they are subjected to deformation. It includes that, if an elastic solid stretched, then sideways trims by the square root of the extension. It is also known as the theory of linear elasticity. The classical rubber elasticity theory [122] can predict the modulus of elastomers. Relation between modulus  $E$  and molar mass of the network chains of the neo-Hookean rubber is possible to describe according to Equation 6. Here  $\nu$  is mole number of network chains,  $V$  is volume of the elastomers.

$$E = \frac{3\nu RT}{V} = \frac{3\rho RT}{M_c} \quad (6)$$

Pure elastomers exhibit nonlinear behavior in high strain due to the stretching of polymer chains beyond their elastic limit, leading to significant molecular reconfiguration and chain entanglement. This nonlinearity arises from the complex interplay of chain orientation, entropic effects, and polymer network deformation, resulting in strain-dependent mechanical properties.

According to the classic rubber elasticity theory of Neo-Hookean rubber, the relationship between stress and molar mass of network chains can be represented in Equation 7. Here,  $\rho$  is density of elastomer,  $R$  is molar gas constant (8.31 J), and  $T$  is temperature in Kelvin.

$$\sigma = \frac{3\rho RT}{M_c} \left( \lambda - \frac{1}{\lambda^2} \right) \quad (7)$$

$M_c$  is the molar mass of the network chains, and it is the contribution of entanglements  $M_e$  and crosslinks  $M_x$ . The modulus of a real elastomer contains contribution from chain entanglements (see Equation 8).

$$E \approx E_x + E_e \propto \frac{1}{M_x} + \frac{1}{M_e} \quad (8)$$

Figure 19 shows the comparison between nonlinear stress-strain curve of realistic pure elastomers and neo-Hookean elastomer. It was observed that the neo-Hookean model does not fit very well with realistic elastomer. It fits only in a small region at the beginning where strain begins with stress. Typical elastomers show less stress in the intermediate region and then strong upturn stress much stronger than predicted by neo-Hookean model. The data of realistic rubber goes below because of strain softening, and it is related to topological rearrangement of entanglements. Stretching of an elastomer involves rearrangement processes of the elastomer coils while they do not capture by the affine model because of the effects like entanglements. According to the affine

model, the deformation of the rubber is homogeneous and isotropic, and the molecular chains within the rubber are stretched or compressed uniformly along the direction of the applied force. After the strain softening, strain hardening is commonly attributed for the finite extensibility because of there are ideal Gaussian chain model breaks down as well as possibility of strain induced crystallization.

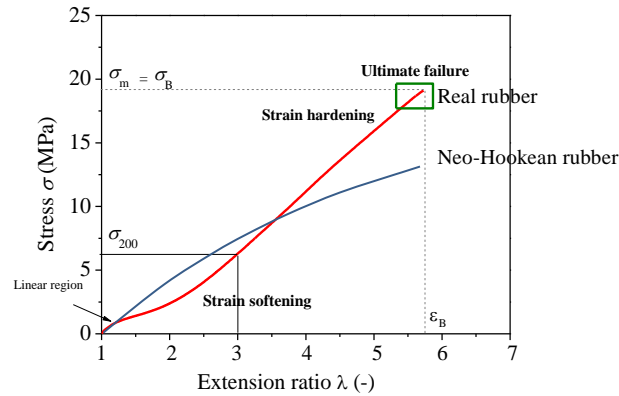


Figure 19: Representation of an exemplary a neo-Hookean (black line) and a realistic stress–strain (red line) curve with parameters

In the context of small-strain deformation, it is commonly observed that the actual modulus  $E$  of a filler-reinforced elastomer is typically higher than that of a pure elastomer (see Figure 20). This enhancement in stiffness arises primarily from the presence of incompressible filler materials where active filler networks. The addition of fillers, such as carbon black nanoparticles, to the elastomeric matrix, introduces a reinforcing effect. These fillers possess a higher modulus  $E$ , and strength  $\sigma$ , compared to the elastomeric material itself. As a result, when the composite material undergoes deformation within the small-strain regime, the presence of the stiff filler imparts additional resistance to the applied stress. The stiffness of the filler material restricts the ability of the elastomer to deform, resulting in a higher effective modulus for the composite. This behavior can be attributed to the reinforcement mechanism, where the fillers effectively increase the overall stiffness of the material by impeding the movement of the polymer chains and reducing their ability to stretch. It is important to note that the specific increase in modulus due to filler reinforcement can vary depending on factors such as filler concentration, filler-matrix interaction, the geometrical arrangement of fillers within the elastomer matrix and presence of oils.

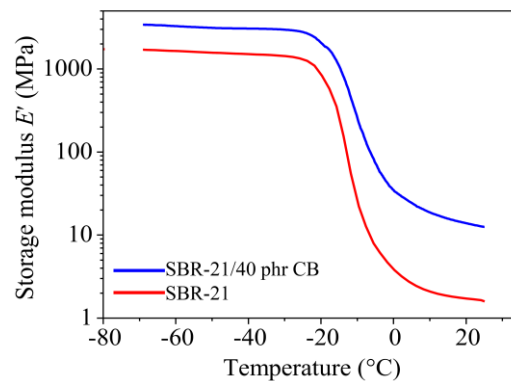


Figure 20: The temperature-dependent actual modulus  $E$  of pure SBR (red line) and Carbon black reinforced SBR (blue line)



The presence of fillers embedded within the rubber matrix has a notable impact on the mechanical properties of elastomers, as also demonstrated by the stress-strain diagram depicted in Figure 21. Specifically, the inclusion of fillers leads to an increase in the modulus of the elastomer. However, when subjected to higher strains, the filler networks within the elastomer matrix typically undergo breakdown due to their incompressible and inelastic nature. Consequently, as the strain increases, the filler networks tend to separate, resulting in an increase in the distance between them. It is important to highlight that in the case of filled elastomers, the breakdown of filler networks is the primary cause of the observed strain softening and sudden decline in the modulus of elastomers. Therefore, the influence of filler particles becomes particularly significant during substantial deformations, and this phenomenon is commonly referred to as the Payne effect. The Payne effect arises from the formation of a filler network within the elastomer matrix, which leads to increased stiffness and decreased mobility of the elastomer chains. The formation of this network can occur through physical interactions, such as van der Waals forces, or chemical bonding between the carbon black particles and the elastomer matrix [33]. The magnitude of the Payne effect depends on various factors, including the size, shape, concentration, and surface chemistry of the carbon black filler particles (refer to Figure 11), as well as the interaction between the rubber and filler. While the small strain behavior is crucial in determining the initial mechanical properties of filled elastomer materials, the Payne effect becomes more significant at larger strains where the behavior is primarily governed by the filler network rather than the elastomer matrix. Therefore, comprehending the contribution of both mechanisms is essential for the design and optimization of filled elastomers with tailored mechanical properties. Neo-Hookean model (green line) is not capable of capturing the Payne effect observed in filled elastomers (red line). It cannot accurately predict the decrease in modulus with increasing strain amplitude. The Neo-Hookean model's limitations stem from its assumption of linear elasticity (small strain) and its inability to account for the complex interactions between the filler particles and the elastomeric matrix.

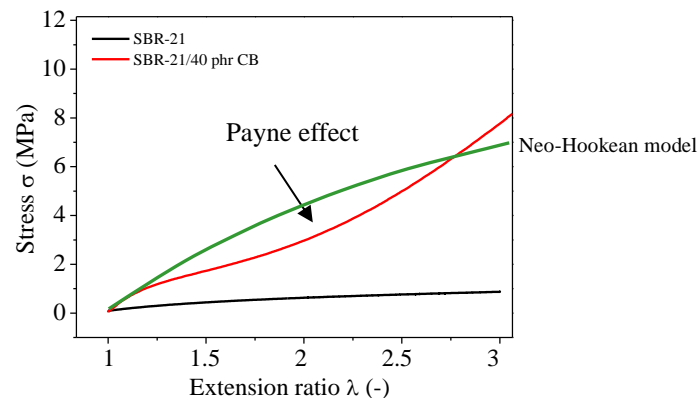


Figure 21: Representation of stress-strain diagram of unfilled and carbon black-filled SBR vulcanizates

The investigations on the modulus  $E$  of small-strained elastomer and stiffness  $\sigma_{200}$  (stress at 200 % strain) of high-strained elastomer were conducted successfully. However, it is worth noting that the analysis of the modulus of the rubber matrix was complicated due to the lack of additional data. Despite this limitation, the researchers were able to effectively carry out the examinations on the modulus of the elastomer in its original state and its stiffness after deformation. These findings contribute to a better understanding of the mechanical properties of elastomers and their response to external forces. Further research with comprehensive data on the rubber matrix is recommended to enhance the accuracy and comprehensiveness of future investigations.

This thesis aims to investigate the modulus of the rubber matrix in carbon black-filled SBR. However, a significant challenge arises due to the non-linear relationship between elastomer modulus and temperature in filled rubber systems. Consequently, accurately measuring the modulus of the rubber matrix becomes a complex task. In order to address this issue, measurement data from a previous article [35] was utilized. The same type of SBR as used in this thesis was employed in the aforementioned article, facilitating the collection of supporting data. Initially, the shear modulus  $G$  was determined through dynamic mechanical analysis (DMA) of unfilled SBR samples with varying concentrations of crosslinking agents, as depicted in Figure 34 (a). For the measurement of crosslink density, qualitative data of residual dipolar coupling ( $D_{\text{res}}$ ) was initially obtained using double quantum nuclear magnetic resonance (DQ NMR) or multi-quantum (MQ) spectroscopy [35,130–132]. These are the well-known method to evaluate the crosslink density of polymer networks. It mainly detects the weak residual dipolar coupling. The presence of crosslinks in rubber vulcanizates shows the non-isotropic fast segmental motion of the rubber chain. Dipole coupling between protons in monomer segments is not the same because of anisotropy chain segmental fluctuation. The methods of NMR measurements are broadly described in chapter 3.2.2.

An optimum networking system can give a better mechanical [98] and crack resistance behavior [120]. The crosslinking reaction develops a rubber networking system. A large number of studies were done on the correlation between crosslink density and mechanical properties, and the previous study [121] claims that a general trend followed between the crosslink density and different mechanical properties of elastomers, as shown in Figure 22. The results of this thesis have compared to this general trend to fit the results, and a general hypothesis created if there are any differences. However, filler or additives such as plasticizers can influence the network density.

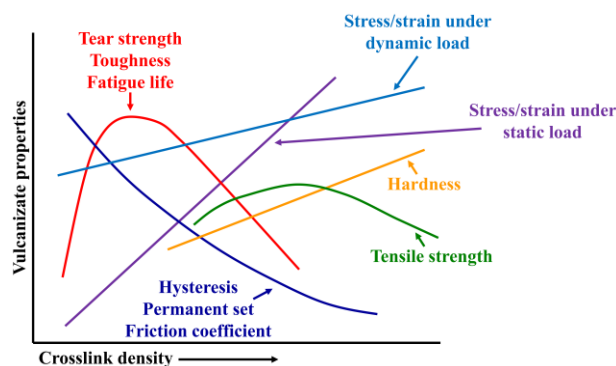


Figure 22: Influence of the crosslink density on the elastomeric properties, adapted from ref [121]

### Dispersion of filler and plasticizing effect

The structure of a filled elastomer is dominated by filler distribution and dispersion and how the filler interacts with elastomers. This means the tightness of rubber by the functionalized filler. The networking system of elastomer vulcanizates also dominated the structural property. When oil penetrates into the elastomer matrix, the discussion about elastomeric structure has to include the plasticized behavior of oils. The penetrated oil can change the networking system of elastomer vulcanizates [3], so it is an important factor and cannot be avoided when discussing about structural properties of elastomers. As a result, there are three factors that have to be included during the discussion of the structural properties of elastomers, such as rubber bounding, and crosslink after vulcanizates.

The addition of plasticizers improves the flow properties and distensibility. Plasticizers provide lubrication among polymer chains without any chemical changes. A study on the influence of plasticizer/oil is not enough to briefly discuss how they interrupt the rubber-filler interactions. A recent article [4] was published on the finding influence of TDAE on rubber-filler systems where the SBR/BR blend system was used with silica filler. This thesis claims that the mixing time, additional time of TDAE during mixing, and concentration of TDAE were the factors that can influence the rubber-layer  $L$ . In the absence of oil, the shear force is high during mixing, which may improve filler dispersion in the rubber matrix by crushing filler agglomerates. When oil is added, it can improve filler dispersion in the matrix by enhancing lubricating rubber chains [118]. The improvement of dispersion during mixing can cause more rubber-filler interactions. However, the type of oil and concentration is another factor to influence rubber-filler interactions. A high content oil addition may cause the plasticization effect and leads to bulk viscosity [119] and due to low internal shear forces during mixing with a high content of oil, resulting a reduction of rubber-filler interactions. However, a higher mixing time can enhance the rubber-filler interactions. The Carbon black undergoes different dispersion states depending upon the material parameters and mixing technology, and it could appear as large agglomerates to small aggregates [133]. The carbon black dispersion investigation was essential because of the well-dispersed Carbon black in the elastomer matrix to obtain optimum vulcanizate properties [134]. Large carbon black agglomerates can play a critical role in improving the mechanical properties and fracture resistance of plasticized elastomers. There are some ways in which carbon agglomerates resist crack initiation and propagation in plasticized elastomers, such as reinforcement which means the carbon agglomerates can increase the stiffness and strength of the elastomer matrix, which can resist the formation of cracks under mechanical stresses. It can absorb and dissipate energy during deformation, reducing the stress concentration at the tip of a crack and preventing its propagation. It toughens the elastomer matrix by bridging the crack faces and preventing their separation, thereby reducing the rate of crack propagation. Carbon agglomerates can also act as a barrier to the diffusion of oxygen and other gases that can accelerate the degradation of the elastomer material, thereby increasing its resistance to crack propagation. The presence of plasticizers in the elastomer can enhance the interaction between the carbon agglomerates and the elastomer matrix. This can lead to a more homogeneous dispersion of carbon agglomerates in the elastomer, resulting in improved mechanical properties and fracture resistance. However, if the plasticizer content is excessive, it can reduce the strength and toughness of the elastomer, making it more susceptible to crack initiation and propagation. Therefore, it is essential to optimize the plasticizer content and the dispersion of carbon black agglomerates within the elastomer matrix to maximize their beneficial effects on crack resistance. Carbon black as a reinforcing filler was used in this thesis and mixed into elastomer to enhance its processing properties and maximize its durability and physical properties. However, its reinforcing capacity cannot be fully realized until it is well dispersed in the rubber matrix. The undispersed agglomerates of carbon black weaken a rubber compound by forming stress concentrations and depriving other areas of the required carbon black concentration [120,121]. A good filler dispersion can result in less filler network formation, it does not necessarily mean that it is detrimental to reinforcement. In fact, a well-dispersed filler can enhance the mechanical properties of an elastomer matrix by improving the interfacial adhesion between the filler and the matrix, which can lead to increased stiffness, strength, and toughness [137]. The formation of a filler network, on the other hand, can provide additional points of constraint that resist deformation, leading to an increase in stiffness and strength. However, the extent of filler network formation and its effect on reinforcement depends on several factors, including the size, shape, concentration, and surface chemistry of the carbon black particles, as well as the elastomer-filler interaction. In some cases, a well-dispersed carbon black filler can still form a network, resulting in an increase in mechanical properties.

Some previous studies [71,98,124–126] claimed that oil penetration in rubber matrix reduces the crosslink density. The crosslink density can be influenced by the type and concentration of oil [98]. Several methods can be applied to measure the crosslink density of rubber materials. The common method is the swelling test [121,127–129], and it was done previously to get the crosslink density of rubber vulcanizates. The test is also used to measure the crosslink density of plasticized rubber vulcanizates [4].

### 2.3.2 Fracture resistance behavior and plasticization effect

Fracture mechanics of elastomers are of great technical importance. Durability is the main priority for developing elastomeric materials for high-performance elastomeric goods like seals, conveyor belts, tires, dampers, and other engineering components. The concept of fracture mechanics was derived before 1960 and applied to materials that obey Hooke's law [138]. The application of fracture mechanics is used to the estimation of the failure reliability of products made of elastomeric compounds. In modern science, fracture mechanics is an essential tool used to improve the performance of mechanical components. Fracture mechanics is a term that discusses the fracture behavior of polymers, and it is characterized as the driving force on a crack to characterize the material's resistance to crack. A crack is a physical process, and crack propagation occurs in the material when material-dependent mechanical limits such as stress intensity are exceeded. For analysis of crack resistance behavior, the complex connection between loading, crack initiation, and propagation in terms of material resistance against unstable and stable crack propagation has to be determined. Whereas fracture mechanics material testing of polymers to ascertain the crack toughness in terms of resistance against unstable crack propagation is already added in industrial testing practice, there are remarkable deficits in the industrial use of parameters from polymer crack resistance curves that characterize the stable crack propagation behavior [139]. Using the  $J$ -integral concept requires paying attention to the fact that the fracture is initiated by stable crack propagation in many cases. The evaluation of crack resistance behavior related to resistance against stable crack initiation and propagation is performed based on the crack resistance  $R$  concept. The crack opening  $J$ -integral is preferred as load parameters for constructing  $R$ -curves.

The resistance against crack initiation is symbolized as  $J_i$ . It is a parameter of strength that is used to describe an elastomer's resistance against crack initiation. The physical unit of  $J_i$  is N/mm. Specifically,  $J_i$  is the critical value of a measure of the energy required to propagate a crack, at the onset of crack initiation. The value of  $J_i$  can be determined experimentally by performing tests in which a crack is introduced into a specimen of the material, and the load required to initiate crack growth is measured. Elastomers with high values of  $J_i$  are typically more resistant to crack initiation and may be better suited for use in applications that require high levels of durability and reliability. The resistance against stable crack propagation is symbolized as  $T_J^*$  [34,140–142]. It is also a parameter of stress that is used to describe an elastomer's resistance against stable crack propagation. The physical unit of  $T_J^*$  is N/mm<sup>2</sup> or MPa. In engineering design, knowledge of the elastomer's fracture toughness, including the parameter  $T_J^*$ , is essential for ensuring the safety and reliability of structures and components. Four different types of loading could be used to investigate fracture mechanics, and the most common loading system is the quasi-static and impact load and some studies were done to apply the quasi-static and impact load [140,141,143]. Figure 25 shows applying stress as a function of times in two different loading conditions. The stress continuously increases during quasi-static loading, as shown in Figure 25 (a). In contrast, Figure 25 (b) shows that the crack happened quickly when impact loading was applied, and stress looked disrupted. Impact loading is applied when a sudden crash occurs. These loadings apply to characterize unstable crack propagation values; this is a relatively very high crack in the respective materials. The propagation of unstable cracks also proceeds with the release of value.

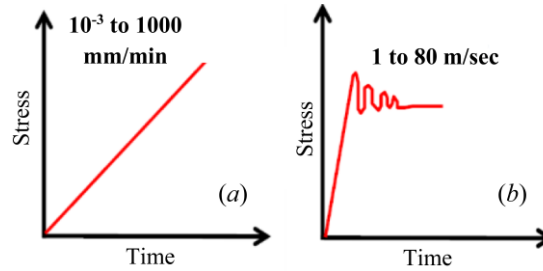


Figure 23: A stress-time deflection under quasi-static loading (a); impact loading (b)

Different research has been ongoing for decades on elastomers' development upon resisting the unexpected crack. Research on fracture mechanics for rubbers started in the middle of the twentieth century [144–146]. Some studies were done on the different elastomers to find the crack resistance behaviors under quasi-static and impact loading systems. A study on the fracture behavior of natural rubber was done by Reincke and Grellmann [34]. They investigated the natural rubber filled with silica and montmorillonite-based filler. The filler concentration was varied in the vulcanization system, and this investigation was done under quasi-static and impact loading system. The aim of this study was to find the crack resistance values on the filler concentration. It was claimed that the filler type and concentrations were a vital factor in the mechanical and fracture resistance behavior of natural rubber. Additionally, the geometry of specimen is the issue to influence the fracture resistance behavior. It was found that the crack resistance values were higher when the filler concentration was 60 to 70 phr and filler types played a key role to influence the resistance against stable  $T_J^*$  and unstable  $J_d$  crack propagation. Crack initiation value  $J_i$  under quasi-static loading was high at low content filler and it reduced and independent after 20 phr filler in the rubber matrix. Agnelli et.al [143] investigated the fracture resistance behavior of different elastomers which reinforced with varieties of filler. Their concentration was on natural rubber, HNBR and EPDM. The investigation of fracture resistance was under quasi-static loading to find the resistance against stable crack propagation. Their study proved that  $T_J^*$  was highly influenced on the type of elastomers, filler type and its concentration. It was found that the  $T_J^*$  continuously raises when filler concentration increase. Although maximum filler concentrations were used 30 phr except carbon black. The HNBR shows the higher  $T_J^*$  compared to other elastomers, and the MWCNT filler was the most efficient filler that helped to enhance the crack resistance values. Another study on the investigation of fracture mechanical properties of SBR was done by Reincke *et al.* [141]. Parallely  $T_J^*$  and  $J_d$  was measured on SBR, which was filled with different types and concentration of filler such as silica and carbon black. They have selected different particle sizes of carbon black to see how the surface area of filler can influence on the crack resistance values. It was depicted that SBR showed higher  $T_J^*$  and  $J_d$  when it was filled with 40 phr of filler, and it was optimum concentration with SBR vulcanizates.

For the first time in plasticizer and fracture mechanics history, Brown [147] used phthalate plasticizers in polyvinyl chloride (PVC) polymer and investigated the fracture resistance behavior under impact and quasi-static loading. A higher fracture resistance performance was found up to 10 weight % of phthalate plasticizers under quasi-static loading, as shown in Figure 26 (a), which is generated for this study using data from the previous study Figure 26 (b) is generated from the same study, showing that plasticized PVC fracture mechanics gradually decreased when plasticizers' content was increased under impact loading. A precise overview was found from this research that plasticizers influenced the fracture resistance behavior of polymers.

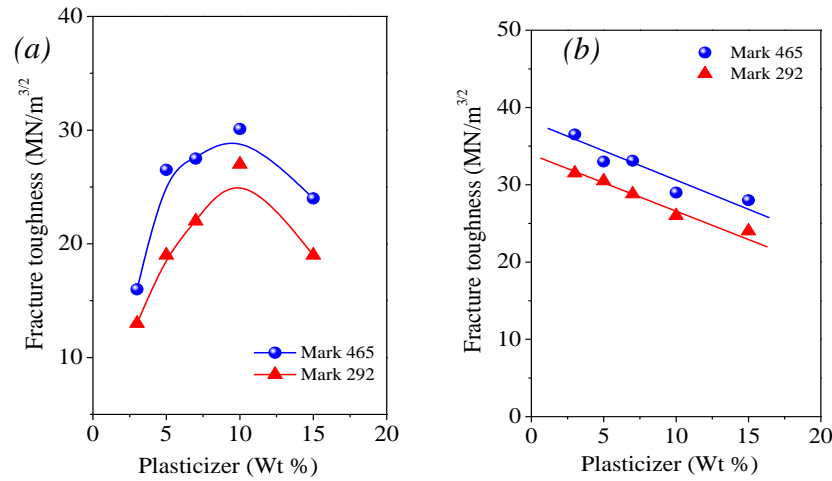


Figure 24: Fracture toughness of plasticized PVC materials: compact tension specimens (a); impact tests (b) data taken from ref [147]

### 2.3.3 Mechanical behavior and plasticization effect

There are some excellent mechanical results for versatile elastomers obtained with bio-oils or modified bio-oils as plasticizers, especially with epoxidized soybean oil [66], linseed oil [127], castor oil [49], and rice bran oil [148]. The characterization aimed to find the possible influence of plasticizers on the mechanical and fracture resistance behavior of elastomers. A list of previous work has been done where the mechanical behavior of elastomers was characterized with different modified bio-oils. Castor and jatropa oil with styrene butadiene rubber (SBR) [126], epoxidized palm oil (EPO) with SBR [128], olive oil and orange with acrylonitrile-butadiene rubber (NBR) [48], palm oil with ethylene-propylene-diene rubber (EPDM) [100], linseed oil with natural rubber NR [127].

The hypothesis of their work to make the prediction that the addition of oils could greatly affect the tensile, tear resistance, resilience, and hardness behavior of elastomers. Research which mentioned above on bio-oil/elastomer blend claimed that modification of bio-oil reduced their molecular size which helps to more penetration in the polymer matrix, that make a good dispersion and overall improved mechanical properties. Previous research also claims that the plasticizer concentration strongly influences mechanical behavior. For example the tear strength was higher when the plasticizer concentration was 6 to 8 phr as shown in Figure 25 [127]. Although a suitable bio-oil is essential for the modification of certain elastomers in order to obtain a homogeneous filler distribution and dispersion, so that mechanical properties and crack resistance can be improved together. Otherwise, the bio-oil can bleed out of the elastomer matrix, rise to the elastomer surface, and begin leaching.

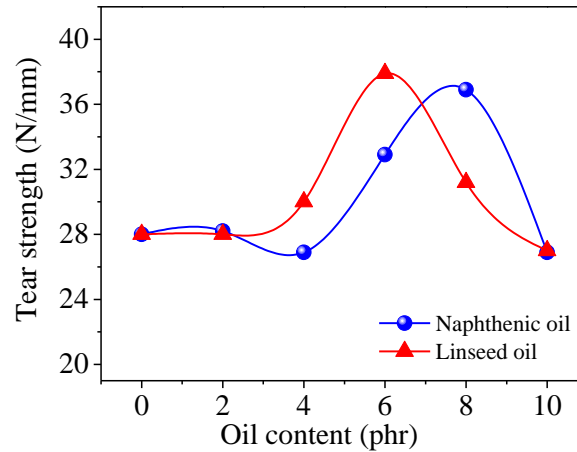


Figure 25: Dependence of tear strength as a function of naphthenic oil and linseed oil contents in the mix, data taken from ref [127]

Plasticizer leaching or external migration is a major problem, reducing properties and shortening service life. Petrović [151] worked on the EPDM mixed with soybean oil. It was found that the oil exuded from the matrix and oil droplets accumulated on the surface as shown in Figure 26. It has a heterogeneous filler dispersion and finally deplorable mechanical behavior.



Figure 26: Bleed-out of soybean oil from cured tensile pad molded from EPDM, photo reproduced with permission from ref [151]

This thesis mainly focused on the gaps of the research mentioned above on bio-oil/elastomer blend systems, and the gap was to know about the fracture mechanics of those elastomers blended with modified bio-oils. The researchers are mainly focused on some typical mechanical properties of elastomers but rarely focus on fracture resistance behavior. This thesis is the research area of finding the fracture resistance of plasticized elastomers, where the type and concentration of plasticizers were of great importance. In addition, this thesis introduced the bio-oil and turned to the replacement of mineral oil with bio-oil, mainly studying various mechanical analyzes such as tensile behavior, tear strength behavior, hardness behavior, resilience and compression set behavior. Some studies have been presented here that have recently been mechanically analyzed, so that their result was a latent motivation to continue this thesis.

The next chapter follows with the experimental part of this thesis. The following part of the experiment is divided into three parts. The introduction of materials, oils and experimental characterization methods are discussed at the beginning. After that, results are shown with

discussion and finally a structure-property correlation is made. I will introduce the oils and essential materials used in this thesis. The rubber mixture is then processed, including vulcanization processes. Then, in the oil characterization part, a description of oil characterization methods is given, including their physical, chemical and thermal characterization. The next part describes the characterization of the rubber raw compound, such as the rubber-layer  $L$  analysis. After vulcanization, the method for measuring the crosslink density is described. The structural properties of plasticized rubber vulcanizates are discussed, including micrographs of cross-sectional areas of fracture surfaces. The methods for investigating the mechanical behavior come next in line and then come to the most interesting part of this thesis, the methods for the fracture resistance behavior of plasticized elastomeric vulcanizates. The exciting and crucial results will be brief of structure, mechanics, fracture strength and aging behavior which will be included in the results and discussion section where the crucial discussion was about the evaluation as part of the benefits of bio-oil blends of elastomers. Finally, the structure-property correlations were discussed and scientific conclusions were drawn.



## 3 Experimental

### 3.1 Investigated oils and materials

#### 3.1.1 Oils

Several bio-oils were used to characterize the influence of plasticizers on the properties of elastomers where a mineral oil-based plasticizer treated distillate aromatic extracts (TDAE) and synthetic plasticizer Mesamoll<sup>®</sup> were used to compare the evaluations. TDAE and Mesamoll<sup>®</sup> were mixed directly in the elastomer without further modification. TDAE was represented as a conventional plasticizer as a non-renewable source of mineral oil. Mesamoll<sup>®</sup> is a commercial name for Alkylsulphonic acid ester with phenol (ASE) which represents the source of synthetic plasticizer. Both oils were used in this thesis as reference oils. In contrast, bio-oils were used after different modifications. This thesis mainly investigated the crack resistance behavior of bio-oil mixed elastomer vulcanizates, where reference oils were used to compare the evaluations. A list of oils, including abbreviations, is given in Table 4.

Table 4: Overview of the used oils

Category	Oils	Abbreviations
Mineral oil	Treated distillate aromatic extract	TDAE
Synthetic oil	Alkylsulphonic acid ester with phenol (ASE)	Mesamoll <sup>®</sup>
Bio-oil-1	Soybean oil epoxidized ester of glycerol formal	EESO
Bio-oil-2	Canola oil epoxidized ester of glycerol formal	EECO
Bio-oil-3	Rapeseed oil epoxidized	ERO
Bio-oil-4	Rapeseed oil epoxidized methyl ester	ROME
Bio-oil-5	Rapeseed oil epoxidized iso-propyl ester	ROPE
Bio-oil-6	Soybean and sunflower oils epoxidized ester	EESS

TDAE (Vivatec 500) was collected from Hansen & Rosenthal KG, Hamburg, Germany. Mesamoll<sup>®</sup> was obtained from Lanxess Deutschland GmbH, Leverkusen, Germany. Bio-oil-1 (EESO), bio-oil-2 (EECO), and bio-oil-6 (EESS) were modified in the laboratory of Glaconchemie GmbH, Merseburg, Germany. Whereas the modification of bio-oil-3 (ERO), bio-oil-4 (ROME), and bio-oil-5 (ROPE) was done in the laboratory of Pilot Pflanzenöltechnologie Magdeburg e. V., Magdeburg, Germany. The listed bio-oils were not commercial plasticizers so there is no technical data, so some general characteristics were done in this thesis. Especially physical (e.g., density, viscosity), chemical (e.g., structure, molecular mass, polarity), and thermal ( $T_g$ , melting point) measurements were done.

#### 3.1.2 Elastomers and Composition

The investigation was performed on styrene-butadiene rubber (SBR) and acrylonitrile-butadiene rubber (NBR) polymers. Clear grade S-SBR Sprintan<sup>™</sup> SLR-4602 (21 % styrene) was used in this investigation. However, for comparison with clear grade S-SBR mixture with TDAE, one single mixture was prepared by using S-SBR Sprintan<sup>™</sup> SLR-4630 (25 % styrene), which is extended with 37.5 phr TDAE. The composition of this mixture was the basic composition, but no additional oil was added. Nevertheless, these SBR materials were supplied by Trinseo Deutschland GmbH, Schkopau, Germany. NBR with three different contents of acrylonitrile monomer was used as named PERBUNAN<sup>®</sup> 1846 F (18 % acrylonitrile), PERBUNAN<sup>®</sup> 3445 F (34 % acrylonitrile), and PERBUNAN<sup>®</sup> 3945 F (39 % acrylonitrile) from Lanxess Deutschland GmbH, Germany. For all the investigations except the compression set (CS), the reinforcing filler carbon black of the type

Corax<sup>®</sup> N220 and for the CS investigation Corax<sup>®</sup> N550 was added, which was supplied by Orion Engineered carbons GmbH, Frankfurt, Germany. Mesamoll<sup>®</sup> was used for the CS investigation after mixing with NBR materials.

Sulfur was used as a crosslinking agent, stearic acid was a processing aid, and it acted as co-activator too, ZnO as an activator, N-cyclohexyl-2-benzothiazolesulfenamide (CBS) as an accelerator, and these materials were supplied by Roth Deutschland GmbH. An antioxidant N-(1,3-dimethylbutyl) -N'-phenyl-p-phenylenediamine (6PPD) was supplied by Avokal<sup>®</sup> GmbH. Polymer, mineral and synthetic oils, Fillers, and other additives were used in this thesis directly from the packet without any modification and kept at room temperature in a standard atmosphere to prevent physical and chemical changes. However, after modification, the bio-oils are also stored in standard conditions as other investigation ingredients.

### 3.1.3 Preparation of rubber mixtures

A basic method was followed for the rubber mixture preparations according to previous studies [66,72,98,148,152]. In the beginning, the recipe was prepared where the amount of elastomers, fillers, crosslinking agents, and antioxidants were fixed though the amount of oil was variable. The SBR with 21 % styrene was named SBR-21 after mixing, whereas SBR with 25% styrene (with 37 phr TDAE) was named S-25T. In contrast, NBR with 34 % acrylonitrile and 39 % acrylonitrile were named NBR-34 and NBR-39 accordingly. The formulation of the materials is reported in Table 5. The compounds were prepared with a two-stage mixing procedure. In the beginning, a lab kneader as Figure 27 (a) with a fill factor of 0.7 was used where the starting temperature was 50 °C, and a rotation speed of 50 rpm was used. The elastomer was introduced first in the chamber, closed the lid, then opened again after 1 min, and the carbon black, oil, stearic acid, ZnO, and 6PPD were poured, then closed the lid again. After 5 min, opened the lid, and the sulfur and CBS were added. After that lid was closed and monitored the torque and temperature on time using software which is showing on the PC monitor. The compounded dough was discharged after 10 min, and as a final step, it was homogenized on a two-roll mill as shown in Figure 27 (b) before curing.

Compression sets (CS) were analyzed as the investigation for NBR materials. PERBUNAN<sup>®</sup> 1846 F (18 % acrylonitrile), and PERBUNAN<sup>®</sup> 3445 F (34 % acrylonitrile) were used for the CS investigations. The recipe was used slight differently from other investigations for this experiment, and the recipe for CS analysis are listed in Table 6. The main difference was NBR types, oil concentrations, and the particle size of the filler.

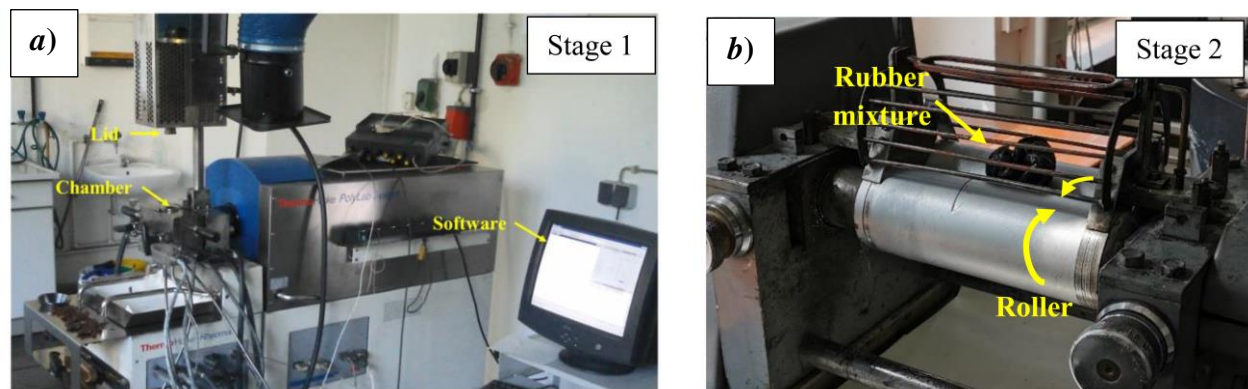


Figure 27: Lab kneader for rubber mixing connected with a PC software (a); two roll mills for mixture homogenization (b)

Further, cure characteristics at a temperature of 160 °C were determined by using a vulcameter (type GÖTTFERT elastograph, GÖTTFERT Werkstoff-Prüfmaschinen GmbH, Buchen, Germany). According to the results of the vulcameter tests, the time  $t_{90}$  was fixed as the vulcanization time for the necessary plates. For each material (formulation), plates with a size of 100 mm × 60 mm × 6 mm and 120 mm × 120 mm × 2 mm were vulcanized. Specimens of the desired form for the tests were cut using a metal cutter from these plates.

Table 5: Composition and time of addition during mixing

Name	Comments	Content (phr)	Time of addition (min)
Polymers	SPRINTAN™ SLR 4602, SPRINTAN™ SLR 4630 PERBUNAN® 3445 F, PERBUNAN® 3945 F	100	0
Carbon black	N 220	40	1
Oil	Mineral oil, bio-oil	0/12.5/25/37.5	1
Stearic acid	Processing aid	1	1
ZnO	Activator	3	1
6PPD	Antioxidant	1.5	1
Sulfur	Crosslinking agent	1.75	5
CBS	Accelerator	1.05	5

Table 6: Composition and time of addition during mixing for CS analysis

Name	Comments	Content (phr)	Time of addition (min)
NBR	PERBUNAN® 1846F, PERBUNAN® 3945F	100	0
Carbon black	N 550	40	1
Oil	Mineral oil, synthetic oil, bio-oil	0/5/15	1
Stearic acid	Processing aids	1	1
ZnO	Activator	3	1
6PPD	Antioxidant	1.5	1
Sulfur	Crosslinking agent	1.75	5
CBS	Accelerator	1.05	5

## 3.2 Experiments

### 3.2.1 Oil characterization

Bio-oils can have different chemical properties, and they are primarily laboratory-modified natural plant oils. The modification might change some significant properties of bio-oils. Without ensuring it was complicated to use as a plasticizer. Some factors can affect here for excellent compatible bio-oils with different elastomers. The primary queries about the bio-oils are to know the modified bio-oils chemical and physical properties. Different characterization methods were used for chemical characterizations. The essential characterization methods are discussed here to ensure the properties of oils.

#### Characterization of chemical structure using infrared spectroscopy (FTIR)

Fourier transform infrared spectroscopy (FTIR) used as a fast and reliable method for monitoring the aromaticity of mineral oil and epoxidation fraction of bio-oils. The FTIR analysis has become a powerful analytical tool in studying plant oils because it is fast, non-destructive, and requires

minimal sample preparation, reducing production costs. It is also environmentally friendly and reduces chemical residues. Furthermore, FTIR spectroscopy is an excellent tool for oil functional group analysis. FTIR spectra are used to characterize bio-oils because of the difference in the intensity and frequency at which the highest absorbance appears, according to the nature and composition of the sample [153,154]. The attenuated total reflection (ATR) sampling technique is used in conjunction with infrared spectroscopy, enabling the oil samples to be examined directly in their liquid state without further preparation. After running the software, a drop of oil sample was placed on the ATR crystal (see Figure 28) and getting the FTIR signal within the wavenumber of 400 to 4000  $\text{cm}^{-1}$  region and this region has chosen because the wavenumber for the corresponding oils functional groups were mainly detected signal within this range.

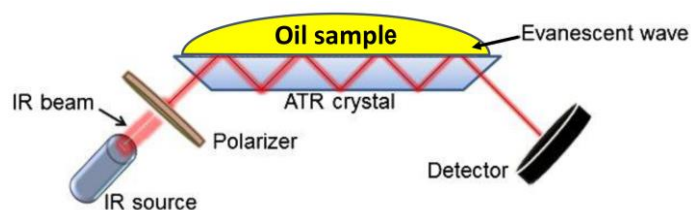


Figure 28: Schematic representation of an ATR-FTIR system. The infrared beam passes through the ATR crystal-covered on the top by the oil sample, reproduced with permission from ref [155]

The IR signal from the ATR crystal has been automatically converted into FTIR by the software with the specific peak for the oil functional groups. The FTIR analysis was done in the chemical analysis lab in Polymer Service GmbH Merseburg. This measurement was done at 23 °C, and three different drops of oil sample were used for three measurements to ensure the precise analysis. One measurement was selected among the three for further analysis. The functional groups for correspondent peaks for the oils were noted and marked on the peaks. However, the intensity of the peak is a concern in getting a quantitative analysis of oils because the intensity is related to the amount of the oil component [156]. During analysis mainly focused on finding the aromatic functional groups for the mineral oil. The corresponding fatty acid peaks and the intensity of epoxidized peaks were noted and compared for the bio-oils. The most common conversion of epoxides from fatty oils is peracids [157,158] oxidation with molecular oxygen using catalytic methods [159], and that can be detected by FTIR spectra. The ATR sampling technique with FTIR spectrum quickly identifies the region for those epoxidized corresponding peaks and makes it easy to analyze bio-oils, and functional groups, including information about the fraction of epoxy conversion.

### Characterization of epoxidation using nuclear magnetic resonance spectroscopy (NMR)

Nuclear magnetic resonance spectroscopy (NMR) can be applied to measure the quantitative information about the bio-oils chemical structure. In this thesis, NMR spectroscopy was applied to find the fraction of epoxidation of bio-oils and the aromatic nature of mineral oils. Bruker Avance TM 400 MHz spectrometer was used for the investigation.  $^{13}\text{C}$  and  $^1\text{H}$ -based NMR were mainly applied for the mineral oil investigations.  $^1\text{H}$  NMR spectroscopy is used for the characterization of bio-oil samples. Because of the low natural abundance of the  $^{13}\text{C}$  nucleus (1.1%) coupled with low inherent sensitivity relative to  $^1\text{H}$  (about 1/64), the  $^{13}\text{C}$  NMR experiment is approximately 6000 times less sensitive than  $^1\text{H}$  NMR. No further sample preparation was needed for the oil analysis. The liquid oil is inserted into a unique NMR tube. Around 2 ml oil samples were filled in the NMR tube, and after adding deuterated chloroform ( $\text{CDCl}_3$ ) solvent, the

level of tube height was not more cross than 4 to 5 cm from the bottom of the tube. Due to high preciseness and an expensive method, only one sample was enough to get the exact quantitative result of the oil component. NMR spectroscopy measurement was carried out in the lab of liquid state NMR analysis lab at Merseburg University of Applied Sciences. The operating temperature of the experiment was 25 °C, and the standard frequency was 400 MHz. The NMR spectrum was received in FID format; then, it was opened in MestReNova software. Previous studies [6,160,161] noted the correspondent peak for the oil component. The area of the correspondence peaks was estimated using software in the same consequence, and the epoxy peaks for the modified bio-oils are calculated to compare among those oils regarding their fraction of epoxy conversions.

### Molar mass investigation using gel permeation chromatography (GPC)

This experiment aims to determine the oil samples' molecular mass and molecular mass distribution. The gel permeation chromatography (GPC) is a part of the size exclusion chromatography (SEC) method, where the component of oils are separated according to their molecular size and this molecular mass (see Figure 29).

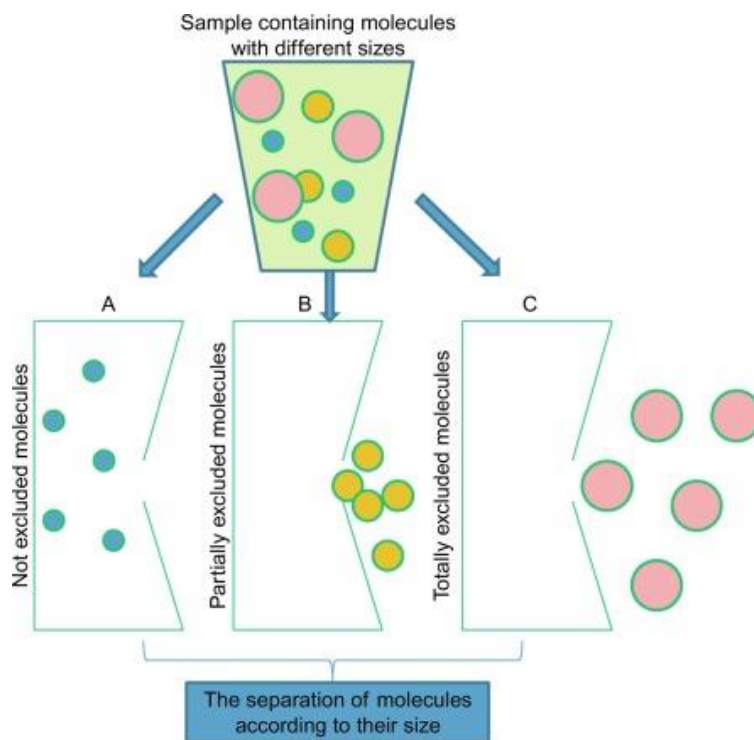


Figure 29: The principle of separating molecules by size exclusion chromatography, reproduced with permission from ref [162]

The measurement was carried out on gel permeation chromatography (GPC) equipment (type 1260 Infinity, Agilent Technologies, Inc. California, USA) at Merseburg University of Applied Sciences. There was no special sample preparation of oil applied to this chromatography. The liquid oil samples are dissolved into toluene solvent in an SEC column, and this capped column has inserted into the equipment. The measuring temperature was applied at around 35 °C, and the liquid flow rate was 0.8 ml/min. The aim was to determine the molecular mass information of oils, and it was evaluated according to a previous study [163]. The number-average molecular weight  $M_n$ , weight-average molecular weight  $M_w$ , and z-average molecular weight  $M_z$  was determined for different oil samples, as shown in Figure 30. However, the value of  $M_n$  represented the molecular mass of the oils.

Additionally,  $M_w/M_n$  and/or  $M_z/M_w$  ratios are applied to calculate molecular weight distribution, also known as polydispersity index (PDI). The modal distribution of oils was determined from the molecular weight distribution curve. The unimodal distribution of oil represents the single component of oils, whereas multimodal distribution depicts multi-components that can be present in the oil. The molar distribution was analyzed using the PSS WINGPC UniChrom V 8.20 software connected to the GPC column.

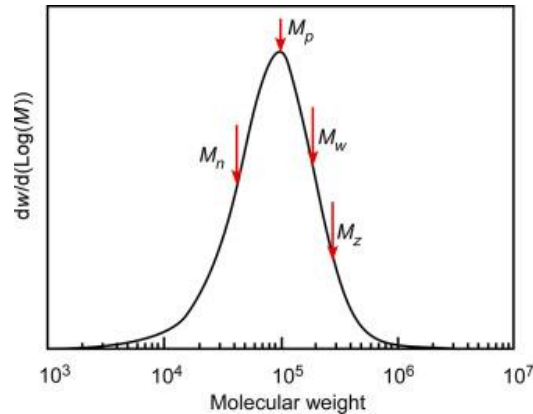


Figure 30: The GPC curve and the relationship between  $M_n$ ,  $M_w$ , and  $M_z$ .  $M_p$  demonstrated the peak of the GPC curve, reproduced with permission from ref [163]

### Thermal analysis using differential scanning calorimetry (DSC)

Differential scanning calorimetry (DSC) was used to investigate the purity of oils, glass transition temperature ( $T_g$ ), and melting point ( $T_m$ ) of the oil samples. It is one of the standard calorimetry methods to find the thermal behavior of oil-type liquid samples. No further preparation was needed for the oil sampling, and a single attempt was enough for the measurement if no unacceptable occurrence happened. A small amount of oil sample (5-8 mg) was poured into a closed crucible and placed into a temperature-controlled DSC cell. Another crucible without oil (empty cell) was used as a reference. The DSC run involves heating/cooling the sample at a controlled, steady rate and monitoring the heat flow to characterize the phase transitions as a function of temperature (see Figure 31).

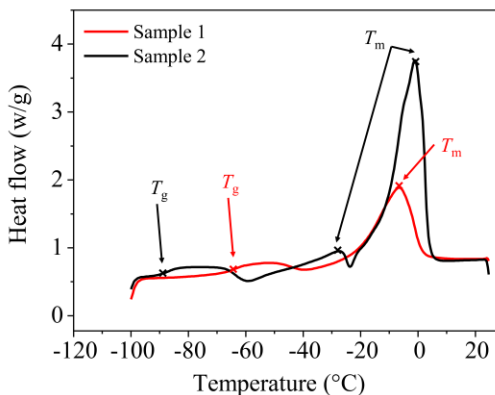


Figure 31: Thermal transitions in oil samples. Both oil samples go through the glass transition  $T_g$  as the temperature increases. Sample 1 has exhibited only one melting peak, and sample 2 undergoes two melting peaks at two different temperatures

More detailed studies can adopt multi heating/cooling steps and isothermal mode. The DSC 214 Polyma device from Erich NETZSCH GmbH is used for the DSC investigations, and it was done in the chemical analysis of Polymer Service GmbH Merseburg. This testing model is especially suitable for the investigation of oligomers and polymers. The standard for the DSC was DIN EN ISO 11357 [164]. The heating and cooling rate were applied  $10 \text{ K min}^{-1}$ , and the temperature range was controlled between  $-100 \text{ }^\circ\text{C}$  to  $25 \text{ }^\circ\text{C}$  because the glass transition temperature and probable phase transition were expected within this region. The measurement was done during two times heating and one cooling time. Firstly, melted the sample up to  $25 \text{ }^\circ\text{C}$ , then it was cooled to  $-100 \text{ }^\circ\text{C}$  and heated again up to  $25 \text{ }^\circ\text{C}$ . The data was considered for the second time heating and cooling. The result is analyzed according to international standards [164] and notes the region of  $T_g$  and melting peaks. However, the intensity of melting peaks is noted for corresponding oil samples. Although some oils perhaps show two melting peaks, it has some explanations, like a minor component present in oil samples [165]. The endothermic transition  $T_g$  starts at the beginning during heating, and the endothermic melting peaks  $T_m$  appear after that for the oil samples. The exothermic crystallization transition  $T_c$  was appeared during the cooling. So, the measurement for  $T_g$  and  $T_m$  were measured during heating and  $T_c$  during cooling.

### **Kinematic viscosity measurements**

The viscosity of bio-oils is the general condition for getting an optimum condition for a good mixture, and this could be the strong reason for the viscosity measurement of the oils. Even after the mixture, the inappropriate viscosity can influence the leaching of plasticizers from the materials. The investigation was done to find the kinematic viscosity  $\nu$  at different temperatures because in oils, it is more common to express viscosity as  $\nu$ , and it is defined by the ratio of dynamic viscosity and density. The unit of  $\nu$  is  $\text{mm}^2/\text{s}$  which is measured in the device HAAKE™ MARS™ rheometer (Thermo Fisher Scientific, USA) with the temperature controlling device of MARS 60. The measurement was performed at Merseburg University of Applied Sciences. There is no sample preparation needed in this method. Some drops of oil sample (5 to 10 mg) were placed on the plates. The gap between the two plates was 0.05 mm, and the rotation speed of the lower plate was  $58 \text{ rad s}^{-1}$ . This thesis measured the viscosity at two different temperatures (e.g.,  $40 \text{ }^\circ\text{C}$  and  $100 \text{ }^\circ\text{C}$ ). After running the device with the connected software, no further calculation was needed to get the viscosity results when all data is automatically getting from the software.

### **Surface tension investigation using contact angle methods**

The surface tension of oil is one of the important parameters that can influence the oil mixing with elastomer, and this is a sharp reason to measure the surface tension of oil. There are different methods can apply to measure the surface tension of oils. However, this thesis focused on the easy, cheap, and less time-consuming methods and then chose the contact angle measurement method. According to the contact angle method, a tiny drop of oil is placed on the untreated polytetrafluoroethylene (PTFE) and measured the contact angle between oil and PTFE surface is in Figure 32. It is the accepted standard reference surface for two-component liquid surface tension determination. An untreated PTFE is assumed to have a surface energy of  $18.0 \text{ mJ/m}^2$  and capable of non-polar type interactions. DIN EN ISO 19403 [166] standard was used to contact angle measurement. The experiment was done in the microscopy lab of Polymer Service GmbH Merseburg. The experiment was done at  $23 \text{ }^\circ\text{C}$ , while no special sample preparation was needed for oil investigation. Around 5 ml of oil was poured into a plastic syringe, and the piston was pressed softly, so easily one drop could become out from the needle dropped on the PTFE surfaces. 10 drops of oil were spread on the different positions of PTFE surfaces.

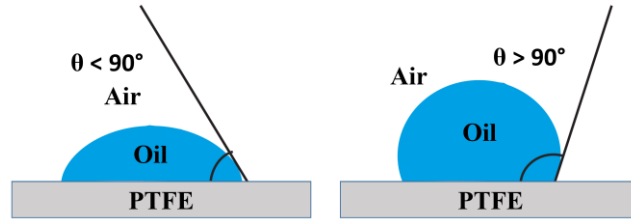


Figure 32: Schematic representation of contact angle of oil on the PTFE surfaces

The first step in determining PTFE surface energy using Fowke's theory is to test the PTFE for contact angle with an oil which has only a dispersive component to its surface tension (i.e., an oil for which  $\sigma_L^P = 0$ , so that  $\sigma_L^D = \sigma_L$ ). The dispersive component is defined as the part of the surface tension of oils that is due to dispersive interactions or van der Waals interactions, and these interactions are caused by temporary fluctuations of the charge distribution in the atom or molecules.

According to Fowkes theory, the interaction between polymer and oil was described by three primary Equations 9-11.

Young's equation:

$$\sigma_S = \sigma_{SL} + \sigma_L \cos \theta \quad (9)$$

$\sigma_S$  is the overall surface energy of the polymer,  $\sigma_L$  is the overall surface tension of the oil,  $\sigma_{SL}$  is the interfacial tension between polymer-oil, and  $\theta$  is the contact angle between polymer and oil.

Dupre's adhesion energy equation:

$$I_{SL} = \sigma_S + \sigma_L - \sigma_{SL} \quad (10)$$

$I_{SL}$  is the energy of adhesion per unit area between oil and polymer surface.

Fowkes adhesive energy theory between polymer and oil was separated into interactions between the dispersive components and non-dispersive (polar) components. Polar interactions construct Coulomb interactions between permanent dipoles and between permanent and induced dipoles or hydrogen bonds.

$$I_{SL} = 2 [(\sigma_L^D)^{1/2} (\sigma_S^D)^{1/2} + (\sigma_L^P)^{1/2} (\sigma_S^P)^{1/2}] \quad (11)$$

Here  $\sigma_L^D$  is the dispersive component of the surface tension of wetting oil,  $\sigma_L^P$  is the polar component of the surface tension of wetting oil,  $\sigma_S^D$  is the dispersive component of the surface energy of the polymer, and  $\sigma_S^P$  is the polar component of the surface energy of the polymer.

Above three equations were combined to get the primary equation of the Fowke's surface energy theory (see Equation 12):

$$(\sigma_L^D)^{1/2} (\sigma_S^D)^{1/2} + (\sigma_L^P)^{1/2} (\sigma_S^P)^{1/2} = \frac{(\cos \theta + 1) \sigma_L}{2} \quad (12)$$

The first step in measuring the solid surface energy using Fowke's theory is to test the polymer for contact angle with an oil that has only a dispersive component to its surface tension. In this case, the primary Equation 1 reduces to Equation 13:

$$\sigma_L = \frac{4 \cdot \sigma_S^D}{(\cos \theta + 1)^2} \quad (13)$$



and  $\sigma_S^D$  can be calculated directly from the contact angle data obtained. Where  $\theta_{PTFE}$  = the contact angle measured between PTFE and the sample oil. Therefore, the dispersive surface tension component ( $\sigma_L^D$ ) can be determined by oil for which the overall surface tension ( $\sigma_L$ ) is known only by measuring the contact angle between that oil and PTFE ( $\theta_{PTFE}$ ) and using Equation 14. The polar surface energy component for the liquid is then determined by difference ( $\sigma_L^P = \sigma_L - \sigma_L^D$ ).

$$\sigma_L^D = \frac{\sigma_L^2 (\cos\theta_{PTFE} + 1)^2}{72} \quad (14)$$

In the second step, the PTFE was replaced by elastomer surfaces, which means contact angle measurement was done separately on untreated raw SBR and NBR surfaces. The untreated flat surfaces were prepared after being pressed within the flat metal plate, and the measurement process was kept the same as done by PTFE surfaces. Thus, the untreated SBR and NBR smooth surfaces were separately used to find the contact angle of the oil drops. In this investigation, the wettability of oil as the contact angle was evaluated on the non-polar PTFE surfaces and on the individual elastomer's surfaces planned for the mixes with oils. The evaluation was done according to a previous study [167], where the contact angle of  $0^\circ$  assumed to be the oil is wholly wetted on the substrate, which means the best possible wet. If the contact angle is between  $0^\circ$  to  $90^\circ$ , this means a high wetting occurs. The contact angle between  $90^\circ$  to  $180^\circ$  means poor wetting behaviors, and the contact angle equal to  $180^\circ$  means the oil does not wet the matrix.

### 3.2.2 Physicochemical characterization of elastomers

#### Rubber-layer $L$ of raw mixtures

The aim of this experiment is to know the influence of oils on rubber bounding. However, the additives can influence rubber bounding [168]. Although additives were the same for all samples, the type of oils is changed, so mainly assumed that oil can influence the rubber-bound. There are two types of rubber-bound surfaces occluded by carbon black, as shown in Figure 33 (left), where the primary layer is a tight layer and mostly does not go in a solvent (e.g., Toluene).

When the carbon black is added to rubber chains, the chains partially bonded to the active center available on the surface of carbon black (see Figure 11). The widely accepted insoluble rubber determination method is bound-rubber fraction, which is calculated according to Equation 15 [169].

$$\text{Bound-rubber fraction} = \frac{m_2 - m_1 * c_R}{m_1(1 - c_R)} \quad (15)$$

Here, mass  $m_1$  resembles the rubber compound before extraction, which is the sum of the mass of the insoluble rubber part and carbon black.  $c_R$  is the weight ratio of carbon black in raw rubber mixture.  $m_2$  is the mass of rubber-filler gel, which is the sum of the insoluble rubber part and the mass of carbon black after extraction.

Oil was used in this thesis with rubber and carbon black, making the investigation complex for bound-rubber determination. It is a reason to select another suitable method of bound-rubber investigation. To find the fraction of rubber in rubber-filler gel named so-called rubber-layer  $L$ , which is defined as the mass fraction of rubber retained in the extracted compound, and an extraction method to determine the rubber-layer  $L$  according to methods used in previous studies [36,37,169,170]. This thesis followed rubber-layer  $L$  determination method to investigate the bound-rubber fractions of oil-enriched raw rubber mixtures [4].

The investigation was done in the immersion lab of Merseburg University of Applied Sciences. According to the method, the uncured rubber mixture of around 0.1 g was stored in 100 ml toluene at  $23^\circ\text{C}$  for seven days. After that, the solution was thrown from the flask, and the rubber-filler

gel was taken out and dried in an oven with a temperature of 70 °C for 3 h to a final mass. A schematic diagram of rubber-layer  $L$  measurements is presented in Figure 33.

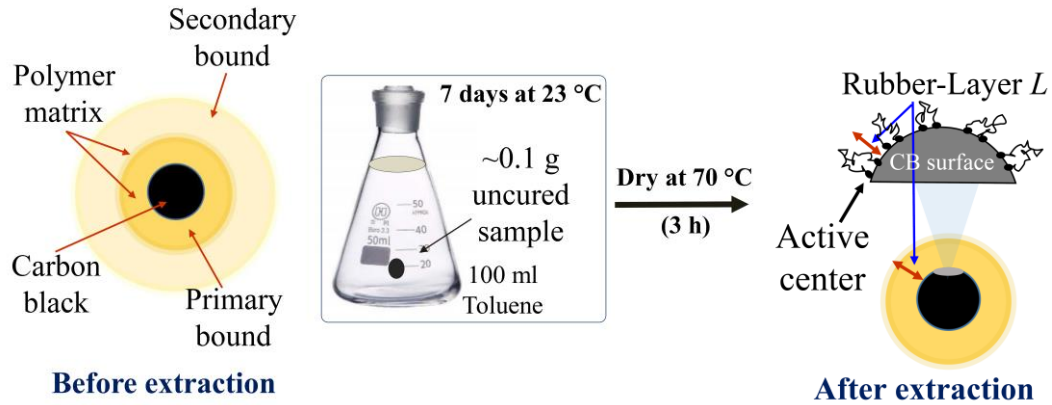


Figure 33: Schematic diagram of rubber-layer  $L$  measurement method

At least three measurements were carried out for each sample for precision. Rubber-layer  $L$  was calculated using Equation 16 [36].

$$L = \frac{m_2 - m_1 \cdot c_R}{m_2} \quad (16)$$

The mass  $m_1$  corresponds to the rubber compound before extraction, which is the sum of the mass of the undissolved rubber part, the mass of the soluble rubber, oil, and carbon black.  $m_2$  is the rubber-filler gel's mass, the sum of the undissolvable rubber part, and the carbon black's mass.  $c_R$  is the weight ratio (see Equation 17) of carbon black. Here  $m_{CB}$  is the mass of the carbon black,  $m_R$  is the mass of rubber,  $m_O$  is mass of oil in the rubber matrix and  $m_A$  is the mass of other additives including crosslinking agents and antioxidants.

$$c_R = \frac{m_{CB}}{m_{CB} + m_R + m_O + m_A} \quad (17)$$

## Determination of the network density and modulus by using DQ NMR spectroscopy

The aim of this characterization was to investigate the influence of crosslink density of elastomers when it is mixed with oils. The double-quantum (DQ) NMR spectroscopy method was used to characterize the crosslinking behavior of the elastomers. The characterization method was applied according to a previous study [121]. It introduces first a tail subtraction from the so-called sum/difference intensities in the DQ experiment, where possible, to find how much signal (proton percent) in the sample is due to elastically inactive material. It is also possible to distinguish shorter and longer relaxation time  $T_2$  and associate this with highly entangled material, which was defined as polymeric defects. A high polymer defect means more mobile material, and this contains chain ends, low-MW-sol), and the numbers are tail fractions. Consider the tail fraction then used the remaining reference intensity to remove the relaxation effect from double quantum curve and this gives the residual dipolar coupling ( $D_{res}$ ). The crosslink density in NMR units  $D_{res}/2\pi$  (unit in kHz) fitted to the normalized DQ build-up curves.  $D_{res}$  is the structural restraints that become available upon the partial orientation of the molecules in the magnetic field [171], which refer only to the network component and its proportional to crosslink density  $\nu$  [35,172] and  $E$  as Equation 18.

$$E \propto D_{res} \propto \nu \quad (18)$$

$D_{res}$  showed a linear relationship with the  $\nu$  of unfilled SBR, as shown in Figure 34 (b), with a slope  $A_{NMR}$  of  $1.027 \times 10^{27} \text{ m}^{-3} \text{ kHz}$ . Thus, to determine  $\nu$  of the filled SBR,  $D_{res}$  was multiplied by  $A_{NMR}$ . Subsequently, Equation 19 was used to calculate  $G$ , here  $k$  is Boltzmann constant  $1.38 \times 10^{-23} \text{ JK}^{-1}$ , and  $T$  is temperature.

$$G = \nu kT \quad (19)$$

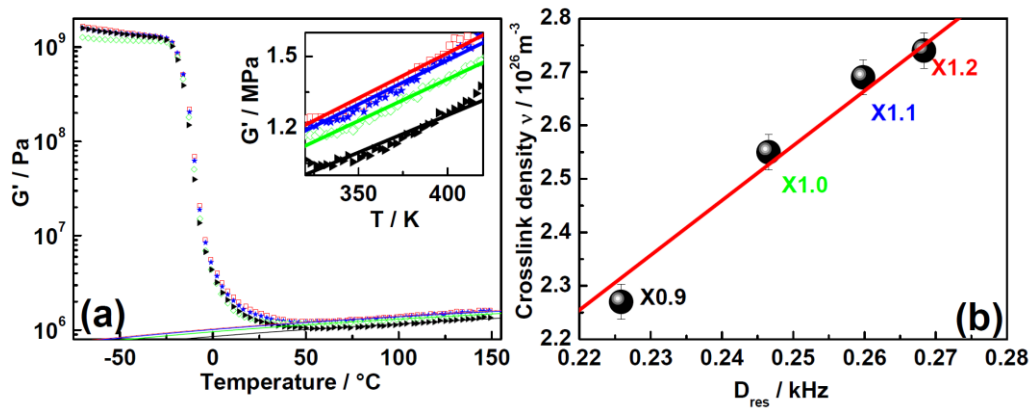


Figure 34: Crosslink density measured by dynamic shear measurement (a) as a function of residual dipolar coupling from DQ NMR measurements (b), reproduced with permission from ref [35]

The relationship between  $G$  and  $E$  is shown in Equation 20. Crosslink density  $\nu$  of filled SBR is incorporated into Equation 21 to calculate  $E_{NMR}$ . Furthermore,  $E_{NMR}$  of the SBR matrix can be determined by multiplying the volume fraction of rubber ( $\phi_R$ ).

$$E = 3G \quad (20)$$

$$E_{NMR} = 3\nu kT \quad (21)$$

In contrast to the investigation on NBR, wherein the availability of data  $A$  was not available, the present study relies solely on the utilization of qualitative data derived from  $D_{res}$  measurements using DQ NMR techniques.

According to a previous study [171], the elastomer was round cut and placed into an NMR tube to be prepared for the sample. The sample was punched into 8 mm diameter and put them into an NMR tube. The thickness of the sample was not more than 8 mm. After that, the samples were sent to Uni Halle for further analysis. The whole experimental part was done in solid-state NMR lab in Martin Luther University Halle-Wittenberg, under the supervision of prof. Kay Saalwächter. The experiment was conducted at 100  $^{\circ}\text{C}$  on a Bruker minispec mq20 spectrometer operating at 0.5 T (20 MHz). The  $90^{\circ}$  and  $180^{\circ}$  pulses had a length of 1.7 and 3.5  $\mu\text{s}$ , respectively, and dead time was 12  $\mu\text{s}$ . The analysis of the DQ curves assumes a bimodal distribution. In the NBR series, there is always a minor component with very high residual dipolar coupling ( $D_{res}$ ), from a small solid-like fraction, either something absorbed to filler or some additive that is still solid at the measurement temperature of 100  $^{\circ}\text{C}$ . Nevertheless, this fraction is always less than 5 % and was ignored. In SBR, the bimodal fit gives a marginally better fitting quality, but the results are not very conclusive. The monomodal fit results are generally satisfactory. However, it is hard to compare these results between NBR and SBR as they are chemically very different.

## Investigation of filler dispersion using an optical microscope

This measurement aimed to know about the influences of oil in elastomer matrices for the carbon black dispersion. The samples are prepared by cutting with a sharp metal razor, as shown in Figure 35 (a); the smooth cross-section surface parallels fit on the glass slide with gum and then focused on the place of the optical microscope. The optical microscope Leica DM 2700M was used to get a photo of the sample's cross-sectional view. The experiment was done in the microscopy lab at Polymer Service GmbH Merseburg. The observation was done at 23 °C and normal atmospheric pressure. The saturation parameter of the microscope was tuned to get the bright matrix, and dark carbon black filler, up to the filler particles, are easily visible to separate, as shown in Figure 35 (b). Each sample takes ten sharp photos in different positions to get a sound comparison among those positions.

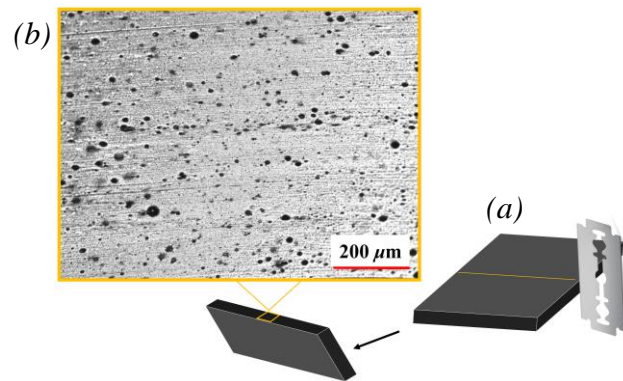


Figure 35: Schematic representation of sample cut (a), a general representation of cross-sectional view of the sample (b)

### 3.2.3 Basic thermo-mechanical and mechanical testing

#### Measurement of viscoelastic behavior of elastomers

This experiment aimed to investigate the viscoelastic behavior of plasticized elastomers. The viscoelastic behavior was analyzed using a dynamic mechanical analysis (DMA) device. According to standard ISO 6721-4 [173], the tensile vibration mode of stretching was used in this thesis. It is also called a thermo-mechanical and non-resonance method. According to standard [173], the tensile storage modulus  $E'$  represents viscoelastic materials' stiffness and is proportional to the energy stored during a loading cycle. It is equal to the elastic modulus for single, rapid stress at low load and reversible deformation. The tensile loss modulus  $E''$  is proportional to the energy dissipated during the loading cycle [173]. For example, energy loss is heat, which measures vibrational energy converted during vibration and cannot be recovered. For  $E'$  and  $E''$ , the modulus value was expressed in MPa. The mechanical loss factor  $\tan \delta$  is the ratio of the loss modulus to the storage modulus [173]. It measures the energy loss, expressed as the restorable energy, and represents mechanical damping or internal friction in a viscoelastic system. The  $\tan \delta$  is a dimensionless number, and a high  $\tan \delta$  value indicates a material with a high nonelastic strain component, while a low value indicates a more elastic one. The relation between  $\tan \delta$ ,  $E'$ , and  $E''$  is expressed in Equation 22. If the material is purely elastic, the stress and deformation phase,  $\delta = 0$ . The general viscoelastic behavior of elastomer is shown in Figure 36, where the  $T_g$  is pointed at the peak of the  $\tan \delta$  curve. This figure is a typical viscoelastic curve for filled elastomer. Rubber matrix value is entropy elastic, and it goes up with heating and due to filler network softening, it goes down. The viscoelastic data from DMA investigation can be compared with stress at 200 %

strain  $\sigma_{200}$  which is a value that characteristic for large deformation where the filler network is broken down (Payne effect).

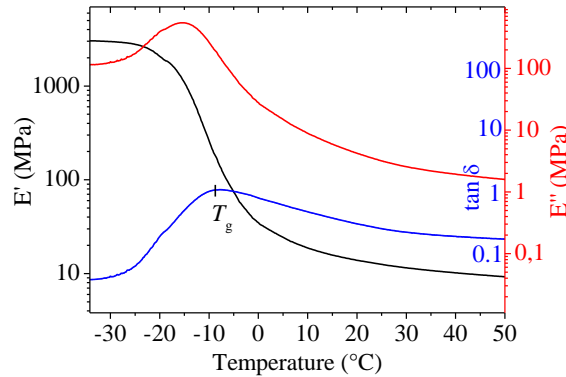


Figure 36: Typical dependence of the storage modulus  $E'$  (black), loss modulus  $E''$  (red), and mechanical loss factor  $\tan \delta$  (blue) of an elastomer, determined in a DMA experiment

$$\text{Tan } \delta = \frac{E''}{E'} \quad (22)$$

According to the standard [174], the following specimen dimensions were used: length 30 mm, width 5 mm, and thickness 2 mm. In this thesis, the device Eplexor 500 N (Gabo Company) was used in the thermo-mechanical laboratory at Polymer Service GmbH Merseburg. Temperature range was controlled between  $-70^{\circ}\text{C}$  to  $+70^{\circ}\text{C}$ , with a frequency of 10 Hz, strain 0.2 %, and the heating rate was 1 K/min. The information about  $E'$ ,  $E''$ , and  $\tan \delta$  was directly received from the PC software and plotted in Origin software.

## Testing methods for mechanical properties of elastomers

### Tensile test

The tensile test was used to measure the stress-strain behavior of plasticized elastomers, and it is the fundamental test in mechanical material testing. The tensile behavior investigation was done in the mechanical analysis lab in Polymer Service GmbH Merseburg, where the international standard ISO 37 [175] was used for the investigation. Zwick Z020 (ZwickRoell, Ulm, Germany) was the testing machine applied for this investigation. According to standard [175] type 2 (S2) dumb-bell specimen where length was 75 mm, width for the narrow portion was 4 mm and thickness 2 mm has chosen for the testing (see Figure 37). An extensometer was connected to the device while the measurement was done. All this measurement process has done at  $23^{\circ}\text{C}$ , and the testing parameters were: crosshead speed  $v_T$  200 mm/min, clamping pressure 5 bars, clamp distance 50 mm, preload 0.5 N, and measuring ranges standard 20 mm. Always five specimens were tested for each type of elastomer vulcanizates.

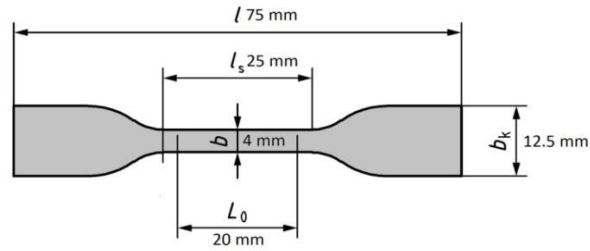


Figure 37: Specification of the dumb-bell-shaped type 2 test specimens for tensile test, photo reproduced with permission from ref [176]

The exemplary stress–strain curve is shown in Figure 19, and this curve describes some essential information on the tensile test, including the tensile strength  $\sigma_m$ , strain at break  $\varepsilon_B$ , and stress at  $x$  % strain  $\sigma_x$  were directly obtained from the experiment protocols, which is generated by PC software.

### Tear resistance

The tear test determines the resistance that an elastomer exerts against tear propagation under tensile loading, and this is the aim to get the tear resistance properties of plasticized elastomeric materials. The tear strength  $T_S$  is a certain material parameter that depends on the composition of the material, structure, and morphology. The standard of tear tests is DIN ISO 34-1 [177], and according to the previous study [133,141,178], the number of specimens used is five in a series to get precise tear resistance behavior. The tear resistance analysis was done in the mechanical analysis lab in Polymer Service GmbH Merseburg, and the universal testing machine (type Zwick Z020, ZwickRoell, Ulm, Germany) was used for this measurement. According to standard [177], a trouser-type specimen (see Figure 38) was used in this experiment where the dimension of the specimens followed its length of 100 mm, the width of 15 mm, and thickness of 2 mm. The whole experiment was done at 23°C room temperature, and the following test parameters were maintained: preload 0.5 N, clamp distance 50 mm, test speed 100 mm/min. After finishing the experiment, the protocol was generated by the software, which informed about the load-clamp distance diagram as shown in Figure 39. The average load  $F_M$  was determined from the curve, and after that, tear strength  $T_s$  were calculated using Equation 23. Here,  $B$  is the thickness of the specimen. However, the software did these measurements and calculations, so there is no need for those further calculations.

$$T_S = \frac{F_M}{B} \quad (23)$$

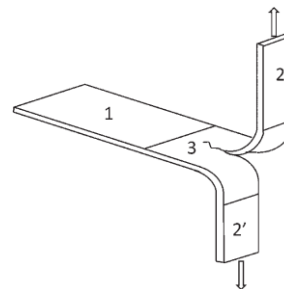


Figure 38: Geometry of the trouser test specimen for the tear test, photo reproduced with permission from ref [179]

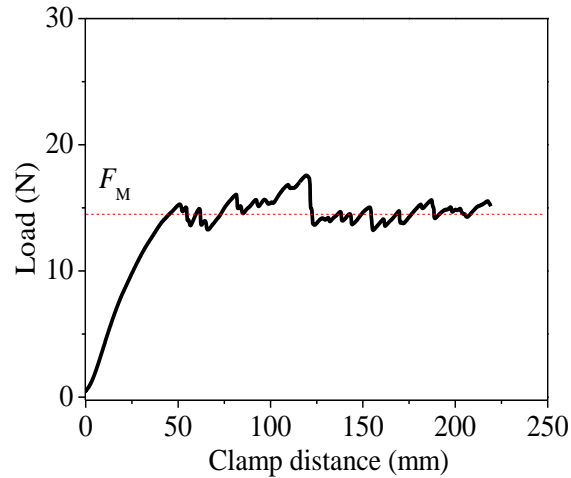


Figure 39: Load-clamp distance curves of tear tests

### Hardness test

The aim of the hardness measurement in this thesis was to investigate the hardness behavior of elastomers when they were mixed with different oils. The hardness test is among the most often applied mechanical material testing methods, and it is defined as the resistance of the material to permanent indentation. There are two common methods that can be applied for the hardness measurement of elastomers, Shore A hardness and International Rubber Hardness Degree (IRHD-M), here “M” for micro. In this thesis, both methods were applied but there are no significant differences observed in hardness of elastomer samples. So, for the detail discussion, only Shore A is selected. Shore A hardness and IRHD-M are both commonly used methods for measuring the hardness of elastomers, but they differ in their measurement techniques and the properties they assess. Measurement Principle of Shore A hardness is based on indentation hardness, where a durometer with a specified geometry and spring-loaded indenting foot is pressed into the elastomer sample, and the depth of penetration is measured. The result is given as a numerical value on the Shore A scale. In contrast, IRHD-M is based on the determination of the indentation depth of an indenter under a fixed load. The indenter is pressed into the sample, and the resulting indentation depth is measured. Indenter Geometry of Shore A Hardness is using a conical-shaped indenter with a specified apex angle. Whereas IRHD-M uses a spherical indenter. Applied load for Shore A Hardness using a spring-loaded system, typically 1 kg. A fixed load is applied for IRHD-M, and usually 5 kg. The sample thickness should be at least 6 mm to ensure accurate results for Shore A hardness. For IRHD-M, the sample thickness is typically around 2 mm. Measurement Units for Shore A Hardness are reported as a numerical value on the Shore A scale, ranging from 0 to 100. IRHD-M is reported as the IRHD scale of ranging from 0 IRHD to 100 IRHD. Shore A hardness and IRHD-M differ in their measurement principles, indenter geometry, applied force, sample thickness requirements, and measurement units. Both methods provide valuable information about the hardness of elastomers, but the choice between them depends on the specific requirements and characteristics of the material being tested.

Figure 40 shows the schematic test setup for hardness testing according to Shore A. It is a durometer that uses a spring-loaded indenter with a conical tip (*a*) to penetrate the surface of the elastomer being tested. The applied load (*F*) of the indenter was 1 kg and a truncated cone with an end face of  $0.79 \pm 0.01$  mm in diameter and an included angle of  $35 \pm 0.25^\circ$  is used as the indenter to determine the Shore A hardness. The durometer measures the depth of penetration of the indenter

( $h$ ), which is directly related to the hardness of the elastomer. The measurement with higher values indicating higher hardness.

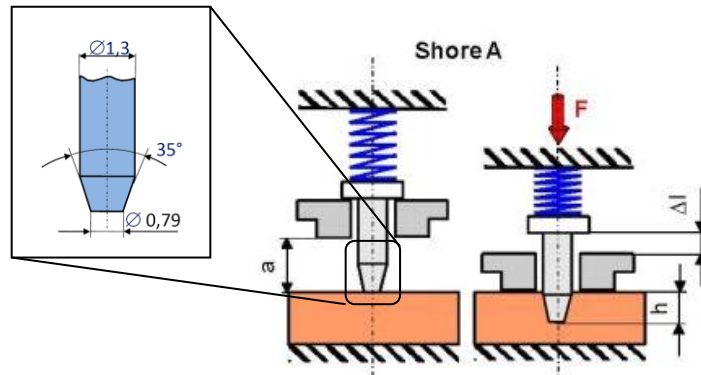


Figure 40: Schematic test setup for hardness testing according to Shore A, photo reproduced with permission from ref [181]

Shore A hardness measurement was performed according to the standard DIN ISO 7619 [180] and the measurement was done in the mechanical testing lab of Polymer Service GmbH Merseburg. The device used for the Shore A hardness measurement was Shore A durometer type 7206.H04, ZwickRoell, Ulm, Germany.

There was no specific shape maintained of the specimens except its thickness, and during this whole measurement, the sample thickness of  $\sim 6$  mm was used. The measurement was done at  $23$  °C, and the testing time was three seconds. There were five single measurements done for each sample in different positions. The individual hardness value in the Shore A scale, including the average Shore A value and standard deviation, was recorded by the software written on the protocol.

The relation between Shore A hardness and elastic modulus of elastomer can be described by the Gents[182] Equation 24. Here  $E$  is elastic modulus in MPa,  $S$  is Shore A hardness.

$$E = \frac{56 + 7.66S}{0.137505(254 - 2.54S)} * 0.0981 \quad (\text{MPa}) \quad (24)$$

In the plasticized elastomers, the relationship between Shore A hardness and modulus of elasticity is complex and non-linear compared to unplasticized elastomers, because the plasticizers are improving the flexibility and processing properties although they affect filler network. The modulus of elastomers is influenced by the crosslink density or bonding between polymer chains, as well as the type and concentration of plasticizers used. So, the modulus of a plasticized elastomer may not be directly proportional to its Shore A hardness. The plasticizer content in the elastomer affects the elastomer's ability to resist indentation, which in turn affects the measured Shore A hardness value. At low plasticizer concentrations, the Shore A hardness value is often used as an approximate measure of the material's modulus. However, as the plasticizer content increases, the Shore A hardness becomes less indicative of the elastic modulus, and other tests such as tensile testing or dynamic mechanical analysis (DMA) are needed to determine the material's true modulus.

### Compression set test

The Compression set (CS) measures a material's elasticity after prolonged compression to characterize the material behavior under a permanent compression, which can be related to ambient



conditions or elevated temperatures. The CS is a characteristic parameter for elastomers, thermoplastic elastomers (TPE), or mainly for sealing materials. The results are used to determine the tendency to leak in service. The aim of this experiments the study to investigate the influence of CS behavior when oil is mixed in an elastomer matrix. According to a previous study [183], the higher the CS, the higher the risk of a leak, which influenced measuring CS behavior as an additional characterization. This method is designated for elastomers with hardness in the range of 10 IRHD to 95 IRHD [184]. A slightly different material composition was applied for this experiment, as shown in Table 6. The standard DIN ISO 815-1 [184] is used for CS investigation, and according to the study, two types of specimens can be used. In this work, the CS test was performed on a standard test specimen type *B* of the cylindrical shape of  $13 \pm 0.1$  mm diameter and  $6.3 \pm 0.5$  mm thickness. The experiment was done in the mechanical testing lab in Polymer Service GmbH Merseburg. The compression apparatus consists of compression plates, steel spacers, and clamping devices (see Figure 41). The compression plates are flat, highly polished stainless-steel plates and smooth surfaces. The test specimen was placed between the compression plates with the spacers on each side, allowing enough approval for the rubber bulging when compressed. The bolts were tightened so that the plates are drawn together uniformly until they contact the spacers.

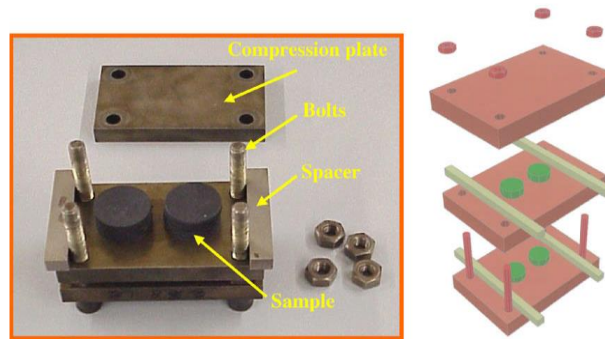


Figure 41: Compression set device, photo reproduced with permission from ref [16]

The percentage of the compression employed was 25 % of the original thickness [16]. The compression duration of 24 hours was used for this work with a surrounding temperature was 23 °C. The specimens are taken out from the compression plate after 24 hours and waited for 30 minutes as the specimen's recovery time. Afterward, the residual thickness of the specimens was measured, and the CS was calculated, according to Equation 25. Here  $t_0$  is the thickness of the sample before compression, where  $t_i$  is the thickness of the sample after recovery, and  $h_s$ , is the height of the spacer.

$$\text{CS (\%)} = \frac{t_0 - t_i}{t_0 - h_s} * 100 \quad (25)$$

### Rebound resilience

The aim of this experiment is to know how the oil has influenced the rebound resilience in the elastomer matrix. Rebound resilience is defined as the ratio of energy returned to energy applied. Generally, rebound resilience is how much kinetic energy a rubber specimen gives back after an impact trial. When rubber is deformed, it absorbs energy, partly recovered when it regains its original shape. The energy which is not restored as mechanical energy is wasted as heat in the rubber. This test was performed according to the standard DIN 53512 [185]. A Hess Werkstoffprüfgeräte (Richard Hess MBV GmbH, Germany) device was used to determine the rebound resilience. The specimen was prepared for this experiment according to standard [185] by cutting

into a round shape and keeping its dimensions of 15 mm and 12.5 mm in thickness. The device consists of an arm and a hammer, including an indenter with a hemispherical surface (see Figure 42).

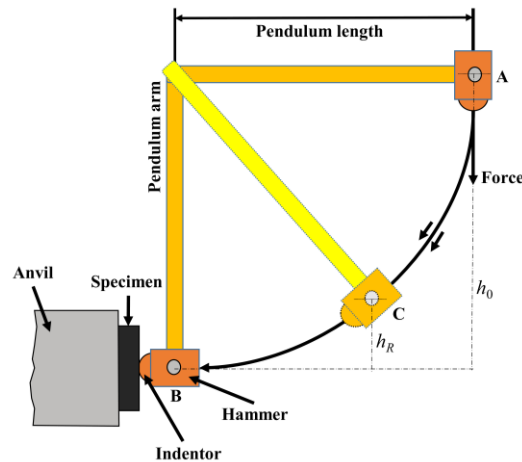


Figure 42: Principle of test apparatus, photo reproduced with permission from ref [185]

The investigations were done at atmospheric pressure and maintained in the room at 23 °C in the elastomeric lab at Merseburg university of applied sciences. The pendulum was hung so that it oscillated circularly under the effect of gravity. The hammer was raised at an angle of 90° from its resting position. After placing the specimen on the anvil with the holder, the pendulum was allowed to fall from the horizontal position. It strikes six times at the same point on the test piece and is caught each time before it impacts again. The first three impacts serve to mechanically condition the specimen, and the last three establish its rebound resilience. The median of the last three readings was determined. According to the test, resilience was established as the ratio of the height of the pendulum to the height of the fall. The rebound resilience is calculated as a percentage according to Equation 26.

$$R = \frac{h_R}{h_0} * 100 \quad (26)$$

Here  $R$  is rebound resilience,  $h_0$  is the height of fall, which is counted as the height between parked hammer position A as shown in Figure 42 and the point where the hammer strike the position marked B.  $h_R$  is the rebound height means the height between returned hammer height after strike marked as C and point where hammer struck position B. The arithmetic mean of the rebound resilience was calculated from the averages for two specimens.

### 3.2.4 Resistance against crack behavior measurement methods

#### Quasi-static fracture mechanics measurement (in-situ) method

A fracture mechanics test under quasi-static loading conditions described in the literature [143,186] was adopted to characterize the influence of the compound composition on the fracture behavior. The aim of this thesis is to find the resistance against crack initiation and propagation under quasi-static loading. Stable crack propagation occurs if the energy wasted, in a material-specific way, compensates for the surplus of available energy caused by crack propagation [139]. When the external mechanical loading is stopped and there is no further growth, the case for cracks is in the linear range of the crack growth curve. Two test procedures are possible for the experimental determination of the resistance against stable crack initiation and propagation under quasi-static

loading: a single-specimen and multiple-specimen method. These specimens techniques were described in previous studies [141,187,188]. In this thesis, single-edged notch tensile (SENT) specimen was used which followed previous studies [143,186]. In the context of SENT specimens for elastomers, the single specimen method offers several advantages over other testing methods: Traditional fracture mechanics testing methods typically require multiple specimens to be tested at different crack lengths to generate a complete stress-strain curve. With the single specimen method, only one specimen is needed to generate a complete stress-strain curve and determine the fracture toughness of the material. This can result in a significant reduction in testing time and cost. The single specimen method can be used to directly measure the fracture toughness of the material. This can result in increased accuracy and reliability of the test results. The single specimen method requires less material than traditional testing methods, which can be especially beneficial for elastomers, which can be expensive and difficult to manufacture in large quantities. The single specimen method can be used to test materials under a variety of loading conditions, including mode I tension as shown in Figure 43. The geometric function  $\eta$  for the SENT test configuration was calculated [189,190] to be  $\sim 1$  in compliance with a previous study by Kim [191]. In this study, the crack was created by Mode I, and this means a simple crack opening characterized by the symmetrical lifting of the opposite crack edges, so tensile stress applies to the plane of the crack. A universal testing machine (type ZwickZ020, Zwick Roell, Ulm, Germany) was used for the investigation. The SENT specimen was prepared according to the dimensions of 100 mm length  $\times$  25 mm width  $\times$  6 mm thickness and  $\approx 5$  mm notch (see Figure 44).

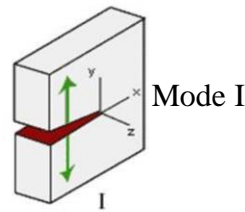


Figure 43: Asymmetrical lifting of the opposite crack edges named mode I, photo reproduced with permission from ref [192]

In contrast to an unstable crack, a stable crack grows under energy consumption and is characterized by a comparably low speed. At the beginning of energy balance at the crack, some authors [193,194] have developed a practical model to determine stable crack propagation. In Figure 44, a sequence of photographs of the deformed specimen (view into the open notch) is shown, and here the left picture shows the state before crack initiation, and the other images the increasing crack opening after crack initiation. The advantage of the single-specimen method is the comparatively low time and material consumption. In this thesis, the test was done at 23 °C, and the testing speed was 50 mm min<sup>-1</sup> applied. The crack opening was monitored with the camera after a time interval. The specimen was well clamped with the clamp and set the camera on the notch spot. Then every click was done after a 10-second interval to complete the fracture when running the test. The crack opening time is determined by observing the notch tip by the eye. It is defined as when a new crack surface is visible over the whole thickness of the specimen. The software has recorded energy consumed during crack propagation, which is analyzed in a computer, measuring the crack length and deformation.

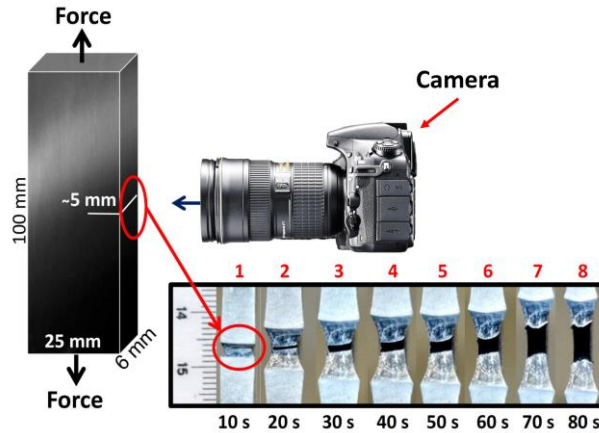


Figure 44: Schematic diagram of SENT specimen and crack opening under quasi-static load

The minimum energy required to initiate the crack is defined as the resistance against the crack initiation  $J_i$ . Crack resistance curves ( $R$ -curves) as the basis for the quantitative characterization of the materials after manual crack length calculation was prepared where the crack resistance values  $J$  (see Equation 27) were determined, which informed the resistance against the crack initiation  $J_i$  and propagation  $T_J^*$ .  $\eta$  is a geometric function,  $B$  is the thickness of the specimens,  $A$  is the energy consumed during crack initiation and propagation,  $W$  is the width of the specimen, and  $a$  is the initial length of the notch. A schematic  $R$ -curves from a single-specimen test is shown in Figure 45, where the slope  $dJ/d(l_R)$  at the crack opening  $l_R$  of 0.5 mm was determined by Equation 28, and it is a quantitative measure of the resistance against stable crack propagation  $T_J^*$  at 0.5 mm of crack open. In this thesis,  $T_{J,0.5}^*$  has been determined from  $R$ -curves by measuring the slope of  $J$ -values at crack open between 0.5 mm to 1 mm.

$$J = \frac{\eta A}{B(W-a)} \quad (27)$$

$$T_J^* = \frac{dJ}{d l_R} \quad (28)$$

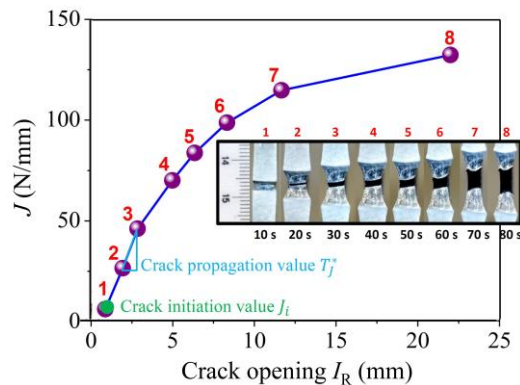


Figure 45: Schematic representation of an  $R$ -curve from the quasi-static fracture mechanics test and an increasingly loaded specimen during a fracture mechanics test, photo reproduced with permission from ref [187]

### Instrumented tensile impact testing method

The instrumented notched tensile-impact test is used to determine the toughness properties of elastomeric materials. The instrumented notched tensile-impact test (ITIT) is a well-known method for characterizing the toughness of elastomers, and this method was applied mainly to crack behavior test on elastomers [34,142,195,196]. Previous studies [197–203] show that the instrumented notched tensile-impact test is a helpful tool to describe the material properties regarding resistance against unstable crack propagation  $J_d$ . The instrumented notched tensile-impact test is an expansion of the conventional notched tensile-impact test according to ISO 8256 [204] and MPK-ITIT [205] and is performed with specimens with razor-blade notches. During the specimen's loading, load-time information was recorded. The analysis of instrumented tensile impact test was done in the fracture mechanics analysis lab of Polymer Service GmbH Merseburg under supervision of Prof. Katrin Reincke. The test is performed with the pendulum device Resil Impactor Junior 25, according to ISO 13802 [206]. This pendulum device has a working capacity of 7.5 J at a 150° falling angle. For the test, a specimen is fixed between a stationary clamp and a crosshead. Double-edge-notched tension (DENT) specimens were applied in this experiment. According to MPK-ITIT [205], DENT specimens with following dimensions: width  $W = 10$  mm, length  $L = 64$  mm, and thickness = 2 mm, and 10 specimens were used for the each series. This thesis was based on the crack by Mode I (see Figure 43). The notching is cut with metal blades, by a pneumatic notching device on the narrow sides of the specimen up to an initial crack length of  $\sim 2$  mm, which means  $\sim 1$  mm at each side.

The measurements were carried out in a normal atmosphere according to ISO 291 [207] with a temperature of 23 °C as used previous study [208]. The specimens were fixed parallel between the stationary clamp and the crosshead in a way that the pendulum hammer hits the crosshead at the lowest point of the circle motion. The initial gauge length was 30 mm, and the notches were made in the middle of the specimens. Experiments with elastomers were performed at a falling angle of 150°; this corresponds to a hammer speed of  $3.7 \text{ ms}^{-1}$ . By this means, the specimen is deformed in the direction of its longitudinal axis until a fracture occurs. After releasing the pendulum hammer moves in a circle and transfers part of its kinetic energy to the crosshead and indirectly to the specimen at the lowest point of its trajectory. The metallic pendulum hammer consists of a cylindrical pendulum arm and an impact construction with metallic blocks at both sides, which meet the crosshead.

Load ( $F$ )-time ( $t$ ) signal is realized over a piezo load cell integrated into the stationary clamp was recorded. From the  $F$ - $t$  diagrams, the deformation was calculated from Newton's second law. In the first integration step in Equation 29, the velocity has been determined, and in the second integration step shown in Equation 30, the extension  $l$  of the specimen is a function of time.

$$V(t) = V_0 - \frac{1}{m} \int_0^t F(\tau) d\tau \quad (29)$$

$$l(t) = \int_0^t V(\tau) d\tau \quad (30)$$

The  $F$ - $t$  signal is transferred to a computer over a data acquisition system. Using the software DAS4Win, one can display and analyze load-time diagrams. In Figure 46, one can see a schematic  $F$ - $l$  diagram of materials. Such diagrams are analyzed by determining the maximum load  $F_{\max}$  and the extension at  $F_{\max}$  -  $l_{\max}$ . The area under the  $F$ - $l$  diagram is divided into two parts which is a energy up to the highest load  $A_{\max}$  and a so-called crack propagation energy  $A_p$ .

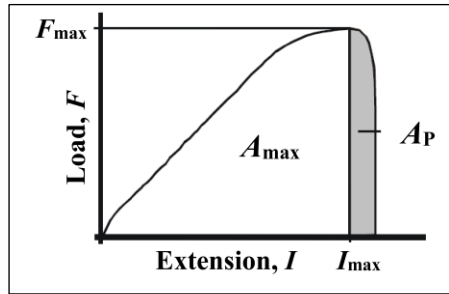


Figure 46: Characteristic load-extension diagram with crack propagation energy ( $F_{\max}$ - maximum load;  $l_{\max}$  - maximum extension;  $A_{\max}$  - energy up to  $F_{\max}$ ;  $A_P$  - crack propagation, photo reproduced with permission from ref [205]

After the test, the recorded load-extension diagram was displayed as Figure 47 (right), and in the beginning highest load  $F_{\max}$  and extension at the highest load  $l_{\max}$  were calculated. Additionally, energy  $A_{\max}$  (corresponds to the area under the diagram up to  $F_{\max}$ ) and crack propagation energy  $A_P$  were specified.

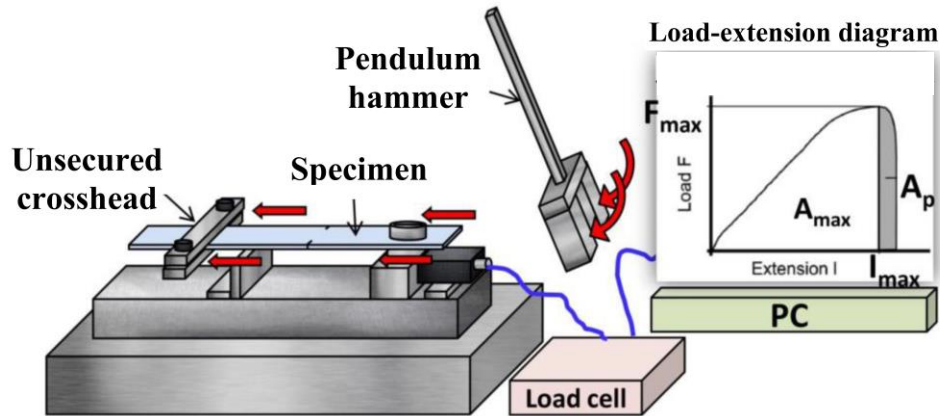


Figure 47: Schematic representation of fracture mechanics testing device for performance of instrumented notched tensile-impact tests

The geometric function  $\eta$  was calculated [138,141] from Equation 31, where  $a$  is the initial notch length, and  $W$  is the width of the specimen. For unstable crack propagation value characterization of polymers with thermoplastic and elastomeric matrix according to this procedure, the resistance against unstable crack propagations is calculated by the following material parameter  $J_d$  [208] as shown in Equation 32. Here  $A_{\max}$  is the energy consumed up to a maximum load of  $F_{\max}$ .  $B$  is the thickness;  $W$  is the width and  $a$  is the initial notch of the specimen.

$$\eta = -0.06 + 5.99 \left(\frac{a}{W}\right) - 7.42 \left(\frac{a}{W}\right)^2 + 3.29 \left(\frac{a}{W}\right)^3 \quad (31)$$

$$J_d = \frac{\eta A_{\max}}{B(W-a)} \quad (32)$$

### 3.2.5 Aging behavior of plasticized elastomers

This investigation was done to know about the aging behavior of oil mixed elastomer vulcanizates. According to a previous study [14], elastomers are easily oxidized and exhibit crosslink reactions under high temperatures. Aging is a normal phenomenon of materials, and aging depends on

different parameters (e.g., temperature, moisture, pressure), including material property [209]. So, this thesis focused on the aging of oils and oil mixed elastomers individually. In the beginning, the oil was poured into a transparent glass bottle, then closed the lid and stored in a hot air oven for six months. The oven temperature was maintained at around 40 °C with circulated air. After finishing six months, the bottle was uncapped, and get ready for mixing with elastomers. The mixing vulcanization and sample preparation conditions were kept the same as used, and this aged oil only replaced unaged oil.

The second part of the aging investigation was done differently; the mixing, vulcanization, and sample preparation conditions were done with unaged oil mixed elastomers. After that, the samples were prepared for aging. The samples were kept in the hot air oven to give them a chance to possible aging, and it was done in the hot air oven at 80 °C temperature for different days. In the beginning, the samples were taken out after three days and characterized the resistance against crack under quasi-static, and impact loading. Furthermore, mechanical behavior was characterized to compare these results to unaged elastomers. Aging was done for fifteen and thirty days and characterized again to inspect the aging behavior of elastomers as a function of time.

## 4 Results and discussion

### 4.1 Structure and properties of the investigated oils

#### 4.1.1 Structure analysis by FTIR and NMR spectroscopy

The modified bio-oils were investigated to identify the chemical bonds present in their chemical structures. This is one of the primary criteria to assess the chemical behavior of the oils. Various analytical techniques were exploited to obtain information about the chemical structures and functional groups, including attenuated total reflection infrared spectroscopy (ATR-FTIR) and nuclear magnetic resonance spectroscopy ( $^1\text{H}$  and  $^{13}\text{C}$  NMR).

Figure 48 shows the FTIR spectra for oils, where figure 47 (a) shows the assigned peak in the fingerprint region, and figure 47 (b) was about the assigned peak of wavenumbers from 1500 to 4000  $\text{cm}^{-1}$ . These figures showed the peaks for oils and responsible functional groups. Sharp peaks of aliphatic hydrocarbons were observed for all oils, at the region of 1460, 2850, and 2920  $\text{cm}^{-1}$ . Additionally, bending vibrations of the  $\text{CH}_2$  at 720  $\text{cm}^{-1}$  [210] and  $(\text{C}=\text{C})\text{-H}$  double bonds in the chain at 2960  $\text{cm}^{-1}$  were observed [211] for all oils. Furthermore, from these figures, glycerides bands within 800-1200  $\text{cm}^{-1}$  [212] were observed in all bio-oils, and there are overall similarities found for the bio-oils.

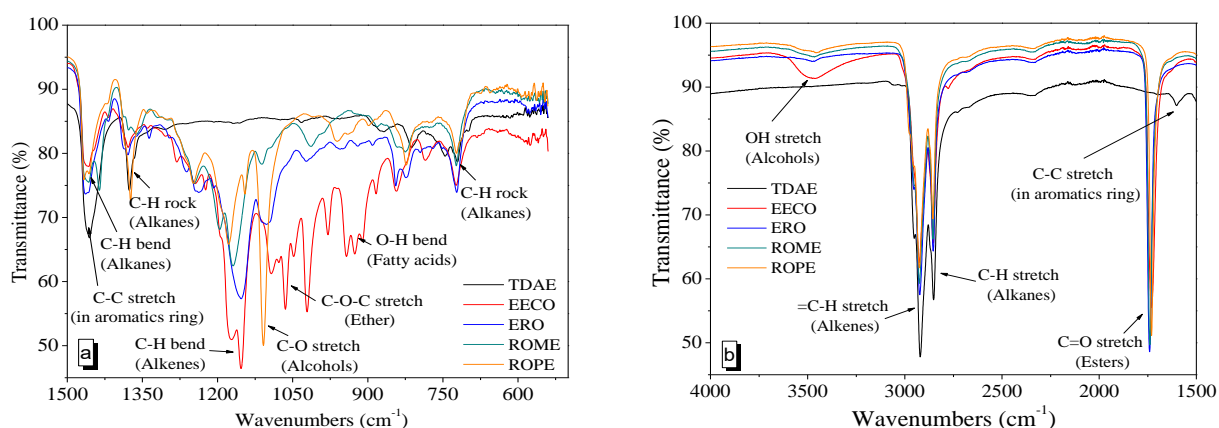


Figure 48: ATR-FTIR spectrum of plasticizers, including traditional plasticizers and bio-oils; fingerprint area (a); wavenumbers of 1500-4000  $\text{cm}^{-1}$  (b)

The epoxy group was common in all investigated bio-oils, and presented a characteristic twin band between 826 and 841  $\text{cm}^{-1}$  associated with symmetric ring deformation [213]. In addition, a distinct hydroxyl group (OH) band at 3470  $\text{cm}^{-1}$  was also observed for bio-oils, and intensity was higher for EECO. An absorption band of ether group stretching vibration ( $\text{C-O-C}$ ) in the region 1053  $\text{cm}^{-1}$  and a more intense hydroxyl band of EECO at 3470  $\text{cm}^{-1}$  [214]. However, the appearance of the -OH group peak at 3470  $\text{cm}^{-1}$ , in the case of EECO, can be associated with the decomposition of the epoxy groups. Due to the side reactions of hydrolysis and acylation taking place owing to the reaction environment (epoxidation reaction with peroxides), which contains water, mineral(catalyst), and organic acids [215], and it is confirmed by the NMR spectrum (see Figure 51).

The EECO is slightly different from the other bio-oils with many identified peaks, making it unique for non-polar elastomers like SBR. Mainly these peaks represent long-chain fatty oils with fatty acids. Contrary, ROPE has an additional  $\text{C-O}$  stretching for the alcoholic group, and these polar alcoholic groups make ROPE unique for fitting polar elastomers. The FTIR spectrum of oils exhibits several absorption peaks, as shown in Figure 49. However, in some modified bio-oils, the



peak nearly disappeared in the same range, and an additional peak appeared in the 820-850  $\text{cm}^{-1}$  range. A previous study [216] described that the characteristic signals in the FTIR spectrum at 820-850  $\text{cm}^{-1}$  represent the quaternary carbons of the epoxy ring, and this is similar to Figure 49 (a). The appearance of an epoxy peak at 820-850  $\text{cm}^{-1}$  provided evidence that the epoxidation reaction took place [160]. The disappearance of C=C bonds in the epoxide spectra further supported almost complete double bond conversion to epoxidized [115]. Figure 49 (b) represents the presence of hydroxyl groups in the bio-oils after their modification. These hydroxyl groups belong to the major fatty acid in modified bio-oil composition.

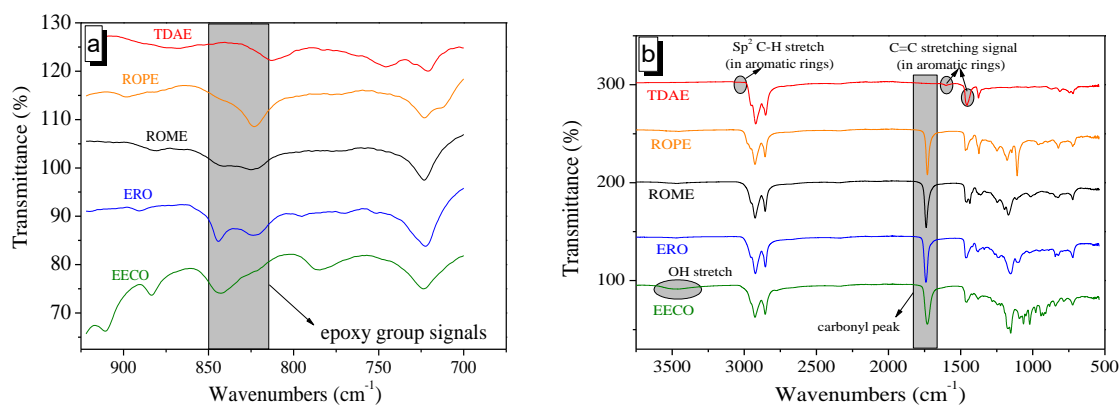


Figure 49: ATR-FTIR spectra with epoxide peaks for bio-oils (a), enlargement of the C = O signal as an internal reference of ester compound, and magnification of absorption peaks at 3400  $\text{cm}^{-1}$  is frequently diagnostic of O-H stretching (b)

$^1\text{H}$  and  $^{13}\text{C}$  NMR spectra of the oils are also collected to further confirm the structure and functional groups in oils. Figure 50 (a) represents the  $^1\text{H}$  NMR of TDAE. As obvious, the methyl group protons gave a multiplet signal at  $\delta = 0.88$  ppm, while the methylene groups presented a strong signal at  $\delta = 1.25$  ppm. Moreover, the phenyl group signals with methyl and ethyl protons appeared at  $\delta = 2.28$  and 2.55, respectively. A weak characteristic signal from the aryl groups was observed at  $\delta = 7.17$  ppm, which were also observed in the  $^{13}\text{C}$  NMR spectra of the oil at  $\delta = 128$  ppm as shown in Figure 50 (b).

These observed signals from NMR spectra also justify claims made using explained FTIR characterization where weak signals from the aromatic rings were observed above 3000  $\text{cm}^{-1}$  wavenumber, and the aromaticity [217] of TDAE is already shown in FTIR analysis (see Figure 48).

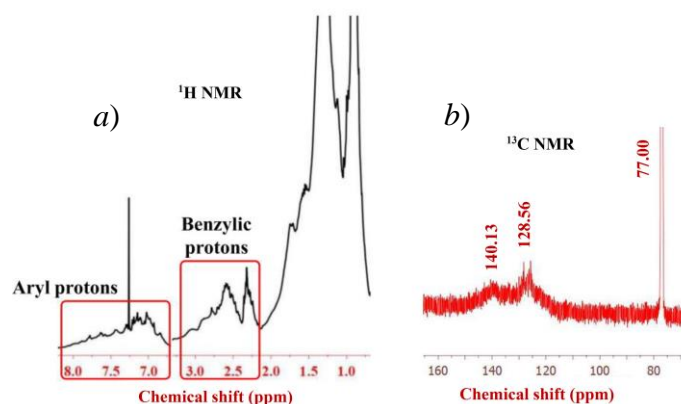


Figure 50: NMR spectrum of TDAE; Proton spectrum (a); Carbon spectrum (b)

The recorded  $^1\text{H}$  NMR spectra of bio-oils are presented in Figure 51. The characteristic multiplet signals from the protons of the epoxy group appeared at  $\delta = 2.80\text{-}3.20$  ppm [160], and the methylene group proton adjacent to the epoxy group gave a multiplet signal at  $\delta = 1.45\text{-}1.60$  ppm [6,161]. As ERO (epoxidized rapeseed oil) is a triglyceride, so the number of epoxy groups is higher in this oil which is obvious in the figure where the peak area from the epoxy group protons is highest as compared to the other investigated oils. The appearance of weak signals at  $\delta = 5.5$  ppm for EECO, and ROPE indicates the presence of unsaturation.

The appearance of hydroxyl group protons at  $\delta = 3.5\text{-}4.0$  ppm, especially in EECO, ROME, and ROPE, indicates the occurrence of the epoxy ring-opening due to side reactions taking place, as earlier explained and discussed in a previous study [211]. The appearance of aryl group protons at  $\delta = 2.39$  ppm indicates the presence of carbonyl groups in all the oils except TDAE. The tertiary proton appears at  $\delta = 5.2\text{-}5.3$ , proving that the bio-oils contain an inside glycerol structure. The methylene proton of the  $-\text{CH}_2\text{-CH-CH}_2-$  backbone appears at  $\delta = 4.1\text{-}4.4$  for all bio-oils. However, ERO has higher intensity, and EECO has medium and the terminal  $-\text{CH}_3$  groups appear at  $\delta = 0.8\text{-}1.0$  region [218] for all bio-oils types, a typical symbol of fatty oils. Nevertheless, the integrated value of the area for peaks at  $4.1\text{-}4.2$  ppm ( $-\text{CH}_2\text{-CH-CH}_2-$ ) is visible for EECO because the EECO has a partial conversion of epoxidation. All the bio-oil samples depict identical characteristic spectra at  $\delta = 5.00\text{-}5.50$  ppm all unsaturated fatty acids ( $-\text{CH}=\text{CH}-$ ) [161],  $\delta 5.20$  ppm glycerol  $\beta$ -position ( $-\text{CH-O-COR}$ ),  $\delta 4.15$  ppm glycerol  $\alpha$ -position ( $-\text{CH}_2\text{-O-COR}$ ),  $\delta 2.76$  ppm bis-allylic protons ( $-\text{CH}=\text{CH-CH}_2\text{-CH}=\text{CH}-$ ),  $\delta 2.39$  ppm all aryl chains ( $-\text{CH}_2\text{-COOH}$ ),  $\delta 2.08$  ppm allylic protons of all unsaturated fatty acids ( $-\text{CH}_2\text{-CH}=\text{CH}-$ ),  $\delta 1.63$  ppm all acyl chains ( $-\text{CH}_2\text{-CH}_2\text{-COOH}$ ),  $\delta 0.88$  ppm all acyl chains except for linolenic ( $-\text{CH}_2\text{-CH}_2\text{-CH}_2\text{-CH}_3$ ) and  $\delta 1.28$  ppm all acyl chains ( $-(\text{CH}_2)_n-$ ) [161].

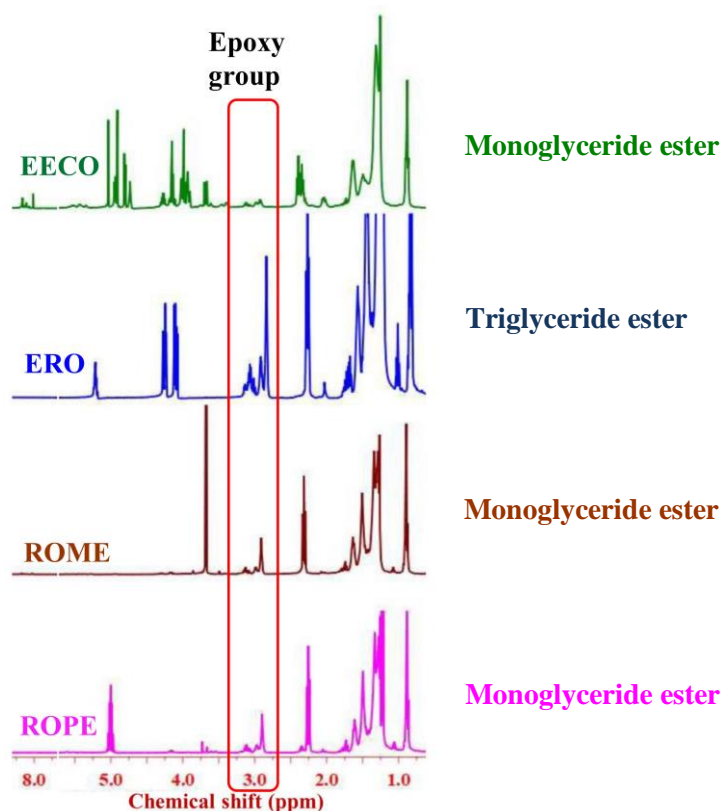


Figure 51:  $^1\text{H}$ -NMR spectra of different bio-oils with conversion intensity of epoxidized parts

The bio-oils spectra indicate that the unsaturated fatty acids were converted into epoxy groups classified as monoepoxides and diepoxides, with signals appearing at  $\delta = 2.9\text{-}3.0$  ppm (-CHOCH-CH<sub>2</sub>-CHOCH-) and  $\delta = 3.09\text{-}3.16$  ppm (-CHOCH-CH<sub>2</sub>-CHOCH-), as well as, at  $\delta = 1.45\text{-}1.60$  ppm methylene protons adjacent epoxy group (-CH<sub>2</sub>-CH<sub>2</sub>-CHOCH-) and at 2.0 ppm methylene alpha group to an acyl group (CH<sub>2</sub>-CH<sub>2</sub>-C=O-O-) [161]. However, in the EECO, ROME, and ROPE spectrum, the signals at  $\delta = 3.40\text{-}3.75$  ppm (OH-CH<sub>2</sub>-CH<sub>2</sub>-OH) methylene hydrogens bonded, -CH<sub>2</sub>-(O-CH<sub>2</sub>-CH<sub>2</sub>-O-CH<sub>2</sub>-CH<sub>2</sub>-OH) alpha-methylene group and (-CH<sub>2</sub>-CH(OH)-CH(OH)-CH<sub>2</sub>-) methine beta group [219], indicated the hydroxyl groups formation, indicating that the monoepoxide and diepoxide rings were opened.

In summary, FTIR and NMR spectra were informed about the chemical characteristics of oils, especially the aromatic characteristics of TDAE was shown, and the ratio of the epoxidized conversion of bio-oils and their glyceride ester of higher fatty acidic characteristics.

#### 4.1.2 Description of polarity, thermal behavior and molecular mass

The elastomer's surface is the first component that comes into contact with the oils. Thus, compatibility is influenced primarily by the elastomer's polarity, surface characteristics, particularly the wettability, surface chemistry of the exposed atoms, surface energy, and surface topography [220]. The polarity of oils was characterized using the contact angle of oils, these were shown in Figure 52 and 52, and measurement data were summarized in Table 7 and 8. The contact angle measurement was done on the untreated elastomer's flat surfaces, and the photo of oil drops was shown in Figure 53. The contact angle of oil drops on flat surfaces reflect the surface tension on the elastomers, and this figure proves that the wetting behavior of oils is identical for specific elastomers. The same oil has two different contact angles on the SBR and NBR. A good wetting can be measured as a low contact angle between oil and elastomer. A variation of contact angles was observed for bio-oils on the polar and non-polar elastomers. Among those bio-oils, only EECO has a lower contact angle on the non-polar SBR, and this is confirmed by the FTIR (see Figure 48) and NMR (see Figure 51) spectra because among bio-oils, EECO has a lower epoxy conversion and it has additional hydrocarbon chains this makes more non-polar behavior than a polar character bio-oils. On the other hand, the ERO and ROME have a lower contact angle on untreated NBR. It was proved that the wetting of oils used in this thesis was high on the ideal non-polar (PTFE) surface. However, it means a probability of high wetting on the polar or non-polar surfaces. The value of surface tensions and wetting conditions on PTFE surfaces were listed in Table 7.

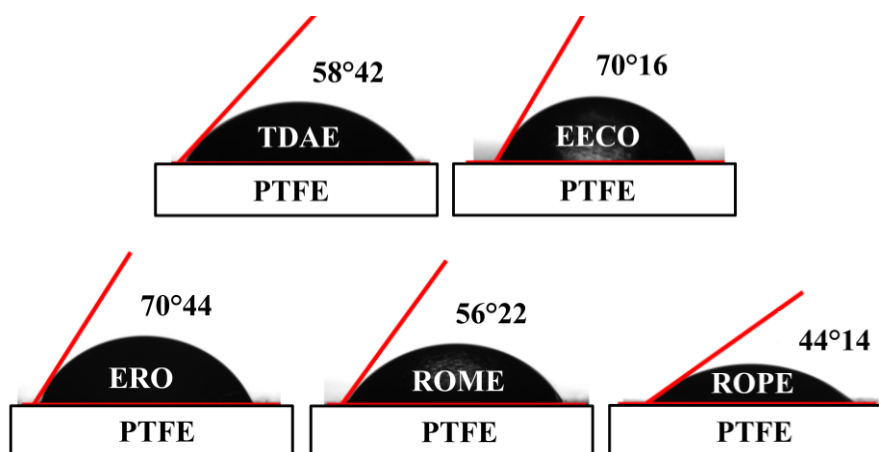


Figure 52: Contact angle of different oils on untreated PTFE surface

The EECO has a moderate contact angle on the PTFE surface, predicting good compatibility with non-polar materials. The calculated surface tension of the EECO was slightly higher than other oils. So, it is perhaps a good choice for non-polar polymers like SBR. Whereas the ROME and ROPE have comparatively lower contact angles on the PTFE surface and calculated surface tension of dispersive part was lower than others, this can be recommended to be compatible with Polar materials like NBR.

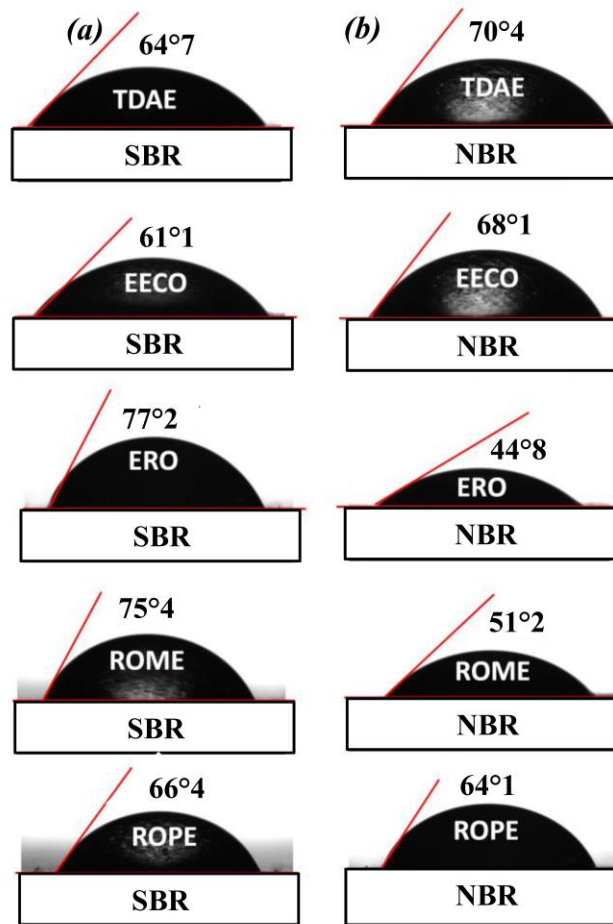


Figure 53: Contact angle of different oils on untreated SBR surface (a) and untreated NBR surface (b)

Table 8 depicts the surface tension for the correspondence contact angles of oils on the SBR and NBR surfaces. A good wetting will count if the contact angle below 90° can be measured, and according to this concept, all oil can show a good wetting on both elastomers; however, for selecting an appropriate oil for a specific elastomer, the lower contact angle and surface tension representing a good wetting [221]. Rubber-filler wetting measurement was done to measure so-called rubber-layer  $L$  to ensure the influence of the oil on rubber-filler interactions. One more point can be added here: additives containing the vulcanized elastomer can be influenced by the bounding of the plasticized elastomer. Additive concentration was identical for all samples, and the surface tension was measured on the untreated and unvulcanized elastomers. The rubbers bounding can change slightly with additives and fillers, and that is not a noticeable account.

Table 7: Contact angle and surface tension  $\sigma_L$  of different oils on PTFE surface

Oils	Contact angle	$\sigma_L$ (mN/m)
TDAE	58°42'	27.9
EECO	70°16'	34.24
ERO	70°44'	34.54
ROME	56°22'	27.00
ROPE	44°14'	23.03

Table 8: Contact angle and surface tension  $\sigma_L$  of different oils on untreated SBR and NBR surface

Oils	Contact angle ( $\theta$ )		$\sigma_L$ (mN/m)	
	SBR	NBR	SBR	NBR
TDAE	64°7'	70°4'	35.3	40.3
EECO	61°1'	68°4'	32.7	38.4
ERO	77°2'	44°8'	48.2	24.6
ROME	75°4'	51°2'	45.9	27.2
ROPE	66°4'	64°1'	36.5	34.8

Table 9 shows different physical and chemical data of oils. Information of oils regarding molecular weight  $M_W$ , density  $\rho$ , glass transition temperature  $T_g$ , and kinematic viscosity  $\nu$  were listed here. Among bio-oils, ERO shows higher  $M_W$  (1200 g/mol),  $\rho$  (1.05 g/cm<sup>3</sup>), and  $\nu$  (136 mm<sup>2</sup>/s). FTIR and NMR spectra shows the ERO was a triglyceride epoxidized ester and it was the reason for exceptional values. Whereas  $\rho$  for other bio-oils were around 1 g/cm<sup>3</sup>,  $\nu$  lies between 12-30 mm<sup>2</sup>/s and  $M_W$  350-500 g/mol. In contrast, TDAE has a lower density 0.94 g/cm<sup>3</sup> and a lower  $M_W$  309 g/mol, although it has a higher  $\nu$  375 mm<sup>2</sup>/s.  $T_g$  of bio-oil comparatively lower than TDAE, and it is correlated to the chemical structures of oils. Bio-oils are epoxidized ester of higher fatty acids, so it contains long chains, especially ROPE has iso-propyl group with epoxidized monoglyceride ester in their structure contains high free-volume, so it shows lowest  $T_g$  (-93 °C), then  $T_g$  (-86 °C) of ROME because of methyl group with epoxidized monoglyceride ester.  $T_g$  of EECO was -74 °C and ERO is a epoxidized triglyceride ester, shows  $T_g$  at - 64 °C. Although,  $T_g$  of bio-oils are significantly lower than  $T_g$  of TDAE (-50 °C).

Table 9: Chemical and physical analysis data of different oils

Oil	$M_W$ (g/mol)	$\rho$ (g/cm <sup>3</sup> ) 23 °C	$T_g$ (°C)	$\nu$ (mm <sup>2</sup> /s)	
				40 °C	100 °C
TDAE	309	0.94	-50	375.01	20.02
EECO	507	1.006	-71	30.67	7.72
ERO	1226	1.055	-64	136.6	16.55
ROME	360	1.001	-86	12.05	3.03
ROPE	403	1.005	-93	12.63	3.21

The variation of molecular weight  $M_w$  and kinematic viscosity  $\nu$  on the density  $\rho$  of oils were shown in Figure 54, and it observed that TDAE did not follow orders like bio-oils. The  $M_w$  of bio-oils were increased with increasing the  $\nu$  except for TDAE.  $\nu$  was very high for TDAE, and a previous studies [222] [223] claimed that the  $\nu$  is higher for aromatic oils than linear or aliphatic oils. So this could be the reason for TDAE having a higher  $\nu$  although it has a lower  $M_w$ . The  $\rho$  of oils increases when it has a high  $M_w$  [224]. The same trend is followed in Figure 54. So molecular weight plays a vital role in the slightly changes  $\rho$  of oils. According to a previous study [224], density and kinematic viscosity were correlated. The  $\rho$  of modified bio-oils was higher than its unmodified bio-oils. Similarly, modified bio-oils  $\nu$  was two and half times higher than unmodified bio-oils. This is perhaps due to the addition of oxygen molecules amid double bonds, thereby increasing the intermolecular forces, molecular weight, and polarity [115].

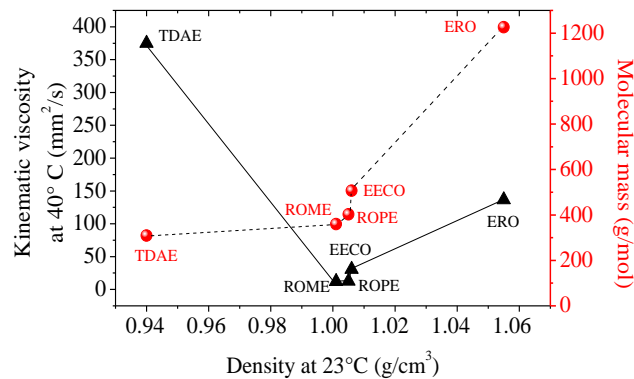


Figure 54: Dependence of kinematic viscosity and molecular mass on the density of different oils

The molar mass distribution can change the properties of a compound, especially oil-type compounds. The investigation was done using GPC analysis, and the results are shown in Figure 55. It was clear evidence that, except for TDAE, the bio-oils were multimodal distribution was shown. TDAE has a simple unimodal but broad distribution, and this means there is no fraction in a trace amount of other components in TDAE. The multi-molar distribution of bio-oils means there was no single chain component. Mostly the bio-oils showed clear bimodal or trimodal distributions. A fraction of the same or different short-chain component could be present with the main structure in the bio-oils [225]. These characteristics could drive bio-oils properties to predict the excellent compatibility with elastomers and reduced migration behavior of bio-oils.

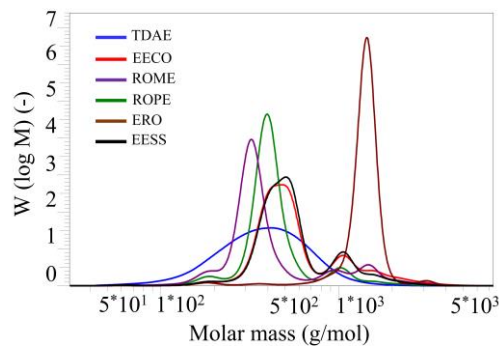


Figure 55: Molar mass distribution of the investigated oils

The thermal behavior of the different bio-oils was determined using DSC measurements given in Figure 56, while the heating and cooling rate was  $10 \text{ K min}^{-1}$  was applied.  $T_g$  has been obtained from the DSC heating curve and is mentioned in Table 9. The DSC heating curve of TDAE exhibits

a glass transition at about  $-52\text{ }^{\circ}\text{C}$ , followed by a small endothermic peak at  $20\text{ }^{\circ}\text{C}$  due to melting processes. The melting curve of EECO showed different major endotherm regions as shown in Figure 56 (a), corresponding to endothermic transitions of the unsaturated (lower-temperature peak) and saturated (higher-temperature peak) fractions. The endothermic region at higher temperature consisted of a peak with a pair of shoulder peaks, while the endotherm region at lower temperature contained four overlapping peaks. However, ERO, ROME, and ROPE showed only one major endotherm in the lower temperature region (unsaturated fraction), and these oil samples had typical melting curves. EECO shows a melting peak at  $12\text{ }^{\circ}\text{C}$ . At the same time, other bio-oils were observed between  $-10$  to  $-1\text{ }^{\circ}\text{C}$ . Figure 56 (b) gives the thermal information during cooling at a rate of  $10\text{ K min}^{-1}$ , where a sharp exothermic peak has appeared for bio-oils onset temperature, which means crystallization event. The crystallization peak for EECO appeared in the temperature range of  $-2.7\text{ }^{\circ}\text{C}$  with a neck at  $0.5\text{ }^{\circ}\text{C}$ , whereas the peak appeared for ERO in the region of  $-26\text{ }^{\circ}\text{C}$ . The exothermic crystallization peaks were associated with the temperature of  $-14\text{ }^{\circ}\text{C}$  and  $-18\text{ }^{\circ}\text{C}$  for ROME and ROPE, respectively. The mineral oil TDAE shows a slightly different behavior than bio-oils, which shows a sharp exothermic peak in the region of  $-94\text{ }^{\circ}\text{C}$ , and two more small exothermic crystallization peaks appeared at the temperature range of  $-12\text{ }^{\circ}\text{C}$  and  $28\text{ }^{\circ}\text{C}$ .

In the bio-oil thermograms, small exothermic peaks are attributed to the fatty acids crystallization, the low density of double bonds, and endothermic peaks lipid melting characteristics [226]. Generally, complex features that were not quickly interpretable during heating in melting curves of bio-oil samples, such as shoulders not separable from peaks, were noticed. These results illustrate the complex nature of glycerol in oil samples. This is a general consequence of the known phenomenon of polymorphism of bio-oils that has interested researchers for many years. Unlike pure glycerol, the polymorphic form of oils cannot be established unequivocally by DSC, which can only be evaluated by X-ray diffraction analysis [227]. Therefore, this thesis has not reported polymorphic transformations in oil samples. Due to the complexity of the measured thermal events, melting and transition points are read at the maximum/minimum of either endo- or exotherm peaks. Complex features were not readily interpretable in the DSC melting curves of oils [228].

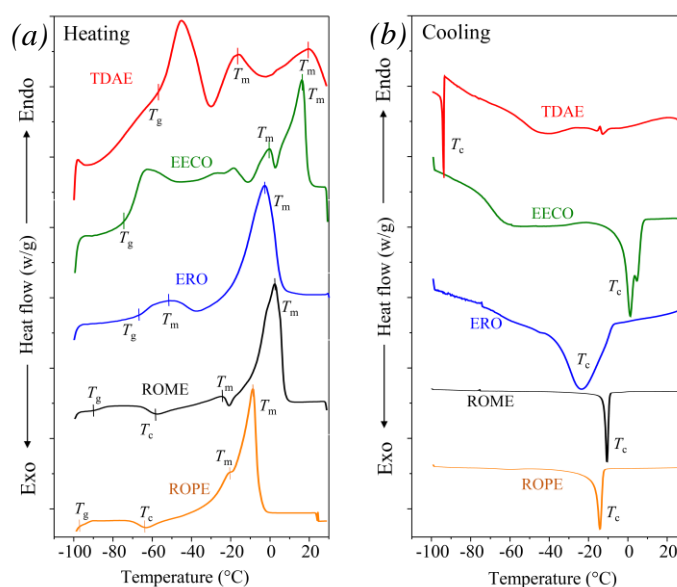


Figure 56: Heat flow evaluation of oils in different temperatures measured by DSC analysis; Heating curves (a), cooling curves (b)

The melting peak of EECO shifted to  $12\text{ }^{\circ}\text{C}$ , whereas other bio-oils were observed between  $-10$  to  $-1\text{ }^{\circ}\text{C}$  due to the formation of hydroxyl groups in EECO that contribute to intramolecular van der

Waals interactions [229]. Furthermore, except for ERO, which was shown in the multi-molar distribution mentioned in Figure 55, the bio-oils have demonstrated two melting peaks. This proved that bio-oils have some fractional components [165]. The highest peak represents the material melting temperature, and the lower represents a second phase or maybe a structural change.

## 4.2 Development of polymer-filler interaction under the influence of oil

It is known that polymer-filler interaction is strongly related to the final vulcanizate properties. Therefore, it is important to gain knowledge of how and to what extent the interaction between polymer and filler is influenced by an oil as a measure of polymer-filler interaction. The rubber-layer  $L$  can be interpreted in this situation. Thus, for selected polymer-filler-oil combination was investigated.

The dependence on the type of oil of the rubber-layer  $L$  for elastomer compounds is presented in Table 10. With changing the oil type, the infiltration of SBR and NBR molecules into carbon black agglomerates and aggregates and the dispersion of carbon black take place simultaneously according to the infiltration model proposed by Manas-Zloczower [230]. Infiltration/dispersion takes place every time and not only by changing the oil type. The variation of rubber-layer  $L$  for the same concentrated filler reinforced elastomers follows the same trend. SBR/EECO has a higher rubber-layer  $L$ , which means the rubber-filler-oil interaction is higher than in SBR/TDAE shown in Table 10. However, the rubber-layer  $L$  is not a very pronounced change in filled NBR systems when the type of oil is changed.

Table 10: Rubber-layer  $L$  of raw mixtures of polymers when mixed with a different type of oils

Oil	Rubber-layer $L$	
	SBR-21/12.5 phr oil	NBR-39/12.5 phr oil
W/O	$0.360 \pm 0.010$	$0.698 \pm 0.002$
TDAE	$0.338 \pm 0.015$	$0.685 \pm 0.006$
EECO	$0.370 \pm 0.018$	-
ERO	$0.179 \pm 0.015$	-
ROME	$0.216 \pm 0.017$	$0.699 \pm 0.004$
ROPE	$0.233 \pm 0.012$	$0.707 \pm 0.005$
EESS	-	$0.703 \pm 0.003$

The data of Table 10 were put in Figure 57 and compared them with surface tension of oils. This shows that the rubber-layer  $L$  decreased with increasing oil's surface tension and happened for SBR raw mixtures. On the other hand, for NBR raw mixtures, no significant change was observed if considered the error margins. The comprehensive study on the rubber-layer  $L$  stated that the type of oil is an essential factor to influence, and low surface tension of oil can develop the rubber-layer  $L$ . There is an inverse and linear relationship between rubber-layer  $L$  and surface tension of oil noticed. So, the surface tension measurement of oil can be the first step to predicting a good rubber-layer  $L$ , which is a cheap and less time-consuming method. Rubber-layer  $L$  for NBR raw mixtures have much higher than SBR raw mixtures although the mixing recipes, time, curing characteristics were maintained in same condition. Type of elastomer and their molecular structure is a factor that influence the rubber-layer  $L$ . NBR is a polar elastomer that contains dipoles and the surface of the filler contains several functional groups that help them bond well and increase the thickness of their primary layer, which remains almost the same after adding 12.5 phr of oil in this matrix.



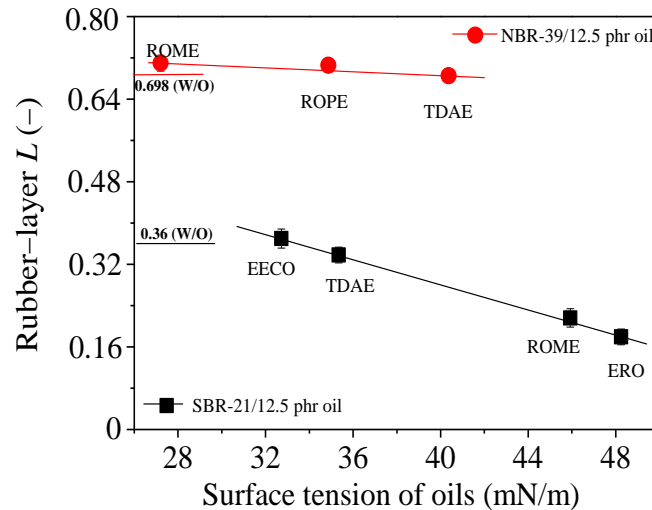


Figure 57: Variation of rubber-layer  $L$  of uncured polymer-filler raw mixtures with different oils as a function of surface tension of oil

A study by Sökmen [4] claimed that TDAE had influenced rubber-layer  $L$  of silica-filled SBR/BR blend and this thesis also proved that the rubber-layer  $L$  dependent on the mixing time. The research on the influence of oil on rubber-layer  $L$  of carbon black-filled elastomers was insufficient. So, comparing the results to previous work is not easy. Nevertheless, some factors can be assumed for the influence of oil on the rubber-layer  $L$  of carbon black-filled elastomers. The carbon black surface contains active groups, including acid, phenolic, quinonic, carboxyl, ketone, pyrone, and lactone groups (see Figure 11) [24,33] that can involve the interaction among rubber and filler. These active groups may change the wetting behavior, and oils can also be a significant cause for changes. Based on the wetting behavior, a correlation was observed between the rubber-layer  $L$  of elastomer raw mixture and the surface tension of oil.

Polarization microscopy was performed as a helpful tool for better understanding the spread of the oils that influenced the dispersion within carbon black-reinforced elastomer vulcanizates. Low concentrated oil (12.5 phr) in elastomer mixture has been chosen for this investigation. The mixing time was 10 minutes, as other investigations were selected for this thesis. Quantitatively, the carbon black agglomerates are assumed to be more than 6  $\mu\text{m}$  in diameter. Figure 58 and Figure 59 show the cross-section areas of plasticized elastomer vulcanizates.

Figure 58 (a), (b), and (f) showed a cross-sectional view of the unplasticized SBR, SBR/TDAE, and SBR/ROPE, respectively. Fewer carbon black agglomerates are noticed in these pictures, and homogenous dispersion of carbon black aggregates is visible through the elastomer matrix. A cross-sectional view of SBR/EECO was shown in Figure 58 (c). It was clearly shown that the number of carbon black agglomerates was higher in SBR/EECO matrix, and the carbon black agglomerates and aggregates were homogeneously dispersed through this matrix. A couple of coagulated oils are visible on the cross-sectional area of the SBR/ERO vulcanizates, as shown in Figure 58 (d). In Figure 58 (e), oil droplets (glareous black spots) were visible on the cross-sectional surface of SBR/ROME vulcanizates.

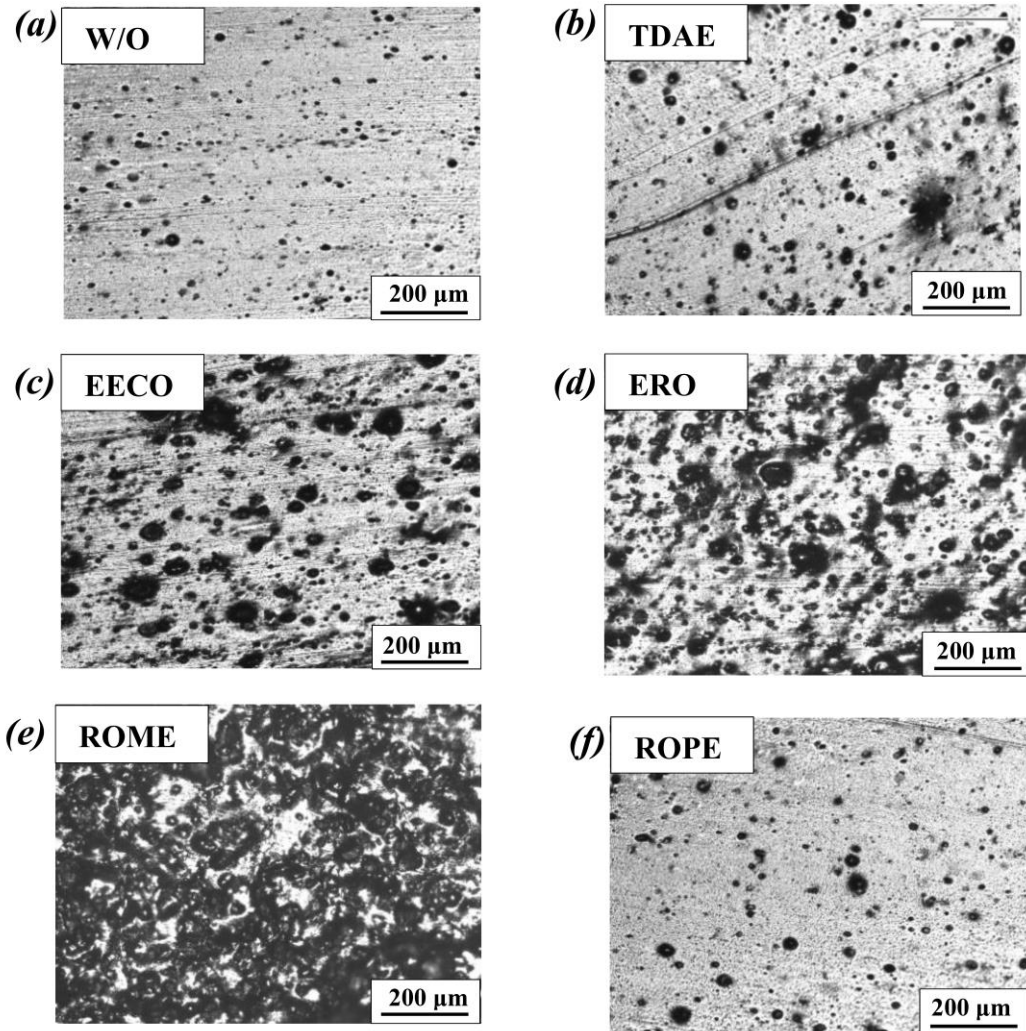


Figure 58: A cross-sectional view in the light microscope of SBR with 12.5 TDAE (a) EECO (b) ERO (c) ROME (d) ROPE (e) and W/O (f) vulcanizates

The visibility of oil droplets in the elastomer matrix and cross-sectional surface have indicated the immiscibility between elastomer-oil. Petrović [151] showed that when oil droplets were visible on the surface, this decreased the mechanical efficiencies. The number of filler agglomerates is decreased, which means the shear stress during mixing was high, and this usually happens for unplasticized filled elastomers. A compatible oil should decrease the shear stress because it increases the chain mobility of elastomers. A previous study [67] stated that the oil reduces the shear stress between the carbon black occluded by the polymer chain. When the oils were immiscible with the matrix, the number of agglomerates decreased [76]. Many agglomerates were present in the SBR/EECO vulcanizates. An optimum number of filler agglomerates indirectly influences the efficiency of the material. When the elastomer is mixed, the elastomer chains have to slip over each other, which is the reason for more agglomerates remaining [74]. From this point of view, the resistance against crack and strain at break of SBR/EECO vulcanizates should give higher values, and partially the arrangement of carbon black agglomerates and aggregates was the reason behind these characteristics. SBR/EECO system has been assumed to show higher efficiency in resistance against stable and unstable crack propagations because the stiff filler agglomerates resisted the crack propagation when they insisted on passing through filler agglomerates.

Figure 59 shows the cross-sectional view of plasticized NBR vulcanizates. The NBR-34 incorporated TDAE, ERO, ROME, and ROPE were investigated and presented in Figure 59 (a), (b), (c), and (d), respectively. It was challenging to see the filler dispersion through NBR matrices. However, the number of visible filler agglomerates was comparatively lower for NBR/TDAE vulcanizates. Bio-oils in NBR influenced the homogenous filler dispersion, and the number of agglomerates was higher and very difficult to distinguish.

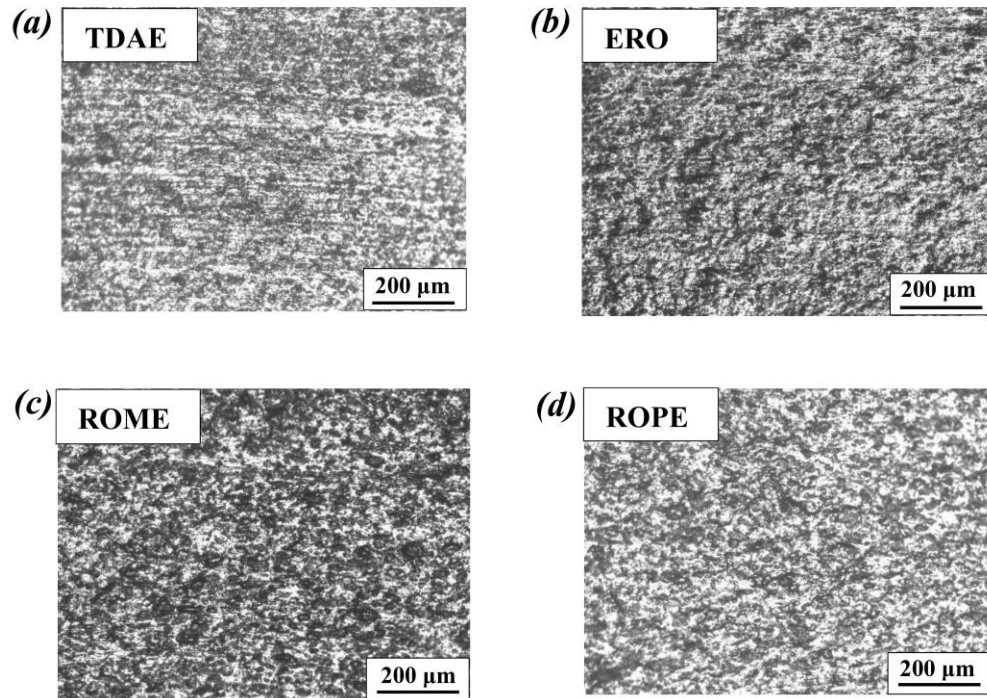


Figure 59: A cross-sectional view in the light microscope of NBR with 12.5 TDAE (a) ERO (b) ROME (c) ROPE (d) vulcanizates

An article [3] on NBR materials was published in 2020, which showed that the oil droplets were visible on the edges of the cross-sectional area of NBR/15 phr TDAE vulcanizates, and a few numbers of carbon black agglomerates were left in the NBR matrix after mixing. This phenomenon partially describes the immiscibility of TDAE in NBR materials where the concentration of TDAE was 15 phr, although, at 5 phr concentration, no TDAE droplets were visible in the cross-sectional area. In contrast, the filler arrangement in the presence of EESO (bio-oil) helps to enhance the mechanical behavior of NBR vulcanizates [3]. In the presence of bio-oils in NBR vulcanizates, crack resistance and mechanical efficiency assumes to be influenced by the homogenous dispersion of aggregates and the optimum number of agglomerates.

### 4.3 Influence of oils on the vulcanization behavior and crosslink density

NMR measurements were done in the Solid-state NMR group of Martin Luther University Halle-Wittenberg under the supervision of prof. Kay Saalwächter. The crosslink density of selected materials was determined by NMR measurement. According to a previous study [35], the residual dipolar coupling  $D_{\text{ress}}/2\pi$  is proportional to crosslink density. So, this thesis only measured the  $D_{\text{ress}}/2\pi$  and represented the crosslink density of plasticized elastomers shown in Table 11. The results show that the crosslink density decreased slightly when oil was added, and this behavior was found for both polymers.

Table 11: Influence of network system of elastomers after oil addition

SBR-21	SBR-21/12.5 phr oil		SBR-21/37.5 phr oil	
	$D_{\text{ress}}/2\pi$ (KHz)	Polymer defects	$D_{\text{ress}}/2\pi$ (KHz)	Polymer defects
W/O	0.25	0.015	0.25	0.015
TDAE	0.24	0.028	0.15	0.16
EECO	0.19	0.072	0.14	0.13
ERO	0.21	0.061	0.17	0.13
ROME	0.20	0.060	0.15	0.07
ROPE	0.20	0.036	0.16	0.03
NBR-39	NBR-39/12.5 phr oil		NBR-34/37.5 phr oil	
W/O	0.32	0.038	0.32	0.05
TDAE	0.30	0.11	0.16	0.13
ROME	0.22	0.097	0.16	0.15
ROPE	0.24	0.092	0.15	0.09

Plasticized rubber vulcanizates exhibited minimal changes when a low content of TDAE was introduced. However, the addition of bio-oils in low quantities resulted in a reduction of crosslink density by approximately 0.05 kHz for SBR and approximately 0.10 for NBR. On the other hand, the incorporation of a high content of oils in the rubber matrix led to a significant decrease in crosslink density, without showing notable differences among the various types of oils used. In the case of SBR vulcanizates, the absence of oils inside resulted in a crosslink density of 0.25 kHz, which closely resembled the findings of a previous study [35]. Conversely, NBR demonstrated a higher crosslink density, indicating a greater prevalence of polymer defects such as entanglements. These outcomes were comparable to those reported in a previous investigation [231]. It is worth noting that NBR vulcanizates cannot be considered equivalent to SBR vulcanizates due to the distinct material properties inherent to each polymer. Overall, the introduction of oils in varying quantities had differential effects on the crosslink density of plasticized rubber vulcanizates, with SBR and NBR displaying distinct behaviors in response to these additives.

Previous authors [4,5] stated that the crosslink density decreased with increasing plasticizer concentration, and the same trend followed in both elastomers in that the crosslink density decreased when oil was added. The dependence of crosslink density with oil concentration was shown in a previous article [232]. The part of this thesis noticed that the same trend was obtained for both polymers. A low crosslink density leads eventually to a low hardness value [232] and a high strain at break [98]. At the same time, SBR/EECO combination showed a low hardness value and comparable tensile strength with high strain at break.

The crosslink density of rubber/bio-oil vulcanizates were reduced up to 25% although the rubber-layer  $L$  of NBR/bio-oils raw mixtures remain unchanged (see Table 10). In general, the rubber-layer  $L$  in the raw mixture can affect the degree of crosslinking in the vulcanized elastomer. For example, a high degree of filler-rubber interaction can lead to more efficient crosslinking, resulting in a higher crosslink density in the vulcanized elastomer [233]. This is because crosslinks act as chemical bonds that hold the polymer chains together, and thus reduce the amount of unbound or free rubber. A higher crosslink density also reduces the mobility of the polymer chains, making it more difficult for the rubber to deform or flow. Although, the relationship between rubber-layer  $L$  in raw mixtures and the crosslink density of vulcanized elastomers is complex and depends on

several factors, including the type and amount of filler and plasticizer, the curing system, and the processing conditions. Sometimes the involvement of oils does not have a major impact on rubber-filler interactions, but they can disrupt the cure of filled elastomers and this depends on molecular size and structure of oils [4]. In this thesis, the proportions of fillers, mixing and curing parameters were kept unchanged, with the exception of oil types, which only interfere curing system for crosslinking but slightly affect the rubber-layer  $L$ , especially for SBR/EECO and NBR/bio-oil systems. The molar mass of bio-oils was slightly higher than TDAE (see Table 9), and these large molecules interrupt during network formation of rubber/bio-oil systems.

SBR/EECO combination resulted in a high tear resistance as well as resistance against stable and unstable crack propagation. According to some previous studies [3,49,98,210,232,234], it was proven that optimization of crosslink density is important for higher efficiency of mechanical behavior. This means the SBR/EECO system was very close to optimum values of crosslink density. A previous study [35] on SBR shows that the polymer defects were slightly higher. Nevertheless, a high fraction of polymer defects reflects more mobile materials, and that value is highest for the SBR/EECO material. The SBR with bio-oil systems had a high fraction of polymer defects affecting the lower hardness with a high strain at break. However, its optimization is also essential to get a higher mechanical behavior.

## **4.4 Thermo-mechanical and mechanical properties of rubber vulcanizates and their dependence on plasticizing oils**

### **4.4.1 Influence of oil type on temperature-dependent linear viscoelastic behavior**

This thesis employed dynamic mechanical analysis (DMA) to assess the viscoelastic properties and modulus of rubber vulcanizates with varying oils, as a dependent variable of temperature. DMA, being a thermo-mechanical analysis technique, enables the acquisition of valuable data, which can subsequently be utilized to anticipate the performance of these materials across diverse application domains and temperature ranges. It was observed that the alterations in viscoelastic behavior and modulus were particularly pronounced in elastomers featuring higher concentrations of oil. Consequently, the evaluation focused on elastomers that were blended with 37.5 phr of oils, aiming to ascertain the influence of oil content on the viscoelastic characteristics of the elastomers. Figure 60 shows the variation of storage modulus  $E'$  of SBR and NBR vulcanizates as a function of temperature. The typical dependencies of the  $E'$  with the high modulus (glassy state), glass transition temperature  $T_g$  (sharp decrease in  $E'$ ), and entropy-elastic range above  $T_g$  with low modulus were obtained. It can be seen that after oil was added to the elastomer, the storage modulus  $E'$  curves shifted to  $T_g$ . The  $E'$  value in the property-elastic range, where application takes place, decreases with the addition of oil. Thus, the highest storage modulus for SBR and NBR was shown when there was no oil inside.

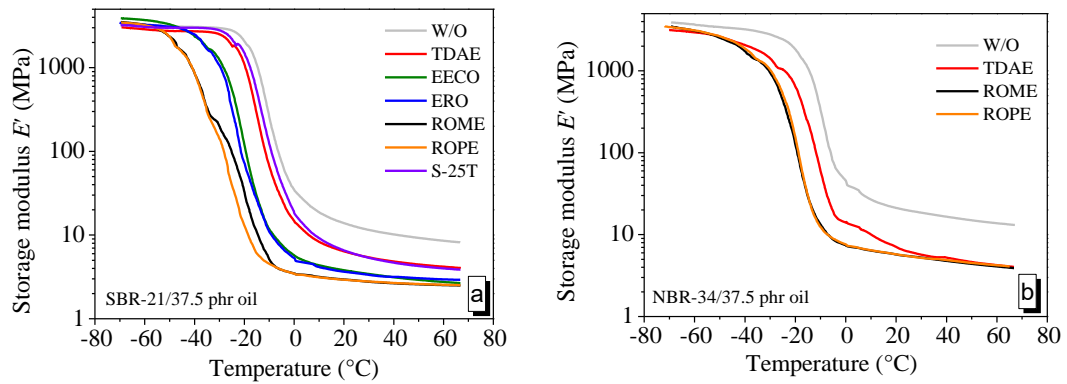


Figure 60: Dependence of storage modulus  $E'$  of SBR (a) and NBR (b) materials on the temperature at the frequency of 10 Hz

A series of bio-oils in rubber matrix used to the lowest  $E'$  comparatively for both elastomers, and they with different oils show  $E'$  very close to each other. It can be stated that the  $E'$  of oil filled elastomers have sharply reduced but  $D_{res}$  is decreases a little as shown in Table 11. Oil types and concentrations are the key factor that reduces storage modulus by 5 times over unplasticized elastomers. In accordance with expectations, the addition of oil has resulted in a decrease in the volume fraction of the elastomer, consequently leading to reductions in both the  $D_{res}$  and the  $E'$ . In particular, the incorporation of specific bio-oils, namely ROME and ROPE, significantly diminishes the modulus of SBR to a considerable extent. Conversely, the addition of oils in the NBR matrix also leads to a significant reduction in the modulus. The underlying rationale for this outcome proved to be unexpected, as the filler network within the elastomer matrix experienced a breakdown due to the presence of oils with a high content, even at a mere 0.2% strain.

The Payne effect of elastomers can only be observed with a large deformation, so no Payne effect is expected to influence elastomers during linear behavior although bio-oils partially destroyed the filler network due to Payne effect, as a result the modulus reduced. During the measurement of stress-strain behavior (tensile test), a large deformation is possible, which can distinguish the modulus at low and high strain. Table 12 shows the values of the storage modulus  $E'$  (DMA) and the stress at 200% strain  $\sigma_{200}$  (tensile test) with normalized decrease factor. For a reasonable comparison, the elastomers filled with a high concentration of oils (37.5 phr) were selected. Table 12 shows that  $E'$  and  $\sigma_{200}$  were higher for unplasticized elastomers with a normalized decrease factor 1. Although  $E'$  was higher where the low strain was applied, at 200% strain,  $\sigma_{200}$  decreased by half. When oil introduced in the polymer network then both elastomers were shown that the reduction of  $E'$  and  $\sigma_{200}$  were very high. However,  $E'$  and  $\sigma_{200}$  varied by oil type, particularly  $E'$  for plasticized elastomers containing bio-oils were comparatively low and in all cases a large reduction in  $\sigma_{200}$  when oil was blended with elastomers.

During measurement of  $\sigma_{200}$ , applied strain was 200%, and it was a large strain where no more filler network remains and it was partially or completely break down due to Payne effect [237].  $\sigma_{200}$  was comparatively lower and was reduced when high content oil was blended into the elastomer network. At high strains, there is negligible influence of the filler network, but only a dependency on the elastomer network and hydrodynamic effect. This relationship was nonlinear due to the variation in crosslink density as oil mixes into the elastomer network. The oil molecules act as lubricants, reducing the friction between polymer chains and increasing their dilution effect. This increased mobility can reduce the  $\sigma_{200}$  of the elastomer, leading to hydrodynamic reinforcement and partial filler network. This measurement used a high concentration of oil in the polymer matrix which depicted the high degree of dilution effect. As the oil concentration increases, the elastomer chains become more mobile due to higher entanglement, leading to a

softening during deformation. When a filler-reinforced plasticized (37.5 phr) elastomer is subjected to stress at 200% strain, it can have a significant effect on the material's dilution.

Table 12: Storage modulus  $E'$  and stress at 200% strain  $\sigma_{200}$  of elastomers after oil addition

SBR-21/37.5 phr oil	$E'$ (MPa)	Normalized decrease factor	$\sigma_{200}$ (MPa)	Normalized decrease factor
W/O	13.03	1	6.48	1
TDAE	6.04	0.46	2.17	0.33
EECO	3.70	0.28	1.16	0.18
ERO	3.55	0.27	2.83	0.44
ROME	2.89	0.22	2.04	0.31
ROPE	2.88	0.22	2.21	0.34
S-25T	6.13	0.47	1.83	0.28
NBR-34/37.5 phr oil				
W/O	20.21	1	13.9	1
TDAE	6.46	0.31	2.39	0.17
ROME	5.55	0.27	1.99	0.14
ROPE	5.56	0.27	2.00	0.14

Figure 61 illustrates a correlation between the actual modulus of the material ( $E_{DMA}$ ), the modulus of the rubber matrix ( $E_{NMR}$ ), and  $\sigma_{200}$ , in relation to the crosslink density of SBR vulcanizates ( $a$ ). Where for NBR samples the correlations of modulus and stiffness were based on linear ( $E_{DMA}$ ) and nonlinear  $\sigma_{200}$  behavior. The figures are demonstrates that unplasticized elastomer exhibits a higher modulus when the filler networks remain active. However, with the addition of a high content of oil, both the crosslinking density and modulus decrease. It is important to note that no linear relationship is observed among these samples, as certain oils, specifically ROME, ROPE and ERO, can disrupt the filler networks. Consequently,  $\sigma_{200}$  is comparatively lower (hydrodynamic reinforcement) due to the high strain, which causes partial or complete destruction of the filler network. This reduction in  $\sigma_{200}$  occurs linearly with decreasing crosslinking density, as anticipated, since the volume fraction of rubber and filler decreases with a high oil load in the recipe. In particular, of SBR/oil and NBR/oil systems were shown that  $\sigma_{200}$  was linearly increased with increasing crosslink density. Conversely, the  $E_{NMR}$  demonstrates a lower modulus because it solely represents the modulus of the rubber matrix without any reinforcement. Furthermore, the  $E_{NMR}$  also decreases as the crosslink density decreases following the addition of oil.

According to the Payne effect [238–240], the strain-like 200 % dependence of filled elastomer can be explained as the filler network is mostly destroyed. At the high strain, van der Waals bonds between carbon black aggregates are broken and reformed. So, the carbon black has a small remaining effect. As a result, the correlation between crosslink density and  $\sigma_{200}$  might not be linear. A previous study [241] claimed that due to the hydrodynamic effect of elastomer, stress at 200 % strain of unfilled elastomers were linearly increased with increasing crosslink density.

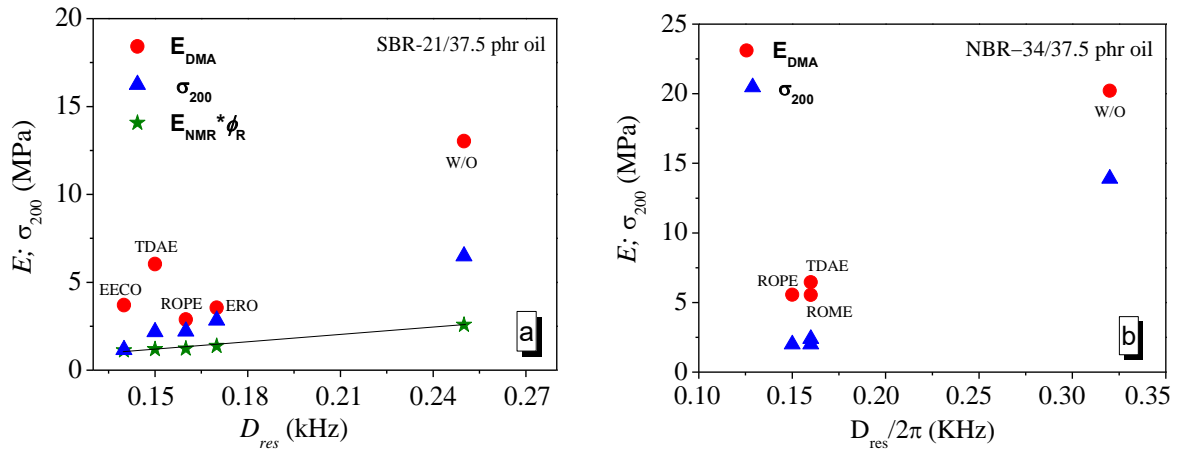


Figure 61: Correlations of modulus and  $\sigma_{200}$  with crosslink density of SBR (a) and NBR (b) vulcanizates

A more detail can be found out about Payne effect at high strain due to filler network breakdown and suffering of hydrodynamic reinforcement of elastomers as seen in a graphical representation in Figure 62. This shows the correlation between the storage modulus  $E'$  and stress at 200% strain  $\sigma_{200}$  (data already given in Table 12). Figures for both elastomers Figure 62 (a) and (b) showed that the  $E'$  and  $\sigma_{200}$  correlations were mostly nonlinear and a very similar way. These were shown to inform the activity of filler network with the elastomer network and properties of hydrodynamic effect.

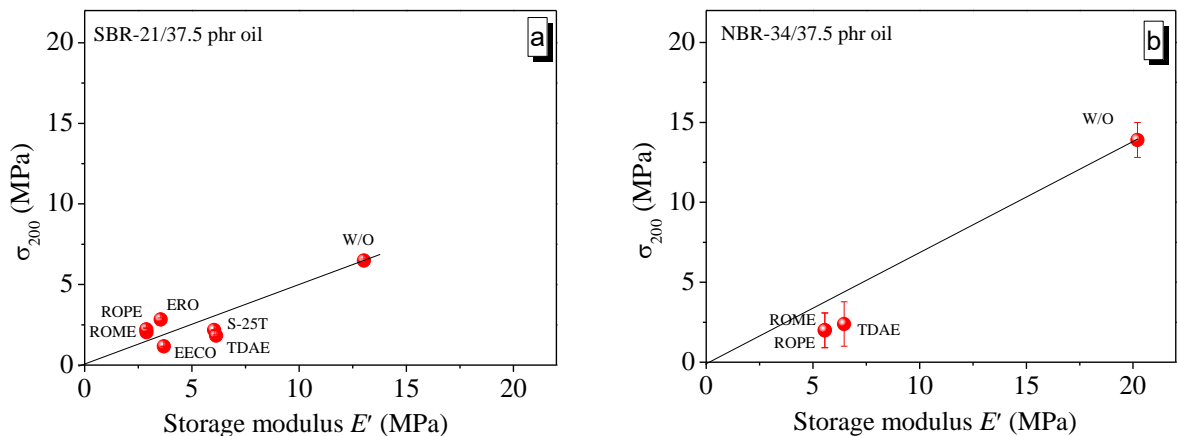


Figure 62: Correlations between stress at 200 % strain  $\sigma_{200}$  and storage modulus  $E'$  of SBR (a) and NBR (b) materials

The hardness of elastomer can be influenced by the Payne effect at high strain. In consequence, Figure 63 shows the correlation between elastic modulus obtained by Shore A hardness and  $\sigma_{200}$ , and it shows that the elastic modulus is linearly proportional to the  $\sigma_{200}$ . This response observed same as for both elastomers as shown in Figure 63 (a) for SBR/oil, and Figure 63 (b) NBR/oil system. As previously discussed, the filler network absents in the strain at 200% due to Payne effect so only the elastomer network, additives and hydrodynamic effects are contributing the relation between hardness and  $\sigma_{200}$ . However, filler, additives, and oils were mixed in the elastomers, so those might have influenced the correlations. Practically it was noticed that these additives and oils slightly influenced the linearity.



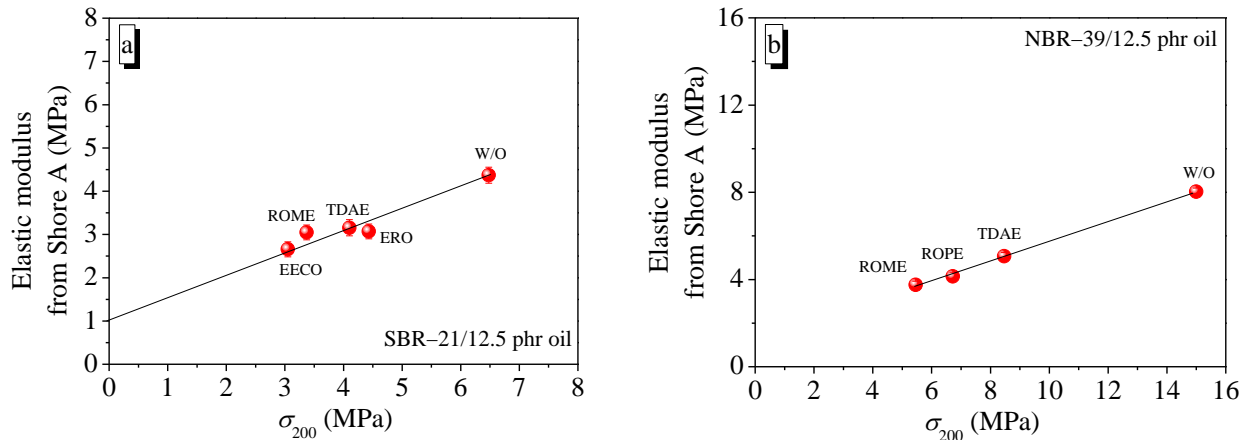


Figure 63: Dependence of Shore A hardness with stress at 200 % strain  $\sigma_{200}$  of SBR (a) and NBR (b) vulcanizates

Figure 64 shows the variation of loss modulus  $E''$  with plasticized polymers as a function of temperature. With oil addition,  $E''$  values decrease with an increase in the modification level. A salient feature is that both SBR and NBR without oil show the highest  $E''$  value. Nevertheless, bio-oils comparatively show the lowest  $E''$  value for both vulcanizates. It is also noticeable from SBR, bio-oils lead to lower  $E''$  values than TDAE. The decrease of modulus, also indicated by lower crosslink density, was measured by NMR measurement. Therefore, it must be due to changes in the filler network.

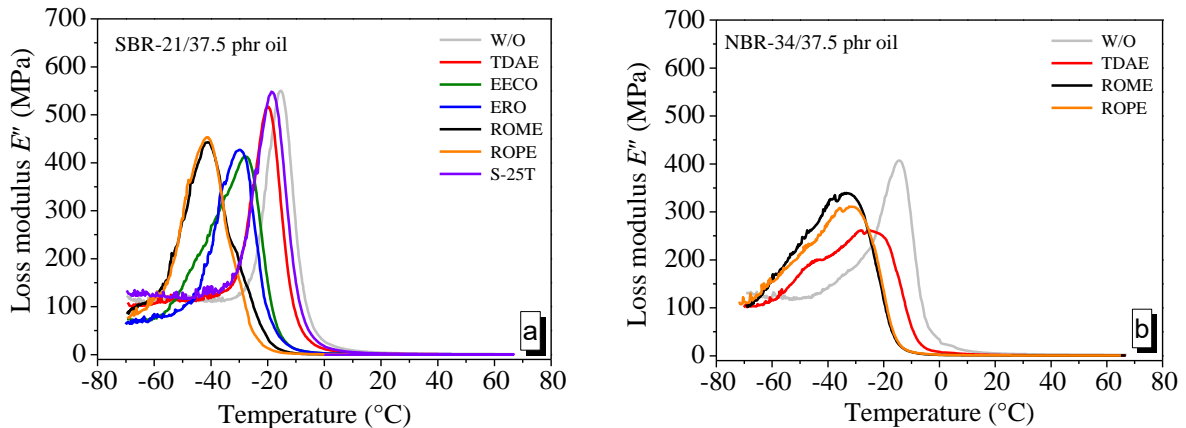


Figure 64: Variation of loss modulus of SBR materials (a), and NBR (b) materials as a function of temperature at the frequency of 10 Hz

Figure 65 represents the  $\tan \delta$  curves as a function of temperature. Figure 66 shows the  $T_g$  of selected materials determined from the  $\tan \delta$  maxima (see Figure 65). Additionally, in Figure 66 the  $T_g$  of the used oils is given with the corresponding  $T_g$  of the materials.

SBR vulcanizates with EECO and ERO show higher  $\tan \delta$  values than TDAE and without oil, which ROME and ROPE show lower  $\tan \delta$  than TDAE. So, ROME and ROPE containing SBR represent the elastic property as they reported the lower  $\tan \delta$ . On the other hand, bio-oils show the  $\tan \delta$  value almost close to each other with TDAE. For SBR, vulcanizates without oil show the lowest  $\tan \delta$ .

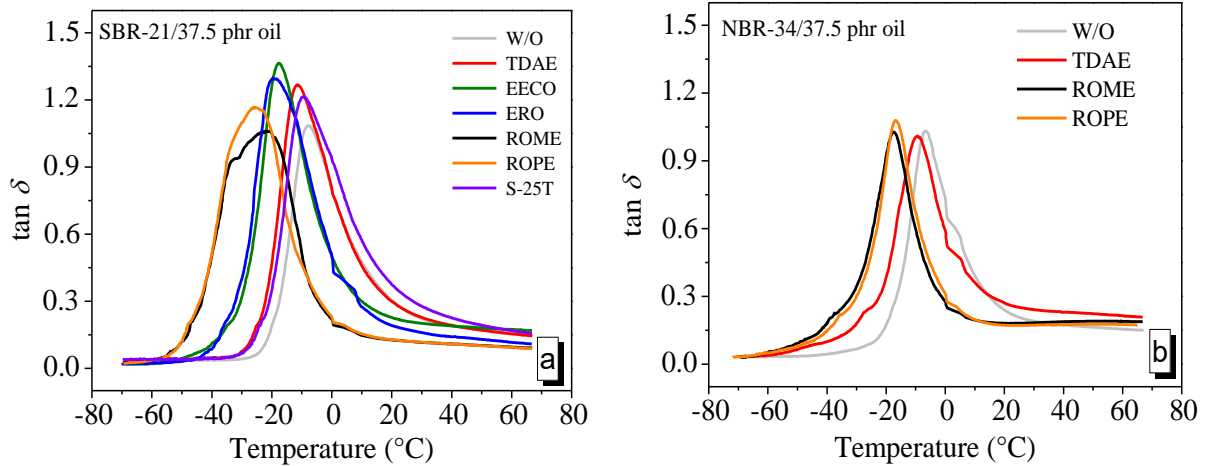


Figure 65: Variation of  $\tan \delta$  of plasticized SBR materials (a), and NBR materials (b) as a function of temperature at the frequency of 10 Hz

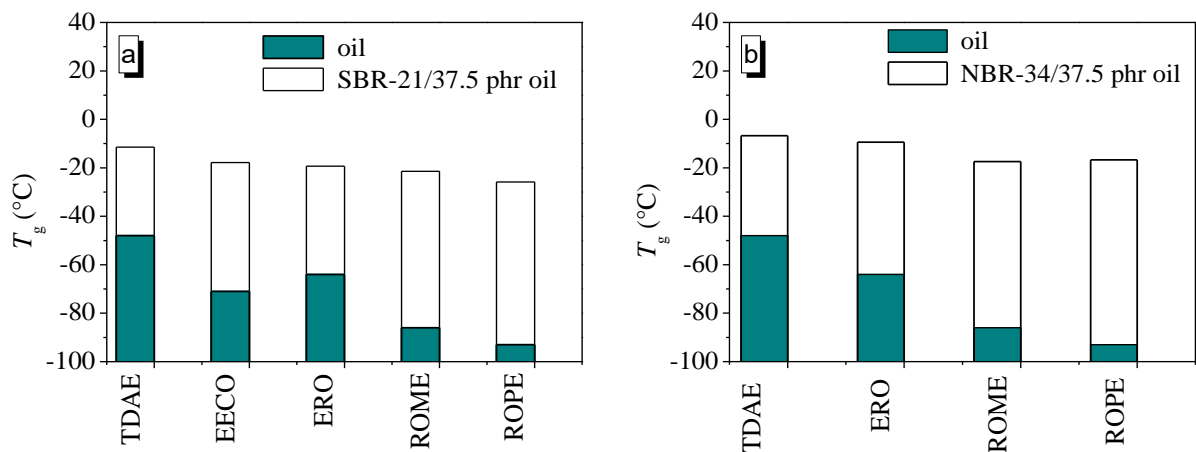


Figure 66:  $T_g$  of different oils (colors) and SBR-21 vulcanizates (a), NBR-34 vulcanizates with oils (b)

NBR-34 shows a higher  $T_g$  than the SBR, and  $T_g$  decreases with increases in the oil content because of mostly the plasticization effect on SBR and NBR vulcanizates. With 37.5 phr, ROPE shows the lowest  $T_g$  value for SBR, and 37.5 phr ROME shows the lowest  $T_g$  value for NBR. This is because bio-oil is the branched and high molecular weight plasticizer that makes higher free-volumes. The oil increases the free volume that reduces the  $T_g$ . The lowest  $T_g$  was obtained with bio-oils for both SBR and NBR than conventional TDAE. The same result was observed by Chen [150], and the previous study [87] claimed that plasticizers' chemical structure and molecular weight control the free-volume within the elastomer. According to free-volume theory [86], the plasticizer with low  $T_g$  is more efficient for reducing the  $T_g$  of the plasticized elastomer, so the  $T_g$  investigation of this thesis was followed the free-volume theory. The high molecular weight and branched plasticizer have higher free-volumes and increased free-volume which decreases the  $T_g$ . The application area of compounded elastomer can be predicted according to the  $T_g$ .

#### 4.4.2 Influence of oil type and content on the mechanical properties

Figure 67 shows the variation of hardness with plasticizer concentration, and it was presented that the hardness of the materials continuously decreases (gray area) when the oil concentration increases for polymer vulcanizates. However, the type of polymer is an essential factor in the hardness behavior, and it was a clear vision of the figure that the material showed higher hardness value when NBR was vulcanized without oil, although SBR showed higher hardness values when no oil was added in the series of SBR vulcanizates. Nevertheless, due to materials property, both polymers cannot be compared. Furthermore, both polymers showed higher hardness when they were mixed with low-content TDAE.

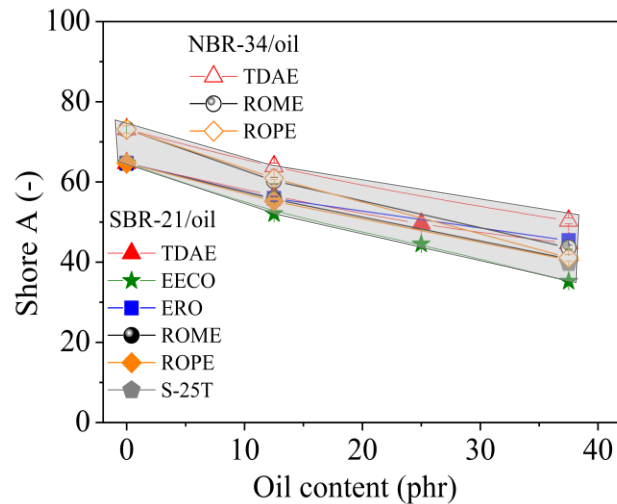


Figure 67: Dependence of hardness values of polymers with changing the oil types and concentrations; solid symbols represent SBR and open symbols for NBR vulcanizates

It was hard to make differences when NBR mixes with low content bio-oils and makes some differences at high concentration of bio-oils where NBR/ROME shows a bit higher hardness value. In contrast, the hardness of SBR materials was almost the same except for EECO when low content oil was mixed, where SBR/EECO vulcanizates had a bit lower hardness, and the variations were higher for high content oils. Hardness values of S-25T were almost similar to other SBR/oil mix materials. Furthermore, Table 13 shows the dependence of hardness values on the ratio of monomer was changed, and it was measured that the hardness values of the NBR-34 show lower hardness compared to NBR-39.

According to the previous study [152], the hardness is higher without the addition of oil, and when the materials containing a higher amount of oils tend to have a lower hardness value than the compound without oil. Petrović [66] and Pechurai [126] also found that the materials with higher oil content tend to have a lower hardness value. An excess amount of oil also increases the coupling action between the Carbon black and polymer, making the polymer chain in the polymers less compact, thus reducing the hardness value.

Table 13: Dependence of hardness values of NBR materials with changing the ratio of acrylonitrile and type of oils; results compared to SBR materials

Oil	Shore A (-)		
	SBR-21/12.5 phr oil	NBR-34/12.5 phr oil	NBR-39/12.5 phr oil
W/O	64.7 ± 1.7	73.1 ± 0.9	77.4 ± 0.5
TDAE	56.6 ± 1.3	63.9 ± 0.8	68.1 ± 0.5
EECO	52.1 ± 0.7	-	-
ERO	55.9 ± 0.6	-	-
ROME	55.7 ± 0.6	60.3 ± 0.8	61.0 ± 0.5
ROPE	55.2 ± 0.7	60.9 ± 0.3	63.4 ± 0.6

Crosslink density is correlated to the hardness values, which decrease with increasing the oil content [98,232]. If the hardness values are compared to Table 11, a correlation between structure-property of crosslink density-hardness can be claimed where they have a direct proportion relation [242]. The excess amount of oil gives better plasticization to the polymers. According to plasticization theories, this excess amount of oil increases the freedom of movement of the polymer chain due to polymer-polymer breakdown interaction, thus reducing the crosslink density and hardness value. For both NBR, vulcanizates with all types of oils were not influenced of the hardness; this is perhaps because of the active contribution of oils during the vulcanization of NBR. Kukreja [72] stated that the highest hardness might be attributed to the high crosslinking participation. This is attributed to the better filler dispersion with bio-oil. This is perhaps attributed to bio-oil containing a higher amount of free fatty acid [92]. However, the hardness of rubber vulcanizates containing different bio-oils was more or less the same. A high crosslink density of elastomers correlates to high hardness behavior [242]. According to the previous research [152], the compound containing a higher amount of oils tends to have a lower hardness value than the compound without oil. Hardness of unfilled elastomers were linearly increased with increasing crosslink density [241].

### Influence of bio-oil type and concentration on the tensile behavior

The tensile behavior of the investigated plasticized elastomers is shown in Figure 68, which gives the dependence of the tensile strength of the elastomer vulcanizates with oil loading. Tensile strength  $\sigma_m$  variation was shown in Figure 68(a), and this depicted that  $\sigma_m$  decreased when the concentration of oil increased in the elastomer matrix.  $\sigma_m$  of NBR vulcanizates was noticeable higher when no oil was added, and it decreased much more than SBR vulcanizates at low content oil.  $\sigma_m$  of SBR had decreased except TDAE when low content of oil was added, and it gradually decreased when oil concentration increased for both polymers. Nevertheless, SBR has a higher  $\sigma_m$  when a high concentration of EECO is mixed. S-25T shows higher  $\sigma_m$  compared to other high oil content SBR samples. For most NBR compounds, the  $\sigma_m$  is slightly dependent or remains nearly constant when the type of oil has changed and even though it continues when high content of the oil is added. The dependence of strain at break  $\epsilon_B$  of polymers on the type and content of the oil is shown in Figure 68(b).  $\epsilon_B$  of SBR materials was higher when no oil was added compared to NBR material. However, due to the variation of material property, the comparison between SBR and NBR was omitted in this thesis. For both polymers, the  $\epsilon_B$  has increased when the low content of the oil is added. Although at high content oil,  $\epsilon_B$  decreased and was almost the same compared to the polymer samples when no oil was added except for SBR, which has higher  $\epsilon_B$  when EECO mixes, and it is almost similar to S-25T.

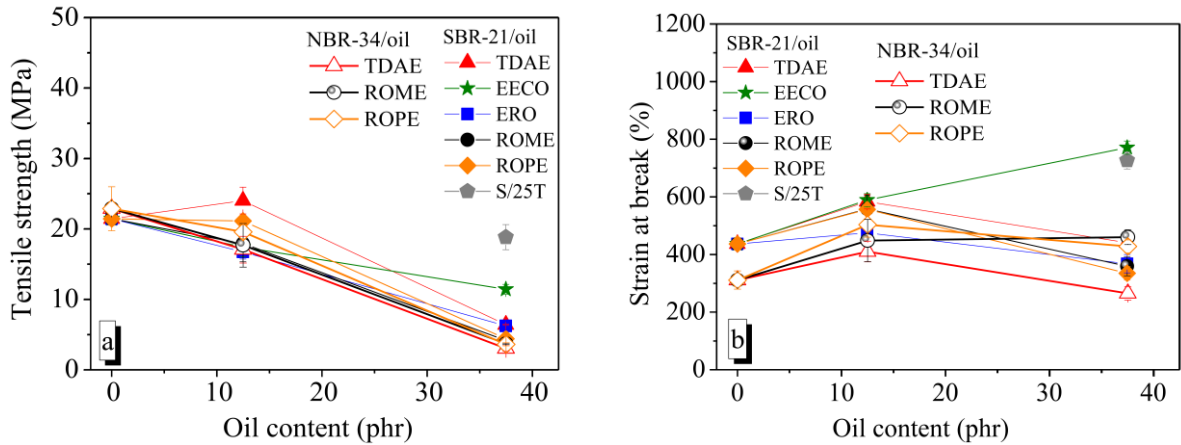


Figure 68: Dependence of tensile strength  $\sigma_m$  (a) and strain at break  $\varepsilon_B$  (b) of elastomers with changing the oil types and concentrations; solid symbols represent SBR and open symbols for NBR vulcanizates

Table 14 summarized tensile behavior when low content of oil mixed with elastomers was monitored the dependence of tensile behavior when the monomer ratio has changed for NBR materials.  $\sigma_m$  of NBR-39 is slightly higher than NBR-34, as shown in Table 14. Nevertheless, when high concentrated EECO is added to SBR,  $\varepsilon_B$  is increased. The same trend follows for NBR when mixed with bio-oils.

Table 14: Tensile behavior of polymers when it mixed with different types of oils

Oil	Tensile strength $\sigma_m$ (MPa)			Strain at break $\varepsilon_B$ (%)		
	SBR-21/12.5 phr oil	NBR-34/12.5 phr oil	NBR-39/12.5 phr oil	SBR-21/12.5 phr oil	NBR-34/12.5 phr oil	NBR-39/12.5 phr oil
W/O	21.4 ± 0.91	22.9 ± 3.12	22.0 ± 1.65	437 ± 13	311 ± 32	275 ± 14
TDAE	24.0 ± 1.89	17.1 ± 1.90	18.8 ± 0.81	584 ± 26	410 ± 36	404 ± 35
EECO	17.4 ± 1.37	-	-	589 ± 23	-	-
ERO	16.7 ± 0.98	-	-	475 ± 37	-	-
ROME	17.9 ± 2.59	17.7 ± 3.09	23.5 ± 1.2	558 ± 49	448 ± 73	569 ± 20
ROPE	21.1 ± 0.63	19.6 ± 0.96	18.6 ± 1.1	557 ± 16	503 ± 43	445 ± 30

A likely reason for higher  $\sigma_m$  is the higher polarity of NBR-39 due to the higher content of acrylonitrile compared to NBR-34 [8]. Generally, a decrease in  $\sigma_m$  is often combined with an increase in the  $\varepsilon_B$  [243]. In detail, some differences can be seen between the different oils. However, with high concentration oils in both elastomers, the  $\varepsilon_B$  has decreased in most cases. This is perhaps due to not having optimal filler dispersion or the antiplasticization effect [87]. If oils are added, the  $\sigma_m$  decreases, contributing to more homogenous filler dispersion in the rubber matrix, as reported in [98], also observed in this thesis that the reduction of storage modulus  $E'$  mentioned in Table 12. However, the macro-dispersion index study gave no correlation with the  $\sigma_m$  values for increasing plasticizers. TDAE does not contain any OH groups, and therefore, compatibility with a polar polymer-like NBR [76] is restricted, leading to a lower  $\sigma_m$ . NBR with higher polybutadiene (NBR-34) shows the higher  $\sigma_m$  and  $\varepsilon_B$  when it contains no oils; this is perhaps due to the higher proportion of the lower  $T_g$  polybutadiene in the polymer chain. A similar effect was reported by Rahman [3], Jiayi [244] and Khalaf [48].

Oils are changing the tensile properties of whatever elastomeric or thermoplastic monomer's contribution to polymer, and results fluctuate according to specific plasticizers. Especially when NBR was mixed with ROME, the tensile properties were enhanced. There is a common trend of increasing deformability with a rising amount of oils until a certain concentration was found in this thesis. According to the study by Petrović [66] and Anis [245],  $\epsilon_B$  also increases significantly as a function of oil content. The structure-property investigation shows the lower polarity of TDAE and SBR, and this correlates with the tensile behavior. In addition, a continuous decrease in  $\sigma_m$  but an increase in  $\epsilon_B$  with increasing the oil loading is attributed to the macro-plasticization effect, which dominates over micro-plasticization and coupling action [26]. From the results, a strong lubrication effect of the bio-oils might be derived; in other words, bio-oils might promote more polymer chain motion in the vulcanizates [100]. Concerning any concentration of oils, for SBR, bio-oils loaded SBR show somewhat lower tensile strength than TDAE; this may be attributed to relatively higher flexibility and lower hardness values discussed before. Due to the lower surface tension of the SBR and bio-oils, the plasticizing effect becomes higher, resulting in proper filler dispersion. The same results were measured by Raju [49] and Anis [245].

### Tear resistance variation of elastomers with bio-oil type and concentration

This thesis evaluated the tear resistance behavior of plasticized elastomer vulcanizates. The target of this study was to find the correlation between the tear strength  $T_s$  of plasticized elastomers and the oil concentration. Additionally, the measurement goal was to find the  $T_s$  of plasticized elastomer when the type of oil and elastomer were changed. The dependences  $T_s$  of oil mix elastomers are shown in Figure 69. It describes the unplasticized elastomers have a poor  $T_s$  and a significant increase of  $T_s$  in the case of elastomer mixes with some of the oils, especially at lower oil loading. For SBR-21 modified with TDAE, ROME, and ROPE, the  $T_s$  remains almost constant at around 12.5 N/mm. In contrast, the  $T_s$  of the SBR/EECO compound increased noticeably at a 12.5 phr loading range. Increasing the amount of TDAE does not much influence the  $T_s$ , and it tends to increase with the addition of 12.5 phr oil. For SBR vulcanizates in all cases, independent of the oil content, EECO results in higher  $T_s$  than TDAE. Moreover, this result was comparable with S-25T, which shows the result between TDAE and bio-oil. In terms of NBR, in every case, whatever the oil content, bio-oils show higher  $T_s$  than TDAE.

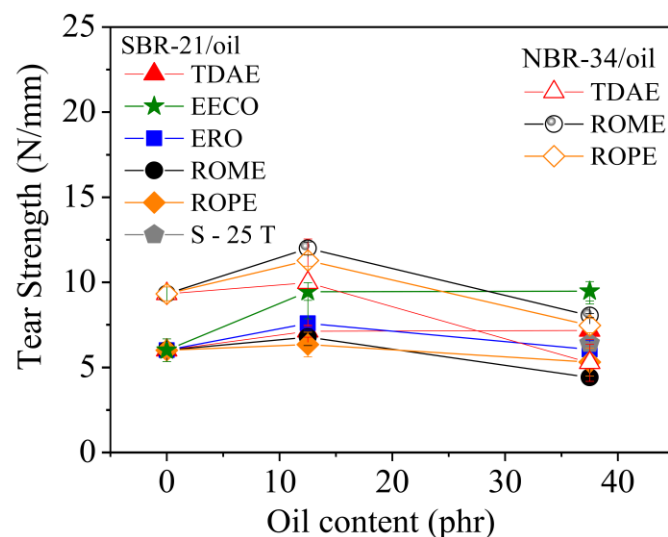


Figure 69: Dependence of tear strength of polymers with changing the oil types and concentrations; solid symbols represent SBR and open symbols for NBR vulcanizates

In addition, Table 15 was added to an easy understanding of how the tear strength  $T_s$  had changed when the elastomers were mixed with different types of oils. Additionally, the table depicted the changes of  $T_s$  of NBR vulcanizates when the types of NBR were different. It is a strong remark that the oil and elastomer types are both key factors for the  $T_s$  changes.

Some previous studies [98,125–127,246] claim that  $T_s$  increased with a further increase in the loading of oil up to a certain concentration. The improvement can explain this increase in polymer-filler-oil compatibility and the decreased crosslink density and better filler dispersion due to increased plasticization. Tearing of SBR vulcanizate occurs due to the propagation of cracks initiated at the stress concentration point through the wearing of rubber molecules at the SBR-Carbon black interfaces [127]. The micro-plasticization of the interfaces using an effective plasticizer can hinder the propagation of cracks [247]. According to a previous study [3], higher  $T_s$  were obtained with better filler dispersion, and a similar result was observed by Chokanandsombat [248] and Raju [232]. Because of the polarity of NBR, bio-oils show a much higher  $T_s$  than TDAE (see Table 15), especially at higher oil loadings.

Table 15: Tear strength of elastomer vulcanizates with changing the oil types and ratio of acrylonitrile monomer in NBR vulcanizates

Oil	Tear strength $T_s$ (N/mm)		
	SBR-21/12.5 phr oil	NBR-34/12.5 phr oil	NBR-39/12.5 phr oil
W/O	5.99 ± 0.67	9.34 ± 0.40	8.09 0.20
TDAE	7.12 ± 0.36	9.99 ± 0.60	11.0 0.25
EEO	9.43 ± 0.50	-	-
ERO	7.58 ± 0.40	-	-
ROME	6.76 ± 0.48	12.0 ± 0.38	14.9 ± 0.29
ROPE	6.33 ± 0.73	11.3 ± 0.34	12.8 ± 0.14

In addition, as expected, the NBR vulcanizates have higher  $T_s$  than those of the SBR, respectively, due to their ability to strain-induced crystallization [249]. However, the polarity of elastomer can influence the tear resistance behavior, and oils enhance the tear resistance behavior to a large extent. In the case of NBR materials, the ROME plays a vital role in enhancing the tear resistance when the polarity of NBR switches to a high level with increasing the acrylonitrile content.

### Compression set variation of elastomers with the bio-oil type and concentration

A low compression set (CS) value represents a better recovery behavior after load release. The materials like NBR have a vast application in keeping it under stress, such as O-rings, gasket, and seals. So, the CS value investigation is so essential for NBR vulcanizates. This thesis only evaluated the CS of NBR vulcanizates and tried to find a correlation between CS and oil concentration in NBR matrices. Two different types of NBR were used in this thesis according to the recipe shown in Table 6. Figure 70 shows the graphical presentation of CS as a function of oil content for both types of NBR vulcanizates.

It is shown that the CS increases somewhat with increasing the oil content. Unplasticized NBR-34 vulcanizates reported higher CS than unplasticized NBR-18. For NBR-18 vulcanizates with lower oil content, the synthetic plasticizer Mesamoll<sup>®</sup> shows the lowest CS among all results. For both

NBR vulcanizates with low oil content, bio-oils show the higher CS values, and both types of NBR vulcanizates with 15 phr bio-oils reported the higher CS values. In contrast, the CS of both NBR vulcanizates is nearly independent of the concentration of TDAE shown in this figure.

A study [3] on this material was published in 2020, where it was shown that CS is correlated to crosslink density. NBR/Mesamoll® shows the lowest CS because it has a high network density claimed by this thesis, whereas the NBR/bio-oils had a low crosslink density and resultant high CS values. A study by Raju [125] also proved that the lowest hardness value represents the highest CS value. In addition, the relation between hardness value and crosslink density is linearly proportional [121]. So, the hardness values, crosslink density, and CS values are dependent on each other. The lower hardness values of NBR/bio-oils were measured in this study, and in parallel, the crosslink density of NBR/bio-oils was shown lower, and these are perhaps the basic reason behind the higher CS values.

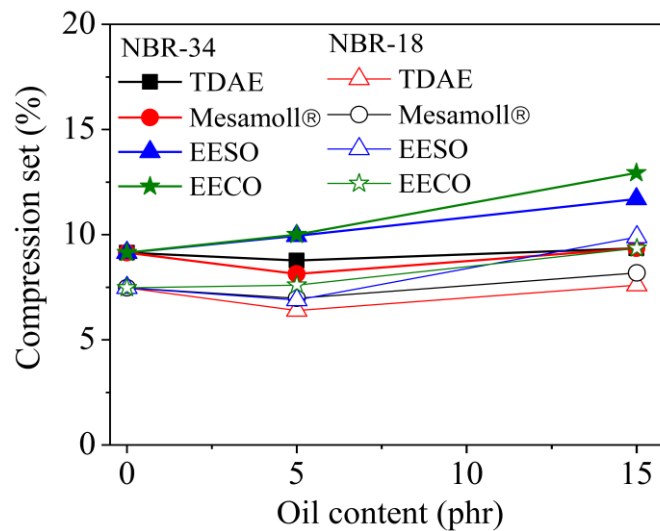


Figure 70: Dependence of compression set (CS) of NBR vulcanizates in different oil types and concentrations

The difference between unplasticized copolymer NBR-34 and NBR-18 were the ratio of monomer in their polymer chain, so the reason for the higher CS of unplasticized NBR-34 than unplasticized NBR-18 is the higher contribution of thermoplastic acrylonitrile monomer in NBR-34 polymer chain. So, recovery behavior after load release was poor than NBR-18. Both NBR vulcanizate with low oil content shows a lower CS, and a previous study [98] claimed the rubber vulcanizate with low oil content reported the filler dispersion was poor. Whereas the plasticizing effect and segmental mobility were pronounced at higher oil content, leading to higher compression set values. However, the bio-oils show the highest CS value of ~12%. In general CS of material as the application of a gasket should be below ~40% [250].

### Rebound resilience behavior of elastomers on bio-oil type and concentration

It is important to know the information on rebound resilience for both plasticized elastomer vulcanizates. The rebound resilience is informed about the amount of kinetic energy of an elastomer specimen gives back after an impact trial. When the elastomer deforms, it absorbs energy and partly recovers when it regains its original shape. The energy which is not restored as mechanical energy is wasted as heat in the elastomer. Hence, the energy is dissipated as heat. If the elasticity is high, less deformation energy is dissipated as heat [126]. This thesis was aimed at finding the correlations between rebound resilience and the oil concentration in elastomer matrices. The rebound resilience of the elastomer vulcanizates is depicted in Figure 71. It represents the



rebound resilience behavior of elastomer vulcanizates as a function of oil content. The unplasticized elastomers showed lower rebound resilience; specifically, unplasticized SBR showed the lowest rebound resilience.

It is clear that the rebound resilience of bio-oils containing elastomer vulcanizates was increased with increasing the oil concentration. A noticeable higher rebound resilience were visible for bio-oils than TDAE for both types of elastomers. Precisely it was exhibited that the rebound resilience were higher when elastomers were mixed with ROME and ROPE, whereas with TDAE, the changes were slightly low. SBR/EECO showed a slight increase when the EECO concentration increased.

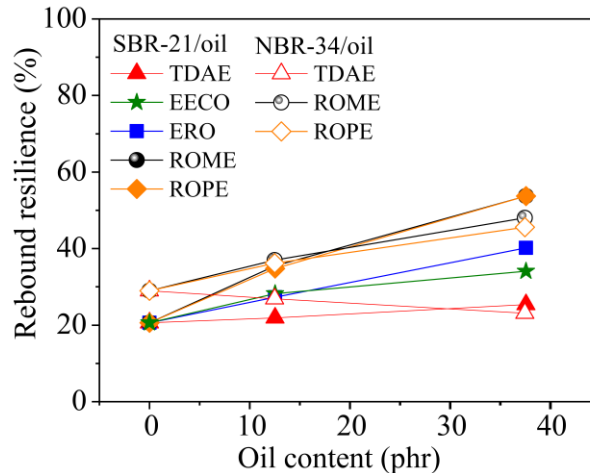


Figure 71: Variation of rebound resilience of SBR-21 with variable concentrations of different oils

A study by Rios [251] claimed that there is an inverse relationship between hardness and rebound resilience. When the hardness values are achieved high, this means the rebound resilience decreases, and this thesis has found the same trend. Generally, the hardness values decreased with increasing the oil concentrations, as shown in Figure 67, and unplasticized elastomers showed high hardness and low rebound resilience. NBR/TDAE has shown the high hardness value among plasticized elastomers, and it has the lowest rebound resilience. The hardness of elastomer/bio-oils was low, and they have shown high rebound resilience. A study [126] proved that the rubber vulcanizates with bio-oils had higher rebound resilience than that of the rubber vulcanizate with aromatic oil and same characteristics were noticed in this thesis.

## 4.5 Fracture mechanics parameters of oil-containing rubber vulcanizates

### Resistance against stable crack propagation behavior

The influence of oil types and concentrations on the carbon black-filled elastomers' resistance against the crack initiation  $J_i$  and stable crack propagation  $T_J^*$  was evaluated in this thesis. Within quasi-static tests, a single specimen method was applied. Only one specimen was loaded from zero up to the point of complete fracture, so error margins of the parameters for quasi-static measurement was absent.  $J_i$  and  $T_J^*$  were determined from the crack resistance curve ( $R$ -curve), which describes the correlations between crack resistance values ( $J$ -value) and crack opening length  $I_R$ . Figure 72 (a) and (b) show  $R$ -curves describing the stable crack propagation process are shown for filler-reinforced, plasticized SBR elastomers with three different amounts of oils. Generally, in these figures, it can be seen that the type and the amount of oil influence the crack

opening and slope of the  $R$ -curves and higher  $J$ -values of the plasticized SBR vulcanizates. Unplasticized SBR has a very small  $I_R$  (inset) because of early break under stress as their strain at break  $\varepsilon_B$  also very small (see Figure 68).  $J$ -values and  $I_R$  of SBR/EECO vulcanizate is comparatively higher than SBR/TDAE vulcanizate.  $J$ -values for SBR vulcanizate are observed higher when a low concentration (e.g., 12.5 phr) of oil is mixed, and it continuously decreases with increasing the oil concentration. In contrast,  $I_R$  has increased with increasing oil content.

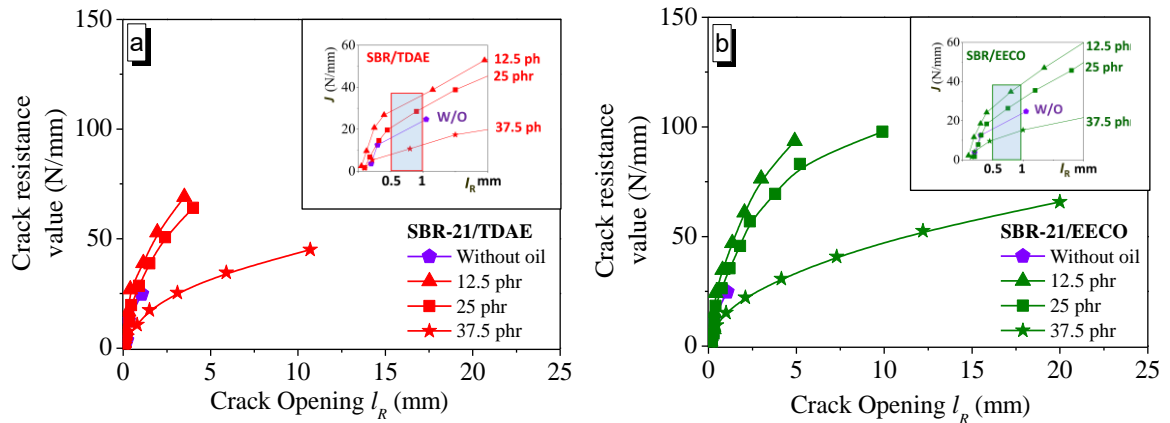


Figure 72: Crack resistance curves  $J$ - $I_R$  of SBR/TDAE vulcanizates (a), SBR/EECO vulcanizates (b) with different oil concentrations (Inset shows the region where  $T_J^*$  measured)

Different behavior of the SBR vulcanizates can be observed when the various but same concentrations of oils are mixed as shown in Figure 73. Due to the different polarities of SBR and NBR, not the same interaction with the used oils is expected. Figure 74 shows the difference in  $J$ -values when changing the polarities in NBR materials, where the interesting responses have recorded changing the polarities of NBR materials. However, depending on the oil content, not the same ranking of the  $R$ -curves are given for SBR and NBR materials, and this means there must be a further factor influencing the crack propagation. Here, the idea of an internal migration process due to the high strain and stress in front of the crack resulting from these different friction conditions at the molecular scale may deliver one additional explanation.

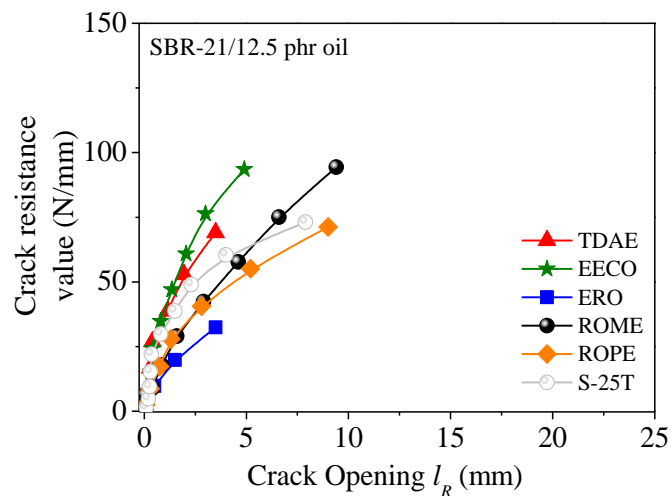


Figure 73: Crack resistance curves  $J$ - $I_R$  of SBR/12.5 phr oil vulcanizates

Concerning SBR materials with 12.5 phr oils was shown in Figure 75, and SBR/EECO shows a higher efficiency in improving the resistance against stable crack propagation  $T_J^*$  than TDAE.

When the oil amount is increased to 37.5 phr, the  $R$ -curves of SBR/EECO and SBR/TDAE are similar, but SBR/EECO has a larger crack opening. Interestingly, the stable crack propagation behavior of the SBR vulcanizate with 37.5 phr TDAE (mixed in) is different from that of the SBR material S-25T, based on an oil-extended SBR; this is shown in Figure 72, 69, and 71. No additional oil was added during mixing, but the amount of TDAE is comparable to the compound. S-25T vulcanizate shows the highest  $J$ -values.

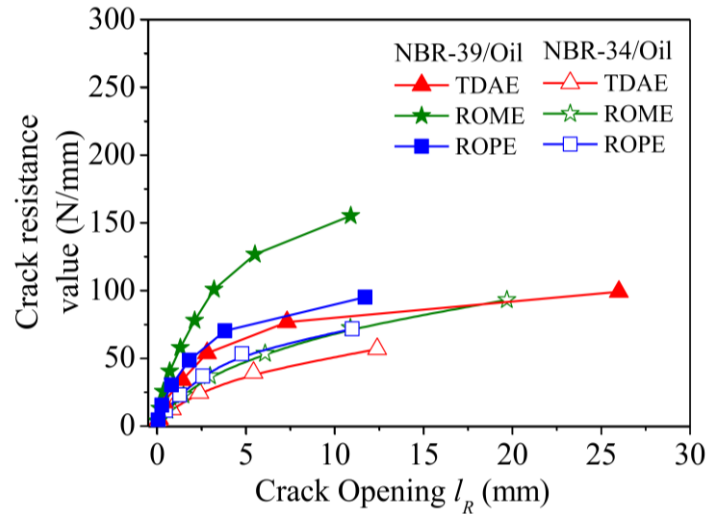


Figure 74: Dependence of oil types on crack resistance behavior  $J$ - $I_R$  of NBR vulcanizates

In some cases, this difference is not as pronounced for mechanical properties. The conditions for energy dissipation at the molecular level in S-25T are different from the vulcanizate with TDAE mixed. The result of the unplasticized SBR is almost similar to previous results [252], it could be stated that the oil influences crack propagation positively. It means the  $J$ -values of the plasticized materials are high the crack opening  $I_R$  values, and it is related to strain at break  $\epsilon_B$ , which was measured in tensile behavior investigation around 770 %.

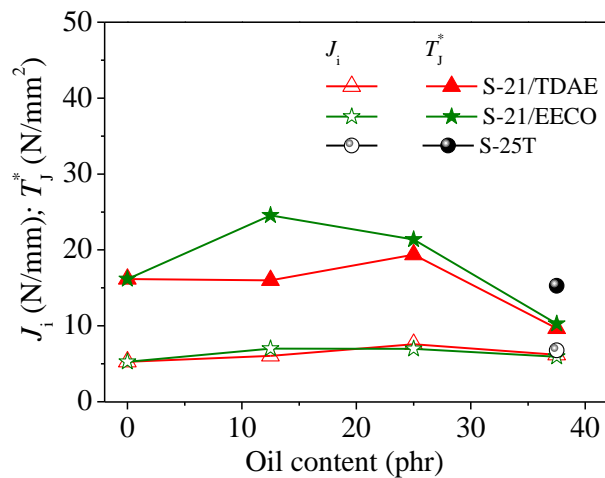


Figure 75: Crack initiation  $J_i$  and propagation values  $T_j^*$  of SBR-21 with different concentrations of oils

Consequently, the crack resistance of S-25T is higher. Here, the internal migration in the area around the crack tip can be a reason for the difference. For material S-25T, oil migration is expected to be lower due to the mixing of oil in the polymer chain. The crack initiation  $J_i$  values are different for the SBR and NBR materials with plasticizer content, as mentioned in Table 16. However, the stable crack propagation value  $T_J^*$  shows significant differences between EECO, ROPE, ROME, and TDAE. One reason for the high crack propagation values is the higher deformability of the material.

Table 16: Crack initiation  $J_i$  and stable propagation values  $T_J^*$  of polymer materials with different oils

Oil	SBR-21		NBR-39	
	$J_i$	$T_J^*$	$J_i$	$T_J^*$
W/O	5.27	16.16	11.26	20.05
TDAE	6.05	19.01	13.43	19.98
EECO	7.01	25.55	-	-
ERO	7.58	10.08	-	-
ROME	6.33	10.93	10.39	31.94
ROPE	7.07	12.58	10.86	22.23

Therefore, a much higher elastic deformation is possible/necessary to reach a critical value in front of the crack tip. Again, the idea of internal migration is pointed out as one possible reason for the different crack propagation. However, the stiffness of the materials may also contribute to the increase in crack resistance. If the deformation controls the stable crack propagation, a decreased stiffness combined with higher deformability will increase crack resistance. The crack initiation values  $J_i$  and stable crack propagation  $T_J^*$  values of the investigated two different polarities NBR materials are shown in Table 17, respectively. For both elastomers, the influence of the oil type is much more pronounced for the crack propagation value.

Further, the different oils lead to different crack resistance  $T_J^*$  levels for both series. For practical application, the crack resistance of the material should be high enough to prevent or slow down crack propagation. NBR vulcanizates generally have higher crack initiation values than SBR. However, NBR is generally known as a material with a low tear and cut resistance, so it was expected to have lower crack initiation values than the SBR vulcanizates. In contrast to the crack propagation, the crack initiation  $J_i$  is higher for the unplasticized NBR material than the SBR vulcanizate. While the crack propagation value of the SBR vulcanizates is relatively less influenced by the type of the oil and oil content except for EECO, in NBR, this quantity is strongly stabled with plasticizer addition except for ROME. EECO is a product having a comparatively low polar percentage [92] due to low conversion of epoxidized. The higher proportion of oleic acid [110] in the fatty acid chain of the chemical structure of EECO is one possible reason for the high level of crack resistance, and other mechanical properties were found in this thesis. Part of this investigation was published in 2021 [5].

Table 17 shows the influence of oil and NBR polarity on the resistance against crack properties. When the polar acrylonitrile monomer increased in materials (NBR-39), it was found that the efficiency of crack initiation  $J_i$  and stable crack propagation  $T_J^*$  value was high. Concerning  $T_J^*$  behavior of high polar NBR, the bio-oils, especially ROME, show excellent efficiency compared to the mineral oil-based TDAE.

Table 17: Crack initiation  $J_i$  and stable propagation values  $T_J^*$  of different NBR materials with different oils

Oil	NBR-34		NBR-39	
	$J_i$	$T_J^*$	$J_i$	$T_J^*$
W/O	8.91	8.83	11.26	20.05
TDAE	6.59	10.63	13.43	19.98
ROME	5.70	13.31	10.39	31.94
ROPE	4.19	14.09	10.86	22.23

Higher efficiency of resistance against stable crack propagation obtained when ERO mixes with low polar NBR materials, which was discussed in the previous article [5] published in 2021. According to a previous study [76] on bio-oils, it contains OH groups most compatible with polar polymers like NBR. Another study [26] claimed that during elastomeric materials' vulcanization, the bio-oil could be co-vulcanized to the elastomer matrix, and the oils may consume sulfur. In this case, the crosslink density would be reduced, which may also explain, e.g., higher deformability. The crosslink density from NMR measurement was investigated in this thesis that the lower crosslink density of elastomers when bio-oils mixed. Although, crosslink density has a large effect on  $E'$  and it was noticeable.

### Resistance against unstable crack propagations behavior

Besides the quasi-static fracture mechanics investigation, the fracture behavior under impact-like conditions was also characterized. Figure 76 shows the resistance dependence against unstable crack propagation  $J_d$  for carbon black-filled SBR and NBR vulcanizates when the type of oil has changed.

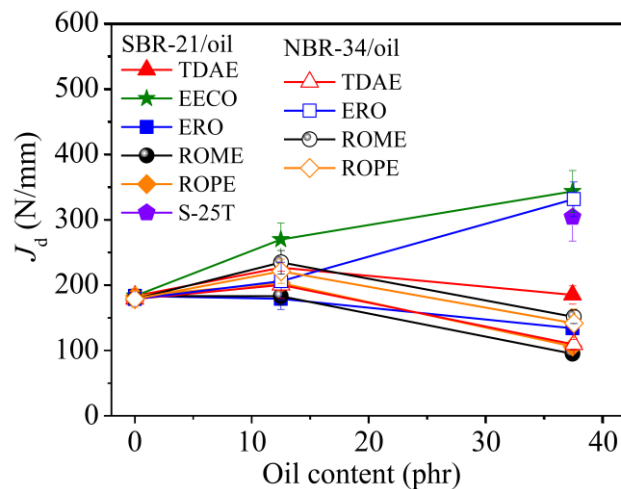


Figure 76: Dependence of unstable crack propagation  $J_d$ -values of polymer materials on the oil concentrations

The  $J_d$  becomes higher for all SBR/oil combinations or remains constant with a plasticizer content of 12.5 phr. The further increase in plasticizer content leads to a relatively substantial decrease in  $J_d$ , except for EECO. This vulcanizate shows continuously increasing  $J_d$ -values. This contrasts with the quasi-static fracture mechanics test, and it was related to viscoelasticity was measured and showed in Figure 59 and it was claimed that low  $E'$  shows high  $J_d$ . The  $J_d$ -value of carbon black filled SBR is similar to previously reported results [140] when no oil is added.

Table 18 shows the  $J_d$ -values for the polymer vulcanizates depending on the oil content and type. The data for SBR-21 and NBR-34 were already given in Figure 72, here added only to see the difference with NBR-39. The polymer type has a more significant influence on the unstable crack propagation behavior of the compounds whenever oils are the same. It appears that the addition of oils increased  $J_d$ , although, at a high concentration of oils,  $J_d$  decreased except for ERO.  $J_d$ -values had changed for specific oils when changes the polarity of NBR was shown in Table 18. Highly polar NBR (NBR-39) enhanced its efficiency when ROME was added instead of ERO. So, it could be a possible clear statement that the polarity of elastomers is a big concern in choosing the oils for it.

Table 18: Dependence of unstable crack propagation values  $J_d$  of polymer materials when the type of oils has changed

Oil	Unstable crack propagation value $J_d$ (N/mm)		
	SBR-21/12.5 phr oil	NBR-34/12.5 phr oil	NBR-39/12.5 phr oil
W/O	184 ± 8	179 ± 13	177 ± 7
TDAE	227 ± 12	200 ± 21	237 ± 19
EECO	270 ± 25	-	-
ERO	179 ± 16	-	-
ROME	183 ± 14	235 ± 18	303 ± 10
ROPE	204 ± 12	221 ± 19	254 ± 20

Furthermore, it is concluded that EECO leads to much higher  $J_d$ -values of SBR vulcanizates than TDAE, and again, this shows the replacement potential of this bio-oil. The reason for the high level of crack resistance of the EECO material is apparent, and further investigations were clarified. A low crosslink density of SBR/EECO was obtained and was shown in table 11, and this could be the strong possible reason for the high elongation of this system, also presented in Figure 68. The  $J_d$ -values were calculated according to load-extension diagram (see Figure 46), and due to the high extension ( $\varepsilon_B = 770\%$ ) of the SBR/EECO system, the overall  $J_d$ -values were noticeably higher than other systems. According to gel theory, plasticizer like EECO containing long aliphatic chains are more potent than plasticizers containing bulky cyclic groups like TDAE, especially at low temperatures and short time investigations [79].

The percolating arrangement of fillers seen at the length scale of micro-dispersion, especially at a high filler loading level, is called a filler network. It is assumed that the filler dispersion and the arrangement of the filler network [34,191] are influenced by EECO, ERO, and ROME and make the carbon black more compatible with the polymer matrix. These bio-oils destroyed the filler networks, so very less filler aggregates (see Figure 58) remains and this means more dispersed filler particles, better dispersion and therefore less filler network. The presented comparison figure, Figure 61, demonstrates that the filler network undergoes significant deterioration in multiple bio-oil blended elastomers, exhibiting varying degrees of damage. However, it is noteworthy that the fracture mechanics analysis fails to exhibit analogous patterns among the bio-oil blended elastomers. Consequently, this indicates that the filler network's contribution to the fracture phenomenon is not of substantial significance.

## 4.6 Dependence of aging characteristics on oil type

### Thermo-oxidative aging of highly plasticized rubber vulcanizates

Thermo-oxidative aging was investigated in selected materials based on SBR vulcanizates. This experiment was carried out on the plasticized SBR vulcanizates when a high content (e.g., 37.5 phr) oil mixes. A high concentration of oil was chosen because the changes can be more visible due to their high amount in the SBR matrix. TDAE was chosen as a conventional plasticizer, and EECO was selected because of the higher resistance against crack propagation found during the investigation. S-25T samples were also used for this investigation because they have 37.5 phr TDAE content and showed comparable mechanical and fracture resistance efficiencies. Figure 77 (a) shows the resistance against stable crack propagation  $T_J^*$  behavior of SBR materials as a function of aging time. It was visible that  $T_J^*$  increases up to 15 days for EECO-loaded SBR with increasing the aging time. After that, it decreases. Whereas SBR with TDAE  $T_J^*$  decreases little when aging time increases. In contrast, for S-25T,  $T_J^*$  changes over aging time. In the beginning  $T_J^*$  decreases, when aging time prolonged, then it was noticed that  $T_J^*$  slightly increased, and when aged up to 30 days, then  $T_J^*$  decreased noticeably. Parallely, Figure 77 (b) shows the dependence of resistance against unstable crack propagation  $J_d$  over the aging time. Remarkable changes in  $J_d$  were observed. It was evidently noticeable that  $J_d$  decreased continuously with aging time, and this characteristic happens for all plasticized SBR vulcanizates. The reduction of  $J_d$  was so sharp for all samples over 3 days of aging, and then  $J_d$  reduced but almost linearly and not intensely.

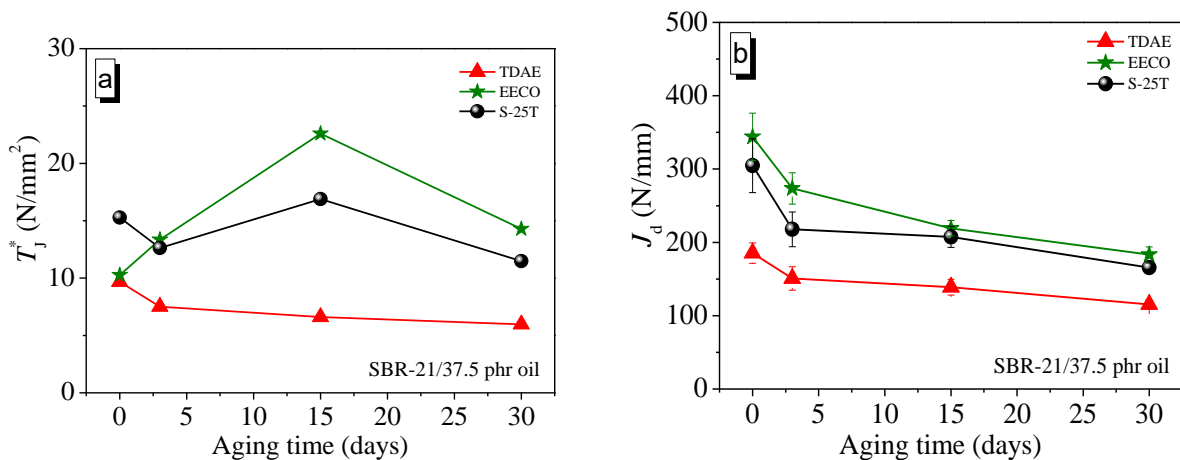


Figure 77: Influence of thermo-oxidative aging of high concentrated plasticized SBR at 80 °C on the fracture mechanics behavior; stable crack propagation value (a), unstable crack propagation value (b)

Tensile behavior of unaged and aged SBR vulcanizates were listed in Table 19. Changes in tensile strength  $\sigma_m$ , strain at break  $\varepsilon_B$ , and stress at 200% strain  $\sigma_{200}$  were mentioned over aging time. A general trend was followed for changing  $\varepsilon_B$  and  $\sigma_{200}$  over aging time was noticed in this thesis. All plasticized SBR samples were shown that  $\varepsilon_B$  decreased over aging time, although the values were different. The  $\varepsilon_B$  difference between unaged and 30 days aged plasticized SBR samples was 150 to 200 %. A considerable reduction was visible for S-25T, and it was 203 %, whereas the difference was smaller, around 150 % for SBR/TDAE system, and SBR/EECO has a 180 % diminution.  $\sigma_{200}$  slightly increases for plasticized SBR samples over aging time, and the difference was between 1 to 2 MPa. A sharp increase of  $\sigma_{200}$  was visible for SBR/TDAE and SBR/EECO systems, and the differences were 1.2 MPa recorded. Changing tensile strength  $\sigma_m$  was not noticeable over aging time for SBR/TDAE, although for SBR/EECO system,  $\sigma_m$  changes slightly. For the S-25T system,

up to 15 days of aging, there was no noticeable change of  $\sigma_m$  observed, but a slight reduction of  $\sigma_m$  was recorded after 30 days of aging.

Table 19: Summary of selected characteristic values from the tensile test for carbon black reinforced SBR compounds with 37.5 phr of different plasticizers

Days	SBR-21/TDAE			SBR-21/EECO			S-25T		
	$\sigma_{200}$ (MPa)	$\sigma_m$ (MPa)	$\epsilon_B$ (%)	$\sigma_{200}$ (MPa)	$\sigma_m$ (MPa)	$\epsilon_B$ (%)	$\sigma_{200}$ (MPa)	$\sigma_m$ (MPa)	$\epsilon_B$ (%)
Unaged	2.17 ± 0.1	6.4 ± 0.1	441 ± 70	1.16 ± 0.1	11.5 ± 1	771 ± 23	1.80 ± 0.0	19.0 ± 2	727 ± 30
3	2.70 ± 0.1	7.0 ± 0.5	416 ± 21	1.50 ± 0.3	12.5 ± 2	713 ± 45	2.20 ± 0.1	18.0 ± 2	699 ± 26
15	3.60 ± 0.2	6.6 ± 0.5	329 ± 20	2.16 ± 0.1	13.0 ± 1	635 ± 22	3.17 ± 0.1	17.5 ± 1	600 ± 27
30	4.20 ± 0.1	6.3 ± 0.0	287 ± 90	2.35 ± 0.2	12.0 ± 1	590 ± 38	3.66 ± 0.1	15.5 ± 2	524 ± 33

Table 20 shows the changes in tear strength  $T_s$  and hardness values over the aging time of different plasticized SBR vulcanizates. A common statement can be expressed here because a general trend was observed in this table.  $T_s$  for all plasticized SBR samples has been decreased when aging time increased. The reduction of  $T_s$  varied from 2 to 3.5 N/mm after 30 days of aging.  $T_s$  of the SBR/TDAE system and for S-25T were reduced by 2 N/mm after 30 days of aging, whereas SBR/EECO system was reduced by 3.5 N/mm. An inverse relation was observed for hardness behavior than  $T_s$  over aging time. For all samples, it was noticed that the hardness values continuously increased with increasing aging time. The hardness difference of plasticized SBR between unaged conditions and 30 days aging was 8 to 11. Hardness value increases for SBR/TDAE system was 8, whereas for SBR/EECO system was 9, and for the S-25T system, it was around 11.

Table 20: Summary of characteristic values from the tear test and Shore A hardness values for carbon black reinforced SBR compounds with 37.5 phr of different plasticizers

Days	SBR-21/TDAE		SBR-21/EECO		S-25T	
	$T_s$ (N/mm)	Shore A (-)	$T_s$ (N/mm)	Shore A (-)	$T_s$ (N/mm)	Shore A (-)
Unaged	7 ± 0.5	45 ± 0.8	9.5 ± 0.5	35 ± 0.5	6.5 ± 0.7	40 ± 0.4
3	6 ± 0.3	45 ± 0.5	8.0 ± 0.5	38 ± 1.5	6.0 ± 0.7	45 ± 0.5
15	6 ± 0.1	50 ± 0.5	7.0 ± 0.1	43 ± 0.1	5.0 ± 0.3	47 ± 0.6
30	5 ± 0.1	53 ± 0.5	6.0 ± 0.9	44 ± 0.5	4.5 ± 0.3	51 ± 0.5

When SBR mixed with EECO, the NMR measurement detected the chemical crosslinking was comparatively lower than with TDAE. So, the rate of post-curing of EECO is probably higher compared to TDAE. Therefore, an increase of  $T_J^*$  and assumed to increase  $\sigma_{200}$  (see Table 19). After that,  $T_J^*$  slightly decreased due to degradation because of keeping the sample at a high temperature for a long time.  $\sigma_m$  also slightly reduced and followed the same order as the fracture resistance behavior. The decrease of strain at break  $\epsilon_B$  is perhaps due to the high crosslinks formation and oxidizing skin, which results from oxygen uptake at the surface of the specimen, as stated by Brown [253].  $T_s$  have decreased because of the oxidative degradation developing rapidly, leading to this



marked decrease, and this phenomenon is more pronounced as the aging temperature increases, as stated by Budruga [254]. A high temperature accelerates post-curing of EECO-loaded SBR and is due to the high crosslink's formation and the oxidizing skin, which results from oxygen uptake at the surface of the specimen. Jhao [14] described the rapid increase of crosslinking density because of butadiene segments of SBR vulcanizates. Elastomers are easily oxidized and exhibit crosslink reactions under high temperatures like 80 °C. As a result, the  $J_d$ -values consistently decrease with increasing aging time and a post-curing is the reason for reducing  $J_d$ -values. In oxygen-containing environments, the mechanical strength of rubbers can be significantly affected by oxidation, especially at relatively high temperatures. A previous study by Coran [255] stated that, after vulcanization, if the materials are kept at a high temperature for a long time, post-curing happens during this time. Shore A hardness increased over aging time because of the post-curing [26],[66] it happened during the aging time at a high temperature like 80 °C. A previous study [14] showed that elastomers are generally becoming stiff and brittle during the thermal oxidation process at high temperatures due to the predominant oxidation and crosslinking reactions facilitated by the double bonds are easily attacked due to electron shifts. This work found the same incident, whether no oil or added low or high content of oil. So, overall, many factors can affect the SBR vulcanizates during aging, especially the type of oil and concentration, aging temperature, aging time, and the presence of oxygen in the atmosphere. These factors can be changed in the resistance against stable and unstable crack propagation, tensile strength, strain at break, tear strength and hardness behavior of plasticized SBR vulcanizates.

#### Influence on crack resistance behavior of materials when mixed with stored bio-oils

Crack resistance behavior of elastomers was investigated when they mixed with stored bio-oils instead of unaged oils. However, selected materials were chosen and investigated. Figure 78 shows the FTIR peaks of the TDAE and different bio-oils. This is interesting to investigate the bio-oils in fresh and after stores. This investigation has been done to discover possible chemical changes during bio-oil storage. The FTIR was measured for the stored oils, including bio-oils and TDAE. The enlargement of changed peaks is shown in Figure 78.

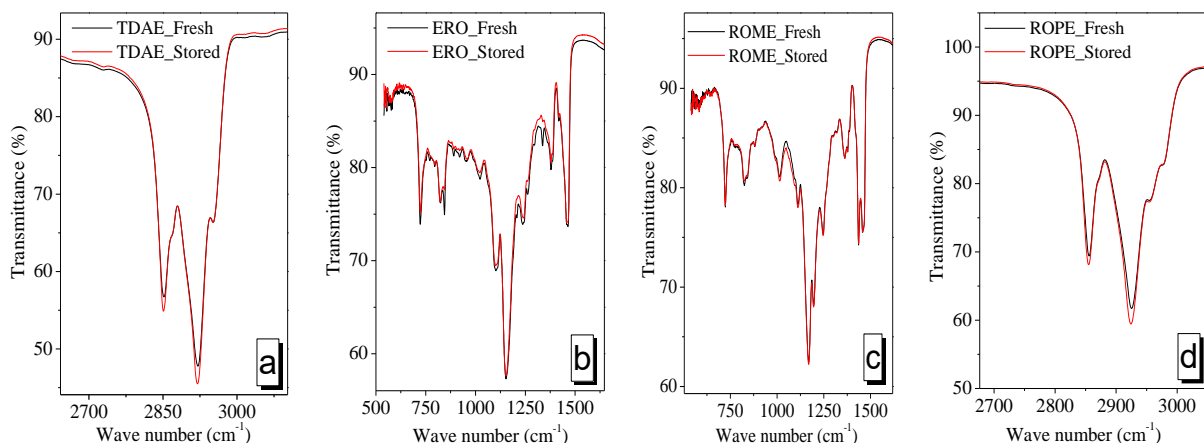


Figure 78: The enlarged ATR-FTIR spectrum of the oils in fresh conditions (black lines) and stored for six months (red lines); (a) TDAE, (b) ERO, (c) ROME, (d) ROPE

There were not well-noticed peaks changes, and the figure depicted that the intensity of peaks has changed in some cases. There is no evidence peaks corresponding to new functional groups. This means only weak evaporation has mostly happened here without any chemical reactions. However, the fracture mechanics behavior can be assumed to be influenced when some of the portions of components were changed. Nevertheless, the stored bio-oils can be positively influencing the

behavior of fracture mechanics when they stored for six months. This thesis was only focused on the changes in peak intensity and the missing peaks were not recognized as changes had been made.

Table 21 shows the  $T_g$  as a result of DSC analysis of different oils in a fresh state and after being stored. No considerable difference was noticed in the concern of  $T_g$ . According to the FTIR measurement, it was proved that the intensity of some hydrocarbon chains in the fatty oils has slightly changed, but it did not influence the  $T_g$  of the compound a lot. As a result, there was no visible change in the compound's molecular mass nor made it more or less branched. These are the criteria that the  $T_g$  did not influence much.

Table 21: Glass transition temperature  $T_g$  of fresh and stored oils

Oil	$T_g$ (°C)	
	Fresh	Stored
TDAE	-50	-52
ERO	-64	-65
ROME	-86	-87
ROPE	-93	-92

Figure 79 shows the rubber-layer  $L$  for plasticized elastomer raw mixtures. The rubber-layer  $L$  of raw mixtures with unaged and stored oils were compared. The influence on the rubber-layer  $L$  has noticeable visibility only in Figure 79(a) and especially for the SBR/ERO mixture and a little change for the SBR/ROPE. Uncured materials' rubber-layer  $L$  behavior can predict vulcanized materials' fracture and mechanical behavior. The materials with higher rubber-layer  $L$  values should have higher fracture and mechanical efficiencies.

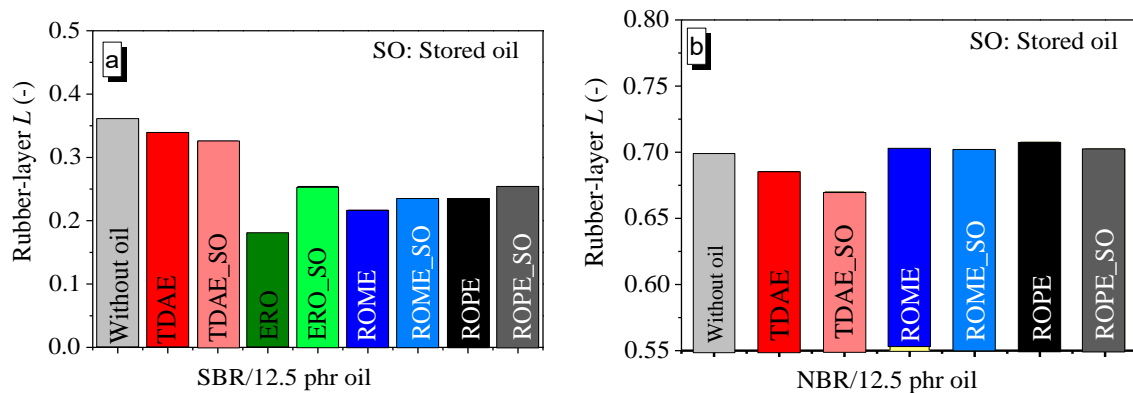


Figure 79: Influence of stored oil on bound-rubber fraction of different types of 12.5 phr oil loaded raw mixtures of SBR-21 (a) and NBR-39 (b)

Crack resistance behavior was investigated for the elastomers mixed with oils before and after stored was shown in Figure 80. The crack resistance ( $J$ -values) for SBR materials were surprisingly enhanced when bio-oils were stored for six months, and the values are shown in Figure 80 (a). Furthermore, Figure 80 (b) shows that NBR materials did not influence the crack resistance behavior much.

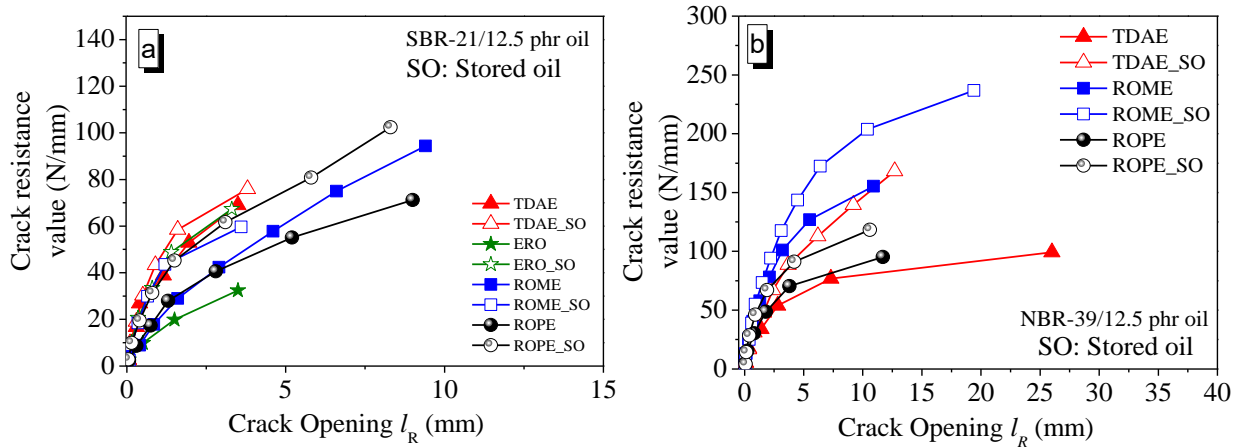


Figure 80: Crack resistance behavior of plasticized SBR (a) and NBR (b) materials where fresh oils (solid symbols) and stored oils (open symbols) were compared

Crack initiation values  $J_i$  and stable crack propagation values  $T_J^*$  were written in Table 22, and the results show that it was correlated to the changes in chemical characteristics describing FTIR analysis and mentioned in Figure 78. However, the exact prediction was made for getting rubber-layer  $L$  values depicted in Figure 79. After storage, ERO and ROPE have slightly changed their chemical behavior, enhancing the rubber-layer  $L$  of uncured SBR raw mixtures. The resistance against crack behavior followed the same trend and enhanced the resistance against crack behavior when they were added into SBR vulcanizates. Table 22 also describes the crack resistance behavior of NBR vulcanizates. As ROPE changes, some component concentrations (see Figure 78) enhance the  $T_J^*$  of NBR vulcanizates. However, rubber-layer  $L$  of NBR/ROPE did not follow the trend for unknown reasons.

Table 22: Crack initiation  $J_i$  and stable crack propagation values  $T_J^*$  of SBR and NBR materials when it was mixed with fresh and stored oil

Oil (12.5 phr)	SBR-21				NBR-39			
	Fresh oil		Stored oil		Fresh oil		Stored oil	
	$J_i$ (N/mm)	$T_J^*$ (N/mm <sup>2</sup> )	$J_i$ (N/mm)	$T_J^*$ (N/mm <sup>2</sup> )	$J_i$ (N/mm)	$T_J^*$ (N/mm <sup>2</sup> )	$J_i$ (N/mm)	$T_J^*$ (N/mm <sup>2</sup> )
W/O	5.27	16.16	×	×	11,26	20.05	×	×
TDAE	6.05	19.01	9.18	18.5	13,43	19.98	11.08	21.56
ERO	7.58	10.08	9.77	24.93	×	×	×	×
ROME	6.33	10.93	8.52	24.15	10.39	31.94	11.50	32.05
ROPE	7.07	12.58	8.72	22.50	10.86	22.23	13.48	32.03

Resistance against unstable crack propagation ( $J_d$ -values) for plasticized elastomers followed a different trend, as shown in Table 23. As discussed before, ERO have some chemical changes (see Figure 78) during storage time, and the resistance against stable crack propagation has been enhanced for this reason. The rubber-layer  $L$  of uncured SBR predicted the same, but resistance against unstable crack propagation has decreased for SBR after storage of ERO and ROPE mentioned in Table 23. Furthermore, it shows that the NBR vulcanizates were not influenced as SBR when mixed with stored ROPE. Overall results show the characteristics changes of ERO, and ROPE only influenced the non-polar elastomers like SBR but not polar elastomers like NBR.

Table 23: Unstable crack propagation value  $J_d$  of SBR and NBR materials when it was mixed with fresh and stored oil

Oil (12.5 phr)	$J_d$ (N/mm)			
	SBR-21		NBR-39	
	Fresh oil	Stored oil	Fresh oil	Stored oil
W/O	184 ± 80	-	177 ± 70	-
TDAE	227 ± 12	213 ± 13	237 ± 19	249 ± 33
ERO	179 ± 16	172 ± 22	-	-
ROME	183 ± 14	186 ± 13	303 ± 10	324 ± 28
ROPE	204 ± 12	129 ± 24	254 ± 20	255 ± 27

The investigation proceeded intensively, where the mechanical behavior was also investigated. The mechanical data for elastomers were mentioned in Table 24 and 25. Changing characteristics of oils slightly negatively influenced the mechanical behavior. The overall mechanical data for plasticized SBR vulcanizates was written in Table 24. SBR vulcanizates' hardness increased after being stored for bio-oils, where tensile strength  $\sigma_m$  and strain at break  $\varepsilon_B$  decreased for SBR when mixed with stored oils. The tear strength  $T_s$  increased for SBR vulcanizates when mixed with stored oils

Table 24: Dependence of mechanical behavior of SBR materials on the type oils mixes before and after stored

SBR-21/ 12.5 phr oil	Shore-A		$\sigma_m$		$\varepsilon_B$		$T_s$	
	Fresh oil	Stored oil	Fresh oil	Stored oil	Fresh oil	Stored oil	Fresh oil	Stored oil
W/O	64.7 ± 1.2	×	21.4 ± 0.9	×	437 ± 13	×	5.99 ± 0.6	×
TDAE	56.6 ± 1.3	56.6 ± 0.4	24.0 ± 1.9	21.5 ± 3.2	584 ± 25	566 ± 53	7.12 ± 0.3	8.16 ± 1.0
ERO	55.9 ± 0.6	57.9 ± 0.3	16.7 ± 10	15.1 ± 1.7	475 ± 36	412 ± 31	7.58 ± 0.4	6.30 ± 0.1
ROME	55.7 ± 0.6	56.3 ± 0.6	17.9 ± 2.6	17.8 ± 10	559 ± 49	474 ± 13	6.76 ± 0.5	6.08 ± 0.7
ROPE	55.2 ± 0.7	56.6 ± 0.6	21.1 ± 0.6	18.5 ± 1.1	557 ± 16	467 ± 19	6.33 ± 0.7	6.53 ± 0.7

The mechanical behavior of plasticized NBR vulcanizates was compared in Table 25. The hardness values and  $T_s$  are not much influenced. On the other hand,  $\sigma_m$  and  $\varepsilon_B$  slightly decreased for NBR when it was mixed with stored oils.

Table 25: Dependence of mechanical behavior of NBR materials on the type oils mixes before and after stored

NBR-39/ 12.5 phr oil	Shore-A		$\sigma_m$		$\varepsilon_B$		$T_s$	
	Fresh oil	Stored oil	Fresh oil	Stored oil	Fresh oil	Stored oil	Fresh oil	Stored oil
W/O	77.4 ± 0.5	×	22.0 ± 1.6	×	275 ± 14	×	8.09 ± 0.2	×
TDAE	68.1 ± 0.5	66.0 ± 0.8	18.8 ± 0.8	16.0 ± 1.4	404 ± 34	405 ± 40	11.0 ± 0.2	9.46 ± 0.1
ROME	61.0 ± 0.5	61.5 ± 0.7	23.5 ± 1.2	19.5 ± 1.7	569 ± 20	501 ± 41	14.9 ± 0.3	15.3 ± 1.4
ROPE	63.4 ± 0.6	63.8 ± 0.5	18.6 ± 1.1	14.2 ± 1.3	445 ± 30	370 ± 33	12.8 ± 0.1	13.7 ± 0.4
EESS	71.9 ± 0.6	62.8 ± 1.6	11.5 ± 0.7	22.6 ± 3.0	240 ± 20	523 ± 43	13.3 ± 0.9	14.4 ± 0.4

The main objective behind the modification of bio-oils was to modify its chemical structure by eliminating unsaturation content into an oxirane oxygen ring, thereby improving the prepared epoxide's thermo-oxidative stability. The use of modified oil is possible as a lubricant base liquid due to its good lubricity and higher thermo-oxidative stability than its structurally unmodified methyl esters [256], and unsaturation content in the oil restricts its direct use as lubricant base stock. Therefore, bio-oil was modified via epoxidation structure to convert unsaturation in oleic, linoleic, and linolenic acids into epoxy-groups, thereby improving the thermo-oxidative stability [216].

## 5 Structure-property correlations

Structure-property correlations link structure to the behavior of a material and are central to polymer science, product development, and design. For example, understanding the relationship between structure and specific physical properties is crucial for the development of advanced materials such as elastomers with bio-based compounds such as vegetable oil-based plasticizers. For traditional elastomers, finding structure-property relationships is easier because some specific properties are well-defined (e.g., chemical properties, fracture behavior, filler dispersion), measured with precise instruments, and are usually inherent in the final structural product. The composition of elastomers creates more and more different new types with different physical properties, such as entanglement length or glass transition temperature. There are several attempts that attempt to estimate properties from microscopic modelling.

Styrene butadiene rubber (SBR) is a non-polar polymer. Measuring the surface tension of oil is a primary option for selection as a plasticizer for SBR vulcanizates. The structure of SBR is favorable for absorbing non-polar oils, while polar oil reduces its general properties. The change in crosslinking density of SBR with changed oil type and concentration was determined in this work using NMR spectra. The rubber layer L of the SBR raw mixture is influenced by the type of oil addition.

In contrast, acrylonitrile butadiene rubber (NBR) is a polar polymer. Information on the surface tension of oils helps to find suitable oil as a plasticizer for NBR vulcanizates. NBR is accepted as a plasticizer by more polar oils, and NBR's general properties decrease when insisting on being blended with non-polar oils, as observed in this thesis. The type and concentration of the oil affect the crosslink density of NBR. The type of oil influenced the rubber layer L of NBR raw compounds. Oil migration from the NBR matrix depends on the type and concentration of the oils.

This chapter aims to establish some important structure-property correlations from this comprehensive study that can help to adopt other material compositions for fracture and mechanical behavior.

The structure-property correlation was established between the epoxidation rate of oil and the crack propagation behavior of polymers as shown in Figure 81. The presence of the epoxide group in oil influenced the cracking behavior of polymers, which was measured in this work.

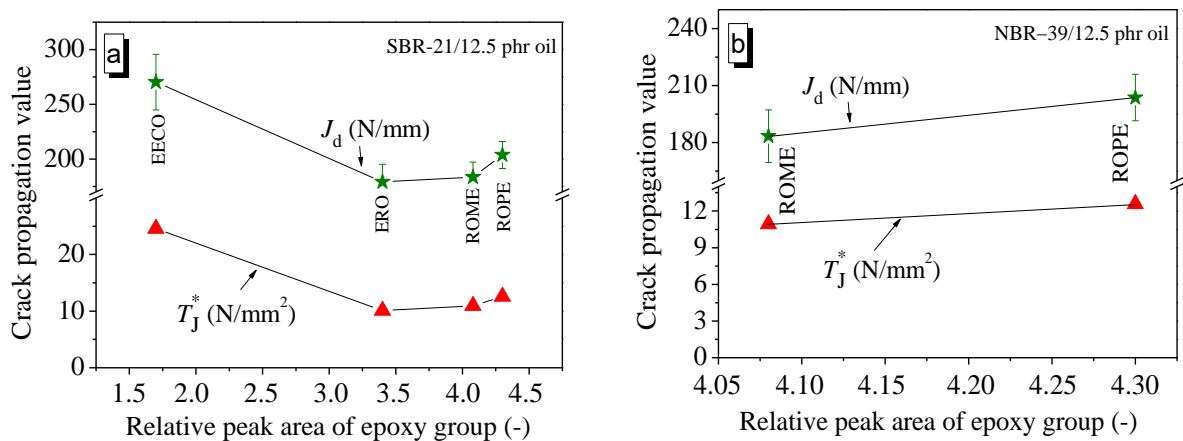


Figure 81: Correlation between the fraction of epoxidation in bio-oils and crack propagation value of SBR (a) and NBR (b) vulcanizates

The low epoxy group content in the oil correlated with the high resistance to crack propagation of SBR. However, when the presence of the epoxy group in bio-oil is high, the effectiveness of resisting crack propagation of SBR is made to be poor. NMR spectroscopy showed that ERO, ROME and ROPE have a higher relative peak area for the epoxy group ranging from 3.4 to 4.4. This does not significantly affect the resistance to crack propagation in SBR vulcanizates.

In contrast, it has been reported that the resistance to crack propagation of NBR is proportional to the level of epoxy groups in the bio-oil. Epoxide rings are polar [107] and more active [104] with polar polymers. So if epoxide conversion is high, this could predict a better fit with polar elastomers like NBR. A study [257] was conducted to find these relationships and showed that the low transformation of the epoxide rings could improve the resistance to crack propagation for non-polar elastomers.

Figure 82 (a) and (b) shows the correlation of the crack resistance behavior of elastomer vulcanizates with their chemical crosslink density as detected by solid state NMR. The influence of resistance to crack propagation behavior was pronounced when the crosslink density of elastomer was changed. In this thesis it was found that lower crosslinking of the SBR/EECO and NBR/ROPE system is essential for higher resistance to crack propagation. When the crosslink density is high then the resistance to crack propagation is as low as unplasticized elastomers shows. However, the linear crack resistance-crosslink density correlations only followed the elastomer when blended with oils, showing low surface tension and better hydrodynamic reinforcement in the elastomer matrix. The fact that the oil disrupts crosslinking during vulcanization has been demonstrated previously [72] and was visible in this study. However, optimization of crosslink density is essential to achieve higher resistance to crack propagation. Some previous studies [241,258] found a correlation between cracking behavior and crosslink density of elastomers, showing that optimizing crosslink density is very important to improve resistance to cracking.

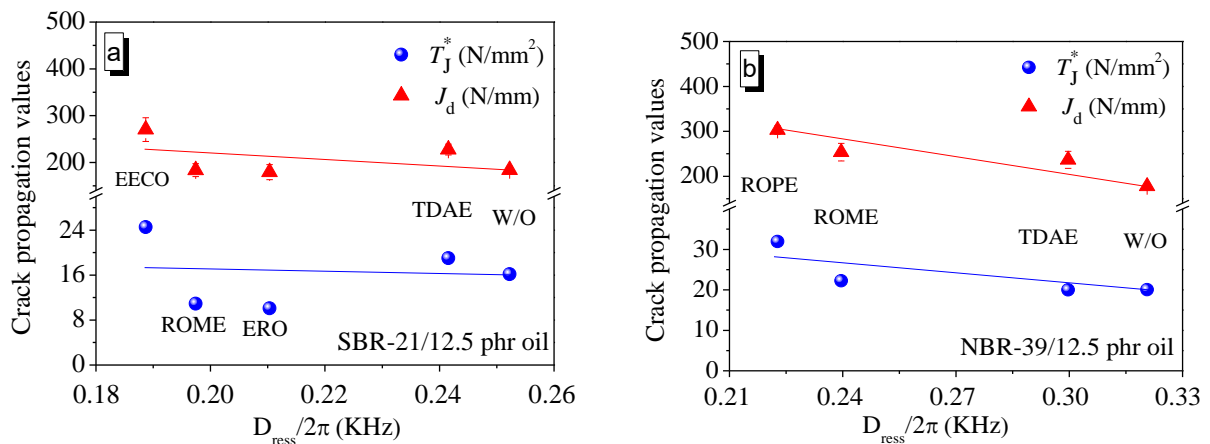


Figure 82: Correlation between crosslink density and crack propagation value of SBR (a) and NBR(b) vulcanizates

In this thesis, an attempt was made to find correlations between the resistance to crack propagation and the rubber-layer  $L$ . Figure 83 suggests that the resistance to crack propagation in SBR materials is linearly proportional to the rubber-layer  $L$ . The correlation of the rubber-layer  $L$  was determined for stable and unstable crack propagation. It was very optimistic that the correlations for both types of loads applied for the crack resistance study followed the same. That means it opens up the possibility of choosing a test method to know the material properties, which can reduce time and material costs.

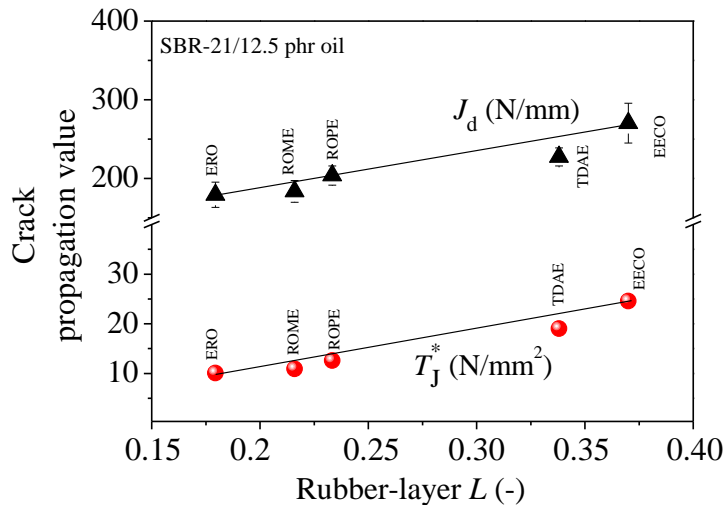


Figure 83: Correlation between rubber-layer  $L$  and crack propagation values of plasticized elastomer vulcanizates

Figure 84 shows the relationship between crack resistance and surface tension of oils. It is a correlation to see how the resistance to crack propagation behaves when measuring the surface tension of oils on the same elastomers. It shows an intriguing relationship between the resistance to crack propagation and the surface tension of oils, where it was observed that crack propagation values decreased linearly with increasing surface tension. The correlation was independent of the polarity of the elastomers and the mode of crack propagation. Both polymer types (e.g. SBR and NBR) and each test method for crack propagation were applicable for this correlation. Some necessary steps like predicting the mechanical behavior and crack resistance of elastomers can be decided to get out of this correlation. The process of selecting oils as plasticizers can be performed first to measure the surface tension on the untreated elastomer surface. Low surface tension can predict high crack resistance, reducing testing cost and time. However, the presence of fillers and additives can create some differences, so this can be a constraint when making a decision. Although this thesis claims a weak influence of fillers and additives, the lower surface tension of oils showed higher resistance to cracking.

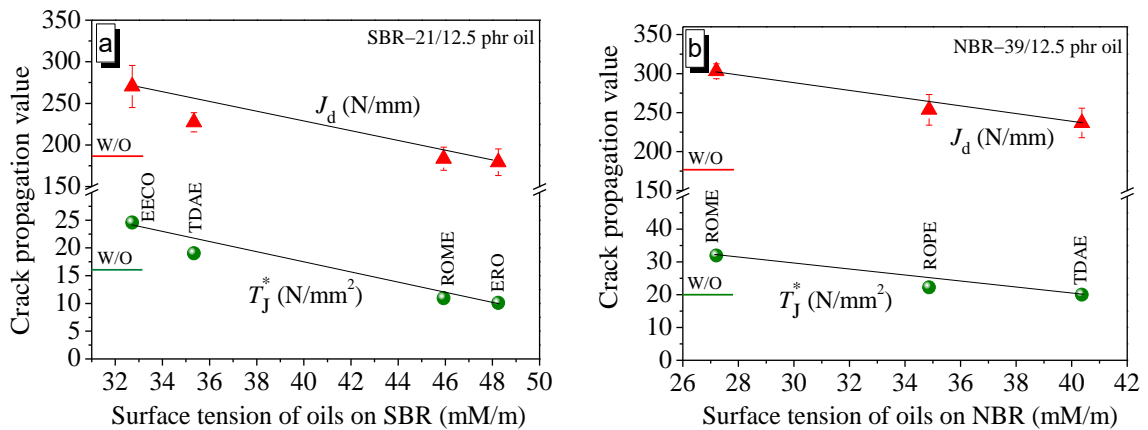


Figure 84: Correlation between surface tension and crack propagation values of SBR (a) and NBR(b) vulcanizates



There are some general results to be gained from structure-property correlations.

Conversion of high epoxidation to bio-oil correlated with high crack resistance of the polar elastomer. The polar elastomers are compatible with those bio-oils that have a high epoxidation conversion.

A thick rubber-layer  $L$  correlates with the high efficiency of crack resistance. Therefore, if a plasticized elastomer has a large rubber-layer  $L$ , then it is normal to expect high crack resistance performance from that elastomer.

The low surface tension of oils correlates with high crack resistance. This information can help predict the crack resistance behavior of plasticized elastomer when the oil on that elastomer has low surface tension under untreated conditions.

The structure-property correlations are the only important tool emerging from findings to characterize the elastomers plasticized with bio-oils. In general, the structure-property correlation is built to reveal some relationships that help to prepare new materials with advanced ideas. The crack resistance behavior can be assumed if the structure and the material behavior of elastomers and their impact on the oils are known. This thesis helps to establish structure-property correlations, so just knowing some general properties of the oil can presume that it is a match for the desired polymers.

## 6 Summary

This thesis is part of an investigation of the carbon black-filled elastomers based on their polarity and tried to fit with appropriate bio-oils as plasticizers. Initially, bio-oils are characterized according to physical, chemical, thermal, and aging behavior. The crack resistance information of the materials was a significant concern. Physical, structural, thermal, mechanical, and aging behavior was considered during the investigation. This thesis was divided into four steps, as discussed in the beginning. These were summarized according to their results.

Step 1: Bio-oils have been studied in a number of ways. Chemical, thermal and physical tests have mainly been carried out to ensure compatibility with the appropriate elastomers capable of developing mechanical behavior and breaking strength. Some important findings have been highlighted and shown in Figure 85. Density and viscosity were part of the physical properties of the tests performed. The density of bio-oils was around 1 g/cm<sup>3</sup> except that ERO was 1.05 g/cm<sup>3</sup>. The viscosity of ERO was 137 mm<sup>2</sup>/s while the viscosity of other bio-oils stayed between 12-31 mm<sup>2</sup>/s. The density and viscosity of TDAE were 0.94 g/cm<sup>3</sup> and 375 mm<sup>2</sup>/s, respectively. The surface tension measurement was taken to see the polarity of the oils. EECO was low polar, hence the surface tension on the SBR was low, whereas ERO, ROME and ROPE were comparatively high polar and low surface tension was observed on NBR materials. GPC, FTIR and NMR measurements were carried out for chemical characterization. The molar mass of ERO was 1226 g/mol, while the molar mass of other bio-oils was 350-500 g/mol. In the FTIR and NMR tests, a high conversion of the epoxidation was observed, while EECO showed a low conversion of the epoxidized ester compound and the decomposed and formed OH group. Thermal DSC analysis was performed and it was found that the  $T_g$  of bio-oils was comparatively low and several melting peaks were observed. DSC was measured after storing it for six months to find that the  $T_g$  had changed slightly.

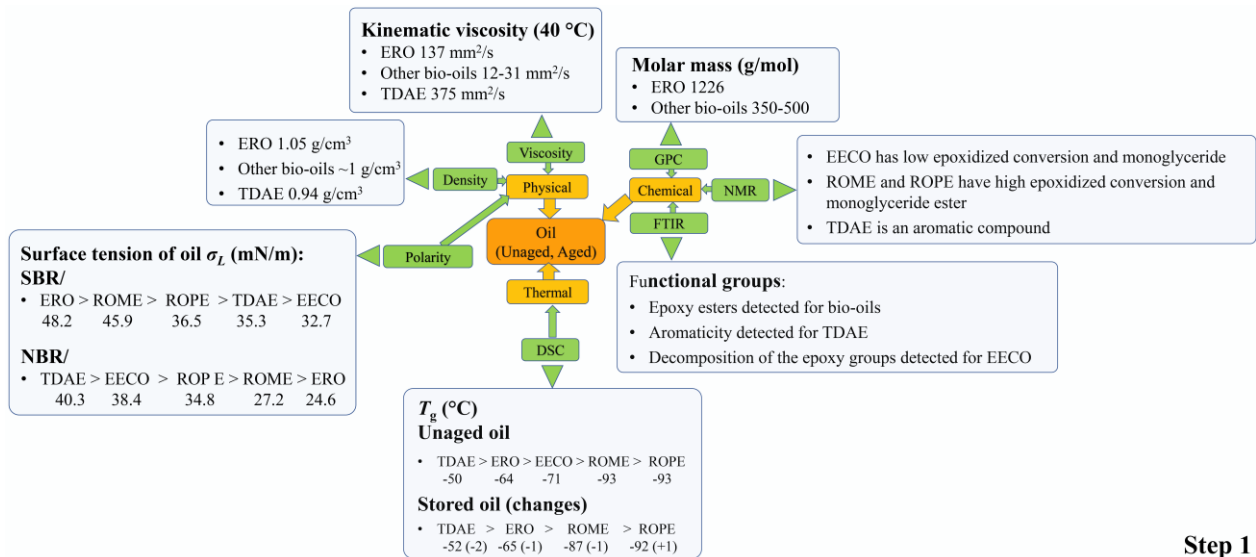
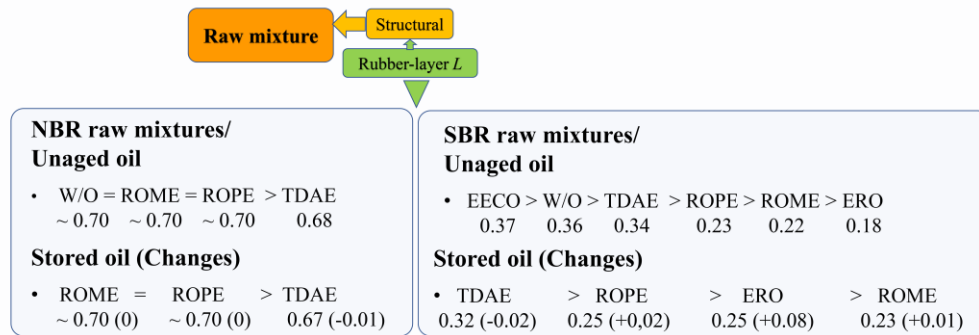


Figure 85: Results from oil investigation

Step 2: Determination of plasticized elastomer raw mixture was done in Step 2 as shown in Figure 86. This investigation was called structural analysis and the rubber-layer  $L$  was measured in part of this thesis. The influence of oils through the rubber-layer  $L$  was found in this investigation, especially in SBR. NBR raw mixtures have a higher rubber-layer  $L$  compared to SBR raw mixtures, and oils had little or negligible effect on the rubber-layer  $L$  of NBR, and stored bio-oils showed no changes in the rubber-layer  $L$  on plasticized NBR stocks. The blending of EECO slightly increased

the rubber-layer  $L$  of SBR raw mixtures, except that these other oils decreased the rubber-layer  $L$ . Mixing stored oil in SBR raw compounds slightly changed the rubber-layer  $L$ .



## Step 2

Figure 86: Results from structural property investigation of plasticized raw mixtures

Step 3: In an important step of this work, the mechanical, fracture resistance, thermo-mechanical, structural and physical properties were investigated. The results have been compiled and shown in Figure 87. This thesis proved that elastomers exhibited higher resistance to crack initiation and propagation when 12.5 phr oils were blended into elastomers. When non-polar SBR is incorporated with EECO, resistance to crack initiation and stable crack propagation improve. Crack resistance and stable crack propagation of NBR is developed when mixed with 12.5 phr ERO, ROME and ROPE. Consequently, it has been observed that SBR exhibits higher resistance to unstable crack propagation when blended with EECO. Resistance to unstable crack propagation was developed for NBR when blended with approximately 12.5 phr of ERO, ROME and ROPE.

Tensile performance was examined, with SBR showing higher tensile strength when blended with TDAE and lower tensile strength when blended with EECO. Also, this thesis showed that the strain of SBR was higher when blended with EECO. In the case of polar elastomer, NBR showed higher tensile strength when blended with ERO and, interestingly, higher strain was observed when NBR was blended with ERO. However, blending NBR with ROME or ROPE showed more developed tensile behavior than TDAE. A highly polar NBR (NBR-39) showed higher tensile strength and strain at break when blended with ROME. SBR showed higher tear strength when blended with EECO and NBR had higher tear strength when blended with ROME and ROPE. It has been observed that NBR-39 has higher tear strength than NBR-34. NBR with bio-oils has a higher compression set than TDAE. It was found that elasticity was higher with increasing oil concentration in elastomers and that bio-oil exhibited higher elasticity compared to TDAE. In particular, both elastomers had higher elasticity when blended with ROME and ROPE. SBR/EECO and NBR/ERO are comparable to TDAE. It was observed that the crosslink density was reduced by the oil blend, which mainly decreased with increasing oil concentration. Crosslink density was higher when low concentrated oil was used. SBR shows high crosslink density when blended with TDAE and blending with EECO shows lower crosslink density. In contrast, the crosslink density of NBR decreased when blended with bio-oils and was higher when TDAE was used. Elastomers blended with a highly concentrated oil were used to determine the viscoelastic behavior of plasticized elastomers to find thermomechanical properties. SBR/TDAE had a higher storage modulus and loss modulus than SBR/bio-oils were measured. At the same time, NBR shows a higher modulus when blended with bio-oils.

In addition, the glass transition temperature of oils was measured using DSC. It has been confirmed that when elastomers are blended with bio-oils, the glass transition temperature of plasticized elastomers is significantly reduced. Filler macro-dispersion was measured as part of the structural

analysis. A clear view of the filler dispersion of the plasticized SBR was observed on the light microscope. When blending SBR with commercial TDAE, a small number of filler agglomerates were visible, while the number of agglomerates was higher when SBR was blended with EECO. In contrast, with plasticized NBR it was very difficult to see the filler agglomerates, but it was observed that the filler dispersion was homogenized when NBR was mixed with bio-oils, but the filler network was still compromised.

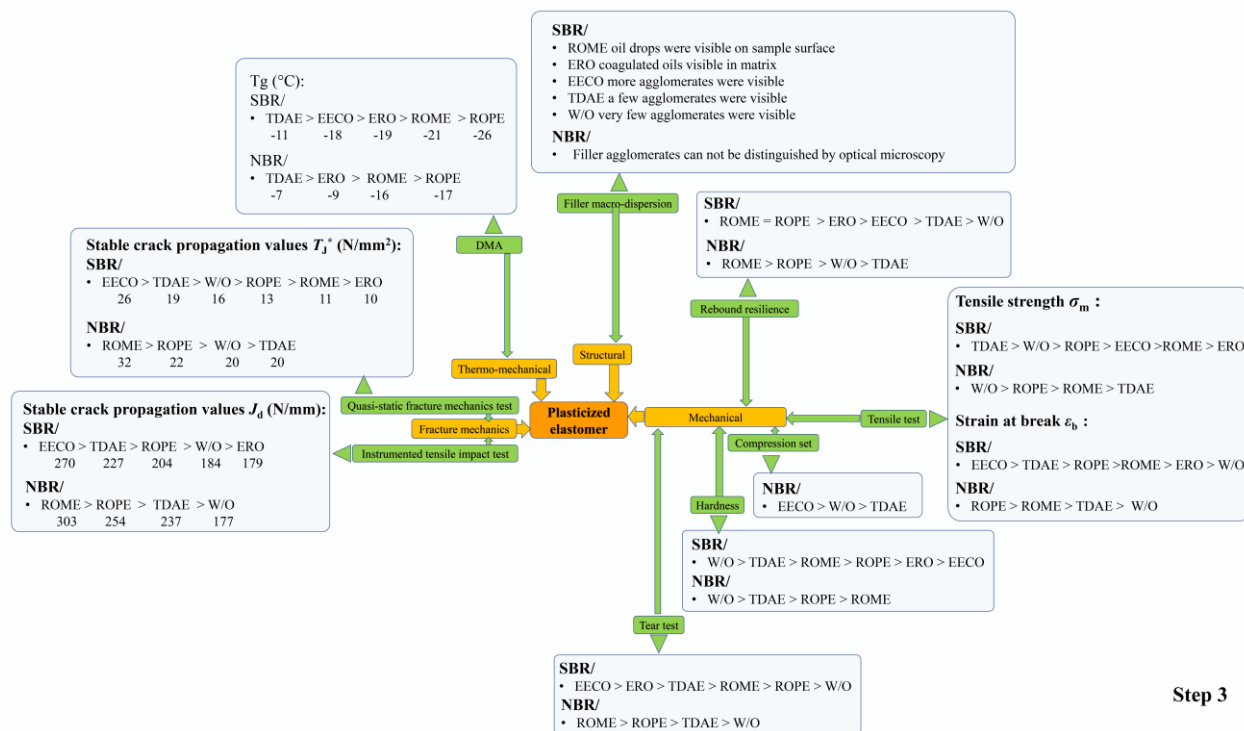


Figure 87: Results from structural, mechanical, crack resistance, and physical characterization of plasticized elastomer vulcanizates

Step 4: Some significant results have been condensed and mentioned in Figure 88. In this step, the main focus was on the aging behavior of oils and plasticized elastomers. A high oil content (e.g. 37.5 phr) was blended into SBR to see how it affects crack resistance and mechanical behavior over aging time. It was found that the aged plasticized SBR developed resistance to stable crack propagation when blended with EECO where crack resistance performance decreased with TDAE. The resistance to unstable crack propagation decreased slightly when SBR was mixed with oils. Tensile strength, strain at break, and tear strength were reduced over aging time for plasticized SBR. Hardness values are higher for plasticized elastomers over time. It was also observed that the resistance to crack initiation and stable crack propagation was surprisingly higher when SBR was blended with stored bio-oils. NBR was not very responsive to stored bio-oils. Resistance to unstable crack propagation for plasticized SBR materials has not been developed when blended with stored bio-oils. Hardness values increased slightly for plasticized SBR and were not greatly affected for plasticized NBR. Tensile strength decreased with SBR/stored bio-oils and was not affected as much with NBR/stored bio-oils blends. When mixed with stored bio-oils, the tensile strength and strain at break of both elastomers decreased slightly.

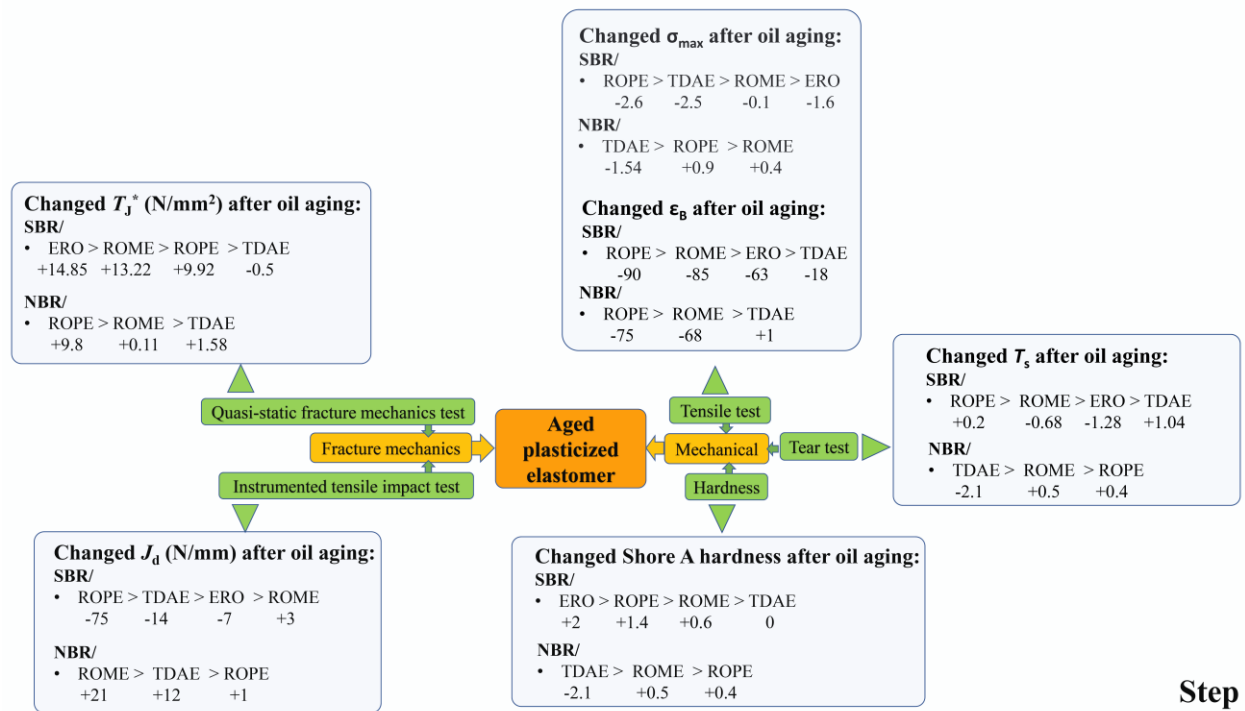


Figure 88: Results from mechanical, and crack resistance characterization of plasticized elastomer vulcanizates when mixed with stored oil

The results of this thesis contribute to the illumination of the relationships between plasticized polar and non-polar elastomers and crack resistance behavior. The chemical structure, polarity, and modification process of bio-oils were a significant concern. The plasticized elastomers' physical, structural, thermal, mechanical, and aging properties were considered. From an application perspective, the application of plasticized elastomers can enhance its resistance against its crack behavior by employing an appropriate modification of fatty oils. The results will be verified by producing different bio-oils with the same properties. Bio-oils have consistently demonstrated advantageous qualities in terms of crack resistance. Nevertheless, it is imperative to conduct a more thorough examination of the effects within the filler network, as its behavior remains challenging to anticipate. The occurrence of filler network breakdowns, which could have occurred or not, still lacks clarity.

## References

- [1] B.N.J. Persson, O. Albohr, G. Heinrich, H. Ueba, Crack propagation in rubber-like materials, *J. Phys. Condens. Matter.* 17 (2005) 1073.
- [2] F. Grasland, L. Chazeau, J.-M. Chenal, J. Caillard, R. Schach, About the elongation at break of unfilled natural rubber elastomers, *Polymer (Guildf).* 169 (2019) 195–206.
- [3] M.M. Rahman, K. Oßwald, K. Reincke, B. Langer, Influence of bio-based plasticizers on the properties of NBR materials, *Materials (Basel).* 13 (2020) 2095.
- [4] S. Sökmen, K. Oßwald, K. Reincke, S. Ilisch, Influence of Treated Distillate Aromatic Extract (TDAE) Content and Addition Time on Rubber-Filler Interactions in Silica Filled SBR/BR Blends, *Polymers (Basel).* 13 (2021) 1–15.
- [5] M.M. Rahman, K. Oßwald, B. Langer, K. Reincke, Influence of Plasticizers Basing on Renewable Sources on the Deformation and Fracture Behaviour of Elastomers, in: G. Heinrich, R. Kipscholl, R. Stoček (Eds.), *Fatigue Crack Growth Rubber Mater. Exp. Model.*, Springer International Publishing, Cham, 2021: pp. 331–346.
- [6] I. Shahzad, M.M. Rahman, S. Wittchen, K. Reincke, B. Langer, V. Cepus, Synthetical modification of plant oil-based plasticizer with CO<sub>2</sub> leads to reduced migration from NBR rubber, *J. Appl. Polym. Sci.* 139 (2022) 1–13.
- [7] E. H. F. Mark, N. G. Gaylord, and N. M. Bikales, *Encyclopedia of polymer Science and technology*, Vol. 15, Interscience Publishers, a division of John Wiley and Sons, Inc., New York, 1971. 703 pp., *J. Polym. Sci. Part B Polym. Lett.* 10 (1972) 227–228.
- [8] L. Gong, M.H.T. Nguyen, E.S. Oh, High polar polyacrylonitrile as a potential binder for negative electrodes in lithium ion batteries, *Electrochem. Commun.* 29 (2013) 45–47.
- [9] G. Henrici-Olivé, S. Olivé, *Molecular interactions and macroscopic properties of polyacrylonitrile and model substances*, in: *Chemistry (Easton)*, Springer Berlin Heidelberg, Berlin, Heidelberg, 1979: pp. 123–152.
- [10] J.S. Dick, *Rubber Technology (compounding and testing for performance)*, in: *J. Chem. Inf. Model.*, Hanser Publishers, Munich, Cincinnati, 2013: pp. 46–67.
- [11] JSP corporation, Japan. Data sheet: Nitrile rubber (NBR), *Tech. Data Information Nitrile Rubber (NBR)*; Japan Synth. Rubber Co., Ltd. (2019) 1–3.
- [12] *Chemistry and manufacturing process of acrylonitrile butadiene rubber (NBR)*, *Worldw. Long Term New Rubber Consum. Forecast by Elastomer Type, IISRP Worldw. Rubber Stat.* (2005).
- [13] Michael Kelly, *Industrial Insulation Nitrile Rubber*, *Insul. – Mater. Sci. Appl.* 4 (2014) 1–18.
- [14] J. Zhao, R. Yang, R. Iervolino, S. Barbera, Changes of Chemical Structure and Mechanical Property Levels During Thermo-Oxidative Aging of Nbr, *Rubber Chem. Technol.* 86 (2013) 591–603.
- [15] L. Ślusarski, G. Janowska, Thermal decomposition of homo- and copolymers of isobutylene, *J. Therm. Anal. Calorim.* 19 (1980) 435–447.
- [16] A. Mostafa, A. Abouel-Kasem, M.R. Bayoumi, M.G. El-Sebaie, The influence of CB loading on thermal aging resistance of SBR and NBR rubber compounds under different aging temperature, *Mater. Des.* 30 (2009) 791–795.
- [17] G. Salomon, Influence of Structure on Polymer-Liquid Interaction. II. Influence of Nitrile Groups, *Polym. Sci.* 3, No.2 (1948) 805–813.
- [18] J.A. Brydson, *Styrene---Butadiene Rubber*, in: A. Whelan, K.S. Lee (Eds.), *Dev. Rubber Technol. Synth. Rubbers*, Springer Netherlands, Dordrecht, 1981: pp. 21–49.
- [19] H.A. Favre, W.H. Powell, *Nomenclature of Organic Chemistry, IUPAC Recommendations and preferred Names 2013*, in: *Cambridge R. Soc. Chem.*, 2014: pp. 1–4.
- [20] W. Obrecht, J.-P. Lambert, M. Happ, C. Oppenheimer-Stix, J. Dunn, R. Krüger, *Rubber*, 4. *Emulsion Rubbers*, in: *Ullmann's Encycl. Ind. Chem.*, John Wiley & Sons, Ltd, 2011.
- [21] Britannica, The Editors of Encyclopaedia. “styrene-butadiene rubber”. *Encyclopedia Britannica*, 24 June. (2018).
- [22] Z. Ahmad, J.E. Mark, *Biomimetic materials: Recent developments in organic-inorganic hybrids*, *Mater. Sci. Eng.* 6 (1998) 183–196.
- [23] Y. Zhang, S. Ge, B. Tang, T. Koga, M.H. Rafailovich, J.C. Sokolov, D.G. Peiffer, Z. Li, A.J. Dias, K.O. Mcelrath, M.Y. Lin, S.K. Satija, S.G. Urquhart, H. Ade, D. Nguyen, Effect of Carbon Black and Silica Fillers in Elastomer Blends, (2001) 7056–7065.
- [24] J.L. Koenig, The chemical reactions of network structures in elastomers, *Acc. Chem. Res.* 32 (1999) 1–8.
- [25] C.. Roland, *The Science and Technology of Rubber: Chapter 3, Structure Characterization in the Science and Technology of Elastomers*, Fourth Edi, Elsevier Inc., 2005.
- [26] P. Kundu, Surface Modification of Carbon Black by Vegetable Oil—Its Effect on the Rheometric, Hardness, Abrasion, Rebound Resilience, Tensile, Tear, and Adhesion Properties, *J. Appl. Polym. Sci.* 84 (2002) 993–1000.

- [27] M. Kang, Y. Heo, F. Jin, S. Park, A review : role of interfacial adhesion between carbon blacks and elastomeric materials, 18 (2016) 1–10.
- [28] Z.H. Li, J. Zhang, S.J. Chen, Effects of carbon blacks with various structures on vulcanization and reinforcement of filled ethylene-propylene-diene rubber, *Express Polym. Lett.* 2 (2008) 695–704.
- [29] J. Fröhlich, W. Niedermeier, H.D. Luginsland, The effect of filler-filler and filler-elastomer interaction on rubber reinforcement, *Compos. Part A Appl. Sci. Manuf.* 36 (2005) 449–460.
- [30] W. Niedermeier, J. Fro, Reinforcement Mechanism in the Rubber Matrix by Active Fillers, *Raw Mater. Appl. KGK Rubber Point.* (2002) 356–366.
- [31] J. Donnet, Filler-Elastomer Interactions, *Br. Polym. J.* 5 (1973) 213–228.
- [32] D. Walter, Primary Particles – Agglomerates – Aggregates, *Lab. Chem. Physics, Inst. Occupational Soc. Med. Justus-Liebig-University.* (2005) 9–24.
- [33] D.J. Kohls, G. Beaucage, Rational design of reinforced rubber, *Curr. Opin. Solid State Mater. Sci.* 6 (2002) 183–194.
- [34] K. Reincke, W. Grellmann, G. Heinrich, Investigation of Mechanical and Fracture Mechanical Properties of Elastomers Filled with Precipitated Silica and Nanofillers Based upon Layered Silicates, *Rubber Chem. Technol.* 77 (2004) 662–677.
- [35] A. Mujtaba, M. Keller, S. Ilisch, H.J. Radosch, T. Thurn-Albrecht, K. Saalwächter, M. Beiner, Mechanical properties and cross-link density of styrene-butadiene model composites containing fillers with bimodal particle size distribution, *Macromolecules.* 45 (2012) 6504–6515.
- [36] H.H. Le, S. Ilisch, G.R. Kasaliwal, H.J. Radosch, Filler phase distribution in rubber blends characterized by thermogravimetric analysis of the rubber-filler gel, *Rubber Chem. Technol.* 81 (2008) 767–781.
- [37] H.H. Le, Z. Ali, S. Ilisch, H.J. Radosch, Time-dependent reinforcement effect of nanoclay in rubber nanocomposites, *J. Mater. Sci.* 46 (2011) 1685–1696.
- [38] G. Kraus, Reinforcement of elastomers by carbon black, in: *Fortschritte Der Hochpolym., Springer Berlin Heidelberg, Berlin, Heidelberg, 1971: pp. 155–237.*
- [39] W. Kaewsakul, K. Sahakaro, W.K. Dierkes, J.W.M. Noordermeer, Factors influencing the flocculation process in silica-reinforced natural rubber compounds, *J. Elastomers & Plast.* 48 (2016) 426–441.
- [40] S.-S. Choi, Effect of bound rubber on characteristics of highly filled styrene-butadiene rubber compounds with different types of carbon black, *J. Appl. Polym. Sci.* 93 (2004) 1001–1006.
- [41] S.-S. Choi, E. Ko, Novel test method to estimate bound rubber formation of silica-filled solution styrene-butadiene rubber compounds, *Polym. Test.* 40 (2014) 170–177.
- [42] S.-S. Choi, Difference in bound rubber formation of silica and carbon black with styrene-butadiene rubber, *Polym. Adv. Technol.* 13 (2002) 466–474.
- [43] I. Pliskin, N. Tokita, Bound rubber in elastomers: Analysis of elastomer-filler interaction and its effect on viscosity and modulus of composite systems, *J. Appl. Polym. Sci.* 16 (1972) 473–492.
- [44] H.H. Le, S. Ilisch, D. Heidebreich, A. Wutzler, Kinetics of the Phase Selective Localization of Silica in Rubber Blends, *Polym. Polym. Compos.* 16 (2008) 101–113.
- [45] G. Oenslager, The development of organic accelerators for rubber vulcanization, *Chem. Ind.* 3 (1933) 91–95.
- [46] M.W. Harman, Vulcanization Characteristics on Mercaptobenzothiazole Derivatives, *Ind. Eng. Chem.* (1937) 205–207.
- [47] J. Kadlcak, I. Kuritka, P. Konecny, R. Cermak, The Effect of ZnO Modification on Rubber Compound Properties, in: *Recent Res. Geogr. Geol. Energy, Environ. Biomed., 2011: pp. 347–352.*
- [48] A.I. Khalaf, A.A. Ward, A.E. Abd El-Kader, S.H. El-Sabbagh, Effect of selected vegetable oils on the properties of acrylonitrile-butadiene rubber vulcanizates, *Polimery/Polymers.* 60 (2015) 43–56.
- [49] P. Raju, V. Nandan, A study on the use of castor oil as plasticizer in natural rubber compounds, *J. Rubber Res.* 10 (2007) 1–16.
- [50] Comprehensive product guide, Varox (Peroxide accelerator), Vanderbilt Chem. LLC. (2014).
- [51] Technical informations of crosslinking Agents, Sigma Aldrich, 40 (1999) 1.
- [52] S. Ellison, J. Blanksby, G. Barney, Bond Dissociation Energies of Organic Molecules, *Am. Chem. Soc.* 36 (2003) 255–263.
- [53] A.Y. Coran, Vulcanization, chapter- 7, in: J.E. Mark, B. Erman, C.M. Roland (Eds.), *Sci. Technol. Rubber (Fourth Ed., Fourth Ed., Academic Press, Boston, 2013: pp. 337–381.*
- [54] O. Chaikumpollert, Y. Yamamoto, K. Suchiva, S. Kawahara, Mechanical properties and cross-linking structure of cross-linked natural rubber, *Polym J.* 44 (2012) 772–777.
- [55] M.-J. Wang, Effect of Polymer-Filler and Filler-Filler Interactions on Dynamic Properties of Filled Vulcanizates, *Rubber Chem. Technol.* 71 (1998) 520–589.

- [56] M.-J. Wang, S. Wolff, J.-B. Donnet, Filler—Elastomer Interactions. Part III. Carbon-Black-Surface Energies and Interactions with Elastomer Analogs, *Rubber Chem. Technol.* 64 (1991) 714–736.
- [57] S. Wolff, M.-J. Wang, Filler—Elastomer Interactions. Part IV. The Effect of the Surface Energies of Fillers on Elastomer Reinforcement, *Rubber Chem. Technol.* 65 (1992) 329–342.
- [58] S. Wolff, M.-J. Wang, E.-H. Tan, Filler-Elastomer Interactions. Part VII. Study on Bound Rubber, *Rubber Chem. Technol.* 66 (1993) 163–177.
- [59] W. Balasooriya, B. Schritteser, G. Pinter, T. Schwarz, L. Conzatti, The Effect of the Surface Area of Carbon Black Grades on HNBR in Harsh Environments, *Polymers (Basel)*. 11 (2019) 1–20.
- [60] G. Heinrich, T. a. Vilgis, Contribution of Entanglement of the Mechanical Properties of Carbon Black Filled Polymer Networks, *Macromolecules*. 26 (1993) 1109–1119.
- [61] M.A. Fazal, A.S.M.A. Haseeb, H.H. Masjuki, Comparative corrosive characteristics of petroleum diesel and palm biodiesel for automotive materials, *Fuel Process. Technol.* 91 (2010) 1308–1315.
- [62] W. Arayaprane, Rubber Abrasion Resistance, *Rangsit Univ. Thail.* (2007) 147–166.
- [63] M. Gerspacher, L. Nikiel, H.H. Yang, C.P.O. Farrell, F. Worth, G.A. Schwartz, Flocculation in Carbon Black Filled Rubber Compounds, (2002) 596–604.
- [64] C.S. Barrera, K. Cornish, Fly ash as a potential filler for the rubber industry, in: *Handb. Fly Ash, 2022*: pp. 763–792.
- [65] M. Klüppel, G. Heinrich, A. Schröder, Carbon Black, *IARC Monogr. Eval. Carcinog. Risks to Humans*. 1995 (2010) 539–550.
- [66] Z.S. Petrović, M. Ionescu, J. Milić, J.R. Halladay, Soybean Oil Plasticizers As Replacement of Petroleum Oil in Rubber, *Rubber Chem. Technol.* 86 (2013) 233–249.
- [67] David F. Cadogan, Phthalic acid and Derivates, *Ullmann's Encycl. Ind. Chem.* (2012) 35–154.
- [68] W. Hofmann, *Rubber technology handbook*, Munich ; New York : Hanser Publishers ; New York : Distributed in the U.S.A. by Oxford University Press, 1989.
- [69] M. Wessling, S. Schoeman, T. van der Boomgaard, C.A. Smolders, Plasticization of gas separation membranes, *Gas Sep. Purif.* 5 (1991) 222 – 228.
- [70] E.P. Favvas, F.K. Katsaros, S.K. Papageorgiou, A.A. Sapalidis, A.C. Mitropoulos, A review of the latest development of polyimide based membranes for CO<sub>2</sub> separations, *React. Funct. Polym.* 120 (2017) 104–130.
- [71] Nasruddin, T. Susanto, The Effect of Natural Based Oil as Plasticizer towards Physics-Mechanical Properties of NR-SBR Blending for Solid Tyres, *J. Phys. Conf. Ser.* 1095 (2018) 1–7.
- [72] T.R. Kukreja, R.C. Chauhan, S. Choe, P.P. Kundu, Effect of the doses and nature of vegetable oil on carbon black/rubber interactions: Studies on castor oil and other vegetable oils, *J. Appl. Polym. Sci.* 87 (2002) 1574–1578.
- [73] M. Bocqué, C. Voirin, V. Lapinte, S. Caillol, J.J. Robin, Petro-based and bio-based plasticizers: Chemical structures to plasticizing properties, *J. Polym. Sci. Part A Polym. Chem.* 54 (2016) 11–33.
- [74] A. Kirkpatrick, Some relations between molecular structure and plasticizing effect, *J. Appl. Phys.* 11 (1940) 255–261.
- [75] Clark F W, *Industrial and engineering chemistry*, *Chem. Ind.* 60 (1941) 1089–1090.
- [76] G. Wypych, Effect of plasticizers on properties of plasticized materials; *Handbook of Plasticizers (Second Edition)*, in: William Andrew Publ., 2nd Editio, 2012: pp. 209–306.
- [77] R. Houwink, *Technology of Synthetic Polymers: in its Chemical and Physical Aspects*, 11th International Congress of Pure and Applied Chemistry, London, 1947.
- [78] F.H. Verhoek, A.L. Marshall, Vapor Pressures and Accommodation Coefficients of Four Non-Volatile Compounds. The Vapor Pressure of Tri-m-cresyl Phosphate over Polyvinyl Chloride Plastics, *J. Am. Chem. Soc.* 61 (1939) 2737–2742.
- [79] W. Aiken, T. Alfrey Jr., A. Janssen, H. Mark, Creep behavior of plasticized vinylite VYNW, *J. Polym. Sci.* 2 (1947) 178–198.
- [80] A.K. Doolittle, Mechanism of Solvent Action, *Ind. & Eng. Chem.* 36 (1944) 239–244.
- [81] P.B. Stickney, L.E. Cheyney, Plasticizers for rubbers and resins, *J. Polym. Sci.* 3 (1948) 231–245.
- [82] T. Alfrey Jr., *The physics of rubber elasticity*. L. R. G. Treloar, Oxford Univ. Press, New York, 1949, 262 pp. Price \$6.00, *J. Polym. Sci.* 5 (1950) 387.
- [83] H.M. Spurlin, The technology of solvents and plasticizers, *J. Polym. Sci.* 18 (1955) 444–445.
- [84] T. Moorshead, *Advances in PVC compounding and processing*, M. Kaufman Son, London. (1962).
- [85] T.G. Fox, P.J. Flory, Second-Order Transition Temperatures and Related Properties of Polystyrene. I. Influence of Molecular Weight, *J. Appl. Phys.* 21 (1950) 581.
- [86] G. Kanig, Zur Theorie der Glastemperatur von Polymerhomologen, Copolymeren und weichgemachten Polymeren, *Kolloid-Zeitschrift Und Zeitschrift Für Polym.* 190 (1963) 1–16.



- [87] J. Kern Sears and J. Darby JR, The technology of plasticizers, John Wiley Sons, New York. 20 (1982) 459–459.
- [88] D.J. Plazek, K.L. Ngai, The Glass Temperature, in: J.E. Mark (Ed.), *Phys. Prop. Polym. Handb.*, Springer New York, New York, NY, 2007: pp. 187–215.
- [89] M.L. Williams, R.F. Landel, J.D. Ferry, The Temperature Dependence of Relaxation Mechanisms in Amorphous Polymers and Other Glass-forming Liquids, *J. Am. Chem. Soc.* 77 (1955) 3701–3707.
- [90] International Lubricants Inc. All rights reserved. No part of this document can be used or reproduced without the express written consent of ILI., (2007).
- [91] E. Aisbl, Replacement of Highly Aromatic Oils in Tyres, *Eur. Tyre Rubber Manuf. Assoc.* (2010) 1–7.
- [92] S. Dasgupta, S.L. Agrawal, S. Bandyopadhyay, S. Chakraborty, Characterization of eco-friendly processing aids for rubber compound, *Polym. Test.* 26 (2007) 489–500.
- [93] V. Null, Safe process oils for tires with low environmental impact, *KGK-Kautschuk Und Gummi Kunststoffe.* 52 (1999) 799–805.
- [94] S. Dasgupta, S.L. Agrawal, S. Bandyopadhyay, R. Mukhopadhyay, R.K. Malkani, S.C. Ameta, Eco-friendly processing oils: A new tool to achieve the improved mileage in tyre tread, *Polym. Test.* 28 (2009) 251–263.
- [95] Evaluation of the carcinogenic risk of chemicals to humans (WHO), *Int. Agency Res. Cancer.* 32 (1983) 33–68.
- [96] M. Meier, J. Metzger, U. Schubert, Plant oil renewable resources as green alternatives in polymer science., *Chem. Soc. Rev.* 36 (2007) 1788–1802.
- [97] Y. Xia, Biorenewable polymeric materials from vegetable oils, *Grad. Theses Diss. Iowa State Univ. Paper 1030* (2011) 124.
- [98] P. Raju, V. Nandan, K.N. Kutty, A Study on the Use of Coconut Oil as Plasticiser in Natural Rubber Compounds, *J. Rubber Res.* 10 (2007) 1–16.
- [99] A. Thomas, Fats and Fatty Oils, in: *Ullmann's Encycl. Ind. Chem.*, Wiley-VCH Verlag GmbH & Co. KGaA, 2000.
- [100] Z. Wang, Y. Peng, L. Zhang, Y. Zhao, R. Vyzhimov, T. Tan, H. Fong, Investigation of Palm Oil as Green Plasticizer on the Processing and Mechanical Properties of Ethylene Propylene Diene Monomer Rubber, *Ind. Eng. Chem. Res.* 55 (2016) 2784–2789.
- [101] V. Nandan, R. Joseph, K.E. George, Rubber seed oil: A Multipurpose additive in NR and SBR compounds, *J. Appl. Polym. Sci.* 72 (1999) 487–492.
- [102] A. Adhvaryu, S.Z. Erhan, Epoxidized soybean oil as a potential source of high-temperature lubricants, *Ind. Crops Prod.* 15 (2002) 247–254.
- [103] Z. Wang, X. Zhang, R. Wang, H. Kang, B. Qiao, J. Ma, L. Zhang, H. Wang, Synthesis and characterization of novel soybean-oil-based elastomers with favorable processability and tunable properties, *Macromolecules.* 45 (2012) 9010–9019.
- [104] P. Saithai, J. Lecomte, E. Dubreucq, V. Tanrattanakul, Effects of different epoxidation methods of soybean oil on the characteristics of acrylated epoxidized soybean oil-co-poly(methyl methacrylate) copolymer, *Express Polym. Lett.* 7 (2013) 910–924.
- [105] L. Yang, H. Dai, A. Yi, B. Lin, G. Li, Structure and properties of partially epoxidized soybean oil, *J. Therm. Anal. Calorim.* 93 (2008) 875–879.
- [106] Y. Chen, Q. Wang, J. Tang, Z. Zhang, Determination of Surface Characteristics of Epoxidized Soybean Oil by Inverse GC, *Chromatographia.* 76 (2013) 91–96.
- [107] J. Zong, Z.; Soucek, M. D.; Liu, Y.; Hu, Cationic photopolymerization of epoxynorbornane linseed oils: The effect of diluents., *J. Polym. Sci. Part A Polym. Chem.* 41 (2003) 3440–3456.
- [108] Y. Feng, Y. Ding, J. Liu, Y. Tian, Y. Yang, S. Guan, C. Zhang, Effects of dietary omega-3/omega-6 fatty acid ratios on reproduction in the young breeder rooster, *BMC Vet. Res.* 11 (2015).
- [109] P. Baladincz, C. Tóth, J. Hancsók, Expanding Feedstock Supplies of the Second Generation Bio-Fuels of Diesel-Engines, *Hungarian J. Ind. Chem.* 38 (2010) 1–7.
- [110] M.A. Gallardo, D.D. Pérez, F.M. Leighton, Modification of fatty acid composition in broiler chickens fed canola oil, *Biol. Res.* 45 (2012) 149–161.
- [111] J. Orsavova, L. Misurcova, J. Vavra Ambrozova, R. Vicha, J. Mlcek, Fatty acids composition of vegetable oils and its contribution to dietary energy intake and dependence of cardiovascular mortality on dietary intake of fatty acids, *Int. J. Mol. Sci.* 16 (2015) 12871–12890.
- [112] Z.S. Petrović, A. Zlatanić, C.C. Lava, S. Sinadinović-Fišer, Epoxidation of soybean oil in toluene with peroxyacetic and peroxyformic acids - Kinetics and side reactions, *Eur. J. Lipid Sci. Technol.* 104 (2002) 293–299.
- [113] S. Sinadinović-Fišer, M. Janković, Z.S. Petrović, Kinetics of in situ epoxidation of soybean oil in bulk catalyzed by ion exchange resin, *J. Am. Oil Chem. Soc.* 78 (2001) 725–731.
- [114] J. La Scala, R.P. Wool, Property analysis of triglyceride-based thermosets, *Polymer (Guildf).* 46 (2005) 61–69.

- [115] V.B. Borugadda, V. V. Goud, Epoxidation of castor oil fatty acid methyl esters (COFAME) as a lubricant base stock using heterogeneous ion-exchange resin (IR-120) as a catalyst, *Energy Procedia*. 54 (2014) 75–84.
- [116] H. Nouredini, B.C. Teoh, L.D. Clements, Densities of Vegetable Oils and Fatty Acids - viewcontent.pdf, *Chem. Biomol. Eng. Res. Publ.* 12 (1992) 1184–1188.
- [117] Standard Test Method for Characteristic Groups in Rubber Extender and Processing Oils and Other Petroleum-Derived Oils by the Clay-Gel Absorption Chromatographic Method, ASTM D2007-19. (2020) 1–9.
- [118] A. Rathi, M. Hernández, S.J. Garcia, W.K. Dierkes, J.W.M. Noordermeer, C. Bergmann, J. Trimbach, A. Blume, Identifying the effect of aromatic oil on the individual component dynamics of S-SBR/BR blends by broadband dielectric spectroscopy, *J. Polym. Sci. Part B Polym. Phys.* 56 (2018) 842–854.
- [119] Y. Chokanandsombat, P. Sea-Oui, C. Sirisinha, Influence of Aromatic Content in Rubber Processing Oils on Viscoelastic Behaviour and Mechanical Properties of Styrene-Butadiene-Rubber (SBR) for Tyre Tread Applications, in: *Multi-Functional Mater. Struct. IV*, Trans Tech Publications Ltd, 2013: pp. 471–474.
- [120] G. Weng, G. Huang, H. Lei, L. Qu, Y. Nie, J. Wu, Crack initiation and evolution in vulcanized natural rubber under high temperature fatigue, *Polym. Degrad. Stab.* 96 (2011) 2221–2228.
- [121] A. Blume, J. Kiesewetter, Determination of the crosslink density of tire tread compounds by different analytical methods, *KGK Kautschuk Gummi Kunststoffe*. 72 (2019) 33–42.
- [122] R.T. Deam, S.F. Edwards, The theory of rubber elasticity, *Philos. Trans. R. Soc. London. Ser. A, Math. Phys. Sci.* 280 (1976) 317–353. <https://doi.org/10.1098/rsta.1976.0001>.
- [123] L.R.G. Treloar, The elasticity of a network of long-chain molecules—II, *Trans. Faraday Soc.* 39 (1943) 241–246.
- [124] T.R. Kukreja, R.C. Chauhan, S. Choe, P.P. Kundu, Effect of the doses and nature of vegetable oil on carbon black/rubber interactions: Studies on castor oil and other vegetable oils, *J. Appl. Polym. Sci.* 87 (2003) 1574–1578.
- [125] P. Raju, V. Nandan, K.N.K. Sunil, A study on the use of castor oil as plasticiser in natural rubber compounds, *J. Rubber Res.* 10 (2007) 1–16.
- [126] W. Pechurai, W. Chiangta, P. Tharuen, Effect of Vegetable Oils as Processing Aids in SBR Compounds, *Macromol. Symp.* 354 (2015) 191–196.
- [127] S. Fernandez, S. Kunchandy, S. Ghosh, Linseed Oil Plasticizer Based Natural Rubber/Expandable Graphite Vulcanizates: Synthesis and Characterizations, *J. Polym. Environ.* 23 (2015) 526–533.
- [128] M.Z. Nurul Ayunie, A.Z. Romli, M.A. Wahab, M.H. Abidin, Effect of Epoxidized Palm Oils Loading on the Crosslink Density and Rebound Resilience Characteristic of SBR Vulcanizates, *Adv. Mater. Res.* 748 (2013) 206–210.
- [129] T. Khanlari, Y. Bayat, M. Bayat, Preparation of a novel polyurethane network based on PPG–PGN–PPG: investigation of the effect of plasticizers on its properties, *Polym. Bull.* (2021).
- [130] K. Saalwächter, B. Herrero, M.A. López-Manchado, Chain Order and Cross-Link Density of Elastomers As Investigated by Proton Multiple-Quantum NMR, *Macromolecules*. 38 (2005) 9650–9660.
- [131] Y.K. Chae, W.Y. Kang, J.-H. Jang, S.-S. Choi, A simple NMR method to measure crosslink density of natural rubber composite, *Polym. Test.* 29 (2010) 953–957.
- [132] T. Saleesung, D. Reichert, K. Saalwächter, C. Sirisinha, Correlation of crosslink densities using solid state NMR and conventional techniques in peroxide-crosslinked EPDM rubber, *Polymer (Guildf)*. 56 (2015) 309–317.
- [133] H.H. Le, S. Ilich, H. Radusch, Characterization of the effect of the filler dispersion on the stress relaxation behavior of carbon black filled rubber composites, *Polymer (Guildf)*. 50 (2009) 2294–2303.
- [134] H. Takino, S. Iwama, Effect of processing additives on carbon black dispersion and grip property of high-performance tire tread compound, *Rubber Chem. ....* (1997) 5–7.
- [135] P.. M. C.W Sweitzer, Dispersion- The fourth dimension of carbon black, *Rubber Ageing*. 92.2 (1962) 251–256.
- [136] B.. Mutagahywa, Carbon black dispersion in rubber assessment methods and process studies, 1984.
- [137] S.-Y. Fu, X.-Q. Feng, B. Lauke, Y.-W. Mai, Effects of particle size, particle/matrix interface adhesion and particle loading on mechanical properties of particulate–polymer composites, *Compos. Part B Eng.* 39 (2008) 933–961.
- [138] T L Anderson, *Fracture mechanics. Fundamentals and application*, 1995.
- [139] W. Grellmann, New Developments in Toughness Evaluation of Polymers and Compounds by Fracture Mechanics, in: W. Grellmann, S. Seidler (Eds.), *Deform. Fract. Behav. Polym.*, Springer Berlin Heidelberg, Berlin, Heidelberg, 2001: pp. 3–26.
- [140] K Reincke W Grellmann G Heinrich, Fracture mechanical investigations of filler-reinforced elastomers, Boukamel A, Laiarinandrasana L, Verron E *Const. Model. Rubber V. Taylor Fr. Group, London.*, (2008) 221–227.
- [141] K. Reincke et al., Investigation of Fracture Mechanical Properties of Filler- Reinforced Styrene-Butadiene elastomers, *KGK-Kautschuk Und Gummi Kunststoffe*. (2009) 246–251.
- [142] K. Reincke, W. Grellmann, R. Lach, G. Heinrich, Toughness Optimization of SBR Elastomers – Use of Fracture Mechanics Methods for Characterization. *Macromolecular Materials and Engineering*, 288 (2003) 181–189.

- [143] S. Agnelli, G. Ramorino, S. Passera, T. Riccò, Fracture resistance of rubbers with MWCNT, organoclay, silica and carbon black fillers as assessed by the J-integral: Effects of rubber type and filler concentration, *6* (2012) 581–587.
- [144] R. S. Rivlin, A. G. Thomas, Rupture of Rubber. I. Characteristic Energy for Tearing, *J. Polym. Sci. X* (1953) 291–318.
- [145] A.A. Griffith, The phenomena of rupture and flow in solids, in: *The royal society, London, 1921*: pp. 582–593.
- [146] A.G Thomas, Rapture of rubbers:II the strain cncentration at an incision., *J. Polym. Sci.* 18 (1955) 177–188.
- [147] H.R. Brown, G. Stevens, Fracture of slightly plasticized polyvinyl chloride, *J. Mater. Sci.* 13 (1978) 2373–2379.
- [148] A.P. Kuriakose, G. Rajendran, Use of rice-bran oil in the compounding of styrene butadiene rubber, *J. Mater. Sci.* 30 (1995) 2257–2262.
- [149] S. Kumar, Recent Developments of Biobased Plasticizers and Their Effect on Mechanical and Thermal Properties of Poly(vinyl chloride): A Review, *Ind. Eng. Chem. Res.* 58 (2019) 11659–11672.
- [150] J. Chen, Z. Liu, K. Wang, J. Huang, K. Li, X. Nie, J. Jiang, Epoxidized castor oil-based diglycidyl-phthalate plasticizer: Synthesis and thermal stabilizing effects on poly(vinyl chloride), *J. Appl. Polym. Sci.* 136 (2019) 1–9.
- [151] Z.S. Petrović, J. Milić, M. Ionescu, J.R. Halladay, EPDM rubber plasticized with polymeric soybean oil of different molecular weights, *Rubber Chem. Technol.* 90 (2017) 667–682.
- [152] P.P. Kundu, Improvement of filler-rubber interaction by the coupling action of vegetable oil in carbon black reinforced rubber, *J. Appl. Polym. Sci.* 75 (2000) 735–739.
- [153] D. Goburdhun, S.B. Jhaumeer-Lauloo, R. Musruck, Evaluation of soybean oil quality during conventional frying by FTIR and some chemical indexes, *Int. J. Food Sci. Nutr.* 52 (2001) 31–42.
- [154] M.D. Guillén, N. Cabo, Fourier transform infrared spectra data versus peroxide and anisidine values to determine oxidative stability of edible oils, *Food Chem.* 77 (2002) 503–510.
- [155] A. Ausili, M. Sánchez, J.C. Gómez-Fernández, Attenuated total reflectance infrared spectroscopy: A powerful method for the simultaneous study of structure and spatial orientation of lipids and membrane proteins, *Biomed. Spectrosc. Imaging.* 4 (2015) 159–170.
- [156] B. Smith, IR Spectral Interpretation Workshop, <https://www.spectroscopyonline.com/view/ir-spectral-interpretation-workshop>, *Spectrosc. MJH Life Sci.* 30 (2015).
- [157] B.M. Abdullah, J. Salimon, Epoxidation of Vegetable Oils- Catalyst, Methods and Advantages, *J. Appl. Sci.* 10 (2010) 1545–1553.
- [158] E. Milchert, A. Smagowicz, G. Lewandowski, Optimization of the reaction parameters of epoxidation of rapeseed oil with peracetic acid, *J. Chem. Technol. & Biotechnol.* 85 (2010) 1099–1107.
- [159] M. chao Kuo, T. chuan Chou, Kinetics and Mechanism of the Catalyzed Epoxidation of Oleic Acid with Oxygen in the Presence of Benzaldehyde, *Ind. Eng. Chem. Res.* 26 (1987) 277–284.
- [160] J. Zhang, J.J. Tang, J.X. Zhang, Polyols prepared from ring-opening epoxidized soybean oil by a castor oil-based fatty diol, *Int. J. Polym. Sci.* 2015 (2015) 1–8.
- [161] W. Xia, S.M. Budge, M.D. Lumsden, <sup>1</sup>H-NMR Characterization of Epoxides Derived from Polyunsaturated Fatty Acids, *J. Am. Oil Chem. Soc.* 93 (2016) 467–478.
- [162] O. Dragostin, L. Profire, Molecular weight of polymers used in biomedical applications, in: M.C. Tanzi, S. Farè (Eds.), *Charact. Polym. Biomater.*, Woodhead Publishing, 2017: pp. 101–121.
- [163] S. Yusa, Chapter 6 - Polymer characterization, in: R. Narain (Ed.), *Polym. Sci. Nanotechnol.*, Elsevier, 2020: pp. 105–124.
- [164] *Plastics – Differential scanning calorimetry – Part 2: Determination of glass transition temperature, ISO 11357-2.* (1999).
- [165] Y. Feng, X. Jin, J.N. Hay, Evaluation of multiple melting peaks of propylene-ethylene copolymers, *Polym. J.* 30 (1998) 215–221.
- [166] *DIN EN ISO 19403: Paints and coatings - Wettability - Part II and III: Determination of surface free energy of solid surfaces by contact angle measurement,* (2020).
- [167] S.-J. Park, M.-K. Seo, Solid-Liquid Interface, in: S.-J. Park, M.-K. Seo (Eds.), *Interface Sci. Compos.*, Elsevier, 2011: pp. 147–252.
- [168] S.H. El-Sabbagh, N.M. Ahmed, G.M. Turkey, M.M. Selim, Rubber nanocomposites with new core-shell metal oxides as nanofillers, chapter 8, in: *Prog. Rubber Nanocomposites*, 2017: pp. 249–283.
- [169] H.H. Le, S. Ilisch, D. Heidebreich, A. Wutzler, Kinetics of the Phase Selective Localization of Silica in Rubber Blends, *Polym. Polym. Compos.* 16 (2008) 101–113.
- [170] H.H. Le, M. Parsaker, M.N. Sriharish, S. Henning, M. Menzel, S. Wießner, A. Das, Q.K. Do, G. Heinrich, H.J. Radusch, Effect of rubber polarity on selective wetting of carbon nanotubes in ternary blends, *Express Polym. Lett.* 9 (2015) 960–971.
- [171] E. Ravera, L. Cerofolini, M. Fragai, G. Parigi, C. Luchinat, Chapter Four - Characterization of lanthanoid-binding

- proteins using NMR spectroscopy, in: J.A. Cotruvo (Ed.), *Rare-Earth Elem. Biochem. Charact. Appl. Lanthanide-Binding Biomol.*, Academic Press, 2021: pp. 103–137.
- [172] J.L. Valentin, P. Posadas, A. Fernández-Torres, M. Malmierca, L.J. González, W. Chassé, K. Saalwächter, Inhomogeneities and Chain Dynamics in Diene Rubbers Vulcanized with Different Cure Systems, *Macromolecules*. 43 (2010) 4210–4222.
- [173] Plastics- Determination of dynamic mechanical properties (Part 1: General principles), ISO 6721-1. (2011) 1–23.
- [174] Plastics — Determination of dynamic mechanical properties, ISO 6721-4. (2008) 1–8.
- [175] Rubber vulcanized or thermoplastic- Determination of tensile stress-strain properties, DIN ISO 372011(E). (2011) 1–28.
- [176] N. AU - Riehle, S. AU - Thude, A. AU - Kandelbauer, G.E.M. AU - Tovar, G. AU - Lorenz, Synthesis of Soft Polysiloxane-urea Elastomers for Intraocular Lens Application, *J. Vis. Exp.* (2019) 1–14.
- [177] Rubber, vulcanized or thermoplastic (Determination of tear strength — Part 1: Trouser, angle and crescent test pieces), ISO 34-1. 2010 (2010) 1–18.
- [178] K. Reincke et al., Influence of Process Oils on the mechanical properties of elastomers, *KGK*. (2009) 506–514.
- [179] N. Stern, I. Dyamant, E. Shemer, X. (Matthew) Hu, G. Marom, Hybrid effects in the fracture toughness of polyvinyl butyral-based nanocomposites, *Nanocomposites*. 4 (2018) 1–9.
- [180] Rubber, vulcanized or thermoplastic — Determination of indentation hardness Part 1: Durometer method (Shore hardness), ISO 7619. (2004) 1–8.
- [181] W. Grellmann, S. Seidler, Mechanical Properties of Polymers, in: *Polym. Test.* (Second Ed., Hanser, 2013: pp. 73–231.
- [182] A.N. Gent, On the Relation between Indentation Hardness and Young's Modulus, *Rubber Chem. Technol.* 31 (1958) 896–906. <https://doi.org/10.5254/1.3542351>.
- [183] D. Turland, Do compression set results measure up?, *Seal. Technol.* 2010 (2010) 11–13.
- [184] Vulcanized and thermoplastic rubber Determination of compression set at ambient, elevated or low temperatures, DIN ISO 815. (1991) 1–11.
- [185] Determining the rebound resilience of rubber using the Schob pendulum, DIN 53512. (2000) 1–4.
- [186] G. Ramorino, S. Agnelli, R. De Santis, T. Riccò, Investigation of fracture resistance of natural rubber / clay nanocomposites by J -testing, *Eng. Fract. Mech.* 77 (2010) 1527–1536.
- [187] W. Grellmann, K. Reincke, Technical material diagnostics – Fracture mechanics of filled elastomer blends, in: *Fract. Mech. Stat. Mech. Reinf. Elastomeric Blends. Lect. Notes Appl. Comput. Mech.*, Berlin, 2013: pp. 227–268.
- [188] K. Reincke, W. Grellmann, G. Heinrich, Engineering fracture mechanics for crack toughness characterisation of elastomers, *Fract. Nano Eng. Mater. Struct. - Proc. 16th Eur. Conf. Fract.* (2006) 763–764.
- [189] N. Ait Hocine, M. Nait Abdelaziz, H. Ghfiri, G. Mesmacque, Evaluation of the energy parameter J on rubber-like materials: Comparison between experimental and numerical results, *Eng. Fract. Mech.* 55 (1996) 919–933.
- [190] N.A. Hocine, M.N. Abdelaziz, A new alternative method to evaluate the J-integral in the case of elastomers, *Int. J. Fract.* 124 (2003) 79–92.
- [191] B.H. Kim, C.R. Joe, Single specimen test method for determining fracture energy ( $J_c$ ) of highly deformable materials, *Eng. Fract. Mech.* 32 (1989) 155–161.
- [192] A.T. Zehnder, Modes of Fracture, in: Q.J. Wang, Y.-W. Chung (Eds.), *Encycl. Tribol.*, Springer US, Boston, MA, 2013: pp. 2292–2295.
- [193] P. Will, R curves for energy dissipative materials, *J. Mater. Sci.* 8 (1994) 2335–2340.
- [194] P. Will, B. Michel, M. Schaper, Justification of nonlinear J-resistance curves, *Eng. Fract. Mech.* 37 (1990) 275–281.
- [195] W. Grellmann, K. Reincke, Quality Improvement of Elastomers. Use of Instrumented Notched Tensile-Impact Testing for Assessment of Toughness. *Materialprüfung*, 46 (2004) 168–175.
- [196] K. Reincke, W. Grellmann, Anwendung der instrumentierten Schlagzugprüfung in der Kunststofftechnik. In: Buchholz, O. W. und Geisler, S. (Hrsg.) Herausforderung durch den industriellen Fortschritt - Tagungsband Werkstoffprüfung, Verlag Stahleisen GmbH Düsseld. (2003) 322–328.
- [197] H. Louis, A. Reckleben, Analyse des dynamischen Reißverhaltens von Elastomeren. In Tagungsband: Kautschuk-Herbst-Kolloquium., 24.–26. Ok (1996) 1–9.
- [198] R. Fernie, N.A. Warrior, Impact Test Rigs for High Strain Rate Tensile and Compressive Testing of Composite Materials. *Strain*, 38 (2002) 69–73.
- [199] D.E. Mouzakis, J. Karger-Kocsis, Effects of Gasoline Absorption on the Tensile Impact Response of HDPE/Selar Laminar Microlayer Composites., *J. Appl. Polym. Sci.* 68 (1998) 561–569.
- [200] J. Karger-Kocsis, O.I. Benevolenski, E.J. Moskala, Toward Understanding the Stress Oscillation Phenomenon in Polymers Due to Tensile Impact Loading., *J. Mater. Sci.* 36 (2001) 3365–3371.

- [201] K. Dijkstra, J. Ter Laak, R.J. Gaymans, Nylon-6/Rubber Blends: 6. Notched Tensile Impact Testing of Nylon-6/(Ethylene-Propylene Rubber) Blends., *Polymer (Guildf)*. (35AD) 315–322.
- [202] C.B. Bucknall, G. Ajroldi, Blends Containing Core-Shell Impact Modifiers. Part 3 - Effects of Temperature on Tensile Impact Behaviour., *Plast. Rubb. Comp.* 30 (2001) 377–383.
- [203] I. Bekar, M.S. Fatt, J. Padovan, Deformation and Fracture of Rubber under Tensile Impact Loading., *Tire Sci. Techn.* 30 (2002) 45–58.
- [204] *Plastics—Determination of tensile-impact strength, ISO 8256, Int. Organ. Stand. Geneva, Switz.* (2004).
- [205] *Testing of Plastics, DIN EN ISO/IEC 17025, MPK-ITIT: 2012-06.* (2012) 1–6.
- [206] *Plastics – Verification of Pendulum Testing Machines – Charpy, Izod and Tensile-Impact Testing, ISO 13802.* (1999).
- [207] *Plastics – Standard Atmospheres for Conditioning and Testing, Geneva, Switzerland, ISO 291.* (2008).
- [208] W. Grellmann, S. Seidler, *Plastics Testing, Carl Hanser Verlag München, Wien, New York,* (2007).
- [209] U. Giese, *Aging Behavior of Elastomers Thermal-Oxidative Aging,* (2014) 1–7.
- [210] S. Allauddin, R. Narayan, K.V.S.N. Raju, Synthesis and Properties of Alkoxysilane Castor Oil and Their Polyurethane/Urea–Silica Hybrid Coating Films, *ACS Sustain. Chem. & Eng.* 1 (2013) 910–918.
- [211] S. Allauddin, V. Somiseti, T. Ravinder, B. Rao, R. Narayan, K. Raju, One-pot synthesis and physicochemical properties of high functionality soy polyols and their polyurethane–Urea coatings, *Ind. Crops Prod.* 85 (2016) 361–371.
- [212] P.A. Ourique, J.M.L. Gril, G.W. Guillaume, C.H. Wanke, S.G. Echeverrigaray, O. Bianchi, Synthesis and characterization of the polyols by air oxidation of soybean oil and its effect on the morphology and dynamic mechanical properties of poly(vinyl chloride) blends, *J. Appl. Polym. Sci.* 132 (2015).
- [213] C. Fu, Z. Yang, Z. Zheng, L. Shen, Properties of alkoxysilane castor oil synthesized via thiol-ene and its polyurethane/siloxane hybrid coating films, *Prog. Org. Coatings.* 77 (2014) 1241–1248.
- [214] S. Dworakowska, D. Bogdal, A. Prociak, Microwave-Assisted Synthesis of Polyols from Rapeseed Oil and Properties of Flexible Polyurethane Foams, *Polymers (Basel).* 4 (2012) 1462–1477.
- [215] E. Milchert, A. Smagowicz, G. Lewandowski, Optimization of the epoxidation of rapeseed oil with peracetic acid, *Org. Process Res. Dev.* 14 (2010) 1094–1101.
- [216] J. Salimon, N. Salih, E. Yousif, Synthetic biolubricant basestocks from epoxidized ricinoleic acid: Improved low temperature properties, *Kem. u Ind. Chem. Chem. Eng.* 60 (2011) 127–134.
- [217] N.R. Babij, E.O. McCusker, G.T. Whiteker, B. Canturk, N. Choy, L.C. Creemer, C.V.D. Amicis, N.M. Hewlett, P.L. Johnson, J.A. Knobelsdorf, F. Li, B.A. Lorsbach, B.M. Nugent, S.J. Ryan, M.R. Smith, Q. Yang, NMR Chemical Shifts of Trace Impurities: Industrially Preferred Solvents Used in Process and Green Chemistry, *Org. Process Res. Dev.* 20 (2016) 661–667.
- [218] A. Adhvaryu, S.Z. Erhan, Epoxidized soybean oil as a potential source of high-temperature lubricants, *Ind. Crops Prod.* 15 (2002) 247–254.
- [219] H.A.J. Aerts, P.A. Jacobs, Epoxide yield determination of oils and fatty acid methyl esters using <sup>1</sup>H NMR, *J. Am. Oil Chem. Soc.* 81 (2004) 841–846.
- [220] J.H. Lee, G. Khang, J.W. Lee, H.B. Lee, Interaction of different types of cells on polymer surfaces with wettability gradient, *J. Colloid Interface Sci.* 205 (1998) 323–330.
- [221] Y. Yuan, T.R. Lee, Contact Angle and Wetting Properties, in: G. Bracco, B. Holst (Eds.), *Surf. Sci. Tech.*, Springer Berlin Heidelberg, Berlin, Heidelberg, 2013: pp. 3–34.
- [222] J.L.E. Chevalier, P.J. Petrino, Y.H. Gaston-Bonhomme, Viscosity and Density of Some Aliphatic, Cyclic, and Aromatic Hydrocarbons Binary Liquid Mixtures, *J. Chem. Eng. Data.* 35 (1990) 206–212.
- [223] J.L.E. Chevalier, P.J. Petrino, Y.H. Gaston-Bonhomme, Viscosity and density of some aliphatic, cyclic, and aromatic hydrocarbons binary liquid mixtures, *J. Chem. & Eng. Data.* 35 (1990) 206–212.
- [224] C.M. Rodenbush, F.H. Hsieh, D.S. Viswanath, Density and viscosity of vegetable oils, *JAOCs, J. Am. Oil Chem. Soc.* 76 (1999) 1415–1419.
- [225] M.E. Nichols, R.E. Robertson, The origin of multiple melting endotherms in the thermal analysis of polymers, *J. Polym. Sci. Part B Polym. Phys.* 30 (1992) 305–307.
- [226] T. Wang, J.L. Briggs, Rheological and thermal properties of soybean oils with modified FA compositions, *J. Am. Oil Chem. Soc.* 79 (2002) 831–836.
- [227] C.P. Tan, Y.B.C. Man, Differential Scanning Calorimetric Analysis of Edible Oils: Comparison of Thermal Properties and Chemical Composition, *77* (2000) 143–155.
- [228] K.G. Berger, E.E. Akehurst, Some applications of differential thermal analysis to oils and fats, *Int. J. Food Sci. & Technol.* 1 (1966) 237–247.
- [229] J.P.P. de Moraes, I.K.C. Pacheco, A.L.M.M. Filho, D.C.L. Ferreira, F.J.C. Viana, F. da Silva Reis, J.M.E. de Matos, M.

- dos Santos Rizzo, A.C.V. Fialho, Polyurethane derived from castor oil monoacylglyceride (*Ricinus communis*) for bone defects reconstruction: characterization and in vivo testing, *J. Mater. Sci. Mater. Med.* 32 (2021).
- [230] Manas-Zloczower I, Analysis of mixing in polymer processing equipment, *Rheol. Bull.* 66 (1997) 5–8.
- [231] I.H. Syed, P. Stratmann, G. Hempel, M. Klüppel, K. Saalwächter, Entanglements, Defects, and Inhomogeneities in Nitrile Butadiene Rubbers: Macroscopic versus Microscopic Properties, *Macromolecules.* 49 (2016) 9004–9016.
- [232] P. Raju, V. Nandan, A Study on the Use of Linseed Oil as Plasticiser in Natural Rubber Compounds, *J. Rubber Res.* 11 (2008) 147–162.
- [233] D.Y. Kim, J.W. Park, D.Y. Lee, K.H. Seo, Correlation between the Crosslink Characteristics and Mechanical Properties of Natural Rubber Compound via Accelerators and Reinforcement, *Polymers (Basel).* 12 (2020).
- [234] Jiayi Li, Modified soybean oil extended SBR compounds and vulcanizates, The University of Akron, 2014.
- [235] A. Charlesby, N.H. Hancock, F.A. Freeth, The effect of cross-linking on the elastic modulus of Polythene, *Proc. R. Soc. London. Ser. A. Math. Phys. Sci.* 218 (1953) 245–255.
- [236] J. Shen, X. Lin, J. Liu, X. Li, Effects of Crosslink Density and Distribution on Static and Dynamic Properties of Chemically Cross-Linked Polymers, *Macromolecules.* 52 (2019) 121–134.
- [237] J. Lacayo-pineda, Filler Dispersion and Filler Networks, 2015.
- [238] A.R. Payne, W.F. Watson, Carbon Black Structure in Rubber, *Rubber Chem. Technol.* 36 (1963) 147–155.
- [239] A.R. Payne, Dynamic properties of heat-treated butyl vulcanizates, *J. Appl. Polym. Sci.* 7 (1963) 873–885.
- [240] A.R. Payne, Dynamic properties of natural rubber containing heat-treated carbon blacks, *J. Appl. Polym. Sci.* 9 (1965) 3245–3254.
- [241] A. Blume, J. Kiesewetter, Determination of the Crosslink Density of Tire Tread Compounds by Different analytical methods, *Raw Mater. Appl. KGK Rubber Point.* 09 (2019) 33–42.
- [242] F. Zhao, W. Bi, S. Zhao, Influence of Crosslink Density on Mechanical Properties of Natural Rubber Vulcanizates, *J. Macromol. Sci. Part B.* 50 (2011) 1460–1469.
- [243] A. Hassan, M.U. Wahit, C.Y. Chee, Mechanical and Morphological Properties of PP/LLPDE/NR Blends—Effects of Polyoctenamer, *Polym. Plast. Technol. Eng.* 44 (2005) 1245–1256.
- [244] J. Li, A. Isayev, Recent development in application of bio-based oils in elastomers, *Rubber Chem. Technol.* 91 (2018) 719–728.
- [245] M.N. Anis Nazurah, A.Z. Romli, M.A. Wahab, M.H. Abidin, Effect of epoxidized palm oil (EPO) on tensile properties and density of rubber compounding, *Adv. Mater. Res.* 812 (2013) 216–220.
- [246] S. Dasgupta, S.L. Agrawal, S. Bandyopadhyay, S. Chakraborty, R. Mukhopadhyay, R.K. Malkani, S.C. Ameta, Characterisation of eco-friendly processing aids for rubber compound: Part II, *Polym. Test.* 27 (2008) 277–283.
- [247] T.R. Kukreja, D. Kumar, K. Prasad, R.C. Chauhan, S. Choe, P.P. Kundu, Optimisation of physical and mechanical properties of rubber compounds by response surface methodology—Two component modelling using vegetable oil and carbon black, *Eur. Polym. J.* 38 (2002) 1417–1422.
- [248] Y. Chokanandsombat, C. Sirisinha, MgO and ZnO as reinforcing fillers in cured polychloroprene rubber, *J. Appl. Polym. Sci.* 128 (2013) 2533–2540.
- [249] S.-R. Ryu, J.-W. Sung, D.-J. Lee, Strain-induced crystallization and mechanical properties of nbr composites with carbon nanotube and carbon black, *Rubber Chem. Technol.* 85 (2012) 207–218.
- [250] L.W. McKeen, 1 - Introduction to Creep, *Polymers, Plastics and Elastomers*, in: L.W. McKeen (Ed.), *Eff. Creep Other Time Relat. Factors Plast. Elastomers (Third Ed., Third Edit, William Andrew Publishing, Boston, 2015: pp. 1–41.*
- [251] S.M.C. Ríos, R. Chicurel, L.F. del Castillo, Potential of particle and fibre reinforcement of tyre tread elastomers, *Mater. & Des.* 22 (2001) 369–374.
- [252] R. Stocck, T. Horst, K. Reincke, Tearing Energy as Fracture Mechanical Quantity for Elastomers, in: *Adv Polym Sci, Springer International publishing AG, Switzerland, 2017: p. 361.*
- [253] R. Brown, G. Soulagnet, Microhardness profiles on aged rubber compounds, *Polym Test.* 20 (2001) 295–303.
- [254] P. Budrugaec, Accelerated thermal aging of Nitrile-butadiene rubber under air pressure, *Polym Degrad Stab.* 47:1 (1995) 29–32.
- [255] A.Y. Coran, Vulcanization: Conventional and Dynamic, *Rubber Chem. Technol.* 68 (1995) 351–375.
- [256] A. Adhvaryu, Z. Liu, S.Z. Erhan, Synthesis of novel alkoxyated triacylglycerols and their lubricant base oil properties, *Ind. Crops Prod.* 21 (2005) 113–119.
- [257] M.M. Rahman, K. Oßwald, K. Reincke, B. Langer, Investigation of the physicochemical properties of bio-based plasticizers for enhancement of the crack resistance behavior of carbon black filled SBR and NBR materials, in: 27. Fachtagung Über Verarbeitung Und Anwendung von Polym. Technomer, Chemnitz, 2021.
- [258] D.S. Campbell, A.V. Chapman, Relationships between structure and performance of vulcanisates, *J. Nat. Rubber Res.*

0127-7065 (1990) 246-258.

## Note of thanks

I would like to sincerely thank Prof. Dr.-Ing. Beate Langer at the Merseburg University of Applied Sciences and Prof. Dr.-Ing. Katrin Reincke at the PSM Merseburg for the valuable scientific supervision of my doctorate and the helpful suggestions and advice, as well as for their understanding and patience with various language issues and grammar. Without their help and support for my academic development in Germany, and this dissertation would have been very tough.

My very special thanks go to Prof. Dr. rer. nat. Kay Saalwächter at the Martin Luther University Halle-Wittenberg for accompanying my research work, the interesting task, his constant supports and the constructive advice and scientific discussions that have made a decisive contribution to the success of this work.

I would like to sincerely thank all my colleagues in the "Materials Diagnostics/Materials Testing" working group (PSM and HoMe) for the scientific, moral, and friendly support that they all gave me in my work. In particular, I would like to express my gratitude to Dr. Katja Oßwald (PSM Merseburg) for her scientific support on rubber processing and testing, Dr. Sybill Ilisch (Synthos Schkopau GmbH) for supporting me in a better understanding of rubber-layer  $L$  analysis, Dr. Ralf Lach (PSM Merseburg) for rubber networking system understanding and Dr. André Wutzler (PSM Merseburg) for the caring instruction of chemical analysis part.

A big thank goes to the following persons for their scientific and technical support: Maximilian Scholz, Paul-Luis Laßbeck (PSM Merseburg) for technical support and machine operations on mechanical testing, Ms. Yvonne Dietze (PSM Merseburg) for DMA and DSC measurements, Mr. Norbert Hinzelmann (HoMe) for GPC analysis, Mr. Sebastian Lebioda (HoMe) for kinematic viscosity measurements. A special thanks to Mr. Carsten Schicktanz (HoMe) for NMR measurements, my condolences on the passing of Mr. Schicktanz, and I wish his soul rest in peace.

My special thanks go to Mr. Walter Kanzler (Glaconchemie GmbH) for the very pleasant cooperation as project partners and bio-oil supplies. I would like to thank Mr. Zuhair Saleem (PPM Magdeburg e.V) for bio-oil supplies and for scientific discussions.

Thanks goes to my friendly colleagues and fellows to helping me to finish this dissertation with their motivation and scientific knowledges: Marcel Auerbach, Selin Sökmen, Irfan Shehzad, Anja Berthold, Sharmin Akter, Newton Sen, Abdus Salam, Akshay Karekar and members of International Graduate Schools in agricultural and polymer sciences (Agripoly) at the Martin-Luther-University Halle-Wittenberg.

I would like to express my heartfelt gratitude to my late parents for making my education possible and for their unconditional love and moral support, I wish from the bottom of my heart that their souls rest in peace. Finally, I would like to thank my sweet wife and parents-in-law from the bottom of my heart for their love. Incredibly, I am very much grateful to my beloved wife for her mental support, although she was in a challenging situation with her pregnancy, studying and our newborn angel daughter Maarit. The little cute face of my little angel motivated me to make myself better.



# **Declaration**

I hereby declare that I have completed this dissertation independently and only using the specified literature and resources.

All services provided by external persons are marked as such.

This dissertation has not previously been submitted to any other university or college.

Halle (Saale), 07.11, 2022

Md Mahbubur Rahman

# Curriculum Vitae

## Personal information

Name	Md Mahbubur Rahman
Date of birth	10 August 1986
Place of birth	Kushtia
Gender	Male
Nationality	Bangladeshi
Academic title	M.Sc

## Education

01/1992-12/1995	Primary school certificate (Mukul Sangha Primary School)
01/1996-12/2002	Secondary school certificate (Kushtia Zilla School)
01/2003-12/2005	Higher secondary certificate (Kushtia government college)
03/2005-10/2009	Bachelor of Science in Applied chemistry and chemical engineering (Islamic University, Kushtia - Jhenaidah)
10/2009-08/2011	Master of Science in Applied chemistry and chemical engineering (Islamic University, Kushtia - Jhenaidah)
10/2014-02/2017	Master of Science in Polymer Materials Science (Martin Luther University, Halle-Wittenberg)
01/2018-Current	PhD in Polymer engineering; title “Influence of modified bio-oils on the fracture mechanics behavior of elastomers” (Martin Luther University, Halle-Wittenberg)

## Scientific profession

08/2010 – 07/2014	Senior chemist (Research and development) Rashid Group of industries limited Bangladesh Rice bran oil production section
07/2017 – 06/2022	Scientific assistant Merseburg University of Applied Sciences Department: Engineering and natural sciences
01/07/2022 – Current	Guest researcher Merseburg University of Applied Sciences Department: Engineering and natural sciences

## Scientific project

15/06/2017 – 14/12/2017

Competence network for applied and transfer-oriented research (KAT) –Development of self-healing elastomer materials with high crack resistance properties

01/09/2017 – 30/06/2020

Development of a non-toxic plasticizer for polymeric materials based on renewable raw materials

01/03/2018 –31/03/2019

Competence network for applied and transfer-oriented research (KAT) – Investigations on the influence of the degree of gelation on the structure and properties of PVC materials

01/04/2019 – 31/12/2019

Investigations into the influence of extrusion parameters on the structure and properties of PVC materials

01/03/2020 – 31.12.2021

Competence network for applied and transfer-oriented research (KAT) - Investigation of the influence of the fracture mechanical assessment of PVC window profiles

01/03/2020 – 30.06.2022

Digitized biotechnological production of biopolymers from residual materials using intelligent model-based process management

01/01/2022 – 30.06.2022

GRAVomer- surfaceCOLLEGE; TP3: Interlocking of engineering university education with professional further qualification in the field of functional surfaces- FKZ 03WIR2005C

## Publications

- 1 Influence of bio-based plasticizers on the properties of NBR materials, **M.M Rahman**, K. Oßwald, K. Reincke, B. Langer. Materials 2020, Vol. 13, issue 9, Page 2095 (Peer Review)
- 2 Influence of Plasticizers Basing on Renewable Sources on the Deformation and Fracture Behaviour of Elastomers, **M.M. Rahman**, K. Oßwald, B. Langer, K. Reincke. G. Heinrich, R. Kipscholl, R. Stoček (Eds.), Fatigue Crack Growth Rubber Mater. Exp. Model., Springer International Publishing, Cham, 2021: Page. 331–346. (Peer Review)
- 3 Influence of modified renewable oils on the fracture mechanics behaviour of SBR polymers. **M.M Rahman**, K. Oßwald, K. Reincke, B. Langer, International Rubber Conference “Innovative Polymers and Polymer Additives”, London, UK 03. – 05.09.2019
- 4 Synthetical modification of plant oil-based plasticizer with CO2 leads to reduced migration from NBR rubber I. Shahzad, **M.M Rahman.**, S. Wittchen, K. Reincke, B. Langer, V. Cepas, J. Appl. Polym. Sci. 2021, e51854. (Peer Review)

## **Conferences and seminars (lectures)**

### **2018**

Influence of plasticizers on the properties of NBR materials. M.M Rahman, K. Reincke, K. Oßwald, B. Langer. “Deutsche Kautschuk-Tagung”, University Session, Hall Madrid, Nürnberg, Deutschland, 02. – 05.07.2018

Influence of plasticizers on the properties of polymeric materials. M.M Rahman, K. Reincke, K. Oßwald, B. Langer. “Tag der Forschung 2018 im Fachbereich INW”, Merseburg, Deutschland, 08.11.2018.

### **2019**

Influence of modified renewable oils on the fracture mechanics behaviour of SBR polymers. M.M Rahman, K. Oßwald, K. Reincke, B. Langer. International Rubber Conference “Innovative Polymers and Polymer Additives”, London, UK, 03.– 05.09.2019.

Influence of modified renewable oils on the fracture mechanics behavior of SBR polymers. M.M Rahman, K. Oßwald, K. Reincke, B. Langer. “Merseburger Elastomertage - elastoMER 2019”, Merseburg, Deutschland, 25.– 26.09.2019

Influence of modified rapeseed oils on the fracture mechanics behavior of polymers. M.M Rahman, K. Oßwald, K. Reincke, B. Langer. Discussion Meeting International Graduate School “Functional Polymers”, Martin-Luther-Universität Halle-Wittenberg, Halle (Saale), Deutschland, 01.10.2019.

Influence of modified bio-oils on the fracture mechanics behavior of SBR polymers. M.M Rahman, K. Oßwald, K. Reincke, B. Langer. Gumference, “Implementation of newest research into rubber industry”, Zlin, Tschechien, 13.11.2019.

### **2020**

Development of crack resistance behavior of bio-plasticized elastomeric materials. M.M. Rahman, K. Oßwald, K. Reincke, B. Langer. 45. “Tagung der Regionalgruppe Ost”, Deutsche Kautschuk-Gesellschaft (DKG), Webinar, 10.12.2020

### **2021**

Investigation of the physical and chemical properties of bio-based plasticizers for enhancement of the crack resistance behavior of carbon black filled SBR and NBR materials. M.M. Rahman, K. Oßwald, K. Reincke, B. Langer. „Technomer 2021“ Technische Universität Chemnitz, 04-05.11.2021

Development of crack resistance behavior of carbon black-filled bio-plasticized polar and nonpolar elastomers. M.M. Rahman, K. Oßwald, K. Reincke, B. Langer. “Plasticizers in Elastomers”, PSM Online research seminar, Polymer Service Merseburg GmbH, Merseburg, 12.07.2021

## **2022**

Investigation of the physicochemical properties of bio-based plasticizers for enhancement of the crack resistance behavior of carbon black-filled SBR and NBR materials. M.M Rahman, Deutschen Kautschuk-Gesellschaft e. V. (DKG) DKT IRC 2021, Nürnberg, 27-30.06.2022

Characterization of the physical and chemical properties of bio-oils to investigate their mixes influence the crack behavior of carbon black-filled SBR and NBR vulcanizates. M.M Rahman, DISCUSSION MEETING-International Graduate School, Functional Polymers, AgriPoly annual retreat, Leucorea, Wittenberg, 16-18.05.2022

### **Conferences and seminars (Posters)**

## **2018**

Influence of plasticizers on the properties of NBR materials. M.M Rahman, K. Reincke, K. Oßwald, B. Langer. PolyMerTec 2018, “16. Problemseminar “Deformation und Bruchverhalten von Kunststoffen” Merseburg, Deutschland, 13-15.06.2018

Development of self-healing elastomers materials with high crack resistance properties. M.M Rahman, K. Reincke, K. Oßwald, B. Langer. PolyMerTec 2018, “16. Problemseminar,, Deformation und Bruchverhalten von Kunststoffen”, Merseburg, Deutschland, 13-15.06.2018

## **2019**

Influence of modified rapeseed oils on the fracture mechanics behavior of polymers. M.M Rahman, K. Oßwald, K. Reincke, B. Langer. Discussion Meeting International Graduate School “Functional Polymers”, Martin-Luther-Universität Halle-Wittenberg, Halle (Saale), Deutschland, 01.10.2019

### **Teaching and supervision of student work**

#### **Introduction to polymer research, Polymer Materials Science, Martin-Luther-Universität Halle-Wittenberg**

Mr. Yashwanth Sai Anjaneya Varma Kosuri, Title: “Investigation of the influence of Fatigue behavior of unfilled SBR when mixed with different types and concentrations of bio-oils”

Ms. Hema Nikhitha Uddaraju, Title: “Investigation of the influence of carbon-black dispersion on plasticizer concentration in SBR materials”

Mr. Jaswanth Kumar Venkataramu, Title: “Investigation of the influence of crosslinking behavior on different bio-oils of carbon black filled NBR vulcanizates”

Ms. Sharmin Akter, Title: “Investigation of curing behavior of free stearic acid loaded SBR as a replacement of commercial stearic acid”

Mr. Kamrul Hasan, Title: “Investigation of mechanical properties of SBR filled with carbon black and processing aids”

#### **Master thesis, Polymer Materials Science, Martin-Luther-Universität Halle-Wittenberg**

Ms. Sharmin Akter, Title: “Investigation of the influences of modified bio-oils on the mechanical and physical behavior of carbon-black filled polymers”

Mr. Kamrul Hasan, Title: “Investigation of the influences of modified bio-oils on the mechanical and physical behavior of carbon-black filled polymers”

### **International Association for the Exchange of Students for Technical Experience**

Ms. Jelena Aksić from Serbia. Title: “Investigation of the influence of carbon-black dispersion on different plasticizers and their concentration of uncured and cured NBR materials”

#### **Lab supervisor (English medium)**

Tensile test of thermoplastic, Lab course “Polymer Testing”, Tensile test and modulus of elasticity in tension. Polymer Material Science (MLU), Room: 131/E/4. 20.04.2018 (2 h), 27.04.2018 (2 h), 04.05.2018 (2 h), 12.04.2019 (1.5 h), 26.04.2019 (1.5 h), 03.05.2019 (1.5 h), 10.05.2019 (1.5 h), Room: Online. 12.06.2020 (1.5 h). 28.05.2020 (1.5 h). 28.05.2021 (1.5 h), Room: Fo/1/8. 06.05.2022 (1.5 h), 13.05.2022 (1.5 h), 20.05.2022 (1.5 h), 03.06.2022 (1.5 h).

Mechanical testing, Lab course “Elastomeric materials”, Manufacturing and characterization of a rubber mixture and vulcanizate, Polymer Material Science (MLU), Room: 131/E/4. 23.11.2018 (3 h), 29.11.2019 (3 h), 06.12.2019 (3 h), 24.01.2020 (3 h), 31.01.2020 (3 h).

Tensile test of elastomers and Macro Dispersion, Lab course “Elastomeric materials”, Manufacturing and characterization of a rubber mixture and vulcanizate, Polymer Material Science (MLU), Room: 131/E/4, 130A/1/202B. 26.01.2018 (2 h), 02.02.2018 (2 h).

#### **Lab supervisor (German medium)**

Elastomere Praktikum “Polymerwerkstoffe”. Studiengang BKT3 (HOME), Room: 131/E/4. 20.11.17 (4 h), 27.11.17 (4 h).

Ermittlung mechanischer Kennwerte bei Zugbeanspruchung “Kunststoffprüfung”. Schwerpunkt Kunststofftechnik im Studiengang MMP, (HoMe), Room: Fo/1/06. 30.11.2021(1.5 h).

Ermittlung mechanischer Kennwerte bei Zugbeanspruchung “Werkstoffcharakterisierung”. Studiengang BGE 2, (HoMe), Room: Online. 21.06.2021 (1.5 h).

Ermittlung mechanischer Kennwerte bei Zugbeanspruchung “Werkstofftechnik-Nichtmetalle (WT2)”. Studiengang BMMP 2, (HoMe), Room: Online. 18.06.2021 (1.5 h).

Kerbschlagbiegeversuch “Werkstofftechnik-Nichtmetalle (WT2)”. Studiengang BMMP 2, (HoMe), Room: Fo/1/04. 05.05.2022 (1.5 h), 19.05.2022 (1.5 h), 02.06.2022 (1.5 h), 09.06.2022 (1.5 h), 16.06.2022 (1.5 h), 23.06.2022 (1.5 h), 30.06.2022 (1.5 h).

Elastomere: Verarbeitung und Prüfung “Polymerwerkstoffe-Vertiefung (PWS 2)”. Studiengang BMMP 6: Schwerpunkt Kunststofftechnik, (HoMe), Room: Online. 08.06.2021 (1.5 h). Room: Fo/1/06. 07.06.2022 (1.5 h).

#### **Management and leadership skills (Advanced training module supervisor)**

Toughness testing and fracture mechanical characterization of polymeric materials, Advanced training module (ATM), “Functional polymers, International Graduate School (AgriPoly),” Room: Online. 06.05. 2021 (3 h).

### **Academic training**

06/02/2020 and 22/02/2020

Academic Writing Course. Lecturer: Anne Wegner (Write English) LLZ, Hoher Weg 8, Gebäude A, 4th floor / Room 4.14, 06120 Halle (1st lecture) and Von Seckendorff Platz 1 Room 1.03, 06120 Halle (2nd Lecture)

21/02/2020

Good Scientific Practice lecture. Lecturer: Thomas Michael (Martin-Luther- Universität Halle-Wittenberg), Von Seckendorff Platz 1 Room 1.29, 06120 Halle

6/11/2019

Poster Design Workshop. Lecturer: Birgit Lukowski (Grafikbüro Suedstern) Von-Seckendorff-Platz 4, SR 4 (1.34), 06120 Halle.

### **Scientific training**

14/03/2019 – 15/03/2019

NMR spectroscopy for the characterization of macromolecular and soft materials. Advanced training module (ATM) functional polymers, International Graduate School (AgriPoly). Lecturer- Prof. Kay Saalwächter (MLU), Betty-Heimann-Str.7, Room: 201.2, 06120 Halle

05/12/2019 – 06/12/2019

IR and Raman spectroscopy for the characterization of macromolecular and soft materials. Advanced training module (ATM) Functional polymers, International Graduate School (AgriPoly). Lecturer- Prof. Valentine Cepus (HOME), Eberhard-Leibnitz-Str.2, Room: Hg/C/1/14, 06217, Merseburg.